CRANFIELD UNIVERSITY
CRANFIELD HEALTH

Ph.D. Thesis

Academic years 2004-2007

GEORGIOS TSEKENIS

Studies towards the development of label-free AC impedimetric immunosensors for healthcare and food quality control

Supervisor: Professor Séamus P.J. Higson

March 2008

This thesis is submitted in partial fulfilment of the requirements for the degree of Doctor of Philosophy

For my parents, Eugenia and Panagiotis

Abstract

This thesis describes work focused towards the fabrication and characterisation of immunosensor platforms for the label-free detection of analytes of importance in the health and food industries. Due to their low unit cost and ease of fabrication, the immunosensor market has significantly increased recently, resulting in a constant demand for new immunosensor applications. Within this thesis, therefore, a novel fabrication protocol is reported towards the production of immunosensor platforms for the detection of the antibiotic, ciprofloxacin, the stroke and multiple sclerosis marker, Myelin Basic Protein (MBP) and the ovarian cancer marker CA-125.

Initial investigations were aimed towards the electrochemical characterization of the available electrode substrates at the onset of this research project namely, gold sputter coated, screen-printed gold and carbon electrodes. They showed that only carbon electrodes provide sufficiently reproducible results and thus these electrodes have been employed for immunosensor fabrication. Due to the advantages of microelectrodes over planar electrodes, attempts to fabricate microelectrode arrays were also made via the ultrasonic ablation of passivated electrode assemblies.

For the site-specific immobilisation of antibodies on polymer modified surfaces biotin-neutravidin affinity technologies were used. The fabricated immunosensors were then interrogated upon exposure to antigen solutions utilising the technique of electrochemical impedance spectroscopy (EIS). Changes in the obtained impedance spectra were used to plot calibration profiles for the detection of ciprofloxacin in buffer and in milk. Similar profiles have been plotted for Myelin Basic Protein (MBP) and the ovarian cancer marker CA-125.

Acknowledgements

First and foremost I would like to thank my supervisor, Professor Séamus Higson, for his invaluable support and guidance throughout these three years.

I gratefully recognise the Sixth Framework Programme of the European Commission for providing the funding for this project and wish to give thanks to all of the members of the ELISHA consortium for a thoroughly enjoyable and productive research programme.

I would also like to thank my colleagues from Silsoe namely, Andrew Barton, Frank Davis, Goulielmos Zois Garifallou and especially Stuart Collyer for their assistance with both technical and non-technical aspects of my research programme.

Thanks must also be given to my colleagues at the University of Leeds namely, Henry Hays, Morsaline Billah and of course Dr. Paul Millner.

I wish to thank Dr. Antonia Vlahou and Dr. Nikolaos Anagnou from the Foundation of Biomedical Research of the Academy of Athens, Greece for offering me a research post even before completing my write-up.

Savvas Amiridis, Stefanos Ntroumakas, Evi Vasilopoulou, Barbara Nawrot, Maria Smirniwtaki and Lefteris Spanos, all played a big part in my university days and their friendship and support is still appreciated more than they know.

A special thank you must also go to Derrick Dring who has been there for me throughout this thesis and for countless more reasons.

Final thanks must be given to all of my family for their continuous support and encourangement, my dad Panagiotis, my brother Alexis and particularly my mum, Eugenia. All my love, thank you.

Declaration

This is a declaration to certify that except as stated below, the contents of this thesis have not been submitted for any other academic or professional award or published in any other form and the contents of this thesis represents entirely my own work.

The results detailed in Chapter 4, 5 and 6 have been collaborative work with Goulielmos-Zois Garifallou, while the results in chapter 7 have contributed to a joint publication in volume 40 of *Analytical Letters*, (2007), pages 1412-1422; this paper is included in the appendix of this thesis.

Georgios Tsekenis

March 2008

CONTENTS

SECTION 1 INTRODUCTION AND METHODOLOGY

CHAPTER 1 **INTRODUCTION** **1**

1.1 RATIONALE FOR THE PHD RESEARCH PROGRAMME 2

1.2 ACADEMIC AIMS OF THE RESEARCH 3

1.3 ELISHA'S RELEVANCE TO THE 6TH FRAMEWORK PROGRAMME 4

1.4 THE ELISHA CONSORTIUM 5

1.5 POTENTIAL IMPACT ON THE BIOSENSOR MARKET 7

CHAPTER 2 **LITERATURE REVIEW** **9**

2.1 BIOSENSORS IN CONTEXT 10

2.1.1 Definition of a biosensor 10

2.1.2 The historical evolution of the biosensor 10

2.1.3 Biosensor applications 17

2.1.4 The design of a commercially successful biosensor 19

2.2 STRUCTURE AND FUNCTION OF TRANSDUCERS 21

2.2.1 Types of transduction 21

2.2.2 Types of electrochemical transduction 22

2.3 ELECTROCHEMISTRY 24

2.3.1 The electrical double layer 25

2.3.2 Equilibrium electrochemistry theory 29

2.3.3 Electrochemistry dynamics 31

2.3.3.1 Electrode kinetics 32

2.3.3.2 Mass transport 34

2.3.3.3 Effect of potential on current flow 36

2.3.4 Voltammetry 39

2.3.4.1 Cyclic voltammetry 41

2.3.5 AC Impedance 44

2.4 MICROELECTRODES 49

2.4.1 Advantages of microelectrodes 50

2.4.2 Microelectrode arrays 52

2.5 ULTRASOUND AND SONOCHEMISTRY 54

2.5.1 The history of Ultrasonics 54
2.5.2 Acoustic cavitation 55
2.5.3 Principles of ultrasound and acoustic cavitation 55
2.5.4 Factors affecting cavitation 57
2.5.5 Applications of ultrasound 58
2.6 POLYMERS 61
2.6.1 Chemically modified electrodes 63
2.6.2 Polymer synthesis 64
2.6.3 Conducting polymers 66
2.6.4 Polymer synthesis validation by the use of a quartz crystal microbalance 68
2.7 ANTIBODIES 70
2.7.1 Antibody structure 70
2.7.2 History of antibody research 72
2.7.3 Antibody immobilisation techniques 73
2.7.4 Fluroquinolones-ciprofloxacin 76
2.7.5 Myelin basic protein 77
2.7.6 Cancer antigen 125 78

CHAPTER 3 **MATERIALS AND METHODS** **80**
3.1 REAGENTS 81
3.2 MATERIALS 82
3.3 BUFFERS AND SOLUTIONS 83
3.4 APPARATUS 85
3.4.1 Gold sputter coater 85
3.4.2 Potentiostat 85
3.4.3 Frequency response analyser 86
3.4.4 Sonication equipment 86
3.4.5 Quartz crystal microbalance 88
3.4.6 Electrodes 89
3.5 EXPERIMENTAL METHODOLOGY 95
3.5.1 Ultra-thin polymer film coatings 95
3.5.2 Microelectrode array fabrication 96
3.5.3 Immunosensor fabrication 96

3.5.3.1 Antibody immobilization using the avidin biotin technology 98
3.5.3.2 Antibody immobilization on aniline boronic acid 103
3.5.4 Quartz crystal microbalance sensor fabrication validation 103
3.5.5 AC Impedance analysis 104

SECTION 2 RESULTS AND DISCUSSION

CHAPTER 4 **ELECTROCHEMICAL CHARACTERISATION OF THE ELECTRODES** **106**
4.1 INTRODUCTION 107
4.2 INVESTIGATION OF THE REPRODUCIBILITY OF DIFFERENT ELECTRODES 111
4.2.1 Gold sputtered gold slides 111
4.2.2 Gold on a silicon substrate planar electrodes and microelectrodes 120
4.2.3 Carbon electrodes 127
4.3 CONCLUSIONS 131

CHAPTER 5 **MICROELECTRODE FABRICATION** **133**
5.1 INTRODUCTION 134
5.2 INITIAL INVESTIGATION INTO THE ULTRASONIC FABRICATION OF MICROELECTRODE ARRAYS 136
5.3 OPTIMISATION OF ULTRASOUNDS CONDITIONS TO FACILITATE THE MASS FABRICATION OF MICROELECTRODE ARRAYS 142
5.3.1 Effects of the duration of sonication upon electrode performance 143
5.3.2 Effects of the power of sonication in association with the positioning of the electrodes upon electrode performance 145
5.3.3 Introduction of a rotating mechanism 149
5.4 CONCLUSIONS 152

CHAPTER 6 **OPTIMISATION OF THE IMMONOSENSOR FABRICATION PROTOCOL** **154**

6.1 INTRODUCTION 155

6.2 OPTIMISATION OF ANILINE ELECTRODEPOSITION ON CARBON ELECTRODES 158

6.2.1 Polymerisation of aniline in a pH 5.0 acetate buffer 158

6.2.2 Polymerisation of aniline in an pH 2.7 solution 160

6.2.3 Polymerisation of aniline in an pH 1.0 solution 162

6.3 QUARTZ CRYSTAL MICROBALANCE PANI DEPOSITION VALIDATION 168

6.4 IMMOBILISATION OF ANTIBODIES FOLLOWING PANI DEPOSITION ON THE ELECTRODE SURFACES 170

6.5 CONCLUSIONS 171

CHAPTER 7 **ELECTROCHEMICAL IMPEDANCE STUDIES ON CIPROFLOXACIN IMMUNOSENSORS** **173**

7.1 INTRODUCTION 174

7.2.1 Electrochemical impedance spectroscopy (EIS) studies on ciprofloxacin immunosensors: Specific sensors 177

7.2.2 Electrochemical impedance spectroscopy (EIS) studies on ciprofloxacin immunosensors: Non-Specific sensors and corrected calibration profile 184

7.2.3 Electrochemical impedance spectroscopy (EIS) studies on ciprofloxacin immunosensors in milk: Specific sensors 190

7.2.4 Electrochemical impedance spectroscopy (EIS) studies on ciprofloxacin immunosensors in milk: Non-Specific IgG sensors 194

7.2.5 Electrochemical impedance spectroscopy (EIS) studies on ciprofloxacin immunosensors in milk: Non-Specific anti-PSA sensors 196

7.2.6 Electrochemical impedance spectroscopy (EIS) studies on ciprofloxacin immunosensors in milk: Corrected calibration profile 201

7.3 CONCLUSIONS 204

CHAPTER 8 **ELECTROCHEMICAL IMPEDANCE STUDIES ON MYELIN BASIC PROTEIN IMMUNOSENSORS** **206**

8.1 INTRODUCTION 207

8.2.1 Electrochemical impedance spectroscopy (EIS) studies on MBP immunosensors: Specific sensors 210

8.2.2. Electrochemical impedance spectroscopy (EIS) studies on MBP immunosensors: Non-Specific sensors and Corrected calibration profile 212

8.3 CONCLUSIONS 221

CHAPTER 9 **ELECTROCHEMICAL IMPEDANCE STUDIES ON CANCER ANTIGEN 125 IMMUNOSENSORS** **223**

9.1 INTRODUCTION 224

9.2.1 Electrochemical impedance spectroscopy (EIS) studies on CA-125 immunosensors: Specific sensors 227

9.2.2 Electrochemical impedance spectroscopy (EIS) studies on MBP immunosensors: Non-Specific sensors and Corrected calibration profile 231

9.3 ANILINE BORONIC ACID 238

9.3.1 PABA electrodeposition 239

9.3.2 Electrochemical impedance spectroscopy (EIS) studies on CA-125 PABA immunosensors: Specific sensors 241

9.3.3 Electrochemical impedance spectroscopy (EIS) studies on CA-125 PABA immunosensors: Non-Specific sensors 246

9.3.4 Electrochemical impedance spectroscopy (EIS) studies on CA-125 PABA immunosensors: Corrected calibration profile 250

9.4 CONCLUSIONS 253

CHAPTER 10 **GENERAL CONCLUSIONS** **255**

CHAPTER 11 **SUGGESTIONS FOR FURTHER WORK** **263**

REFERENCES **267**

APPENDIX **285**

Introduction and Methodology

Chapter 1

Introduction

1.1 Rationale for the PhD Research Programme

An ever increasing demand for improved healthcare, environmental protection and process control has driven a global surge in chemical measurement technologies. Traditionally such analyses have been performed in the laboratory and are associated with delays in measurement and disproportionate expenses for equipment and highly trained personnel. It seems reasonable therefore that industry and society has pushed towards lower cost solutions which can be used even by the consumer. As a consequence of these priorities and in order to meet the existing demand in this research PhD programme, we strove to produce a prototype nano-constructed immunosensor system that can be manufactured with high reproducibility and at low unit cost, which in practice will work similarly to the most successful commercial biosensors.

To achieve this goal, a consortium of 9 European partners has been brought together, each of which was involved in fulfilling a set of work packages that are inter-related. Further to the main goal of the project, the team has been working towards, three further objectives. Firstly, to provide detailed knowledge of a novel signal transduction mechanism observed in nano-constructed affinity-reagent based biosensors. Secondly, to produce electronic, label free, immunosensor model prototypes that can be developed into simple, low-cost and reliable affinity sensors for a range of clinical, environmental and related analytes. And finally, to develop dedicated electronics to be used in the newly constructed immunosensor system. The structure of this consortium as well as its project management are further discussed in section 1.3.

The project is based on previous work in the field of antibody loaded electroconductive matrices which when interrogated with DC pulsed and AC impedance electronics give antigen concentration dependant responses (Grant *et al.*, 2003; Grant *et al.,* 2005). However the approach is markedly different and hence the European project was entitled ELISHA (Electronic Immuno-interfaces and Surface Nanobiotechnology: A Heterodoxical Approach).

ELISHA's approach to the subject of antibody-antigen binding recognition is heterodoxical since although it shares the same principles with the widely used diagnostic technique in immunology, ELISA (Enzyme-Linked ImmunoSorbent Assay), it contrasts the latter by suggesting an alternative way of quantifying the binding event between an antibody and its antigen. This alternative approach offers a number of advantages over ELISA based tests when considering the ease of use of diagnostic tests by end users as well as the potentially significant cost savings, since there is no need for a specialised laboratory and trained personnel to perform analyses.

The range of analytes that may eventually be measured by these devices is vast; however, the primary research carried out in this PhD programme was concentrated on a number of model analytes of great significance in bio-surveillance, medical monitoring, and population screening.

1.2 Academic Aims of the Research

The primary aim of this research, as outlined in the previous chapter was to produce an electronic, label-free immunosensor model prototype that can be further developed into a simple, reliable and low-cost sensor suitable for healthcare and food quality control applications.

Alongside the primary goal, the research carried out promotes knowledge at many levels relevant to the interests of the academic community in the field of sensor fabrication, such as:

- The investigation of a range of different materials (carbon, gold).
- The employment of a number of different monomers and their electrosynthesis.
- The development of various protocols for antibody entrapment and immobilisation on the sensors.

1.3 ELISHA's relevance to the 6th Framework programme

ELISHA targets several priority areas in nanotechnology as set out by the European Union and the sixth framework programme. These priority areas as outlined in the annex of the contract are the following.

- NMP-2002-3.4.1.1 *Molecular and bio-molecular mechanisms and engines*

The programme clearly addresses this area as antigen recognition by its counterpart antibody immobilised on the sensor surface is an event at the molecular level that can be detected and quantified.

- NMP-2002-3.4.1.2 *Molecular interfaces between biology and materials*

The project exploits novel forms of integration of biological and non-biological systems at the nano-level.

- NMP-2002-3.4.2.1 and 3.4.2.2 *Understanding materials phenomena*

Creating new processing pathways for multifunctional materials and mastering their chemistry are both addressed by the project in the creation of different molecular matrices to enable the communication of antibodies affinity reaction with the matrix and to provide new methods of molecular immobilization of the biological structures to or within the matrix.

- NMP-2002-3.4.4.3 *Developing a new generation of sensors for health applications*

The project aims to deliver a largely generic technology that can be made selective to many different analytes. In fact, the range of analytes that may be eventually measured could be as vast as the number of known antibodies.

ELISHA therefore forms part of a larger family of EU contracts on nanotechnology promoting research on cutting edge technologies. In addition, there is a strong advantage at this present time for nanotechnology based ideas, as they are being more exposed to the general public and the success of the glucose biosensor for monitoring diabetes has created an attitude of acceptance of high technology based personal or point of care instrumentation. This is directly related to the framework's priorities in generating enthusiasm for science.

1.4 The ELISHA consortium

So as to fulfill the priorities listed above, nine partners were brought together from five European countries. Seven of these were academic and academic related laboratories, namely the University of Leeds, Cranfield University, the Ecole Centrale de Lyon, the Technical University of Munich, the National Microelectronics Research Centre in Ireland, the Applied Molecular Receptors group of the National Council of Scientific Research in Barcelona and the Institute of Molecular Chemistry in Grenoble. Finally there were two SMEs (Small and Medium Enterprises) involved in the project, namely Uniscan Instruments Ltd. and Technology Translators Ltd.

The project management was co-ordinated through the Enzyme Biotechnology Group in the School of Biochemistry of the University of Leeds and its structure consisted of the following two committees: the steering committee which was made up of one named person from each project partner and the technical committee which was made up of named representatives of the work packages. EBG acted as the central management core for the consortium partners but also as the point of contact for the European Commission (EC) and external organizations showing interest in the progress of the project.

The project partners met regularly to review the project in detail and based on the performance, achieved milestones and delivery of listed work packages decided on any changes necessary to bring success. Reviews were drafted after each meeting that were available to all project partners as well as the EC. The mid-term review and more importantly the final review were much more detailed evaluations involving the EU project officer.

There was a significant complementarity between the partners while the skills they represented were vital for the success of the project. What follows is a brief description of the responsibilities and expertise held by the partners involved in ELISHA.

The Technical University of Munich (TUM) along with the Applied Molecular Receptors Group are experts in the design and production of antibodies. The former concentrated on recombinant antibodies, to insert immobilization tags to simplify the

entrapment process on the surface of the sensors whilst the latter focused on hapten antibodies and the conjugate chemistry to produce and purify them. Between them the project had access to exceptionally pure sources of affinity reagents in the correct formulation and in sufficient amounts.

Our academic institution, Cranfield Health, in conjunction with the Ecole Centrale de Lyon were responsible for sensor production and evaluation of the nanoscale responses observed. Both institutions have a worldwide reputation for biosensor development. Cranfield University is renowned for the invention of the blood glucose biosensor and it contributed to the project through its expertise with nanoscale electrochemical microscopy, AC impedance and DC pulse interrogation and electrode screen printing. The Ecole Centrale de Lyon brought to the project its expertise on capacitive immunosensors and collaborated with the Institute of Molecular Chemistry (ICMG) to produce new techniques for antibody incorporation into immunosensors. ICMG, further to its contribution on antibody entrapment techniques, focused on the synthetic organic chemistry necessary for the production of the immunosensors matrices, as it is an internationally acclaimed institution for substituted pyrrole chemistry.

The role of the National Microelectronics Research Centre in Ireland was to manufacture specifically designed electrodes, as feedback on sensor design and their geometries of sensors can make their interrogation much easier. As transduction experts their contribution was invaluable in signal processing and the extraction of the most useful parameters in any type of signal generated.

Uniscan, one of the two SMEs involved in the project designed, produced and developed the dedicated electronics necessary for the interrogation of the nanostructured immunosensors developed in the project. Technology Transfers Limited, the second SME, are experts in market investigation and IP issues and assisted towards a commercially successful outcome. External alliances were also investigated by them.

Finally the role of the University of Leeds, as discussed previously was to co-ordinate the project; moreover it contributed to the investigations into the nano-interfaces and molecular mechanisms to understand the signal generation. In addition, a quartz

crystal microbalance linked to a potentiostat, at the University of Leeds, enabled the direct detection of deposition and binding events onto the immunosensor films.

1.5 Potential impact on the biosensor market

The strategic impact of the project will be very high, as the work to be carried out opens up a whole new field in sensing and detection of analytes for healthcare, environmental, medical, food, pharmaceutical, manufacturing control and biotechnology applications. Whenever an antibody assay is used now, there will be the prospect of producing an immunosensor for the same analyte. Therefore there is also the capability of starting a new company or companies to manufacture and market the new immunosensor formats, which relates directly to the future plans to develop economic growth within the EU.

The EU is at present one of the leaders in the field of nanotechnology and also was the birthplace of the most successful commercial biosensor devices to date. Even now the bulk of the manufacture of glucose biosensors occurs in the UK. The basic technology behind this huge commercial operation was discovered and developed in the EU, taking around seven years from first concept to full production. In 2003 glucose biosensors accounted for 85% of the total biosensors market which was worth in excess of $5 billion, compared to $500 million in 1996 (Newman *et al*., 2004).

However, the traditionally strong growth in the biosensors market will not last forever. For example, while the annual growth in the blood glucose market was 10-11% in 2000 it slowed down to 5% in 2004 mainly due to the failure of the big players of the field to introduce new technologies and innovations, with the exception of the non-invasive or minimally invasive devices for blood glucose monitoring, such as Glucowatch® and Pendragon® (Newman *et al*., 2004).

Nevertheless other applications of biosensors still await to be commercially developed with the potential of becoming even bigger success stories than the glucose sensors. Defence security, crime prevention and forensics are more important than ever. Technologies for toxin biological threat agents, explosives are growth areas for biosensors and are key areas for many countries including the US and the UK. Food safety, quality and traceability are also important and key issues include the presence

of pathogens, consistency of taste and product verification. Taking into consideration these financial figures, ELISHA could benefit enormously from the increased interest in biosensors and blooming market and be a huge success story.

Chapter 2

Literature Review

2.1 Biosensors in context

2.1.1 Definition of a biosensor

According to Stetter, sensors can be subdivided into two categories: physical sensors and chemical sensors (Stetter *et al*., 2003). Physical sensors are used to measure physical properties such as temperature and pressure. Chemical sensors on the other hand quantify the concentration of a molecular target. Biosensors therefore can be considered as a subset of chemical sensors. The term biosensor has been variously applied to a number of devices either used to monitor living systems or those incorporating biological elements describing such diverse devices such as a thermometer, a mass spectrometer, *daphnia* in pond water, electrophysiology equipment, chemical labels for imaging and ion selective electrodes. However, according to IUPAC the term should be reserved to sensors incorporating a biological element such as an enzyme, antibody, nucleic acid, micro-organism or cell. Thus, a biosensor can be defined as 'a compact analytical device incorporating a biological or biologically-derived sensing element either integrated within or intimately associated with a physicochemical transducer (Turner *et al.*, 1987). It therefore combines the specificity and selectivity that biological systems offer, with the computing power of a microprocessor (Varma *et al*., 2003). The type of transduction varies as much as the biological recognition entity itself, and can be optical, acoustic, thermal or electrochemical in nature. The objective of all transducing systems used in biosensors though is essentially the same, i.e. to translate the response produced by the sensing element into a quantifiable signal (Bridge, 2001).

2.1.2. The historical evolution of the Biosensor

The need for a greater degree of selectivity towards one particular analyte within a complex mixture led to the production of the predecessor of biosensors, by Free *et a*l., in 1956, in the form of the first enzyme strip test (Free *et al*., 1956). In this test, glucose could be detected by a change in the colour of a strip of litmus paper that was first impregnated with glucose oxidase (GOD).

However, the definition of a biosensor as stated in the previous chapter, allows us to clearly identify Professor Leland C Clark Jnr. as the father of the biosensor concept,

since he was the first person to introduce an electrical transducer into a sensor format. In 1956, Clark published his definitive paper on the oxygen electrode (Clark, 1956). A membrane permeable to oxygen, was positioned over a platinum working electrode polarised at -700mV (vs. Ag/AgCl). The electrochemical reduction of oxygen at the cathodically polarised platinum electrode surface produced an amperometric response, thus allowing for the quantification of oxygen levels present in a tissue sample (Equation 2.1).

$$O_2 + 2H_2O + 4e^- \xrightarrow{-700mV \text{ vs. Ag/AgCl}} 4OH^- \qquad \textit{Eqn. 2.1}$$

Based on the oxygen electrode and addressing the need to expand the range of analytes that could be measured, Clark made a landmark address in 1962 at a New York Academy of Sciences symposium in which he described how "to make electrochemical sensors (pH, polarographic, potentiometric or conductometric) more intelligent by adding enzyme transducers as membrane enclosed sandwiches". The concept was illustrated by an experiment in which glucose oxidase was entrapped at a Clark oxygen electrode using a dialysis membrane. An amperometric transducer was once again employed to produce a quantifiable electrical signal. Within this sensor however, the signal produced could be directly related to the electrochemical reduction of oxygen at the electrode via the catalytic oxidation of glucose by glucose oxidase (GOD), Eqn2.2. The decrease in measured oxygen concentration was proportional to glucose concentration.

$$\beta\text{-D-glucose} + O_2 \xrightarrow{-700mV \text{ vs. Ag/AgCl}} \text{gluconolactone} + H_20_2 \qquad \textit{Eqn. 2.2}$$

In the published paper (Clark, 1962), Clark and Lyons coined the term *enzyme electrode*, a term mistakenly attributed to Updike and Hicks. The latter, in 1967, expanded on the experimental detail necessary to build functional enzyme electrodes for glucose, by entrapping GOD in a gel of polyacrylamide adjacent to the surface of the oxygen-detecting electrode. This allowed for increased operational stability of the enzyme and at the same time simplified the sensor preparation (Updike and Hicks, 1967).

Further work on sensors for glucose measurement in tissues and blood samples resulted in the successful application of an enzyme electrode in a prototype blood glucose analyser by Reitnauer in 1972 (Reitnauer, 1972).

The original oxygen detection demonstrated by Clark in 1962 was found to be susceptible to drift due to fluctuations in the ambient environmental oxygen levels. For that reason, in 1974, Yellow Springs Instrument Co. (Ohio) utilised an alternative method of detection to produce the world's first commercial biosensor for whole blood glucose determination, YSI 23A (Fig. 2.1).

Fig 2.1 The Yellow Springs Instrument Co.'s whole blood glucose biosensor, YSI 23A.

The polarity on the working electrode of this glucose analyser, YSI 23A, was reversed and hence the enzymic production of H_20_2 could be amperometrically monitored (Eqn 2.3).

$$H_20_2 \xrightarrow{+650mmV \text{ vs. } Ag/AgCl} O_2 + 2H^+ + 2e^- \qquad \textit{Eqn 2.3}$$

There were certain considerations to be taken into account such as the fact that the potential (+650mmV) at which the working electrode was polarised could oxidise other electroactive components of blood (e.g. ascorbate, urea) and produce erroneous responses. Yellow Springs Instruments overcame this issue, by introducing a novel permselective barrier for the exclusion of interferents, that was placed between the enzyme layer and working electrode and consisted of an anionic cellulose acetate membrane that hindered the passage of anionic solutes via a natural change exclusion mechanism.

Furthermore, the YSI 23A biosensor utilised an outer microporous polycarbonate membrane in the form a substrate diffusion limiting barrier to prevent saturation of the enzyme and thus allow for the linearisation of sensor responses over wider concentration ranges.

Guilbault and Montalvo were the first to detail a potentiometric enzyme electrode, as early as 1969. These workers described a urea sensor based on urease immobilised at an ammonium-selective liquid membrane electrode (Guilbault and Montalvo, 1969). In 1975, the biosensor took a further fresh evolutionary route, when Divies suggested that bacteria could be harnessed as the biological element in microbial electrodes for the measurement of alcohol (Divies, 1975; Rechnitz *et al*., 1978).

In 1976, La Roche produced the "Lactate Analyser LA640", where the enzyme was dissolved in buffer and placed in a reaction chamber directly in front of the electrode in order for the soluble mediator, hexacyanoferrate, to shuttle electrons from lactate dehydrogenase to an electrode (Hall, 1990). Although this was not a commercial success at the time, it turned out in retrospect to be an important forerunner of a new generation of mediated-biosensors and of lactate analysers for sports and clinical applications.

In the same year, a NADH sensor using mitochondria was constructed by Guibault (Guibault, 1976), while the first enzyme sensors with calorimetric indication were developed in 1977 by Mosbach (Mosbach, 1977).

The new devices, called thermal enzyme probes (Cooney *et al*., 1974) and enzyme thermistors (Mosbach, 1974) exploited the fact that many enzyme reactions are highly

exothermic. Thus, the released heat associated with the metabolism of analytes, such as glucose, lactate, urea, ethanol and sucrose could be monitored and quantified. However, these devices had considerable drawbacks, namely complex instrumentation and fluctuations in ambient temperature (Gulce, 1995).

Spectrophotometric techniques were used for the first time in biosensors by Leubbers and Opitz in 1975 (Lubbers and Opitz, 1975). They offer an unrivalled degree of selectivity by exploiting a range of optical properties, such as adsorption, fluorescence, bio/chemiluminescence and reflectance phenomena. Leubbers *et al* coined the term optode to describe a fibre optic sensor by immobilising a reagent on the end of an optical fibre to measure carbon dioxide or oxygen. They further extended the concept to make an optical biosensor for alcohol by immobilising alcohol oxidase at the end of a fibre-optic oxygen sensor (Voelkl, 1980). Commercial optodes are now showing excellent performance for *in vivo* measurement of pH, pCO_2 and pO_2, but enzyme optodes are not yet widely available.

In 1976, Clemens *et al* (Clemens, 1976) incorporated an electrochemical glucose biosensor in a bedside artificial pancreas and this was later marketed by Miles (Elkhart) as the Biostator. Although the Biostator is no longer commercially available, a new semicontinuous catheter-based blood glucose analyser has recently been introduced by VIA Medical (San Diego).

The idea of building direct immunosensors by fixing antibodies to a piezoelectric or potentiometric transducer had been explored since the early 70's, but it was a paper by Liedberg *et al.* (Liedberg *et al.,* 1983) that was to pave the way for commercial success. They described the use of surface plasmon resonance to monitor affinity reactions in real time. The BIAcore (Pharmacia, Sweden) launched in 1990 is based on this technology. However, the first 'direct' immunoelectrode had already been assembled by Janata in 1975 (Janata, 1985), and the electrochemical interrogation of immunoassays has now become common practice.

Many groups are also studying the applications of biological receptor proteins. In 1979 Ray *et al*. (Ray *et al*., 1979), devised a chromatography column with immobilised receptors, while in 1986 Belli and Rechnitz described the first 'receptode' (Belli and Rechnitz, 1986).

Nowadays, the miniaturisation and creation of multifunctional sensors via the use of small-scale devices is the direction in which a considerable amount of biosensor research is directed. Danielson *et al* were the first to biochemically modify gas sensitive or ion selective field effect transistors to produce semiconductor biosensors. These transistors are regarded as the first example of applied microbioelectronics, since they are based on the combination of microelectronics and biotechnology (Danielson *et al.*, 1985).

It becomes apparent that a recurring theme in the history of biosensors is the extensive research on glucose sensors. Throughout the past decades several groups have produced different sensors for the measurement of glucose in tissue and in blood samples - Clark's enzyme electrode being the first example.

It comes as no surprise then that the most commercially successful hand-held biosensor for home use is the electrochemically based Exactech® glucose meter. At this point it is worthy of note that in 1982, Shichiri *et al.* (Shichiri *et al.,* 1982), described the first needle-type enzyme electrode for subcutaneous implantation, a major advance in the *in vivo* application of glucose biosensors and although companies are still pursuing this possibility, no device for general use is available yet.

The Exactech® glucose meter belongs to a new generation of sensors that utilise a chemical mediator. A mediator is a chemical species that may be used within biosensors to facilitate charge transfer between an enzyme and working electrode. A much cited paper in 1984, by Turner *et al.*, on the use of ferrocene and its derivatives as an immobilised mediator for use with oxidoreductases in the construction of inexpensive enzyme electrodes, forms the basis for this glucose meter (Turner *et al.,* 1984). Ferrocene in this case is an alternative to a double membrane structure and replaces O_2 as the natural electron donor-acceptor in the reaction pathway, allowing electron transfer from GOD to the electrode surface at approximately -240mmV vs. Ag/AgCl via the following reaction scheme (Fig 2.2). The lowered polarising potentials, as permitted by the use of ferrocene, have the additional advantage of minimising the risk of oxidation of other electrochemically active solutes in blood samples.

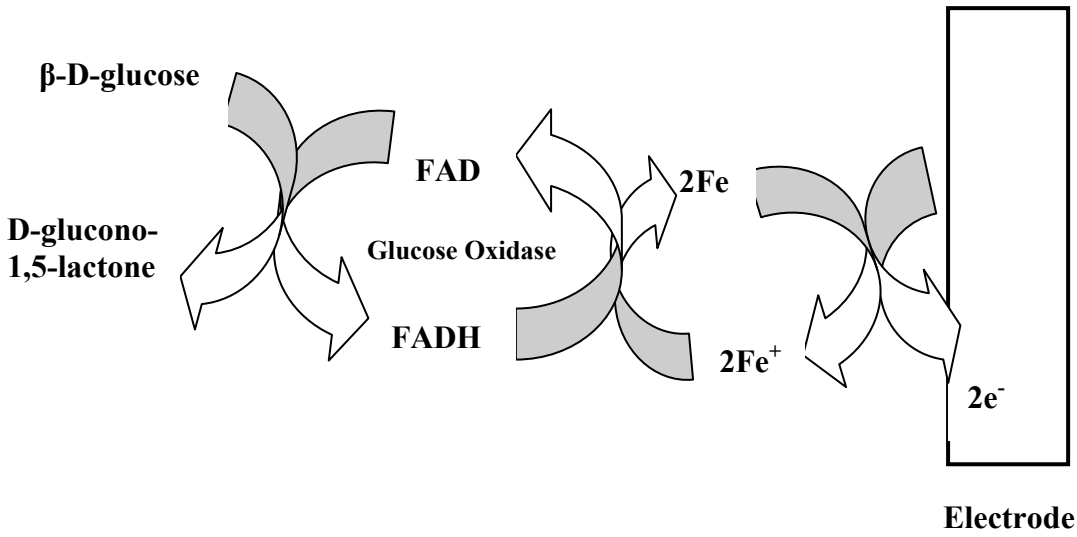

Fig 2.2 Ferrocene mediated glucose oxidase electron transfer

The Exactech® glucose meter was marketed by MediSense (Cambridge, USA). It was first launched in 1987 with a pen-sized meter for home blood-glucose monitoring. The electronics were redesigned into popular credit-card and computer-mouse style formats, and MediSense's sales showed exponential growth reaching US$175 million by 1996 when they were purchased by Abbott (Fig 2.3). This growth is attributed to the portability and inexpensiveness of the sensor and its disposable electrode/sensors strips as well as to the rapid response times (c. 30 seconds). Roche and Bayer now have competing mediated biosensors and the combined sales of the three companies dominate 85% of the world market for biosensors and are rapidly displacing conventional reflectance photometry technology for home diagnostics (Eggins, 1997).

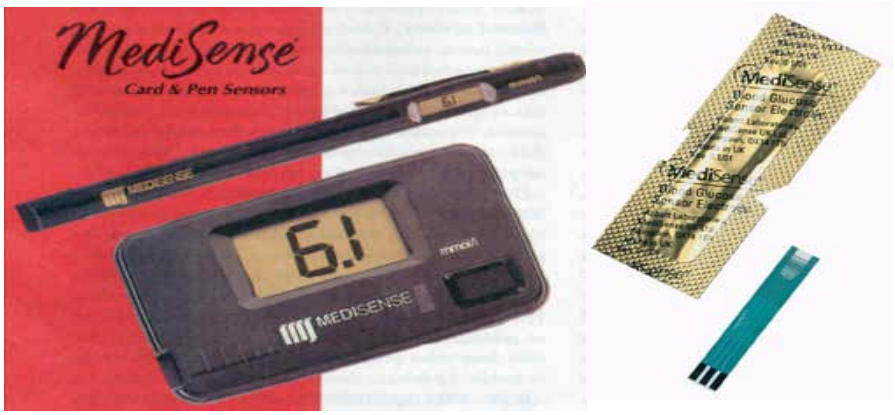

Fig 2.3 MediSense pen and credit card shaped glucose meters along with the disposable strips.

No other biosensor applications have proved as successful as the blood glucose biosensor mainly due to stability issues and batch-to-batch variations posed by other enzymes. Notable exceptions are the home pregnancy kits, based on antibody entrapment, as well as the motor vehicle oxygen sensors.

Academic journals now contain descriptions of a wide variety of devices exploiting enzymes, nucleic acids, cell receptors, antibodies and intact cells, in combination with electrochemical, optical, piezoelectric and thermometric transducers. Within each permutation lies a myriad of alternative transduction strategies and each approach can be applied to numerous analytical problems and not exclusively in healthcare.

2.1.3. Biosensor applications

Although, the over optimistic forecasts back in the 1980s, that the biosensor market would be in the order of several $100 billion by the year 2000 (Freitag, 1996), have not been realised, food industries, environmental agencies and organisations, farmers and even defence and security companies are now all making good use of biosensors, with the potential of further more industrious exploitation in the future in an even greater range of fields.

Medical Applications

The need for portable, remote and cheap analyses of bodily fluids – blood and urine – had led to a rapid expansion of the field of biosensors and their applications in medicine. The single, most successful biosensor to day is without doubt the glucose oxidase enzyme electrode marketed by Exactech® in the shape of a pen. Recently, a new non invasive sensor that does not require a blood sample, and works by measuring blood glucose by IR radiation, the Diasensor 1000^{TM}, became commercially available. However, biosensors are not only used for monitoring glucose levels in the blood. They have already been used for the diagnoses of overdoses, since they do not only offer rapid analysis but also differentiate between different drugs, i.e. paracetamol and salicylic acid. The possibilities are endless, since for each medical condition, with one or more biomarkers associated with it, a different sensor can theoretically be developed. One of the main goals of ELISHA was the

fabrication of immunosensors for the detection of biological markers, such as the ovarian cancer antigen (CA-125) and myelin basic protein (MBP).

Food Industry Applications

The detection of contaminants, such as toxins, pesticides and microorganisms has always been important for the food industry. Therefore, it is not surprising that there is considerable interest in the applications of biosensors in this industry. Biosensors can also be used though, to evaluate the freshness of food, meat and fish for example, or to provide a list of components contained in a food product, such as vitamins, allergens, emulsifiers and preservatives. For example electronic 'noses' or 'tongues' have emerged that can detect hundreds of compounds which contribute to an aroma or flavour (Kress-Rogers *et al.*, 2001). Furthermore, biosensors are already employed to measure alcohol and sugar levels in fermentation procedures (Turner *et al.,* 1984) as well as to determine penicillin levels in milk (Thrust, 1996). Ciprofloxacin which belongs to the family of fluoroquinolines has been examined in an immunosensor format within this PhD programme.

Environmental applications

Environmental monitoring applications of biosensors is an ever expanding field since the determination of air and water pollutants is vital. Applications include the monitoring of herbicides, pesticides, insecticides, fertilisers, along with inorganic ions such as nitrate, sulphate, phosphate, potassium, fluoride, sodium and phenols. The most widely used biosensor in environmental applications is for determining BOD (Biological Oxygen Demand). This type of sensor measures oxygen depletion, used in the oxidation of organic pollutants present in a sample, by microorganisms such as *Clostridium butyricum* and *Trichosporon cutaneu* (Eggins, 1997).

Defence and security applications

The uses of biosensors by the military and the police are primarily aimed at the detection and monitoring of warfare agents such as mustard or nerve gases, as well as explosives, and illicit drugs (Eggins, 1997; Kiyoyuki *et al.*, 1995). Biosensors can

also be used for the monitoring of biological threat agents such as anthrax and plague, within a counter-terrorism context (Iqbal *et al.*, 2000).

2.1.4 The design of a commercially successful biosensor

As briefly outlined in its definition, a biosensor always comprises of a biological component and a transducer. The biological component may be an enzyme, an antibody, a nucleic acid or even a whole cell or tissue slice, giving rise to different generations of biosensors. In the same fashion, the transducer element of a biosensor can vary as well. There are several different modes of transduction, based on optical, thermal, acoustic or electrochemical means, which are further analysed in the following chapter. This report, however, is primarily concerned with electrochemically based sensors.

A further consideration to be taken into account, when designing a biosensor, is the immobilisation of the biological component at an electrode surface. The techniques that have been employed are numerous and depend on the specific biological element and the polymer used in the biosensor.

In its simplest form, a biosensor's circuit consists of a working electrode together with a suitable counter electrode and/or reference electrode. Many interrogation techniques of the circuit are possible; however the most typical are a) the potentiometric approach that measures the potential difference generated between two electrodes, b) the amperomtric approach that monitors the current flow between the electrodes and c) the conductimetric approach, where the biological components' modulated conductivity is monitored within a polymer.

Having decided on the biological entity, transducer and interrogation technique, a commercially successful biosensor must meet certain criteria. To be competitive with existing techniques, a biosensor should be designed to offer a simplified monitoring approach that incurs low capital and running costs, while providing a rapid and accurate determination of a biological agent in a sample as well as meeting the requisite selectivity, accuracy, reproducibility, sensitivity and stability.

Selectivity refers to the ability of a sensor to discriminate between different substrates. This is usually provided by the use of a membrane, such as Nafion, which screens analytes based on size and charge exclusion or by an ion selective frit such as the ion selective glasses used in pH electrodes. Specificity, a term mistakenly used interchangeably with selectivity should not be used as no sensor system is absolutely specific.

Accuracy and precision are two criteria that are closely associated. The former one refers to how close the measured value is to the real value and in a typical biosensor the error margin is expected to be better than ±5%. Precision or reproducibility on the other hand is a measure of how repeatable the obtained results are from a test. In theory reproducibility should be 100% however in practise this will never be case since there are experimental and manufacturing limitations, many of which are introduced by human error and are unavoidable.

Another criterion for a commercially successful biosensor is its sensitivity range. As with every analytical method, biosensors have a lower and upper detection limit that can be different from the range another method can measure. A successful biosensor must have a sufficiently dynamic working concentration range that covers the range of clinical importance for healthcare applications or the range an analyte occurs in nature for food quality and environmental monitoring applications.

Stability is also an important concept to be taken into consideration when designing a sensor, especially if the sensor is to be used for continuous measurements. When exposed to complex solutions, materials can adhere to the surface of the electrode over time, resulting in the decrease of the sensor response. Single use sensors largely circumvent this problem.

One final performance criterion is the response time for a sensor. In other words, a measurement should not take too long, which is typically in the range of 60 seconds or even less, depending on the construction of the sensor and the reaction kinetics.

Nevertheless the most important parameter in designing a biosensor is its production cost. A biosensor that is considerably expensive will not be a success story no matter

how sensitive, selective, reproducible, accurate and quick a measurement it provides is.

2.2 Structure and Function of transducers

2.2.1 Types of transduction

As briefly outlined in the previous chapter, transducers are quintessential in every biosensor format since they are responsible for converting a biological recognition event, into a quantifiable signal. There are a number of different modes of transduction used in biosensors. Electrochemical transduction is of prime interest in this report, and that is why these transducers are examined in more detail. The fundamental principles of electrochemistry governing electrochemical transduction are also presented in the following chapter. In the list that follows, other types of transduction are briefly mentioned.

- ***Thermometric/ Calorimetric transduction***

Since most biological reactions are exothermic, the released energy in the form of heat (25-200kJ/mol) can be exploited to quantify and specify the reaction that has taken place by heat sensitive devices (Palmer, 1991). Mosbach *et al*, were the first to describe a thermal enzyme probe, which consisted of an enzyme bound to a temperature transducer. The latter, however, suffered from low sensitivity and for this reason Mosbach and Danielsson, introduced the enzyme thermistor, which provided more reliable and therefore accurate readings by the use of enzymes immobilised on the surface of columns (Mosbach, 1974). By these calorimetric based sensors, analytes such as uric acid, oxalic acid and glucose have been quantified in samples.

- ***Piezoelectric transduction***

Sensors of this type are gravimetric in operation, i.e. they detect changes in the mass of materials absorbed onto the surface of oscillating piezoelectric crystals by measuring the shift in the resonant frequency (Turner *et al.,* 1987). They are much more sensitive than calorimetric sensors and although to date most of their applications focus on the detection of volatile species, they could be used for

antibody/antigen immunoreactions (Vagdama and Crump, 1992) - or for the sequence selective detection of DNA (Zhai *et al.,* 1997).

• ***Optical transduction***

These biosensors operate on the principle of monitoring optical properties, such as bio or chemiluminsescence, reflectance, absorbance and are also known as optrodes (Turner *et al.,* 1987). The recognition of change in the properties of light of a system can be either a direct consequence of the reaction or an indirect effect on pH sensitive dyes, for example, which, in this case recognise changes in the pH. The latter are called indicator sensors and are able to detect non-optical active properties such as changes in O_2 or H_2O_2 levels indirectly (Seitz, 1984; Prencipe *et al.,* 1987). Recent advances in the technology of optical fibres have led to the development of evanescent wave technology and surface plasmon resonance techniques (Michelsen, 1996).

2.2.2 Types of electrochemical transduction

Electrochemical transducers function by detecting a target molecule or ion redox mechanism occurring on the surface of the working electrode of the circuit. These transducers can be potentiometric, amperometric or conductimetric.

• ***Potentiometric transduction***

This type of transducer relates the zero-current potential (relative to a reference) developed at a selective membrane or electrode surface in contact with a sample solution to the concentration of the analyte. The best known potentiometric sensors are the ion selective electrodes or ISEs. ISEs are devices that develop an electrical potential proportional to the logarithm of the activity of an ion in solution (Eggins, 1997). ISFETs (ion-sensitive field-effect transistors), a subtype of ChemFET devices (chemical field-effect transistor), act in a similar way to ISEs in that they detect ions in electrolytes. The most common example of an ISE, is the pH electrode first described by Cremer and later developed by Haber and Klememsiewicks (Turner *et al.,* 1987). In the original pH electrode, which was essentially a thin bulb of glass,

migration of hydrogen ions through the thin glass wall allowed for a potential difference across the glass membrane. Nowadays, sensor membranes do not need to be made of glass. Solid-state electrodes and liquid exchange electrodes used as ISEs are employed to detect a wide range of ions such as Na^+, K^+, Mg^{2+}, Ca^{2+}, Br^-, Cl^- and Cn^-.

The first potentiometric enzyme electrode or biosensor was produced in 1969 by Guilbault and Montalvo (Guilbault and Montalvo, 1969). By coupling an ion-selective electrode with the enzyme urease, the determination of urea in a sample was possible. Further applications of potentiometric biosensors to date include sensors measuring glucose (Guilbault and Hrabankova, 1970), amino acids (Naggy *et al.*, 1973) and penicillin (Nilsson *et al.*, 1973).

• ***Conductimetric transduction***

Conductimetric transducers are based on enzyme modulated changes in conductivity within a polymer. Measurements involve the determination of the impedance or resistance between two electrodes. Therefore, the same redox-modulated impedance changes within polymer films that are used to coat and thereby modify an electrode surface, can be used as a transduction approach. Watson *et al.* were amongst the first to report a conductimetric based enzyme electrode (Watson *et al.*, 1987). The products, for example, generated by glucose oxidase, such as H_2O_2 (Hall, 1990), gluconolactone (Skinner and Hall, 1997) or even a direct electron transfer between the enzyme and the polymer (Newman and Turner, 1994), can result in a decrease in conductivity that can be monitored. Other enzymes are known to result in an increase to the conductivity within a polymer (Soto *et al*., 2001).

• ***Amperometric transduction***

Amperometric sensors are based on heterogeneous electron transfer reactions. They monitor, in other words, current related to the oxidation and/or reduction of an electroactive species at the surface of a working electrode since the resistance of the electrolyte is low. It is common practice, to polarise the working electrode at a suitable potential relative to the reference electrode so that the rate of the whole process can be controlled by mass transport (Reitnauer, 1972). The fact that

amperometric sensors are able to detect concentrations of analyte in the range of 10^{-8} to 10^{-9}M has resulted in their wide exploitation for measurements in biological media and hence they present the most highly developed and studied sensors (Turner, 1989). By coupling an amperometric sensor to an enzyme, one gets the additional advantage of the high specificity and selectivity offered by the enzyme. The catalytic reaction occurring at the surface of a working electrode, when an enzyme is in the presence of its substrate, gives rise to a current proportional to the concentration of the species produced or consumed. Based, on this simple observation, Clark proposed the first amperometric enzyme electrode, based upon the oxygen electrode (Clark, 1962).

2.3 Electrochemistry

As mentioned in the previous chapter, the type of transduction used in the immunosensors fabricated in this PhD programme is electrochemical. For this reason, the fundamental principles of electrochemistry will be discussed in the following chapters. The phenomena observed throughout this PhD programme can be described using the theory behind dynamic electrochemistry.

Dynamic electrochemistry allows for a detailed investigation into the rates, mechanisms of reactions and fundamental factors involved in an electrochemical process and therefore represents a powerful tool by which electron transfer reactions between electrodes and reactant molecules can be analysed (Fisher, 1996). The dynamics of such a reaction are affected by a number of different factors, such as the potential, the nature and/or the structure of the electrode surface, as well as the reactivity of the solution species and its mass transport. All these can and do alter the rate at which a charge transfer process progresses, and therefore change the dynamics of the reaction. For this reason, they will be analysed in the following chapters, after taking a closer look at the processes occurring at the metal solution interface.

If a metallic electrode (*m*) is placed into a source of electrodes, i.e. reactant molecules in a solution (*aq*), a transfer of electrons and hence of charge will take place across the electrode/solution interface. The following example illustrates this:

$$Fe^{3+}(aq) + e^{-}(m) \leftrightarrow Fe^{2+}(aq) \qquad \textit{Eqn 2.4}$$

Gradually, this reaction reaches equilibrium and thus the transfer of electrons across the electrode/solution interface produces a net charge separation between the two phases, ultimately creating a potential difference (Fisher, 1996).

Therefore, the potential drop across the electrode/solution interface $\Delta\varphi_{m/s}$, is given by:

$$\Delta\varphi_{m/s} = \varphi_m - \varphi_s \qquad \textit{Eqn 2.5}$$

where φ_m is the metal potential and φ_s is the solution potential.

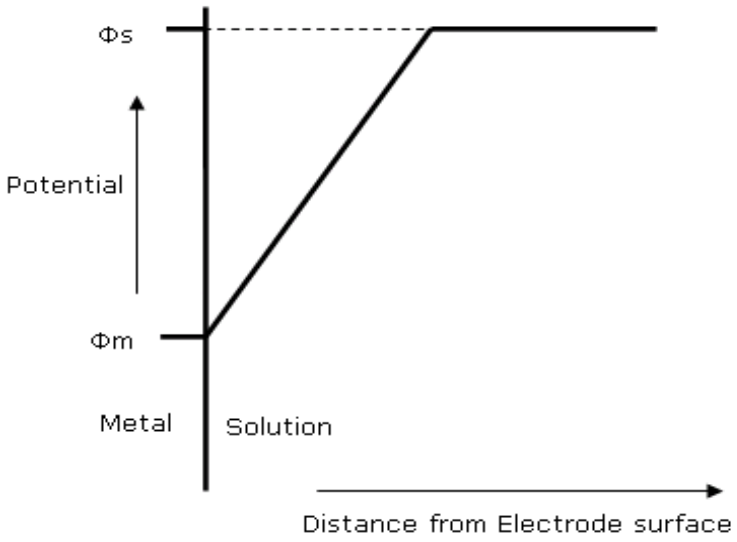

Fig 2.4 Potential drop across the metal/solution interface.

2.3.1 The Electrical Double Layer

The charge separation that results in the potential difference between the two phases can be thought to be analogous to the accumulation of charge across the plates of a parallel plate capacitor.

By the application of a polarising potential, the charge at the surface of the electrode can be controlled, giving rise to electrostatic interactions between the electrode and the electrolyte solution.

A segregation of positive and negative charged species is observed, caused by the discontinuity at the interface and consequent disruption of the behaviour of the

electrolyte in bulk solution. This charge distribution is known as the electrical double layer and several models have been developed to establish the nature of the procedure.

The earliest and simplest model describing an electrical double layer was proposed by *Helmholtz* in 1879. According to this early model, excess charges on the metal electrode are neutralised by a monolayer of ions of opposite charge in the solution. This redistribution of charges due to electrostatic forces or reorientation of dipoles in solvent molecules achieves electrical neutrality on the surface.

$$q_m = - q_s$$

where q_m is the charge density on the metal surface and $- q_s$ is the charge density of the monomolecular layer of solution adjacent to the metal surface.

Helmholtz assumed that there exists a monolayer of solvation between the ions in the solution and the electrode and so ions attracted to the electrode are only able to approach the interface to a distance limited by the solvation shell of that ion. Thus the potential drop, created by the redistribution of ions, is linear and occurs only across the region between the electrode surface and the edge of this monolayer, which is known as the Outer Helmholtz Plane (OHP).

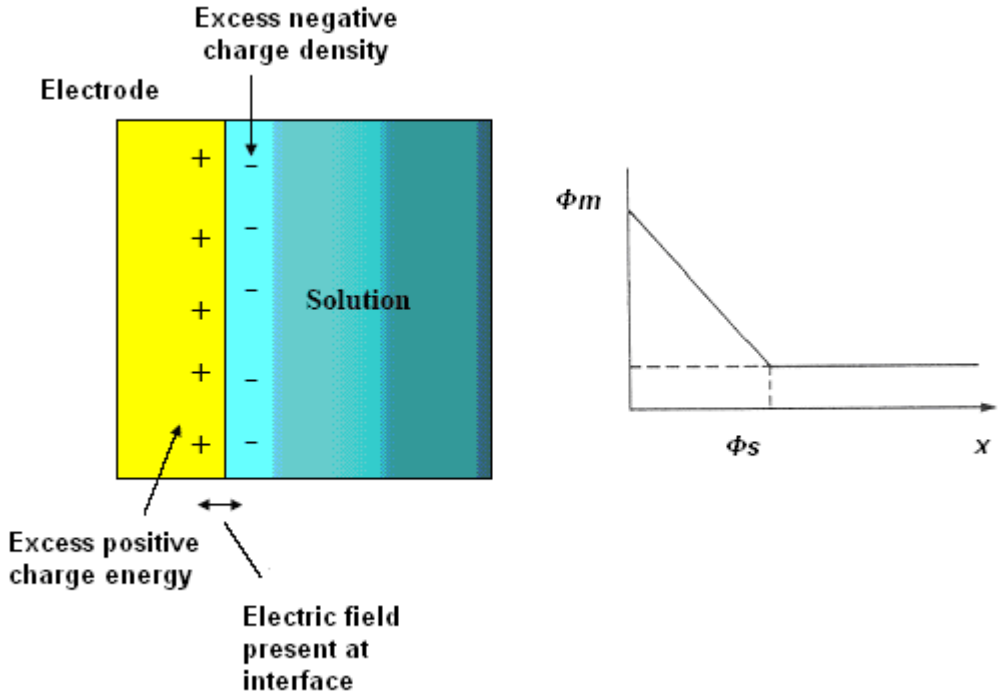

a. ***b.***

Fig 2.5 The Helmholtz model of the electrical double layer a) arrangement of ions, b) variation of the electrostatic potential with distance from the electrode.

Gouy and Chapman, working independently in 1910 expanded the original two layer concept proposed by Helmholtz by allowing for the Brownian motion of ions. Since ions in a solution are free to circulate and are subject to thermal motion, the excess charges within an electrolyte solution are not exclusive to the OHP. Consequently, the electrostatic attraction between an ion and the metal surface is somewhat counteracted, and charge is dispersed into a diffuse layer, resulting in a gradually decreasing concentration of the latter until reaching the homogeneous distribution of ions that exists in bulk electrolyte. The potential drop therefore is mainly concentrated in the close vicinity of the electrode surface but not exclusively contained in the OHP. A new model, postulated in 1924 by Stern essentially brings together the two previous descriptions of the double layer. The significant advancement is the fact that the *Gouy-Chapman-Stern* model takes into account the finite size of solvated ions and furthermore the fact that such ions will be surrounded by ionised water molecules. Therefore, ions cannot near the electrode surface beyond a plane of closest approach giving rise to a sharp potential drop between the electrode surface and the OHP, when compared to the gradual one proposed by Gouy and Chapman.

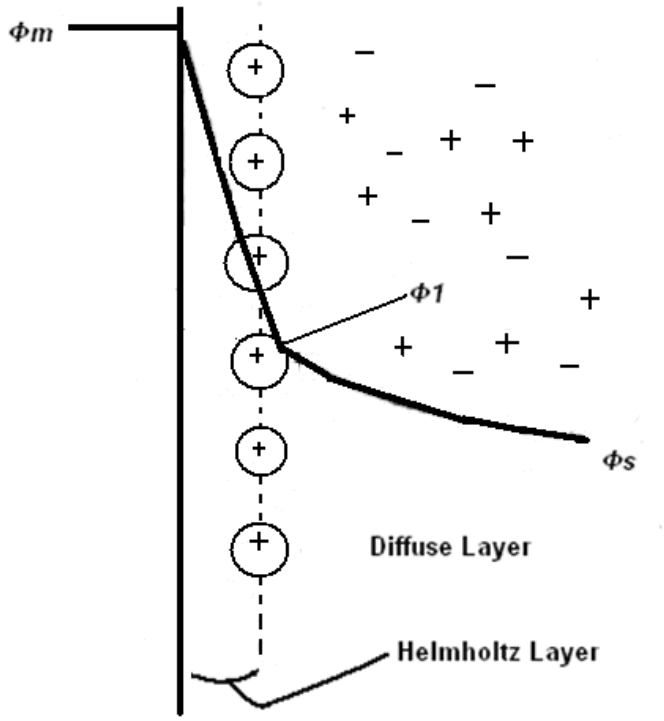

Fig 2.6 Schematic showing the Gouy-Chapman-Stern model of the electrical double layer and the potential drop across the electrode/surface area.

In 1947, *Grahame* extended Stern's model by suggesting that two planes of approach are required to fully describe the electrical double layer phenomenon. In this model, a non solvated ion or an ion that has lost its solvation shell can be found closer to the electrode surface than a solvated ion. Hence, ions that are directly in contact with the electrode are said to be specifically adsorbed, forming an Inner Helmholtz Plane (IHP). On the other hand, ions that are solvated are non-specifically adsorbed and occupy the OHP region.

Finally, in 1963 *Bochris, Devanathan and Muller* proposed a model that took into consideration the presence of solvent, namely water, at the interface of the solution with the metal electrode. The dipoles of these water molecules have a fixed alignment due to their close proximity to the electrode surface, whilst in the following layers of water the dipoles will not be as fixed. This model is nowadays considered to describe the electrical double layer at the electrode surface.

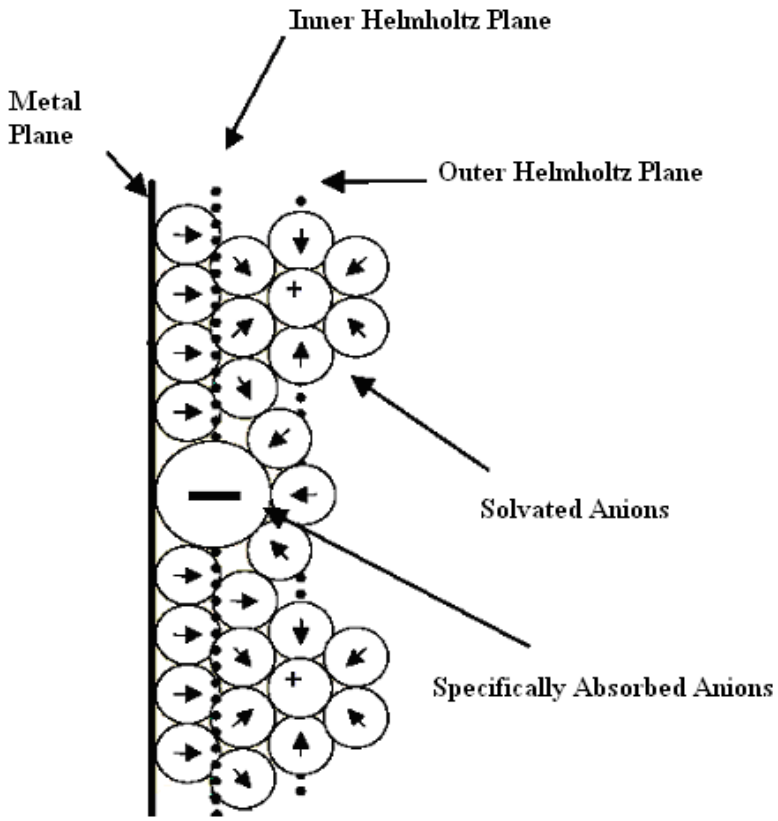

Fig 2.7 Schematic showing the BDM model of the electrical double layer and the potential drop across the electrode/surface area).

2.3.2 Equilibrium electrochemistry theory

The measurement of the potential drop produced by a redox reaction such as the one shown in Eqn 2.4 across the metal/solution interface requires a complete electrical circuit. For this reason, a reference electrode is introduced to the system. The latter maintains a constant potential drop, so in other words it is completely non-polarisable and hence has stable electrical double layer properties (Higson, 2004). Examples of commonly used reference electrodes for electrochemical reactions include the silver/silver chloride (Ag/AgCl) electrode and the saturated calomel electrode (SCE).

• The Standard Hydrogen Electrode (SHE)

This was the first reference electrode to be reported. It is based on the following redox half cell:

$$2H^+(aq) + 2e^- \leftrightarrow H_2(g) \qquad \textit{Eqn 2.6}$$

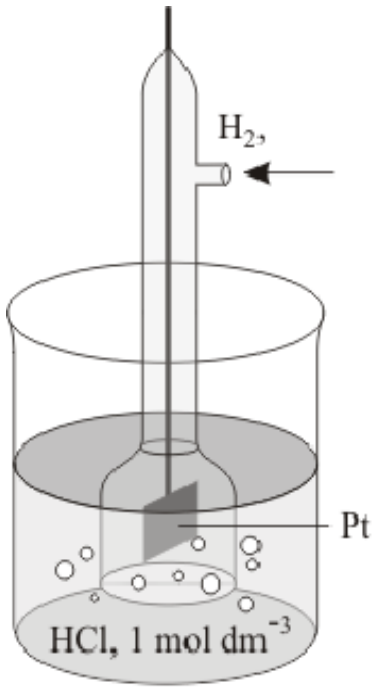

Fig 2.8 The scheme of the standard hydrogen electrode.

Its potential is arbitrarily declared to be zero. The potential of any electrode at standard conditions (temperature 298K, solutes at 1M and gases at 1 atm), is known as its standard electrode potential, $E^{Ø}$.

• The silver/silver chloride (Ag/AgCl) electrode

The silver-silver chloride electrode is the most common reference electrode used for electrochemical reactions due to its ease of manufacture and its superior temperature range. The electrode is a silver wire that is coated with a thin layer of silver chloride either by electroplating or by dipping the wire in molten silver chloride. When the electrode is placed in a saturated potassium chloride solution it develops a potential of 199 mV with respect to the standard hydrogen electrode. Commercially available silver-silver chloride electrodes generally consist of a cylindrical glass tube containing a 4 Molar solution of KCl saturated with AgCl.

The lower end is sealed with a porous ceramic frit which allows the slow passage of the internal filling solution and forms the liquid junction with the external test solution. A silver wire coated with a layer of silver chloride (it is chloridised), is immersed in the filling solution and is joined to a low-noise cable which connects to the measuring system. The silver-silver chloride is the reference electrode of choice in this project since all of the supporting electrolytes in the buffers used where chloride based.

Considering once again the reaction shown in Eqn 2.4, the general charge transfer reaction is the following:

$$O\ (aq) + ne^{-}(m) \leftrightarrow R\ (aq) \qquad \textit{Eqn 2.7}$$

where n represents the number of electrons transferred, and O and R, the reactant species.

Energy is the driving force for all chemical reactions and the energies of the oxidation and reduction half cells shown in general charge transfer reaction above (Eqn 2.7) are related to the electrochemical potentials that develop. The Gibbs free energy change for this equation, therefore, can be given by:

$$\Delta G = \Delta G^{0} + RT\ln\frac{[O]}{[R]} \qquad \textit{Eqn 2.8}$$

Where ΔG^{0} is the Gibbs free energy at standard conditions. However it is known that

$$\Delta G = -\, n\, F\, \Delta E \qquad \textit{Eqn 2.9}$$

Where F stands for the Faraday's constant, equal to 96485 C which is the electric charge carried by one mole of electrons and ΔE the electrical potential of the reaction.

Therefore under equilibrium conditions the potential established will be given by the following equation:

$$E = E^{Ø} - \frac{RT}{nF} \ln \frac{[O]}{[R]} \qquad \text{Eqn 2.10}$$

Where:

- R is the universal gas constant, equal to $8.314510\ J\ K^{-1}\ mol^{-1}$
- T is the temperature in degrees Kelvin
- F is the Faraday constant
- n is the number of electrons transferred in the reaction
- [O] is the concentration of the oxidised species
- [R] is the concentration of the reduced species

It is important to stress the fact that the equation assumes that the system is at equilibrium and therefore no net current flows between the bulk solution and the metal. A reaction of this type is called reversible or Nernstian, after the German physical chemist Walther Nernst who first formulated it. The Nernst equation links the actual reversible potential of an electrode, E, to the standard reversible potential of the electrode couple, $E^{Ø}$ which is a thermodynamic value. It accounts therefore for conditions that alter the standard electrode potential such as the temperature and the concentration of the reactant species.

2.3.3 Electrochemistry dynamics

The equilibrium established when the concentrations of reactants and products are constant results in a net current flow equal to zero. However it is a dynamic equilibrium and not a static one, meaning that both the oxidation and reduction reactions shown below will occur at equal rates.

$$O(aq) + ne^{-}(m) \rightarrow R\ (aq) \qquad \textit{Eqn 2.11}$$

$$R\ (aq) \rightarrow O(aq) - ne^{-}(m) \qquad \textit{Eqn 2.12}$$

The current (i) involved in driving the redox reactions (Eqn 2.12 and 2.13) is given by:

$$i_c = - FAk_{red}[O]_o \qquad \textit{Eqn 2.13}$$

$$i_a = FAk_{ox}[R]_o \qquad \textit{Eqn 2.14}$$

where A is the electrode surface, $[O]_o$ and $[R]_o$, are the surface concentrations of the reactants and $k_{red,}$ $k_{ox,}$ the rate constants for the electron transfer. The net current flow for the reaction is:

$$i = i_a + i_c \qquad \textit{Eqn 2.15}$$

So at the dynamic equilibrium $i = i_a + i_c = 0$ and hence:

$$i_o = i_a = - i_c$$

where i_o is the exchange current density at equilibrium.

If an external voltage is applied to the electrode then the system will no longer be in dynamic equilibrium.

The surface concentrations of O and R will adjust to fit the Nernstian equation and this will ultimately result in current flow. The observed electrolytic current will be dependent on either rate-determining kinetics or rate determining mass transport (Eqns 2.13 & 2.14), both of which are controlled by the potential of the electrode.

2.3.3.1 Electrode Kinetics

The current flowing in either the reductive or oxidative steps can be predicted using the equations 2.13 and 2.14. To establish how the rate constants k_{Ox} and k_{Red} are influenced by the applied voltage the transition state theory will be employed. In this theory the reaction is considered to proceed via an energy barrier and the summit of this barrier is referred to as the transition state. In order to overcome this barrier energy is required. The activation free energy, ΔG^*, for the reduction and oxidation reactions are:

$$\Delta G^*_{red} = G^* - G^O \qquad \textit{Eqn 2.16}$$

$$\Delta G^{*}_{ox} = G^{*} - G^{R} \qquad \textit{Eqn 2.17}$$

And therefore the corresponding reaction rates are given by:

$$k_{red} = Z\exp\left(\frac{-\Delta G^{*}_{red}}{RT}\right) \qquad \textit{Eqn 2.18}$$

$$k_{ox} = Z\exp\left(\frac{-\Delta G^{*}_{ox}}{RT}\right) \qquad \textit{Eqn 2.19}$$

where Z is the frequency of the rate of collision of the electroactive molecule with the electrode surface.

By plotting a series of these free energy profiles as a function of voltage it is apparent that the plots alter as a function of the voltage. The activation energy can be seen to alter as a function of the applied voltage and therefore the rate constants for the forward and reverse reactions are altered too. By simplifying the model one can assume that the effect of voltage on the free energy change will follow a linear relationship. By using this linear relationship the activation free energies for reduction and oxidation will vary as a function of the applied voltage (E) as follows:

$$\Delta G^{*}_{red} = \Delta G^{*}_{red\ \text{no voltage}} + \alpha F(E-E_{eq}) \qquad \textit{Eqn 2.20}$$

$$\Delta G^{*}_{ox} = \Delta G^{*}_{ox\ \text{no voltage}} - (1-\alpha)F(E-E_{eq}) \qquad \textit{Eqn 2.21}$$

The deviation of the applied E from the equilibrium potential is described as the overpotential, η:

$$\eta = E-E_{eq}$$

The parameter α is called the transfer coefficient and typically is found to have a value of 0.5. Physically it provides an insight into the way the transition state is influenced by the voltage. A value of one half means that the transition state behaves mid way between the reactants and products response to applied voltage, whereas a value of zero signifies the fact that the transition state shows no potential dependence.

Substituting the activation free energy terms in Eqn2.16 and 2.17 into the expressions for the oxidation and reduction constants in Eqn2.18 and 2.19, leads to:

$$k_{red} = \mathrm{Z}\exp\left\{\left(\frac{-\Delta G_{RED}^{no_{voltage}}}{RT}\right)\left(\frac{-\alpha F\eta}{RT}\right)\right\} \qquad \textit{Eqn 2.22}$$

$$k_{ox} = \mathrm{Z}\exp\left\{\left(\frac{-\Delta G_{OX}^{no_{voltage}}}{RT}\right)\left(\frac{(1-\alpha F\eta}{RT}\right)\right\} \qquad \textit{Eqn 2.23}$$

According to the results, the rate constants for the electron transfer redox reactions are proportional to the exponential of the applied voltage. So the rate at which the redox reactions occur can be changed simply by varying the applied voltage. This provides the fundamental basis of the experimental technique called voltammetry.

2.3.3.2 Mass transport

Having examined the way the electrode voltage can affect the rate of the electron transfer, one could anticipate that as the voltage is increased the reaction rate and therefore the current will increase exponentially. This would mean that it is possible to pass unlimited quantities of current. In reality this is not the case and the rate of transport of the reactant species to the surface of an electrode from the bulk solution also affects the overall reaction rate, since reactions occur in a localised region at, or close to, the surface of the electrode (Eqn2.13, 2.14). There are three forms of mass transport which can influence an electrolysis reaction: diffusion, convection, migration.

• Diffusion

Diffusion occurs in all solutions and arises from local uneven concentrations of reagents, such as those produced in an electrochemical system where there is a consumption of a reagent at the electrode surface. Entropic forces act to smooth out these uneven distributions of concentration, by the transport of the reactant species

down a concentration gradient, and are therefore the main driving force for this process (Cooper and Cass, 2004).

• Convection

Convection results from the action of a mechanical force on the solution. This can be a pump, a flow of gas, heat or even gravity. There are two forms of convection: the first is termed natural convection and is present in any solution. This natural convection is generated by small thermal or density differences and acts to mix the solution in a random and therefore unpredictable manner. In the case of electrochemical measurements these effects tend to cause problems if the measurement time for the experiment exceeds 20 seconds. It is possible to swamp the natural convection effects from an electrochemical experiment by deliberately introducing convection into the cell. This form of convection is termed forced convection. It is typically several orders of magnitude greater than any natural convection effects and therefore effectively removes the random aspect from the experimental measurements, as it is well defined and can be quantitatively determined. The use of a magnetic stirrer or stirring rod does not produce calculable and reproducible mass transport conditions; however methods such as the rotating-disk, wall-jet or channel flow geometries produce a calculable forced convection (Cooper and Cass, 2004).

• Migration

This is essentially an electrostatic effect which arises due the application of a potential on the electrodes. This effectively creates a charged interface. Any charged species near this interface will either be attracted or repelled from it by electrostatic forces. Due to ion solvation effects and diffuse layer interactions in solution, migration is notoriously difficult to calculate accurately for real solutions. Consequently most voltammetric measurements are performed in solutions which contain a background electrolyte (e.g. KCl) that does not undergo electrolysis itself but helps to shield the reactants from migratory effects. By adding a large quantity of the electrolyte it is possible to ensure that the electrolysis reaction is not significantly effected by migration. The purpose of introducing a background electrolyte into a solution is not

however solely to remove migration effects since it also acts as a conductor to help the passage of current through the solution (Cooper and Cass, 2004).

2.3.3.3 Effect of potential on current flow

To gain a quantitative model of the current flowing at the electrode, the electrode kinetics and the mass transport phenomena of all the species involved must be taken into account. As mentioned before, both of the above are influenced by the applied voltage and most electrochemical systems with high conductivity electrolytes display current versus potential curves that look like the plot below.

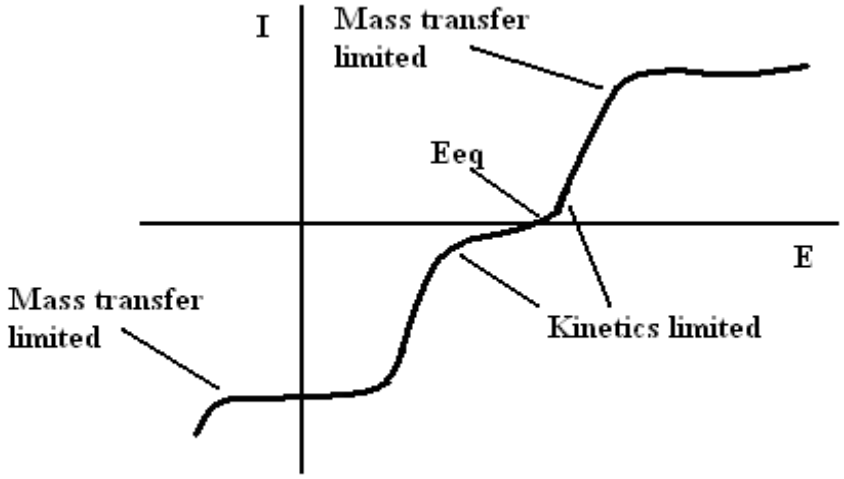

Fig 2.9 Schematic of typical current vs. potential behaviour for an electro chemical system with high conductivity electrolyte.

If the electrode potential is set more anodic than the equilibrium value, from Eqn 2.8, E-$E^{\emptyset}$ will be a positive number and hence $\ln \frac{[O]}{[R]}$ will be negative and therefore a net oxidation will occur on the electrode.

Conversely, if the electrode is set negative of the equilibrium potential, then a reduction reaction will occur on the electrode.

Eqn 2.15 gives the net current flow. By substituting Eqn 2.13 and Eqn 2.14 in Eqn2.15, the following expression of the current flow is derived.

$$i = FA(k_{ox}[R]_o - F\alpha k_{red}[O]_o) \qquad \textit{Eqn 2.24}$$

Also by simplifying Eqn 2.22 and 2.23, by introducing k^o_{red} and k^o_{ox} , called standard heterogeneous rate constants, which are independent of the overpotential, η, the following expressions for the rate constants for the oxidation and reduction half cell reactions can be obtained.

$$k_{red} = k^o_{red} \exp\left(\frac{-\alpha F\eta}{RT}\right) \qquad \textit{Eqn 2.25}$$

$$k_{ox} = k^o_{ox} \exp\left(\frac{(1-\alpha)F\eta}{RT}\right) \qquad \textit{Eqn 2.26}$$

By substituting Eqn 2.25 and 2.26 into Eqn 2.24, and also taking into consideration that $i_o = FAk^o[R]^{\alpha}_{bulk}[O]^{1-\alpha}_{bulk}$ the relationship for the net current flowing at the working electrode is

$$i = i_o\left(\frac{[R]_o}{[R]_{bulk}}\exp\left\{\frac{(1-\alpha)F\eta}{RT}\right\} - \frac{[O]_o}{[O]_{bulk}}\exp\left\{\frac{-\alpha F\eta}{RT}\right\}\right) \qquad \textit{Eqn 2.27}$$

Eqn 2.28 predicts how the observed current varies as a function of the overpotential and transfer coefficient as well as the exchange current density. If the solution under investigation is sufficiently stirred then the surface concentrations of the reactants will be equal to their bulk values. Under these conditions Eqn 2.28 simplifies to:

$$i = i_o\left(\exp\left\{\frac{(1-\alpha)F\eta}{RT}\right\} - \exp\left\{\frac{-\alpha F\eta}{RT}\right\}\right) \qquad \textit{Eqn 2.28}$$

known as Butler-Volmer equation.

As expected, no current flows when $\eta = 0$. The imposition of small overpotentials results in two limiting cases corresponding to large or small values of i_o. When i_o is

large (a) little or no applied overpotential is required to drive the reaction and current flows readily in both directions (anodic and cathodic), according to the sign of the overpotential applied, as analysed previously. Essentially there is little or no activation barrier to either of the electrolysis reactions. For this case the electrode reaction is said to be reversible. The opposite is true for small values of i_o (b). Large overpotentials need to be applied and hence the reaction is termed irreversible.

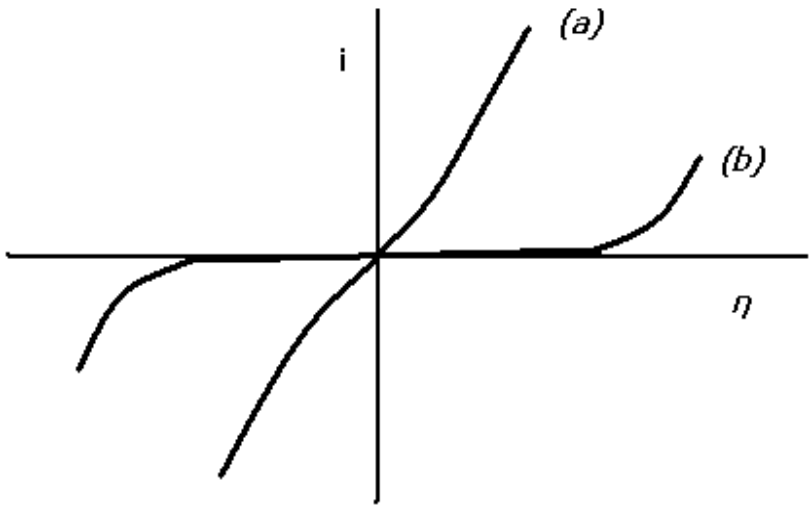

Fig 2.10 The variation of current as a function of overpotential for (a) a reversible and (b) an irreversible electrode reaction.

Therefore, at modest deviations away from equilibrium the current is determined by the charge transfer kinetics at the electrode and the current flow can be determined by Eqn2.28.

At large deviations from equilibrium, the rate that reactant is transported by convection and diffusion often limits the current, since ionic migration is negligible due to the high conductivity of the electrolyte introduced. Furthermore one of the terms in equation 2.29 will be negligible compared with the other. At large positive overpotentials, $i_a >> i_c$, negligible oxidation current flows and Eqn2.29 will become:

$$i = i_o \exp\left(\frac{(1-\alpha)F\eta}{RT}\right) \qquad \textit{Eqn 2.29}$$

and hence:

$$\ln i = \ln i_o + \frac{(1-\alpha)F}{RT}\eta \qquad \textit{Eqn 2.30}$$

At large negative overpotentials, $i_c >> i_a$, negligible reductive current flows and Eqn 2.28 will become:

$$\ln(-i) = \ln i_o - \frac{\alpha F}{RT}\eta \qquad \textit{Eqn 2.31}$$

This logarithmic current-potential dependence was derived by Tafel, and hence they are known as Tafel equations (Eqn 2.30 and 2.31). Such plots are only linear at high values of overpotentials; severe deviations from linearity are observed as η approaches zero. Extrapolation of the linear portion of these plots to the zero overpotential gives an intercept which corresponds to $\ln i_o$; the value of the transfer coefficient can be obtained using the slope.

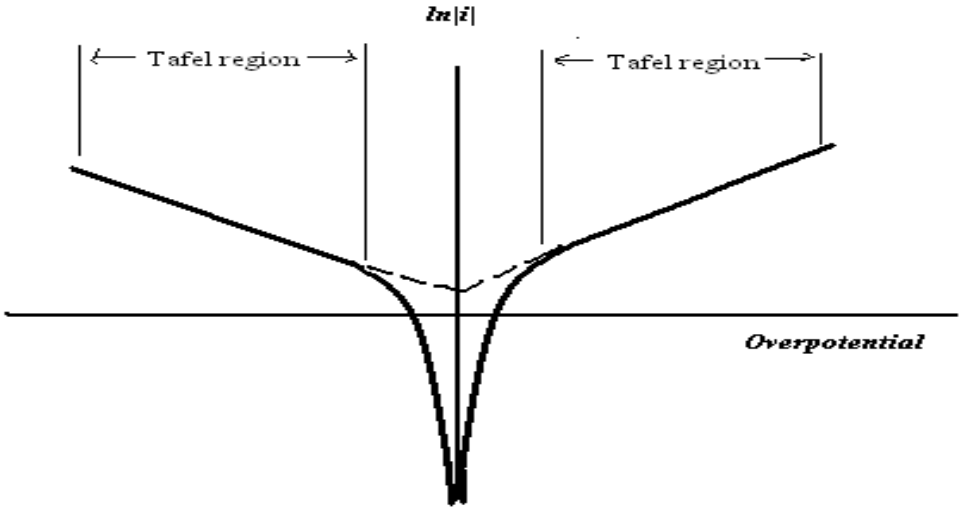

Fig 2.11 Tafel analysis.

2.3.4 Voltammetry

Voltammetry involves the study of current-voltage relationships at a polarized working electrode within an electrochemical cell and can provide remarkably detailed information about the mechanism of the reaction of interest. The concepts introduced in the previous chapters provide the basis for the rationalisation of such voltammetric experiments. Working electrodes may be potentiostatically polarised using pulsed,

linear waveforms. Pulsed voltammetric techniques introduced by Baker and Jenkin (Barker and Jenkin, 1952), involve the polarisation of the working electrode from a potential E_1 to a potential E_2 instantaneously. On the other hand, in linear sweep voltammetry, the polarisation potential is applied at a constant potential sweep rate, v, from a potential E_1 to a potential E_2 as previously. Cyclic voltammetry, being an extension of linear sweep voltammetry, involves first sweeping the potential from E_1 to E_2, before scanning in reverse from E_2 back to E_1. A very large number of electrochemical analyses, such as adsorptive stripping voltammetry and polarography, are based upon linear sweep or cyclic voltammetry. However there are techniques, such as flow analysis, that are based on the principle of maintaining the potential fixed and hence they are amperometric, in contrast with voltammetric techniques which are potentiometric.

The potential difference, E, measured between a working electrode and a reference electrode will be the sum of potential drops at the working electrode/solution interface ($\varphi_m - \varphi_s$) and reference electrode/solution interface ($\varphi_s - \varphi_{ref}$), given by:

$$E = (\varphi_m - \varphi_s) + iR + (\varphi_s - \varphi_{ref}) \qquad \textit{Eqn 2.32}$$

The term iR describes the voltage drop in the solution due to passage of current between two electrodes. R is the electrical resistance of the intervening solution.

For microelectode experiments the term iR can be neglected and since ($\varphi_s - \varphi_{ref}$) is fixed, Eqn 2.33 simply reduces to:

$$E = (\varphi_m - \varphi_s) + \text{constant} \qquad \textit{Eqn 2.33}$$

Consequently, changes in the applied potential are directly reflected in the driving force for the reaction, ($\varphi_m - \varphi_s$), and voltammetry is meaningful with two electrodes. With large electrodes, though, iR is no longer negligible, since the current flowing through the cell will also be induced to change. Moreover, the passage of large currents through the reference electrode can change its chemical composition and so the term ($\varphi_s - \varphi_{ref}$), may no longer be constant. To circumvent the problem, a third electrode is introduced, namely a counter or auxiliary electrode.

2.3.4.1 Cyclic Voltammetry

Cyclic voltammetry is the most widely used technique for acquiring qualitative information about electrochemical reactions. The power of cyclic voltammetry results from its ability to rapidly provide considerable information on the thermodynamics of redox processes, on the kinetics of heterogeneous electron-transfer reactions, and on coupled chemical reactions or adsorption processes.

Cyclic voltammetry is often the first experimental approach performed in an electroanalytical study, since it offers rapid location of redox potentials of the electroactive species and convenient evaluation of the effect of media upon the redox process. For these reasons, it is the voltammetric technique of choice in this project.

Cyclic voltammetry consists of scanning linearly the potential of a stationary working electrode using a triangular potential waveform, shown below:

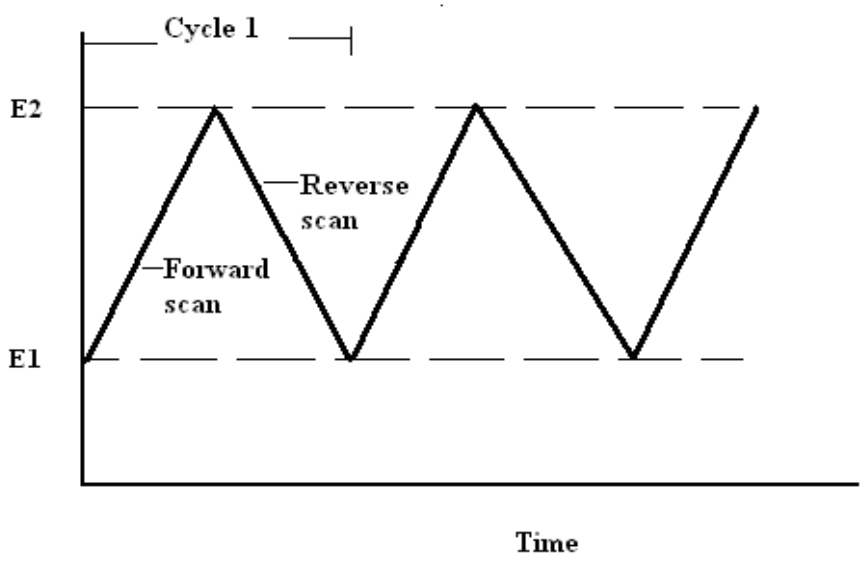

Fig 2.12 Variation of the applied potential as a function of time in a cyclic voltammetry experiment.

Depending on the information sought, single or multiple cycles can be performed. The resulting plot of current versus potential is termed cyclic voltammogram. The following voltammogram illustrates the expected response for a reversible redox

couple during a single potential cycle, assuming that the solution contains only a single electrochemical reactant.

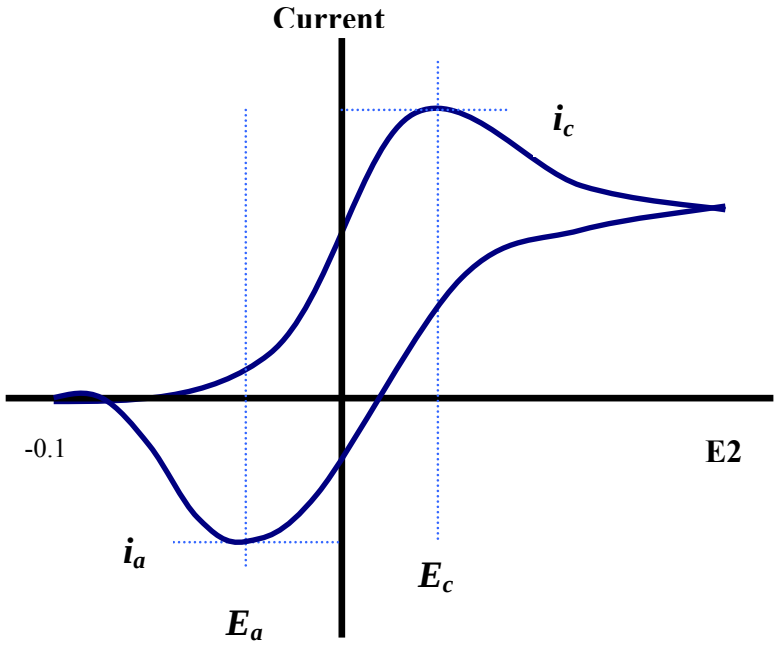

Fig 2.13 Typical cyclic voltammogram.

As the potential is swept in the cathodic direction, species O (Eqn 2.5) is reduced to form increasing amounts of species R, until a reduction peak is reached (Ec). Following this peak, the large quantity of species R present surrounding the electrode creates a diffusion layer and the flux of species O towards the electrode is no longer enough to satisfy an equilibrium situation, as described by the Nernstian equation, resulting in a steady decrease in current. Upon reaching E_2, species R that has been formed at the electrode during the forward scan begins to oxidise to species O. The current observed initially increases due to the availability of species R in the diffusion layer surrounding the electrode.

As the potential becomes more anodic, the rate of oxidation of O to R increases until all of species B present in the diffusion layer is reoxidised and the current gradually decreases. For such a reversible electrochemical reaction the cyclic voltamogram recorded has certain well defined characteristics.

1. The voltage separation between the current peaks is:

$$\Delta E = E_{p.a} - E_{p.c} = \frac{59}{n} \text{ mV} \qquad \textit{Eqn 2.34}$$

where n equals the number of electrons involved in the electrochemical reaction. Accordingly, a fast one-electron process exhibits a separation between the peaks of 59mV. The peak separation does not alter as a function of the scan rate. Thus the peak separation can be used to determine the number of electrons transferred, and as a criterion for a Nernstian behaviour.

2. The peak current is given by the Randles – Sevcik equation:

$$i_p = (2.69 \times 10^5)\, n^{3/2}\, \text{ACD}^{1/2}\, v^{1/2} \qquad \textit{Eqn 2.35}$$

where n is the number of electrons, A is the electrode area, C is the concentration, D is the diffusion coefficient and v is the scan rate (Wang, 2000). According to the equation the peak current is proportional to the square root of the scan rate. Higher scan rates result in higher magnitudes of current, while slower scan results have the opposite effect. Furthermore, the ratio of the anodic to cathodic, reverse to forward peak currents in other words, $i_{p,a}/i_{p,c}$ equals one.

For slow, irreversible processes the situation is quite different to the one pictured above. The applied voltage does not result in the generation of the concentrations at the electrode surface predicted by the Nernst equation, while the position of the current peaks shifts depending upon the rate constant of reduction and oxidation and also on voltage scan rate. The effect rate constants have on redox processes is shown below. As far as the effect of voltage scan rate has on the absolute magnitudes of the peak currents, the dependence is the same as that for a reversible redox process.

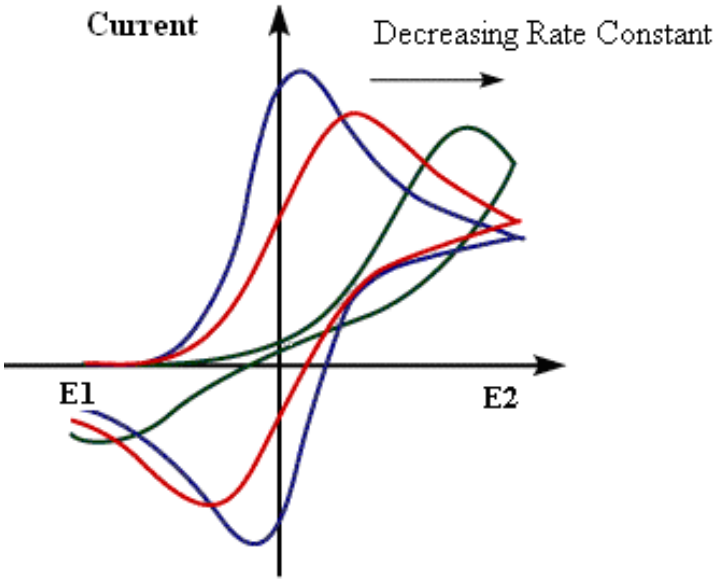

Fig 2.14 Cyclic voltammograms for reversible (blue), quasi-reversible (red) and irreversible (black) redox processes.

2.3.5 AC Impedance

The models discussed in the previous chapters have shown that the double layer is a region in which charges electrolyte ions can be accumulated or depleted in comparison with their bulk values. This in effect means that the interface is capable of storing charge and therefore acts like a capacitor. The integral capacitance of a simple parallel capacitor is defined as:

$$C = \frac{q}{E} \qquad \textit{Eqn 2.36}$$

where q is the quantity of charge stored on the capacitor plates when a potential difference E is applied across them. The capacitance of such a device is constant, independent of the potential applied since the separation of plates is fixed. For an electrochemical cell, though the situation is more complex, since the thickness of the double layer depends on the applied potential. This differential capacitance can be measured using alternating current impedance spectroscopy. This method employs the

excitation of an electrochemical cell by a sinusoidal signal and analysis of the currents produced to gain an insight into the properties of many electrochemical processes. Experimental measurements are performed using an oscillating sinusoidal potential:

$$E = \Delta E \sin \omega t \qquad \textit{Eqn 2.37}$$

where ω is the angular frequency ($= 2\pi f$, where f is the frequency in Hertz) and ΔE is the maximum amplitude.

The oscillating potential across the cell causes a current to flow given by:

$$i = \Delta i \sin(\omega t + \varphi) \qquad \textit{Eqn 2.38}$$

The current therefore will also be sinusoidal and of the same frequency, but different in amplitude and phase from the voltage. Both of them can be represented as rotating vectors, or phasors in the complex plane (Armand diagram) shown below.

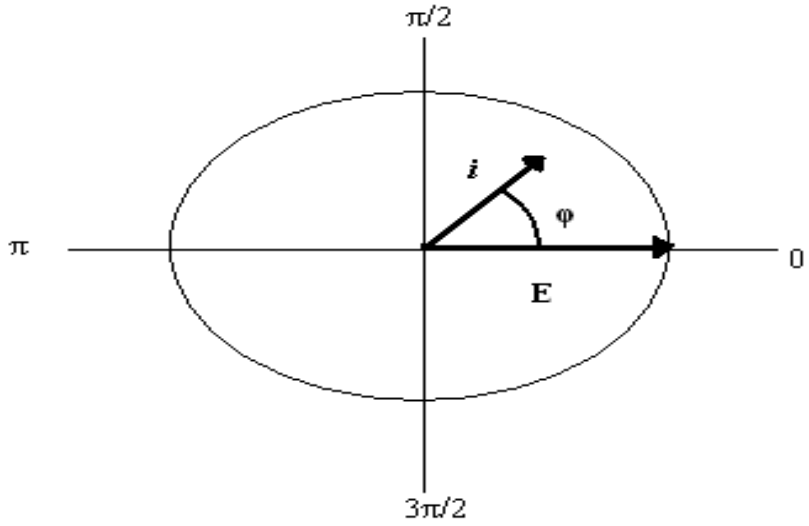

Fig 2.15 Phasor diagram showing current and voltage phasors separated by the phase angle φ.

By applying Ohm's Law, for a system with a simple resistance R, the relationship between the current and the applied potential is given by:

$$i = \frac{E}{R} \qquad \textit{Eqn 2.39}$$

and the phase angle is zero. For a capacitor a similar relationship can be derived from equations 2.36, 2.37.

$$i = \frac{\Delta E}{X_C} \sin(\omega t + \pi/2) \qquad \textit{Eqn 2.40}$$

R is replaced by *Xc* (capacitive reactance) and the phase angle is π/2. Eqn 2.40 can be written as

$$E = -jXci \qquad \textit{Eqn 2.41}$$

By introducing j ($=\sqrt{-1}$) that represents the sinusoidal response of the system in a complex plane. For a resistor and capacitor connected in series, the sum of the voltage drop across each element must sum to the total E, so $E = E_R + E_C = i\,(R - jXc)$ and therefore:

$$E = iZ \qquad \textit{Eqn 2.42}$$

where Z is the impedance.

It provides a measure of how the passage of current is impeded by the circuit and as such a generalisation of the idea of resistance of a circuit. The current will no longer be in phase or 90° out of phase with the voltage. The phase angle will be given by:

$$\tan\varphi = \frac{Xc}{R} = \frac{1}{\omega RC} \qquad \textit{Eqn 2.43}$$

The values R and $-jXc$ are also called the real and imaginary components, Z′and Z′′, respectively of the total impedance Z and are represented in the following Armand diagram.

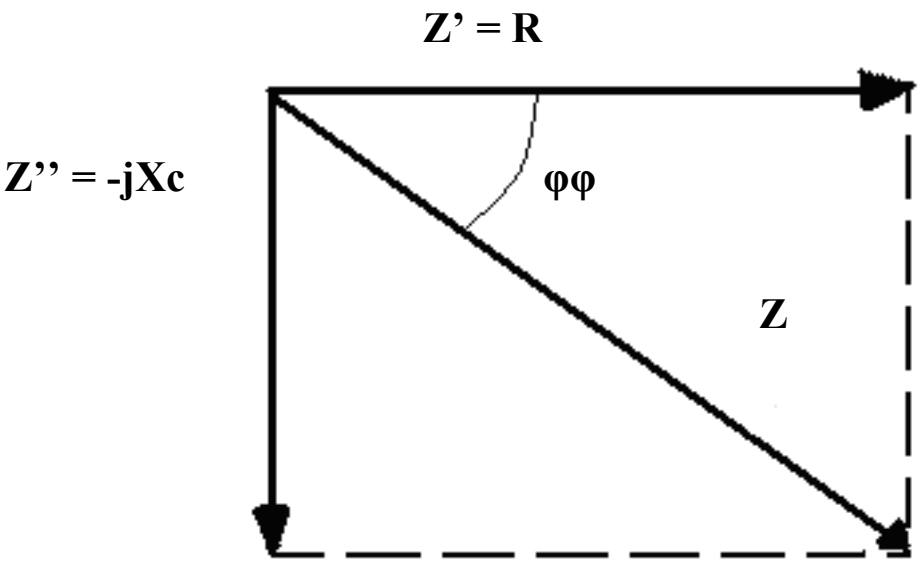

Fig 2.16 Armand diagram for a series resistor and capacitor, showing the total impedance in relation with the resistive and capacitive components of it.

The overall impedance for parallel systems is the reciprocal of the sum of the reciprocal impedances of each circuit component. The quantity defined by the reciprocal of impedance, 1/Z, is called the admittance Y.

There are certain considerations that should be taken into account when interrogating a circuit by means of its impedance. Firstly, the range of the applied frequencies should be as wide as possible, ideally in the range of 6 to 7 decades or even more. Furthermore, since a.c. impedance theories are all linear in nature, in contrast with reality where electrochemical processes are non-linear, the amplitude of the exciting signal must be kept small enough so that the system becomes linear to a close approximation. Typically the peak-to-peak amplitudes used do not exceed 10mV.

It is common practice to use electrical circuits that are equivalent to and model the electrochemical behaviour of a system under impedimetric interrogation. Fig 2.16 shows a typical impedance plot obtained when an electrolytic reaction is taking place at the electrode surface.

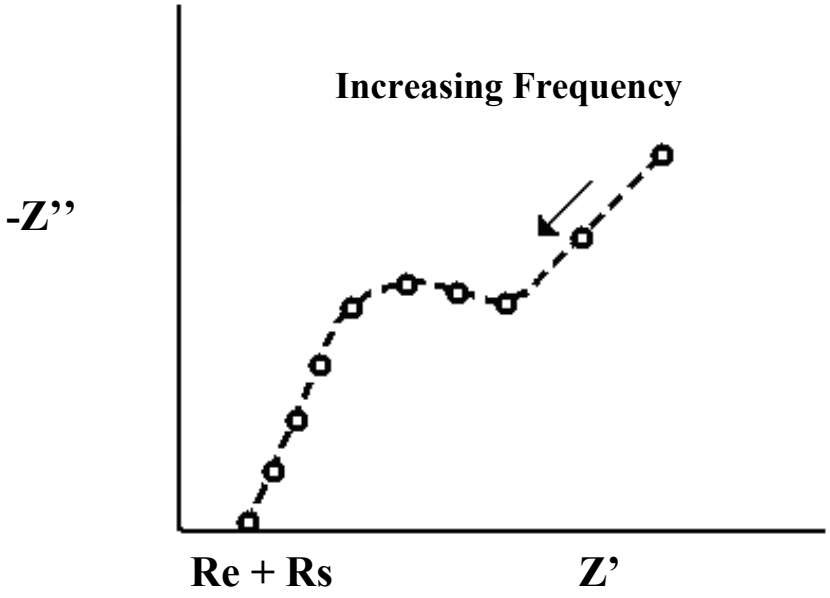

Fig 2.17 Impedance plot for a typical electrochemical reaction.

This may be explained using the Randles circuit shown in Fig 2.18. It consists of a capacitor, C, in series with a resistor, R_s, corresponding to the double layer at the electrode surface and the solution resistance respectively. Furthermore a resistance, R_e, connected in parallel to the capacitor, allows for the faradaic charge transfer reaction and the resistance at the electrode surface associated with the transfer. The final term, the Warburg Impedance, *W*, represents the frequency dependent diffusive transport to the electrode.

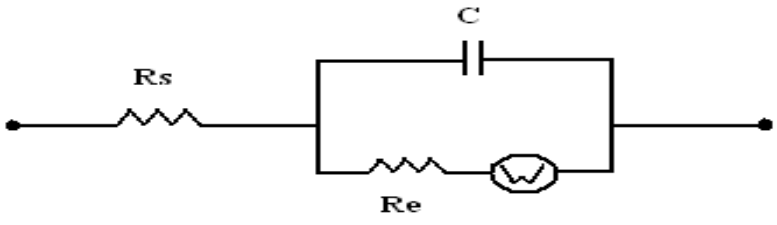

Fig 2.18 The Randles circuit.

According to Fig 2.17, at high frequencies the dominant contribution to the total impedance is that of the solution resistance and therefore at these range of frequencies no electrolysis takes place. As the frequency is lowered, the effect of the resistance at the electrode surface gives rise to the characteristic semicircular part of the impedance plot. Finally, at low frequency ranges, the significant concentration changes induced by the a.c. current (non-faradaic), become increasingly difficult to replenish by diffusion and hence the impedance displays a rise.

2.4 Microelectrodes

Until now we have considered electrochemical processes occurring at electrodes of macroscopic dimensions and these electrodes are commonly referred to as being planar. The fast rate of electron transfer when working with planar electrodes and the relatively slow linear diffusion renders the measured current to be under diffusional control. However, diffusion controlled behaviour is frequently problematic for electroanalysis, since any convection in the solution will affect the diffusion gradients in the solution and result in a change of the electrode response. Miniaturisation of electrodes is one answer to this problem and microelectrodes are the growing trend in the field of electrochemistry. Their use in electrochemistry is not however a new phenomenon. William Wollaston was the first to use microelectrodes as far back as the early 1800s but advances in technology and instrumentation have only permitted the widespread employment of microelectrodes in recent times (Imisides *et al*, 1996)

There is no one definition for what constitutes a microelectrode. According to Dayton *et al*., the electrode must be smaller than the thickness of the diffusion layer to prevent the electrode response being diffusion limited (Dayton *et al.*, 1980). This in principle means that the surface dimension of a microelectrode is smaller than 25 μm, or even less than the width of a human hair (Bard *& Faulkner*, 2001). Recent developments in carbon nanotube technology have allowed for the reduction of microelectrode dimensions to the sub-micron level (~100nm) (Dimaki *et al.,* 2004) and even 10nm, microelectrodes that are called nanodes (Zoski, 2002).

A range of different configurations and materials have been employed in microelectrodes, however, the most commonly used is a circular conductor embedded in an insulating plane. Other common geometries include microcylinders, microhemispheres, microbands or even interdigitated electrodes (Fig 2.19) (Zoski 2002). The same types of materials as the ones used for the fabrication of common working electrodes have been employed in the fabrication of microelectrodes, such as noble metals, carbon fibres or thin metal films.

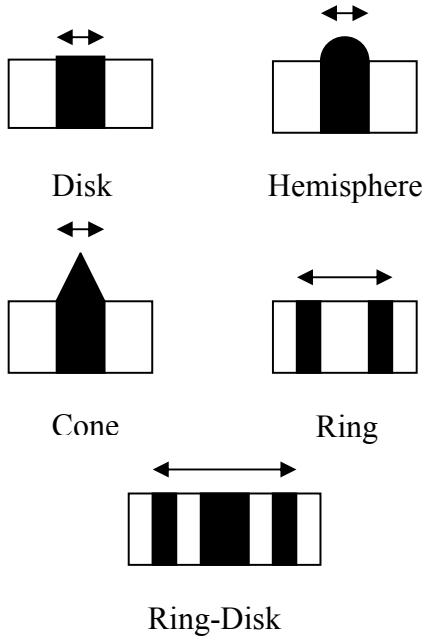

Fig 2.19 Cross-sections of various Microelectrodes.

Microelectrodes have some obvious practical advantages but also open up some fundamentally new possibilities. Such advantages include the exploration of microscopic domains, detection in microflow systems, and analysis of very small sample volumes. Recent studies, for example, have shown the detection of even a single molecule and the *in-vivo* monitoring of neurochemical events (e.g. stimulates dopamine release) (Fan *et al.,* 1996; Kennedy *et al.,* 1993).

2.4.1 Advantages of Microelectrodes

The advantages of microelectrodes go far beyond the simple restrictions of space mentioned in the previous chapter. Because of the fact that the currents passed by microelectrodes are extremely small (of the order of $1x10^{-9}$ amps or even less), since measured current is a function of area, there are certain advantages associated with their use:

- Firstly, it is possible to work in highly resistive solutions that would develop large ohmic (*iR*) drops with conventional electrodes. The decreased ohmic distortions allow electrochemical measurements to be made using non-polar

solvents such as benzene or toluene in the presence of trace pollutants, since a background electrolyte is not necessary and hence a polar solvent is not required. In addition microelectrodes have also been used in frozen solvents, supercritical fluids and even in the gas phase (Fisher, 1996; Wang, 2000).

- Microelectrodes have a smaller surface area which significantly reduces the transient current that flows when an electrode is investigated via cyclic voltammetry. It follows that microelectrode systems suffer less distortion from the so-called 'capacitive charging' and hence the rate at which the potential is swept can be made much greater (higher than 10^{-6} V s^{-1}). Very fast electron transfer and coupling-chemical reactions and the dynamic of processes such as exocytosis can often in this way be investigated (Andrieux *et al.,* 1990).

- Enhanced rates of mass transport of electroactive species result from the radial (nonplanar) diffusion to the edges of microelectrodes. This is because of minute currents passing microelectrodes, inducing tiny amounts of electrolysis. The diffusion layer is hence very thin and the concentration gradient induced across them very high. This becomes valuable in the study of electrolysis mechanisms of fast processes, such as rapid rates of electron transfer between electrode and substrate - or a fast chemical reaction forming part of the overall mechanism (Higson, 2004).

Microelectrodes are therefore fully and uniformly accessible for the supply of materials and are not subject to the rate-limiting diffusional mass transport. As a result of their small size and enhanced hemispherical diffusion, microelectrodes exhibit a modified form of the cyclic voltammogram (Fig 2.20).

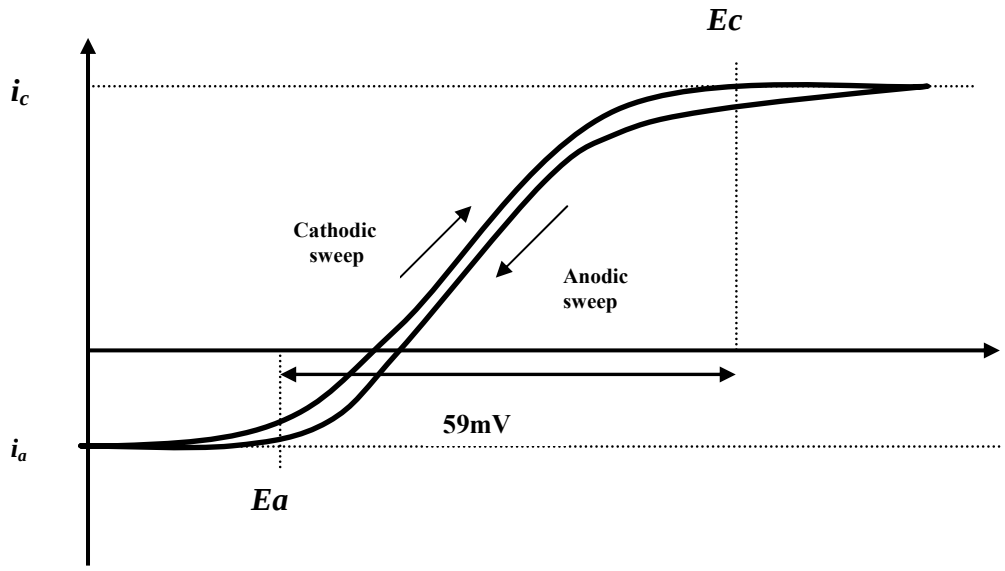

Fig 2.20 Cyclic voltammogram for a reversible electron transfer reaction at a microelectrode.

2.4.2 Microelectrode Arrays

The main disadvantage associated with microelectrodes is the small signal they produce due to their size. This places a serious demand on the instrumentation equipment used to prevent the signal being swamped by electrical noise. Composite electrodes, strive to combine the advantages of single microelectrode systems with significantly higher currents due to larger surface areas. The surfaces of composite electrodes consist of uniform (array) or random (ensemble) dispersions of a conductor region within a continuous insulting matrix (Fig 2.21).

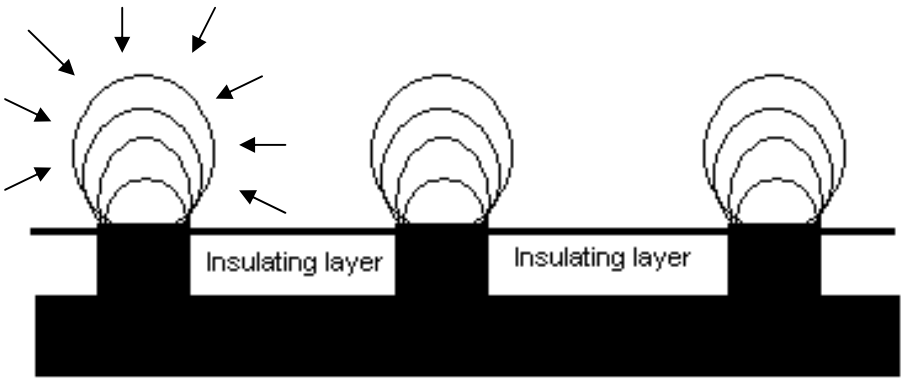

Fig 2.21 Schematic representation of a microelectrode array.

As long as there is a negligible overlap of the diffusion layers from adjacent sites, in the case of relatively low packing density, the current from a composite electrode is the sum of currents of the individual sites. However, at sufficiently long experimental times, if the spacing between the electrodes is not large enough, they will start to compete for mass transport, the diffusion layers will overlap and this in turn will cause a miniaturisation in the hemispherical diffusion of material to the electrode surfaces. This effect is termed shielding and in extreme cases it may result in the sensor array behaving like a macroelectrode of the same total area (Amatore et al, 1983).

There are several ways to fabricate microelectrodes. Techniques based on glass capillary/epoxy encapsulation of metallic wires on carbon fibres have been widely used in the field of neurophysiology for over 50 years, but they are suitable for the production of single microelectrodes (Zoski, 2002).

For the fabrication of microelectrode arrays, microfabrication techniques are employed that take advantage of thin-film and thick-film technologies originally developed for the fabrication of integrated circuits (Feeney *et al*, 2000). These include deep UV and extreme UV photolithography, phase-shift photolithography, electron-beam writing, focused ion beam lithography, scanning probe lithography, X-ray lithography and others. Despite their success in nano-fabrication these techniques are all extremely expensive and require specialized reagents. For this reason soft lithographic techniques (microcontact printing, micromolding in capillaries, microtransfer molding) have been recently developed that are based on self-assembly and replica molding of organic molecules and polymeric molecules (Xiao-Mei Zhao, 1997). Even this approach, however is costly and that is why in this research we used an innovative technique to fabricate microelectrodes developed by previous members of our research group.

Towards this end, we used ultrasound to ablate an insulating polymer film previously deposited on the electrode surface. This resulted in the formation of small abrasions on the polymer film through which we grew a conductive film. The process is further analysed in the following chapter which is devoted to the fundamental principles of ultrasound and sonication. Polymer chemistry is discussed in chapter 2.7.

2.5 Ultrasound and Sonochemistry

2.5.1 The History of Ultrasonics

Ultrasound is a general term used to describe the oscillation of particles of matter at frequencies greater than the upper limit of human hearing, ie. above approximately 20 kHz. The physical upper threshold of ultrasound is thought to be around 5 MHz for gases and 500 MHz for liquids and solids. The field of ultrasound, the equipment used to generate it, and its practical implications and applications are collecticely known as ultrasonics (Glickstein, 1960).

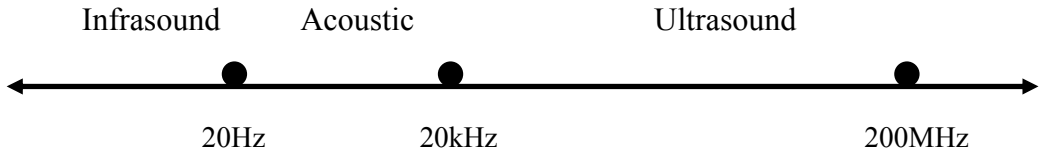

The generation of ultrasound was first established in the 1880's with the discovery of the piezoelectric effect by the Curie brothers (Curie J. & P., 1880). It describes the relationship found between mechanical vibrations and electricity in certain minerals. In their experiments they conclusively measured surface charges appearing on the faces of crystals such as tourmaline, quartz, topaz and cane sugar, when subjected to mechanical stress.

One of the first applications of ultrasound was an ultrasonic whistle demonstrated by Galton in 1883 to investigate the threshold frequency of human hearing (Peason, 1924). Whistles of this type are still used today for calling dogs. It was not until 1918 though, that the piezoelectric effect and ultrasound gave rise to the 'echo sounder', invented by Paul Langevin. The latter patented a quartz-driven ultrasonic transducer and detector to gauge the depth of water beneath a boat's keel and was later on developed further to allow the detection of the presence of enemy submarines, hence the name SONAR (SOund Navigation And Ranging) (Langevin P., 1918).

2.5.2 Acoustic cavitation

Cavitation is a general term used to describe the behaviour of voids or bubbles in a liquid. Cavitation is usually divided into two classes of behaviour: inertial (or transient) cavitation and non-inertial (or stable) cavitation (Leighton, 1994). Stable cavitation is the process where a void or bubble in a liquid medium grows over several thousand acoustic cycles and oscillates as the ultrasonic waves pass through the medium. This oscillation produces micro currents in the surrounding medium, an effect known as microstreaming (Nyborg, 1996). Such cavitation often occurs in pumps, propellers, and in the vascular tissues of plants. Transient cavitation is the process where a bubble in a fluid is forced to oscillate in size or shape due to some form of energy input, such as an acoustic field and collapse when unstable (Leighton, 1994).

Cavitation as a phenomenon was first described in 1895 by Sir John Thornycroft and Sidney Barnaby whilst assessing the damage to the rapidly rotating propellas of HMS Daring (Thornycroft *et al*., 1895). It was found that the rapid motion of the blades caused the surrounding water to rupture and the propeler to loose grip. This problem increasingly concerned the Royal Navy, who commissioned Lord Rayleigh in 1917 to investigate it further and his research concluded that the turbulenece, heat and pressure created when cavitation bubbles implode in the close vicinity of the propellas quickly erode their surface (Lord Rayleigh, 1917).

2.5.3 Principles of ultrasound and acoustic cavitation

Energy in the form of sound can be transmitted through any substance which possesses elastic properties. On the basis of vibration sound waves can be further categorised into transverse and longitudinal waves. When the particles of the medium vibrate in a direction perpendicular to the direction of wave propagation, then the wave is transverse. Such waves are produced on the surface of solids and liquids. For longitudinal waves, vibrations of the particles of the medium are in the direction of wave propagation and the wave proceeds in the form of compression and rarefaction. At places of compression the pressure and density are maximum, while at places of

rarefaction these are at a minimum (Fig. 2.22). Sound waves as well as waves produced in gases and liquids are longitudinal waves (Blitz, 1963).

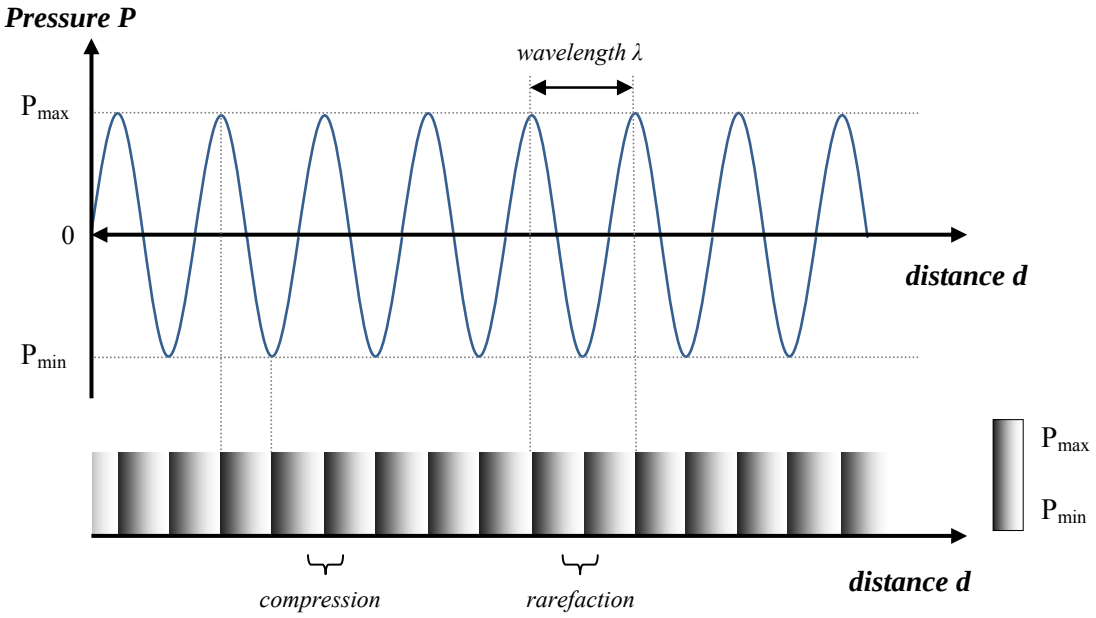

Fig 2.22 The pressure variation (P) associated with a sound wave.

During regions of rarefaction, a negative pressure is applied to liquid medium and when the frequency and amplitude of the longitudinal waves becomes sufficiently high, molecular spacing within the medium becomes so large that voids are created, and the liquid 'tears apart', or cavitates, to form a bubble. For pure water a negative pressure of around 10.000 atmospheres is required to force the water to cavitate. However, in reality the situation is different since the tensile strength of a liquid is significantly lowered due to dissolved gases or suspended particles in the medium. Such factors affecting the phenomenon of cavitation are discussed in the next chapter (Lorimer and Mason, 1987).

The cavities will continue to grow in size over a few compression and rarefaction cycles, taking in some of the dissolved gas from the medium, until they reach an unstable size and thus collapse. This process is called rectified diffusion (Crum 1984). Theoretically, the cavities would grow until they reached an equilibrium which matches the frequency of the bubble resonance. In reality any individual bubble is unstable because of the interference caused by other bubbles collapsing in its vicinity.

An implosion of any of these cavitational nuclei may generate temperatures of up to 5000°C and pressures of approximately 2000 atmospheres and the areas where the bubbles collapse are referred to as hot spots (Suslick *et al*, 1986). When these hot spots are close to a solid surface then the liquid trying to fill the burst cavity will be hindered from that side (Blake, 1986). The majority of the liquid medium will enter the void from the other side, creating in this way a jet targeted towards the sold surface as speeds of several hundred ms^{-1} (Fig 2.23) (Chahine, 1982). The elevated temperatures and pressures associated with the collapse of cavitation voids along with the jet of liquid generated in the process are exploited in an ultrasonic bath or tank, such as the ones used in the research described within this thesis. Stable cavitation, described briefly in the previous chapter, will also contribute to the sonochemical events but to a lesser degree.

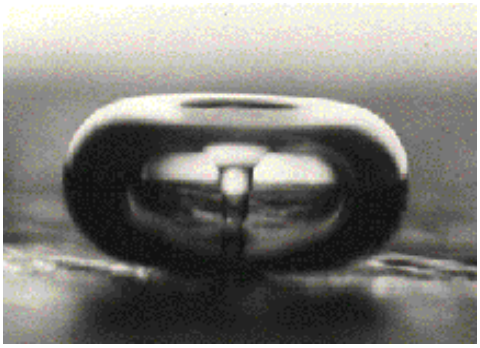

Fig 2.23 An imploding cavitation bubble near a solid surface (Suslick, 1994).

2.5.4 Factors affecting cavitation

Cavitation is a complex phenomenon dependant on many factors. As mentioned previously, *dissolved atmospheric gases* will always exist in a liquid medium and serve as weak spots, lowering the power required to form cavitation voids. Similarly, *impurities* in the form of suspended particles can act as preferential nucleation sites for bubble formation (Zima *et al*, 2003).

However, of equal importance is the effect the *frequency* and *amplitude* of the applied ultrasonic wave have on the formation of bubbles. In general, the higher the frequency of the wave the more difficult it is for the liquid medium to cavitate. This is due to the fact that as the frequency increases, the rarefaction phase shortens. When the frequency of the ultrasound reaches the MHz region, the rarefaction phase is so short that cavitation becomes extremely difficult and it has been shown that at frequencies greater than 2.5 MHz cavitation even ceases to occur (Gaertner, 1954). Transducers

operating at high frequencies exploit this phenomenon for non-invasive medical diagnostic purposes.

As far as amplitude is concerned, the opposite of what holds true for frequency occurs. The higher the intensity or amplitude of the ultrasonic source the greater is the intensity of the ultrasonic cavitation that occurs. In fact the intensity of the latter is directly proportional to the square of the amplitude. However there are limits. If the intensity of the source exceeds the limits of any given system, cavitation voids will start to coalesce in larger entities which are longer lived and act as a barrier to the transfer of energy through the medium. Furthermore, decoupling can occur which refers to the loss of contact between the source and the medium at large vibrational amplitudes.

2.5.5 Applications of ultrasound

Cavitational phenomena created by the application of ultrasound to a liquid medium have been exploited for cleaning purposes, the most widely used application of ultrasound. Ultrasonic cleaning is particularly efficient in removing surface contaminants such as dirt or bacteria. Large crates used in the food industry and surgical equipment are typical objects cleaned in this way (Kuttruff, 1991).

Ultrasound is used in the medical field for other purposes other than cleaning. For example, sound waves can be used for the diagnosis of a number of heart defects, fetal monitoring within pregnancy and also medical imaging of tumours. For such purposes high frequency ultrasonic waves are applied so as to minimise damage to tissues and organs. Lower frequency waves have been shown to remove kidney stones by cavitation (Leroy, 1994), as well as cancer cells (Shuqun *et al*, 2000) and blood clots (Shlamovitz *et al,* 2003), in the new field of medicine termed therapeutic ultrasound. Finally, gene therapy can be carried out with the use of ultrasound since under certain conditions the latter can cause a transient permeability of cell membranes thus allowing large molecules to enter the cell (Miller, 1999).

In the food industry, ultrasound can be used for mixing, tenderizing, ageing emulsifying, cutting and even thawing. Sterilisation of milk can be achieved by the

action of sound waves on micro-organisms found in it while the emulsion bases for sauces such as ketchup and mayonnaise can be prepared using ultrasound (Roberts, 1993).

Of great commercial interest is the use of ultrasound in chemistry. The immense temperatures and pressures associated with cavitation offer a unique set of conditions for chemists to employ. In the last two decades of the 20^{th} century, the field of sonochemistry has arisen as a result. The chemical effects of ultrasound fall into three areas: homogeneous sonochemistry of liquids, heterogeneous sonochemistry of liquid -liquid or liquid-solid systems, and sonocatalysis (which overlaps the first two) (Suslick, 1999).

Homogeneous reactions refer to the effect that ultrasound has on the liquid medium alone, e.g. pure water. The primary products of water sonication are molecular hydrogen (H_2) and hydrogen peroxide (H_2O_2). Other high-energy intermediates may include HO_2 (superoxide), H· (atomic hydrogen), OH· (hydroxyl), and $e^-_{(aq)}$ (solvated electrons). As expected, the sonolysis of water, which produces both strong reductants and oxidants, is capable of causing secondary oxidation and reduction reactions (Misik *et al*, 2000). In contrast, the ultrasonic irradiation of organic liquids has been little studied. Almost all organic liquids will generate free radicals (uncharged, reactive intermediates possessing an unpaired electron) when they undergo ultrasonic irradiation. The sonolysis of simple hydrocarbons creates the same kinds of products associated with very high temperature pyrolysis. Most of these products - H_2, CH_4 (methane), and the smaller 1-alkenes, derive from a well-understood radical chain mechanism (Davidson, 1987).

For many heterogeneous organic and organometallic reactions the use of high intensity ultrasound to enhance the reactivity of metals as stoichiometric reagents has become an important synthetic technique, especially those involving reactive metals, such as magnesium, lithium, and zinc. Reactivity rate enhancements of more than 10 fold are common, yields are often substantially improved, and by-products avoided (Suslick, 1999).

While the chemical effects of ultrasound on aqueous solutions have been studied for many years, the development of aqueous sonochemistry for biomaterials synthesis is very recent. Microencapsulation, the enclosing of materials in capsules a few micrometers in size, has diverse important applications; these include uses with dyes, flavours and fragrances, as drug delivery systems, and as medical diagnostic agents (Narayan, 2004; Suslick, 1999).

Finally ultrasound has been shown to both enhance polymer synthesis and control their cleavage under specific conditions. Polymer degradation produces chains of smaller lengths with relatively uniform molecular weight distributions, with cleavage occurring primarily in the centre of the polymer chain, whereas cleavage by thermal degradation methods results in random breaks, providing a more controlled polydisperity (Mason & Lorimer, 2002). This polymer fragmentation has been used by G. J. Price at the University of Bath to synthesize block copolymers of various kinds. Block copolymers are long chain polymers with two different, but linked, parts (Suslick & Price, 1999).

On the other hand it has been shown that the use of ultrasound can enhance polymerisation reactions and most of the work on this area refers to the radical polymerisation of vinyl polymers. Sonication allows improved control over the molecular weight, tacticity and polydisperity of the forming polymer. Similarly, enhanced polymerisation of small cyclic polycarbonate oligomers and of cyclic siloxanes to silicones has been observed with the application of ultrasound (Mason & Lorimer, 2002).

2.6 Polymers

Polymers are substances whose molecules have high molar masses and are composed of a large number of repeating units or monomers that are joined by covalent bonds. They are both naturally occurring and synthetic and include such diverse molecules as proteins and plastics. Natural polymers such as amber have been in use for centuries while biopolymers like proteins and nucleic acids play crucial roles in biological processes. Synthetic polymers on the other hand are used as adhesives, coatings, foams, and packaging materials to textile and industrial fibres, composites, electronic devices, biomedical devices, optical devices, and precursors for many newly developed high-tech ceramics (IUPAC, 1996).

Although polymers have existed since the beginning of times, the term was first coined by Jöns Jakob Berzelius in 1833 while Henri Braconnot around the same time pioneered cellulose compounds (Labrude, 2003). Development of the technique of vulcanisation (specific curing process of rubber involving high heat and the addition of sulfur) later on in the 19^{th} century improved the durability of natural polymer rubber, which was the first semi-synthetic polymer widely used. However, the first wholly synthetic polymer, Bakelite, was not manufactured until 1909 by Dr. Leo Baekaland (Farber, 1970).

The exact structure of polymers was not fully understood until 1922, when Herman Staudinger proposed that polymers consisted of long chains of atoms held together by covalent bonds, an idea for which he received the Nobel Prize. Up until then, scientists believed that polymers were loose clusters of smaller moleculers, called colloids, held together by an unknown force, a concept known as association theory (Mülhaupt, 2004). Progress in polymer chemistry has been tremendous ever since, with Giulio Natta and Karl Ziegler winning the Nobel Prize in Chemistry in 1963 for the Ziegler-Natta catalyst and a vast number of polymers such as nylon, polyethylene, teflon and silicone being widely employed nowadays (Heeger, 2001).

Depending on the level on which one examines polymers several properties can be attributed to them. At the nano-micro scale the structure of a polymer is under

scrutiny. Polymers that contain only a single type of monomer are known as homopolymers, while polymers containing a mixture of monomers are known as copolymers. The simplest form these monomers can be arranged is in a linear form. If there are one or more substituent side chains to the main chain then the polymer is refered to as branched. If the side chain has a different composition to the main chain then the resulting polymer is known as graft polymer. The polymer's bulk properties may be strongly dependent on the size of the polymer chain. In polymers, the molecular mass can be expressed in terms of degree of polymerisation, which is essentially the number of monomers which comprise the polymer. The space occupied by a polymer molecule is generally expressed in terms of radius of gyration or excluded volume. One final consideration at the microscopic level is the tacticity of the polymer which describes the relative stereochemistry of adjacent chiral centres within a macromolecule (meso, racemo- diad and isotactic, syndiotactic and heterotactic triad) (Painter and Coleman, 1997).

At an intermediate mesoscopic level are properties that describe the morphology of the polymer matrix in space. A polymer may be described as crystalline if it contains regions of three-dimensional ordering on atomic (rather than macromolecular) length scales, usually arising from intramolecular folding and/or stacking of adjacent chains. Synthetic polymers may consist of both crystalline and amorphous regions. Tacticity of a polymer therefore influences the level of its crystallinity (Painter and Coleman, 1997).

Finally, by examining a polymer at the macroscopic level, its bulk properties which are usually the most valuable commerically can be diserned. The tensile strength of a material quantifies how much stress the material will endure before failing. This is very important in applications that rely upon polymer's physical strength or durability. For such applications the Young's Modulus of elasticity is of equal importance and is yet another way of measuring how much stress a polymer can withstand. Transport properties such as diffusivity relate to how rapidly molecules move through the polymer matrix and are important in those polymers used as films and membranes. The melting point of a polymer describes a transition from a crystalline or semi crystalline form to a more amorphous state whereas the boiling point is not relevant since polymers will decompose before reaching the theoretical boiling point values. A

parameter of particular interest in synthetic polymer manufacturing is the glass transition temperature which describes the temperature at which amorphous polymers undergo a second order phase transition from a rubbery, viscous amorphous solid to a brittle, glassy amorphous solid (Painter and Coleman, 1997).

The bulk properties of polymers are greatly dependent on the structure and mesoscopic behaviour of a polymer. For example increasing the chain length tends to decrease chain mobility, increase strength and toughness, and raise the glass transition temperature. Random length and atactic short chains, on the other hand, may reduce polymer strength. The variations are endless giving rise to a huge range of synthetic and natural polymers whose properties can be easily manipulated (Painter and Coleman, 1997).

2.6.1 Chemically modified electrodes

Chemically modified electrodes (CMEs) represent a modern approach to electrode systems. They alter the electrode surface by means of a reagent placed on the electrode surface. Such deliberate alterations can thus meet the needs of and be beneficial to many electroanalytical problems, such as electron-transfer reactions, imparting higher selectivity, sensitivity and stability (Murray *et al.,* 1987; Wang, 1999). The chemical modifier can be an organic compound, a metal oxide or even a polymer layer. The placement of the modifier on the electrode surface is achieved in a variety of schemes, like covalent attachment, sol-gel encapsulation, physical adsorption, spontaneous chemisorption and others. All of the electrodes used in the research project were coated with a thin film of polymer either to insulate them or to provide a conducting substrate upon which an immunosensor platform could be built on. For this reason, it is worth examining the mechanisms of polymer formation on an electrode substrate as well as the individual properties of polyaniline and *poly (1,2diaminobenzene),* the two polymers used in this research.

2.6.2 Polymer synthesis

Polymer modified electrodes can be prepared by casting a solution containing the dissolved polymer onto the surface and allowing the solvent to evaporate, or via electropolymerization (Sittampalam, 1983).

The latter method offers precise control of the film thickness, its morphology and is particularly attractive in connection with miniaturized sensor surfaces and hence the reason it was used in this project. Monomers such as aniline, pyrrole, and 1, 2 diaminobenzene can be electrosynthesised via electrochemical polymerization. In contrast, monomers such as the methacrylates can only be electropolymerised on the working electrode surface via cathodic gel-point mechanistic processes (Sadki *et al.,* 2000).

Electrochemical polymerization can be further subdivided into step growth and chain polymerization. In the former, the polymer chains grow by reactions that occur between two molecular species and that is way step growth polymerization is also commonly referred to as condensation polymerization. Chain-reaction polymerization, sometimes called addition polymerization, requires an initiator to start the growth of the polymer chain. This can be a free radical, an anion or a cation and the addition reaction that follows is named after the initiator. In the three electrode system used in the research the role of initiator was played by the working electrode which removed electrons from the monomers of aniline and 1, 2 diaminobenzene, thus creating a radical monocation. This phenomenon is further illustrated in the results section of this thesis (Bobalek *et al*, 1964).

The progression of the reaction, no matter what the initiator is, involves three steps: the initiation, the propagation and the termination. The first step refers to the creation of the smallest entity that may produce the growing-end group or active centre by addition of a monomer. Polymerisation is initiated by the rearrangement of π orbitals in the monomer and thus the creation of a radical. In *free radical polymerization*, the electrons in the pi bond split up. One combines with the unpaired electron in the initiator (or growing chain end) to form the new bond, and the second ends up on the chain end, reproducing the attacking species. In *anionic polymerization*, the electrons

in the pi bond more together instead of separately. The initiator (or growing chain end) attacks with a pair of electrons, used to form the new bond. The pi-bond electron pair "flows" away from the attacking species, reproducing the anion at the chain end. Finally, in *cationic polymerization* exactly the same mechanism occurs, except that the initiator (or chain end) lacks a pair of electrons. The electron "flow" is simply in the opposite direction, leaving behind a positive charge at the chain end to continue the process. This rearrangement of the double bonds, in all types of chain polymerization, forms a polymer active centre which in turn 'attacks' the following monomer. It is therefore the initiator radical (Bobalek *et al*, 1964).

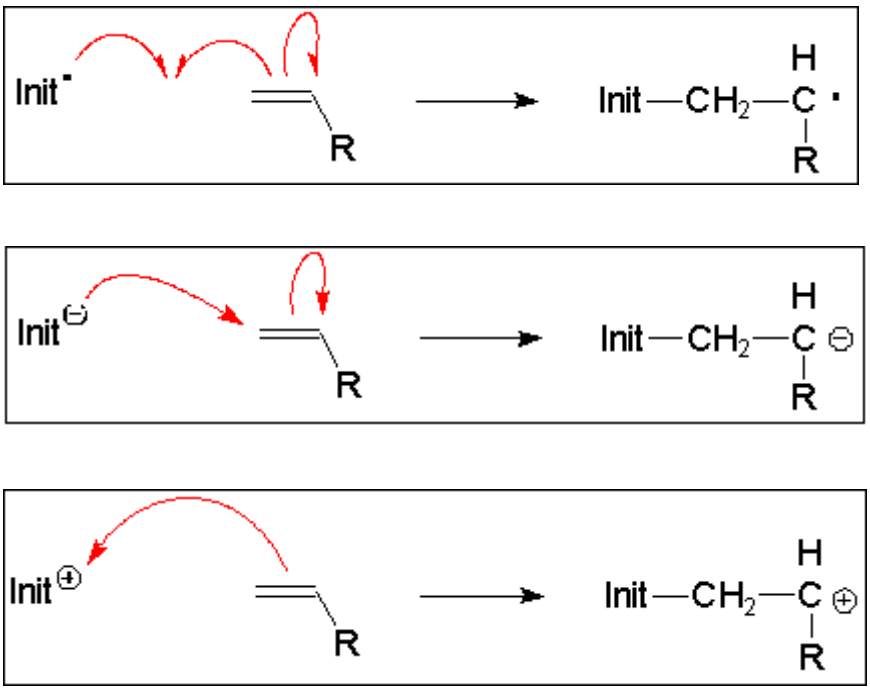

Fig 2.24 Chain polymerizations, the initiation step by a A. free radical, B. anion, C. cation.

The polymer molecule then propagates by the addition of a single monomer to the active centre generating a new one each time thereby producing an ever lengthening polymeric chain. The propagation step ends when there are no more monomer units being added to the growing polymeric chain. The cause of termination can be a chance reaction of the active centre or can be achieved deliberately by the addition of a suitable reagent, such as water (Bobalek *et al*, 1964).

2.6.3. Conducting polymers

Conjugated polymers also known as conducting polymers are characterised by alternating single and double bonds between carbon atoms on the polymer backbone. The essential structural characteristic of all conjugated polymers is their quasi-infinite π system extending over a large number of recurring monomer units. The double bonds connecting adjoining carbon atoms possess therefore a strong localised σ bond and a delocalised π bond.

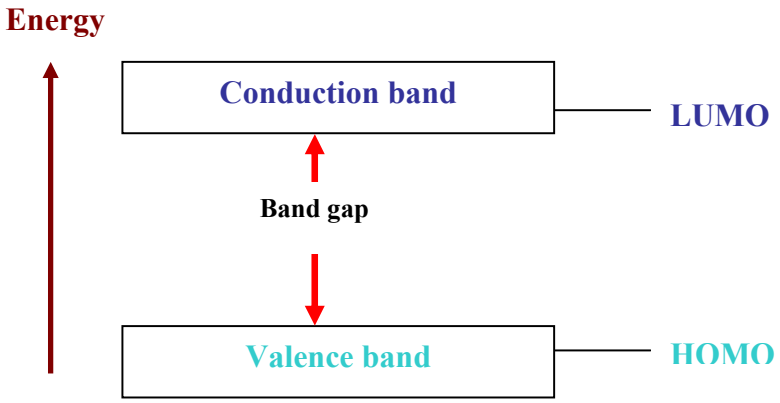

Fig 2.25 Band structure in a conducting polymer.

This creates degeneracy in the frontier molecular orbitals (the highest occupied and lowest unoccupied orbitals named HOMO and LUMO respectively). The frontier orbitals are important because they are key factors in the amount of energy needed to add or remove electrons in a molecule. When an electron is removed from one atom/molecule it is taken from the HOMO and when an electron is added, it is added to the LUMO. These bands stem from the splitting of interacting molecular orbitals of the constituent monomer units in a manner reminiscent of the band structure of solid state semiconductors. The HOMO level is to organic semiconductors what the valence band is to inorganic semiconductors, such as conducting polymers. The same analogy exists between the LUMO level and the conduction band. The energy difference between the HOMO and LUMO level is regarded as band gap energy (Prasanna Chandrasekhar, 1999).

However, conductive polymers generally exhibit very low conductivities because conjugation alone is not sufficient to make a polymer conducting. It is not until an

electron is removed from the valence band (p-doping) or added to the conduction band (n-doping, which is far less common) that a conducting polymer becomes highly conductive. Charge carriers, positive charges (holes) and negative charges (electrons), serving to remove or add electrons from the polymer respectively are termed dopants and generally take the form of an acid or an inorganic molecule (Winokur *et al*., 1987).

In positive charging (p-doping), the commonest doping method, the electron removed from the valence band will create a radical cation, called polaron. The latter is partly localised because of the Coulomb attraction it experiences from the counterion that created it. A high concentration of dopant in the polymer, will allow the polaron to move in the tightly packed counter ions, thereby permitting the flow of current. Therefore in conducting polymers, charge transfer through the polymer is simply transfer of localised charged states (Bredas & Street, 1985).

If the band gap energy required for an electron to jump from the valence band to the conductive band is sufficiently small, such excitation becomes possible. An application of a charge to the conducting polymer leads therefore not only to transfer of electrons between bands but also to the rearangement of the energy levels of those bands and thus to their optical absorption levels. The optical properties of polymer thin films depend exclusively on the structure of the energy bands created following excitation and colour changes corresponding to differences in radiation absorption can be seen by the naked eye. All conducting polymers can be potentially electrochromic in nature and polyaniline is no exception. Its structure and electrochromic properties are further analysed in chapter 4.

Electrochromisn, as a phenomenon has many applications in industry. As the color change is persistent and energy need only be applied once to effect a change, electrochromic materials are used to control the amount of light and heat allowed to pass through windows ("smart windows"), and has also been applied in the automobile industry to automatically tint rear-view mirrors in various lighting conditions. Furthermore, Viologen is used in conjunction with titanium dioxide (TiO_2) in the creation of small digital displays. It is hoped that these will replace LCDs as the viologen (which is typically dark blue) has a high contrast to the bright color of the titanium white, therefore providing a high visibility for the display (Somani, 2003).

2.6.4 Polymer synthesis validation by the use of a Quartz Crystal Microbalance

The first demonstration of the direct piezoelectric effect was in 1880 by the Curies. They combined their knowledge of pyroelectricity - the ability to generate an electrical signal when the temperature of the crystal changes - with their understanding of the underlying crystal structures that gave rise to the former, to predict crystal behaviour, and demonstrated the piezoelectric effect using crystals of tourmaline, quartz, topaz, cane sugar, and Rochelle salt (sodium potassium tartrate tetrahydrate). They showed that a flow of electrons was produced when pressure was applied in certain crystallographic directions (Barton, 2007).

The converse effect was mathematically deduced from fundamental thermodynamic principles by Gabriel Lippmann in 1881. Piezoelectricity did not receive a lot of interest originally and a more detailed study of piezoelectricity did not commence until 1917 when it was reported that quartz crystals could be used as transducers and receivers of ultrasound in water. In 1919 several devices of everyday use, based on the piezoelectricity of Rochelle salt were described; i.e. loudspeakers, microphones and sound pick-ups. In 1921 the first quartz crystal controlled oscillator was introduced (Lewis, 1990).

From the Curies' initial discovery in 1880, it took until the 1950s before the piezoelectric effect was used for sensing applications. Depending on how a piezoelectric material is cut, three main modes of operation can be distinguished, namely transverse, longitudinal, and shear.

The transverse mode refers to the generation of charges along the (x) direction, perpendicular to the line of applied force along a neutral axis (y). The amount of charge depends on the geometrical dimensions of the respective piezoelectric element. For a piezoelectric material operating in longitudinal or shear mode, on the other hand, the amount of charge produced is strictly proportional to the applied force and at the same time independent of the size and the shape of the piezoelectric element.

In 1959, Sauerbrey published a paper that showed that the frequency shift of a quartz crystal resonator is directly proportional to the added mass. Sauerbreys work is

generally taken as the breakthrough and the first step towards a new quantitative tool to measure very small masses; i.e. the quartz crystal microbalance (Sauerbrey, 1959).

The quartz crystal microbalance (QCM) used in this research is therefore an ultra-sensitive mass sensor. The heart of the QCM is the piezoelectric AT-cut quartz crystal sandwiched between a pair of electrodes. 'A' refers to the quartz crystal operating in the shear mode while 'T' specifies a cut with minimal temperature dependence of the resonant frequency. When the electrodes are connected to an oscillator and an AC voltage is applied over the electrodes the quartz crystal starts to oscillate at its resonance frequency due to the piezoelectric effect.

This oscillation is generally very stable due to the high quality of the oscillation (high Q factor). If a rigid layer is evenly deposited on one or both of the electrodes, then the resonant frequency will decrease proportionally to the mass of the adsorbed layer according to the Sauerbrey equation (Eqn 2.44).

$$\Delta f = - [2 \times f_0 \times \Delta m] / [A \times (\rho_q \mu_q)^{1/2}] \qquad \textit{Eqn 2.44}$$

Where:
Δf = measured frequency shift,
f_0 = resonant frequency of the fundamental mode of the crystal,
Δm = mass change per unit area (g/cm^2),
A = piezo-electrically active area,
ρ_q = density of quartz, 2.648 g/cm^3,
μ_q = shear modulus of quartz, 2.947×10^{11} g/cm x s^2.

There are situations where the Sauerbrey equation does not hold, for example, when the added mass is a) not rigidly deposited on the electrode surface, b) slips on the surface or c) not deposited evenly on the electrode. Therefore, the Sauerbrey equation is only strictly applicable to uniform, thin-film deposits. It was not until the beginning of the 1980s that scientists realised that a quartz crystal can be excited to a stable oscillation when it was completely immersed in a liquid. Much of the pioneering work in liquid phase QCM measurements has been done by Kanazawa and co workers, who showed that the change in resonant frequency of a QCM taken from air into a liquid is

proportional to the square root of the liquid's density-viscosity product (Eqn 2.45) (Kanazawa & Gordon, 1985).

$$\Delta f = - f_u^{3/2} [(\rho_L \eta_L) / (\pi \times \rho_q \mu_q)]^{1/2} \qquad \textit{Eqn 2.45}$$

Where:

Δf = measured frequency shift,

f_u = resonant frequency of the unloaded crystal,

ρ_L = density of liquid in contact with the crystal,

η_L = viscosity of liquid in contact with the crystal,

ρ_q = density of quartz, 2.648 g/cm^3,

μ_q = shear modulus of quartz, 2.947 x 10^{11} g/cm x s^2.

After it was established that an excessive viscous loading would not prohibit use of the QCM in liquids and that the response of the QCM is still extremely sensitive to mass changes at the solid-liquid interface, QCMs have been used in direct contact with liquids and/or visco-elastic films to assess changes in mass and visco-elastic properties.

2.7 Antibodies

2.7.1 Antibody structure

Antibodies (also known as immunoglobulins) are glycoproteins that are found in blood or other body fluids of vertebrates, and are used by the immune system to identify and neutralize foreign objects, such as bacteria and viruses. Antibodies are produced by B cells, a kind of white blood cell (Mattu, 1998). However, antibodies can be raised against any biomolecule even those found naturally in an organism to act as recognition molecules. The antibodies used in this research were all against naturally occuring agents in the human organism apart from anti-ciprofloxacin, which is an antibody against the fluoroquinoline antibiotic ciprofloxacin.

All antibodies are made of the same structural units, called chains. Each antibody possesses two heavy chains and two light chains. Based on the type of heavy chain they are composed of antibodies are classed into isotopes. Each heavy chain has two regions, the *constant region* and the *variable region*. The constant region is identical

in all antibodies of the same isotype, but differs in antibodies of different isotypes. The variable region of the heavy chain differs in antibodies produced by different B cells, but is the same for all antibodies produced by a single B cell or B cell clone. Mammals produce five different isotypes known as IgA, IgD, IgE, IgG and IgM. In a similar fashion, light chains are composed of two fragments, a constant one and a variable one. Each antibody contains identical light chains and in mammals they are of two types lambda (λ) and kappa (κ) (Janeway, 2001).

This huge diversity of antibodies allows the immune system to recognize an equally wide diversity of antigens. The unique part of the antigen recognized by an antibody is called an epitope. These epitopes bind with their antibody in a highly specific interaction, called induced fit that allows antibodies to identify and bind only their unique antigen in the midst of the millions of different molecules that make up an organism (Rhoades, 2002). The region of the antibody that recognised its complimentary antigens is located at the tip of the former and is called the Fab fragment (fragment, antigen binding). It is composed of one constant and one variable domain from each heavy and light chain of the antibody. The base of the antibody is commonly referred to as Fc fragment (Fragment, crystallisable). This region binds to specific proteins and in this way modulates the activity of the antibody (Putnam, 1979).

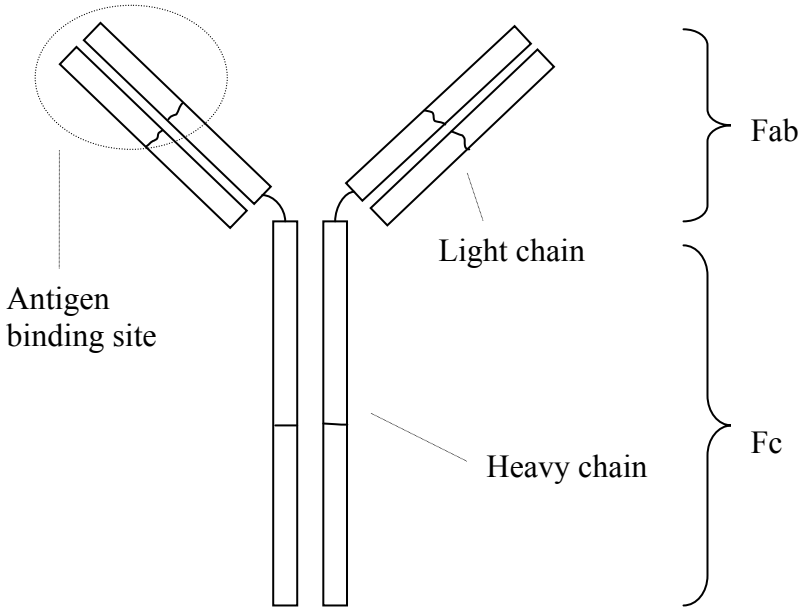

2.26 The basic structure of an antibody.

2.7.2 History of antibody research

Antibody activity against diphtheria and tetanus toxins was first noticed by Emil von Behring and Shibasaburo Kitasato who introduced the concept of humoral immunity, proposing that a mediator in serum could react with a foreign antigen (AG.N., 1931). This idea prompted Paul Elrich to propose the side chain theory that in a similar fashion to the lock-and-key hypothesis proposed by Emil Fisher for enzymes, theorised that living cells possess side chains (receptors) that can link to toxins and foreign agents. According to Elrich, a cell under threat grew additional side-chains to bind the toxin, and that these additional side chains broke off to become the antibodies that are circulated through the body. It was these antibodies that Ehrlich first described as "magic bullets" in search of toxins (Winau *et al*., 2004). Almroth Wright in 1904 suggested that antibodies exist freely in the blood and coat bacteria to target them for phagocytocis, a process he named opsonisation (Silverstein, 2003).

In the 1920s, Michael Heidelberger and Oswald Avery, observed that antigens can be precipitated in conjuction with antibodies and most importantly proved that antibodies are made of proteins (Van Epps, 2006). In the 1940s Linus Pauling confirmed the lock-and-key theory proposed by Elrich by showing that antibody antigen interactions depend more on their configurations than to their chemical compositions, while in 1948, Astrid Fagreaus discovered B cells (Silverstein, 2004).

Further work was directed towards discerning the structure of the antibodies, with Gerald Edelman and Joseph Gally being the first to report the existence of the antibody light chain (Edelman, 1962). They also were the first to realise that the Bence-Jones protein, a monoclonal globulin protein found in the blood or urine and known since 1845 was the same to the light chain they found (Stevens, 1991). Edelman went on to discover that antibodies are composed of disuphide bond-linked heavy and light chains, while Rodney Porter around the same time characterised the Fab and Fc regions of an antibody (Raju, 1999). Most of the studies of this period concentrated on IgM and IgG isotopes. Thomas Tomasi was the first to describe an IgA isotope (Tomasi, 1992), David Rowe and John Fahey identified IgD while IgE (Preud'homme, 2000) was identified by Kikishige Ishizaka and Teruki Ishizaka (Johansson, 2006).

2.7.3 Antibody immobilisation techniques

A number of different antibody entrapment techniques on polymeric films are available, involving either the simultaneous entrapment of the antibody whilst the polymer film is being electrodeposited or via attachment after polymer deposition. The former approach has several drawbacks although it allows for the fast fabrication of sensor platforms. Most importantly, the simultaneous entrapment of biomolecules in a polymer film results in the random entrapment of antibodies, thus hiding some of their active centres from the surface of the polymer film and ultimately rendering the assembly inadequate as a sensor.

On the contrary, the attachment of biomolecules following polymer formation, allows for a much more regulated entrapment process. In other words, the active centres of the antibodies can be guaranteed to face outwards so that they are readily available for antigen binding and recognition. A number of techniques allow for targeted immobilization of biomolecules to single defined sites of immobilization on the polymer film with most employing molecular biology to engineer a defined 'tag'.

The tag can be either a group of amino acids attached to the protein such as a His_6 tag (Fig 2.27) or alternatively can involve whole biomolecules. Examples of the latter include Protein A/Protein G and avidin/biotin. For the purpose of this study, the avidin / biotin pair was selected.

The avidin biotin pair is one of the strongest (non-covalent) binding affinities known with a Kd of $\sim 10^{15}$ M. The bond formation between biotin and avidin is very rapid and, once formed, is unaffected by most extremes of pH, organic solvents and other denaturing agents (Wooley *et al.,* 1942).

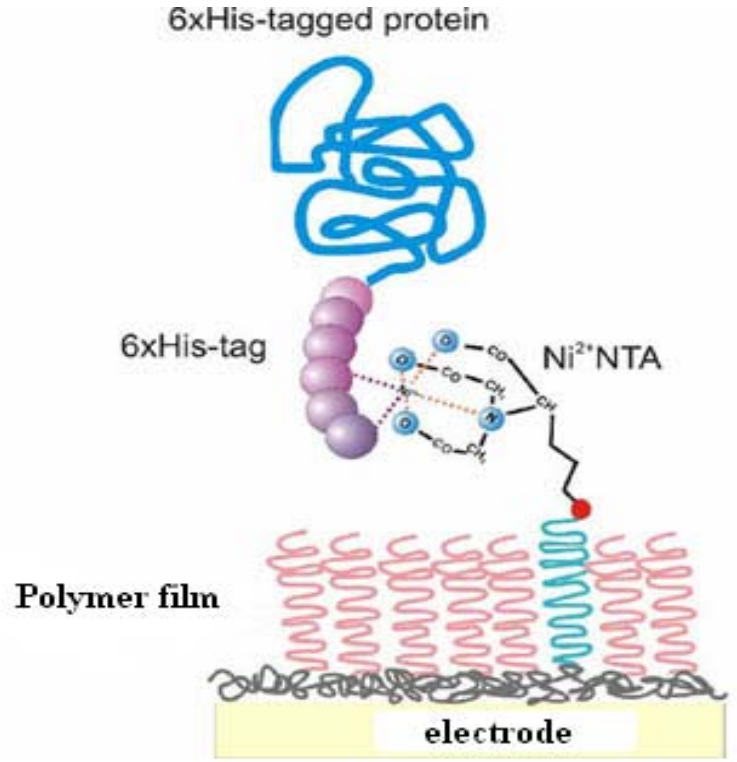

Fig 2.27 Attachment of a biomolecule on a polymer coated electrode by means of a His_6 tag.

Biotin is a 244 Da naturally occurring vitamin found in every living cell with a molecular composition of $C_{10}H_{16}N_2O_3S$ Avidin is a basic glycoprotein found in the egg white and tissues of birds, reptiles and amphibian with an isoelectric point of approximately 10. It is tetrameric molecule with four identical subunits having a combined mass of Mr~60 kDa (Wooley *et al.,* 1942). Each subunit consists of 128 amino acids and binds one molecule of biotin (DeLange and Huang, 1972). Avidin is highly glycosylated with carbohydrate accounting for about 10% of the total mass of avidin. The heterogeneous oligosaccharide is linked to Asn 17 of each subunit of avidin (Wooley *et al.,* 1942).

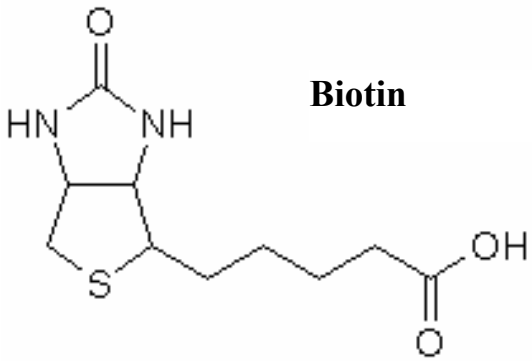

Biotin

The avidin family includes streptavidin and neutravidin. NeutrAvidin has a mass of 60,000 Da and is an engineered deglycosylated form of avidin. As a result, lectin binding is reduced to undetectable levels,

yet biotin-binding affinity is retained because the carbohydrate is not necessary for this activity. NeutrAvidin Protein offers the advantages of a neutral pI to minimize nonspecific adsorption, along with lysine residues that remain available for derivatisation or conjugation. NeutrAvidin Protein yields the lowest nonspecific binding among the known biotin binding proteins. For the reasons mentioned above, NeutrAvidin was used in the fabrication of sensor platforms (Hiller, 1987).

The simplest way of using the neutravidin/biotin reagents is to biotinylate the polymer surface, bind to the neutravidin and finally allow binding to the biotinylated antibody. The commercial kit BK101, purchased from Sigma, employs an NHS activated biotin. *N-hydroxysuccinimide* (NHS) esters of biotin are available with varying properties and spacer arm lengths (Mock and Horrowitz, 1990). The biotin used throughout this project was a water-soluble Sulfo-NHS-Biotin with a caproyl spacer from hexanoic acid, between the NHS group and biotin, which greatly diminishes steric hindrance present at the biotin binding sites of neutravidin (Green, 1971). The NHS group targets primary amines on deposited polyaniline and attaches biotin to it. In the same way, antibodies were biotinylated using the same commercial kit. Following labelling, the biotinylated antibodies were separated from unreacted ones by a fast gel-filtration step and the extent of biotinylation was determined by an avidin-HABA assay since 'over-biotinylation' may damage the antibody.

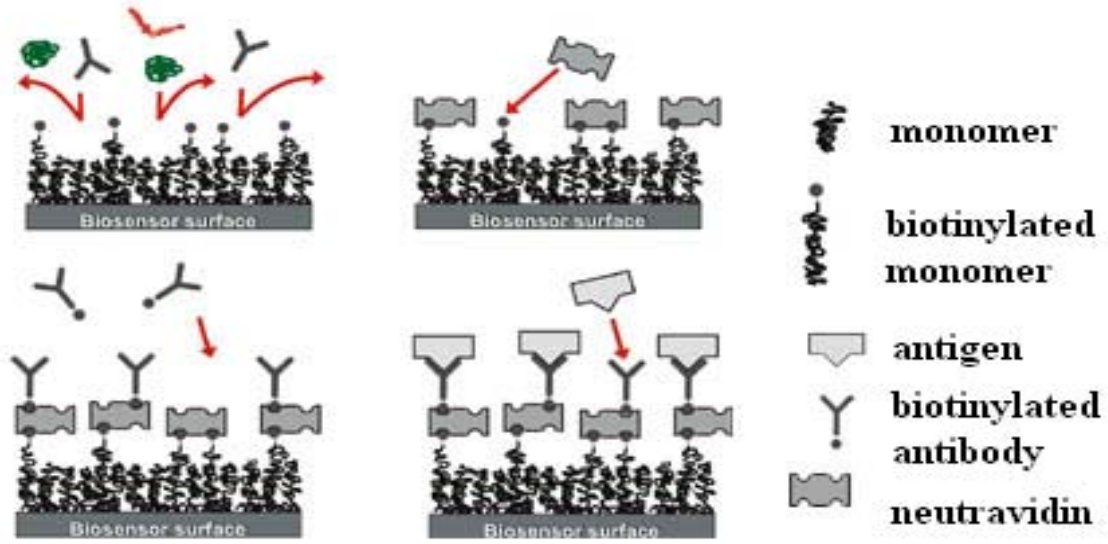

Fig 2.28 Schematic representation of a complete immunosensor.

2.7.4 Fluoroquinolones – Ciprofloxacin

The quinolones are a family of broad spectrum antibiotics, based on nalidixic acid. They are antimicrobial agents effective in the treatment of selected community-acquired and nosocomical infections and are usually administered orally, although some can be given intravenously for treatment of serious infections. This class of antibiotics acts bacteriostatically or bactericidally on both Gram positive and Gram negative bacteria and depending on the concentration, operate by inhibiting the bacterial DNA gyrase and/or topoisomerase II enzyme. In this way the antibiotic inhibits DNA replication and transcription of the bacterium. The quinolones are divided into generations based on their antibacterial spectrum. The earlier generation agents have a narrower spectrum of potency than most of the later ones (Hooper, 1999; Owens and Ambrose, 2000).

The majority of quinolones in clinical use belong to the subset of fluoroquinolones, named after the fluoro group attached to the central ring system. Ciprofloxacin, the agent agent used in this study, is a second generation fluoroquinolone. Ciprofloxacin is the generic international name for the synthetic antibiotic manufactured and sold by Bayer Pharmaceutical under the brand names Cipro® and Ciproxin® (as well as a number of other brand names, for example, as veterinary drugs) (Mason *et al.,* 1995). Ciprofloxacin is bactericidal and its mode of action depends on blocking of bacterial DNA replication by binding itself to DNA gyrase.

At one time ciprofloxacin was considered relatively safe. With increasing experience however, a variety of side effects have become evident, including nausea, vomiting, diarrhoea, abdominal pain, rash, headache, and restlessness. Many of these side effects are also associated with a number of other conditions common with many antibiotics. Because of its potency and broad spectrum activity, ciprofloxacin was initially reserved as a "last-resort" drug for use on difficult and drug-resistant infections. As with any antibiotic, however, increasing time and usage has led to an increase in ciprofloxacin-resistant infections, mainly in the hospital setting. Also implicated in the rise of resistant bacteria was the use of lower-cost, less potent fluoroquinolones, and the widespread addition of ciprofloxacin and other antibiotics

to the feed of farm animals, which led to greater and more rapid weight gain, for reasons which are not yet fully clear (Campi and Pichler, 2003).

Bearing in mind the side effects of ciprofloxacin as well as the increase in the number of bacteria that are non-sensitive to it, it is important for the medical and food industries to control its levels in food. Since ciprofloxacin is an important veterinary antibiotic for livestock, it is of paramount significance to monitor its levels in meat and milk products available for public consumption.

2.7.5 Myelin basic protein

Myelin basic protein (MBP) is a protein believed to be important in the process of myelination of nerves within the central nervous system (CNS). The myelin sheath of the central nervous system (CNS) is formed by membranes that extend from oligodendrocytes and that wrap concentrically (up to a hundred times) around nerve fibers (Arroyo and Scherer, 2000) (Fig 2.29).

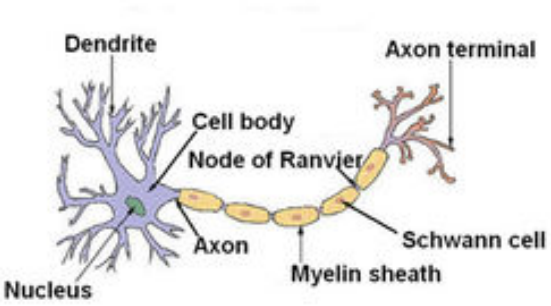

Fig 2.29 Structure of a typical neuron.

The myelin sheath of the peripheral nervous system is similar in overall structure, but differs somewhat in molecular composition (Arroyo and Scherer, 2000). Most of CNS myelin is made up of lipid (up to 70% by dry weight), making it unusual compared to other cellular membranes. The two major protein components of CNS myelin are myelin basic protein (MBP) and proteolipid protein (PLP), occurring in roughly equimolar proportions, although there are many other proteins associated with both compact and non-compact regions of myelin (Kramer *et al*., 2001).

The main consequence of a myelin layer is an increase in the speed at which impulses propagate along the myelinated fibre. Along unmyelinated fibres, impulses move continuously as waves, but, in myelinated fibers, they hop (or "propagate by saltation"). Myelin increases resistance by a factor of 5,000 and decreases capacitance

by a factor of 50. Myelination also helps prevent the electrical current from leaving the axon. When a peripheral fiber is severed, the myelin sheath provides a track along which regrowth can occur. Unmyelinated fibers and myelinated axons of the mammalian central nervous system do not regenerate (Baumann and Pham-Dinh, 2001).

Demyelination, or the loss of the myelin sheath insulating the nerves, is the hallmark of some neurodegenerative autoimmune diseases, including multiple sclerosis, transverse myelitis, adrenoleukodystrophy and stroke (Lamers *et al.,* 2003). Stroke and multiple sclerosis are of particular interest to this thesis.

A stroke, also known as cerebrovascular accident (CVA), is an acute neurologic injury in which the blood supply to a part of the brain is interrupted. That is, stroke involves sudden loss of neuronal function due to arterial or even venous disturbance in cerebral perfusion. The part of the brain with disturbed perfusion no longer receives adequate oxygen. This initiates the ischemic cascade which causes brain cells to die or be seriously damaged, impairing local brain function. An indirect result of stroke is active myelin breakdown or demyelination and therefore the levels of myelin basic protein in cerebral spinal fluid (CSF) can act as markers for stroke (Lamers *et al.,* 2003).

Normal values of MBP in CSF are below 4ng/ml, whilst values between 4 and 8ng/ml may indicate a central nervous system trauma, chronic breakdown of myelin, or recovery from a central nervous system trauma acute episode. If the myelin basic protein levels are greater than 9 ng/ml, active demyelination occurs (Lamers *et al.,* 2003). This value range can be used in an immunosensor platform for MBP so as to obtain information, which can be used to determine the type of a stroke, the onset of occurrence and the extent of brain damage as well as to allow a physician to determine quickly the type of treatment required by the patient.

2.7.6 Cancer antigen 125

CA-125 is an abbreviation for cancer antigen 125, which is a tumour marker that may be elevated in the blood of patients with specific types of cancer. It is a mucinous

glycoprotein and the product of the MUC16 gene (Beatrice *et al*, 2002). CA-125 was initially detected using the monoclonal antibody designated OC125. Dr. Robert Bast and his research team first isolated this monoclonal antibody in 1981 (Bast *et al.*, 1981).

Raised levels of CA-125 are most often associated with ovarian cancer; however its levels may be elevated in other malignant cancers such as those originating in endometrium, fallopian tubes, lungs, breast and gastrointestinal tract (Niloff *et. al*., 1984). Raised levels of CA-125 do not necessarily imply the presence of a malignant condition. CA-125 may also be elevated in a number of relatively benign conditions, such as endometriosis (Bagan, 2008), several diseases of the ovary, and pregnancy (Sarandakou, 2007) as well as in the presence of any inflammatory condition in the abdominal area, both cancerous and benign. For this reason, monitoring CA-125 levels in a patient's blood does not provide definitive answers as to the condition someone is suffering from. Furthermore, CA-125 is not perfectly specific for cancer nor is it perfectly sensitive since not every patient with cancer will have elevated levels of CA-125 in the blood. For example, 79% of all ovarian cancers are positive for CA-125, whereas the remainder does not express this antigen at all.

CA-125 is clinically approved and useful for following the response of an ovarian cancer to treatment and detecting its recurrence. However its prognostical role for early detection of ovarian cancer is controversial and has not yet been adopted for widespread screening efforts in asymptomatic women due to its lack of specificity and its inability to detect early stage cancers. An operation would be necessary to confirm that a woman with elevated CA-125 has ovarian cancer, with the associated risk of surgical complications or even death. In addition, even if cancer was confirmed in such circumstances, it usually would be at an advanced stage where therapy is less effective. Having said that elevated levels of CA-125 can be an indication of a malignancy and women, especially post-menopausal individuals, should in such cases receive further diagnostic screening or treatment. In pre-menopausal women, the test is less reliable as values are often elevated due to a number of non-cancerous causes. The range of CA-125 values that are considered normal is between 0 and 35 units/ml of blood (Amin *et. al.*, 1992).

Chapter 3

Materials and Methods

3.1 Reagents

Orthophosphoric acid, acetic acid, sodium chloride, sodium di-hydrogen orthophosphate 1-hydrate and di-sodium hydrogen orthophosphate 12-hydrate, all analytical grade, were purchased from BDH (Poole, Dorset, UK).

Myelin Basic Protein (from mouse, M2941), Myelin basic protein antibody (monoclonal anti-MBP from rat, M9434), CA-125 (ovarian carcinoma cell line, A97180H), monoclonal antibody to CA-125 (from mouse, M86294M), polyclonal IgG for the control sensors exposed to MBP and CA-125 (from mouse, I5381), ferrocene carboxylic acid, aniline, the biotinylation kit (part no. BK101), biotin 3-sulfo-N-hydroxysuccinimide, bovine serum albumin (BSA), potassium hexacyanoferrate, potassium ferricyanide, potassium fluoride, sodium acetate and 3-aminobenzylboronic acid (aniline-boronic acid) were obtained from Sigma-Aldrich, Gillingham, Dorset, UK.

Prostate specific antigen (PSA) and monoclonal antibodies against PSA were developed and supplied by Canag Diagnostics, Ltd. (Gothenburg, Sweden).

Potassium chloride, hydrochloric acid and *o*-phenylenediamine were obtained from Fisher Scientific Ltd, (Loughborough, UK).

Immunopure neutravidin was purchased from Perbio Sciences UK Ltd (Northumberland, UK).

Ciprofloxacin, a fluoroquinolone antibiotic, was provided by the Applied Molecular Receptors group in Barcelona. Antibodies raised in rabbits against a fluoroquinolone derivative linked to Horseshoe Crab Hemocianyn were supplied by the same partner.

All chemicals were used without further purification.

3.2 Materials

Silver conductive paint (Electrolube Ltd., Berkshire, UK) and multicore wires were purchased from Maplin Electronics Ltd. (Luton, UK) were used for the construction of gold-sputter coated working and counter electrodes.

Epoxy resin was purchased from RS (Corby, UK) and was used for the construction of gold-sputter coated working and counter electrodes.

Centrifugal filters were obtained from Amicon Ltd. (Stonehouse, Gloucestershire, UK) and were used to remove sodium azide from antibody samples.

All water used was obtained from an Elga Purelab UHQ-II Water System (Vivendi Water Systems, High Wycombe, Buckinghamshire, UK).

Commercial screen-printed carbon ink electrodes containing carbon working and counter electrodes and an Ag/AgCl reference electrode were obtained from Microarray Ltd (Manchester, UK).

Project specific gold and platinum on a silicon substrate electrodes were provided by the Tyndall Institute (Cork, Ireland).

The REF321 Ag/AgCl type reference electrode was purchased from Radiometer Analytical SAS (Villeurbane, France) and was used for all electrode interrogations involving gold-sputter coated working and counter electrodes as well as project specific electrodes.

Menzel ‘Superfrost’ twin frosted-end microscope slides were purchased from Fisher Scientific UK Ltd (Loughborough, UK) and were used for the construction of gold-sputter coated working and counter electrodes.

3.3 Buffers and Solutions

A phosphate buffer PBS (pH 7.4) of di-sodium hydrogen orthophosphate 12-hydrate ($5.3x10^{-2}$M), sodium dihydrogen orthophosphate 1-hydrate ($1.3x10^{-2}$M) and sodium chloride (0.1M) was prepared in deionised water.

An acetate buffer (pH 5.0) of sodium chloride ($4x10^{-2}$M), sodium acetate ($4x10^{-2}$M) and acetic acid (aq) ($4x10^{-2}$M) was prepared in deionised water.

A buffer (pH 2.7) of orthophosphoric acid ($9x10^{-4}$M), sodium dihydrogen orthophosphate ($8x10^{-3}$M) and of potassium chloride ($7x10^{-3}$M) was prepared in deionised water.

A solution (pH 1.0) of potassium chloride (0.5M) and of hydrochloric acid (0.3M) was prepared in deionised water.

5mM *o*-phenylenediamine monomer solutions were prepared in pH 7.4 phosphate buffer for the electropolymerisation of *o*-phenylenediamine and insulation of planar carbon electrodes.

1mM ferrocene carboxylic acid solutions were prepared in pH 7.4 phosphate buffer for further electrochemical characterisation on all types of electrodes throughout sensor fabrication.

0.2M aniline hydrochloride monomer solutions were prepared in pH 5.0 acetate buffer, pH 2.7 buffer and pH 1.0 buffer for the electrogeneration of polyaniline and the determination of the optimal conditions of aniline deposition on the surface of the electrodes.

Biotin 3-sulfo-N-hydroxysuccinimide ester sodium salt solutions were prepared for the biotinylation of polyaniline modified (pH 1.0 chloride monomer solution) carbon sensors at a concentration of 1mg ml^{-1} in distilled deionised water.

Neutravidin biotin-binding protein solutions were prepared in distilled deionised water at 10μg ml^{-1}.

Antibodies against PSA, ciprofloxacin, MBP and CA-125 were supplied with sodium azide preservative and reconstituted in pH 7.4 phosphate buffer. These were stored at -20ºC in working aliquots following their biotinylation for non covalent affinity attachment to the PANI-modified working electrode. Prior to biotinylation sodium azide was removed by centrifugation since the presence of the preservative can impair the efficiency of the biotinylation process.

All solutions used for biotinylation of antibody and determination of extent of biotinylation were prepared following the instructions provided with the Immunoprobe biotinylation kit.

BSA blocking solution was prepared at a concentration of 10^{-6}M in de-ionised water.

All antigen solutions for A.C. impedimetric measurements were prepared by diluting the required concentration of antigen in 30ml of PBS pH 7.4.

Potassium hexacyanoferrate (IV) (10mM) and potassium ferricyanide (III) (10 mM) in 50ml PBS 7.4 buffer were utilised as a redox couple for impedimetric measurements.

Aniline boronic acid was prepared by dissolving 110mg of 3-aminobenzylboronic acid and 29.5mg of potassium fluoride in10ml of deionised water. The final pH of the solution was adjusted to 1.5 by the addition of hydrochloric acid.

3.4 Apparatus

3.4.1 Gold sputter coater

An Agar B7341 Automatic Sputter Coater (Agar Scientific Ltd., Essex, UK), in conjunction with a Pfeiffer Rotary Vane Vacuum Pump (Pfeiffer Vacuum Ltd., Newport Pagnell, UK), was used for the preparation of gold sputter-coated working and counter electrodes (Fig 3.1).

Fig 3.1 The Agar Auto Sputter Coater.

3.4.2. Potentiostat

For all electrochemical studies a Sycopel Scientific AEW2-10 Potentiostat was used (Sycopel Scientific Ltd., Washington, Tyne & Wear, UK) (Fig 3.2).

Fig 3.2 Sycopel Scientific AEW2-10 Potentiostat.

3.4.3 Frequency response analyser

AC Impedance measurements were performed using an ACM Auto AC DSP frequency response analyser (Grange-over-Sands, Cumbria, UK) (Fig 3.3), linked to an IBM compatible PC utilising ACM software for data acquisition.

Fig 3.3 ACM Instruments Gill AC frequency response analyzer.

3.4.4 Sonication equipment

A bench-top ultrasonic bath was initially employed for the sonochemical fabrication of microelectrode arrays. A 25 kHz Transsonic T460 sonication bath was used.

The rest of the sonication experimental set ups were built using a custom-made 2 kW, 25.1 kHz ultrasound tank (Fig 3.4) with internal dimensions of 750 x 750 x 600 mm (working volume 750 x 750 x 500 mm) (Ultrawave Ltd., Cardiff, UK), employing 10 transducers (horns) geometrically arranged and bonded to the base of the stainless steel housing. The tank incorporates a frequency sweep of ± 1 kHz in 100 Hz steps three times per second, and a temperature control system allowing the temperature of the water to be maintained at 25□C. Software incorporated within the power generation system allows sonication times to be varied between 1 and 99 seconds and for the power to be varied between 50 and 100 % of the maximum power output. The

software also supports a square wave sonic pulse (50% duty cycle) to facilitate de-gassing of the water, which was carried out for 60 minutes prior to use.

Fig 3.4 Custom built sonication tank.

As the purity of the water is critical to the efficiency of the cavitation process, ultrasound tank water was continually purified via a 100 µm particulate filter, a 'CC9' carbon filter and a 'DC9' deioniser (Purite Ltd., Thame, Oxfordshire, UK), producing water with a conductivity of <0.1 µS.cm^{-}1 (>18 MΩcm^{-1}), confirmed by an integrated conductivity meter (Fig 3.5).

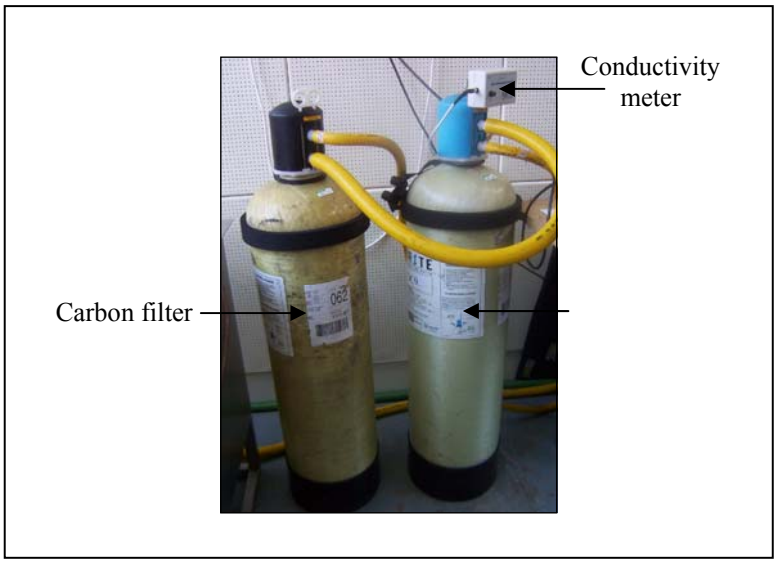

Fig 3.5 Water purification system for 2kW ultrasound tank.

A perforated stainless steel baffle was also custom designed and built to minimise the formation of standing waves and wave reflections from the tank walls, thus improving ultrasound homogeneity (Fig 3.6). Baffle sides were set at a distance of 50 mm from tank walls, including the base which was separated by vibration damping rubber feet.

Fig 3.6 Sonication tank baffling.

3.4.5 Quartz Crystal Microbalance

Aniline deposition on the surface of carbon electrodes was monitored with the use of a quartz crystal microbalance (QCM) at the University of Leeds. The specific QCM used was an RQCM from Maxtek (Cypress, CA, USA).

Fig 3.7 RQM Real-Time Crystal Frequency, Mass and Conductance Measurement Analyser, research crystals and crystal holder.

3.4.6 Electrodes

The ground glass ends of twin frosted microscope slides (cut to 2x1.5cm in size) were coated with gold using the Agar Auto sputter coating machine in order to render one face electrically conductive. Multicore wires were attached to this face using silver conductive paint. Glass/wire junctions were coated with epoxy resin in order to insulate the joint and to provide additional mechanical strength (Fig 3.8).

Platinum and/or gold electrodes on silicon substrates as provided by Tyndall Institute (Cork, Ireland) were also used. They were labeled P3, P4, P5 and P10 by their manufacturer and hence these labels were retained throughout the studies for simplicity. Schematics of these four types of electrodes are shown in the following figures (Figs 3.9, 3.10, and 3.11). The surface area of the P3 and P4 electrodes was $0.785mm^2$. P5 electrodes were interdigitated electrodes. Redox cycling at the surface of interdigitated electrodes results in enhanced current due to close proximity of working and counter electrodes (D.G.Sanderson et al, 1985). The total surface of the working electrode digits is $0.8mm^2$. Finally, P10 electrodes are microelectrode arrays whose advantages have been discussed in the previous chapters. The total surface of the microelectrodes is roughly 0.8 mm^2. Despite their different geometries and consequently electrochemical properties all types of project specific electrodes have similar surface areas.

Screen printed carbon ink electrodes were purchased from Microarray Ltd. (Manchester, UK) (Fig 3.12). The surface area of the working electrodes was $0.2178cm^2$.

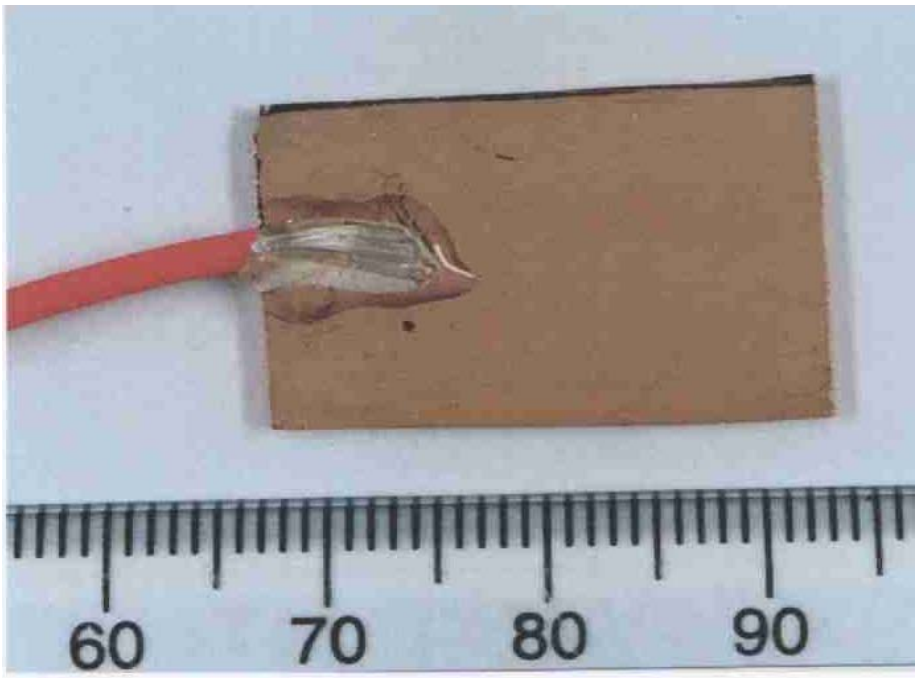

Fig 3.8 Gold coated glass slide.

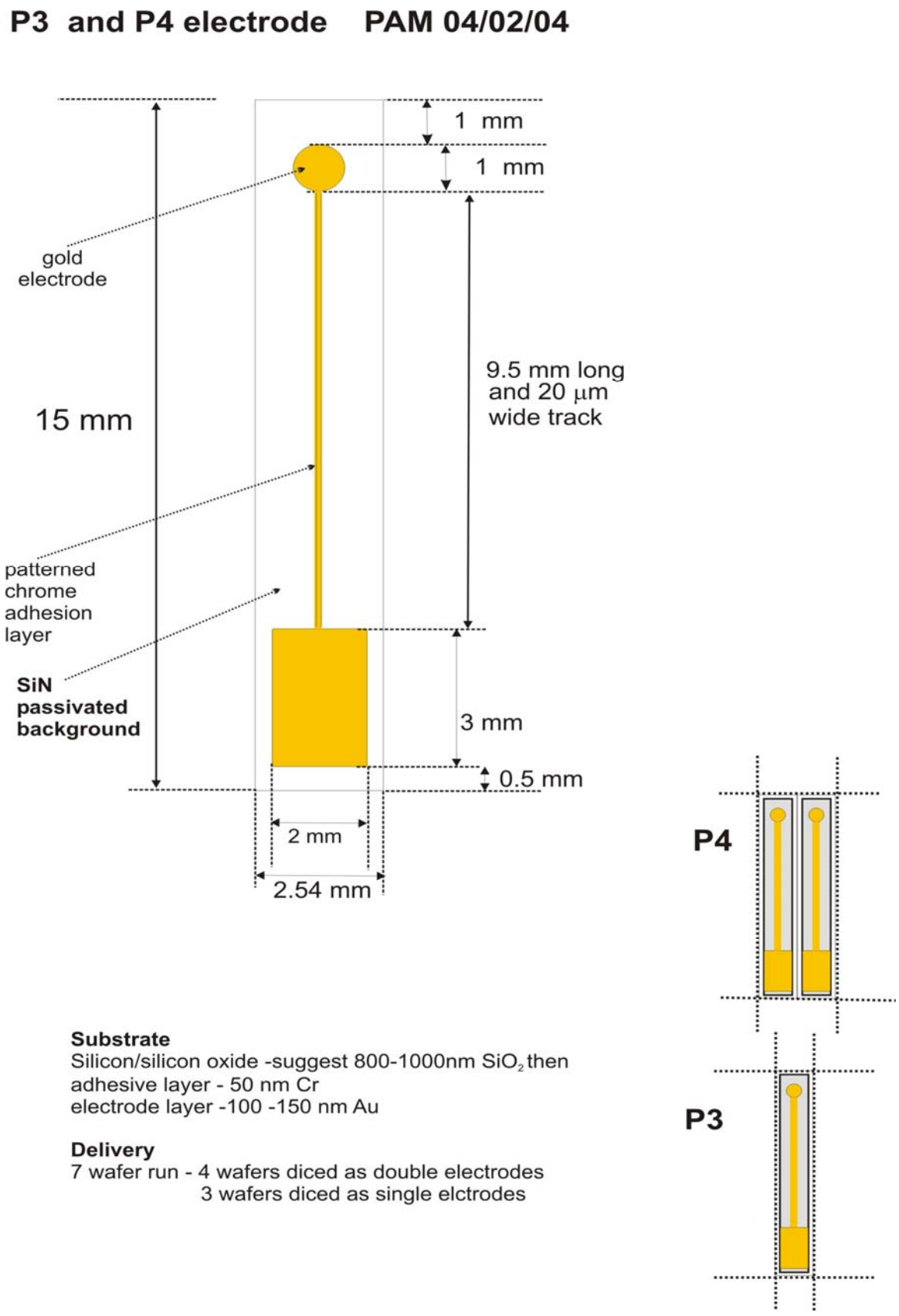

Fig 3.9 P3 and P4 electrodes.

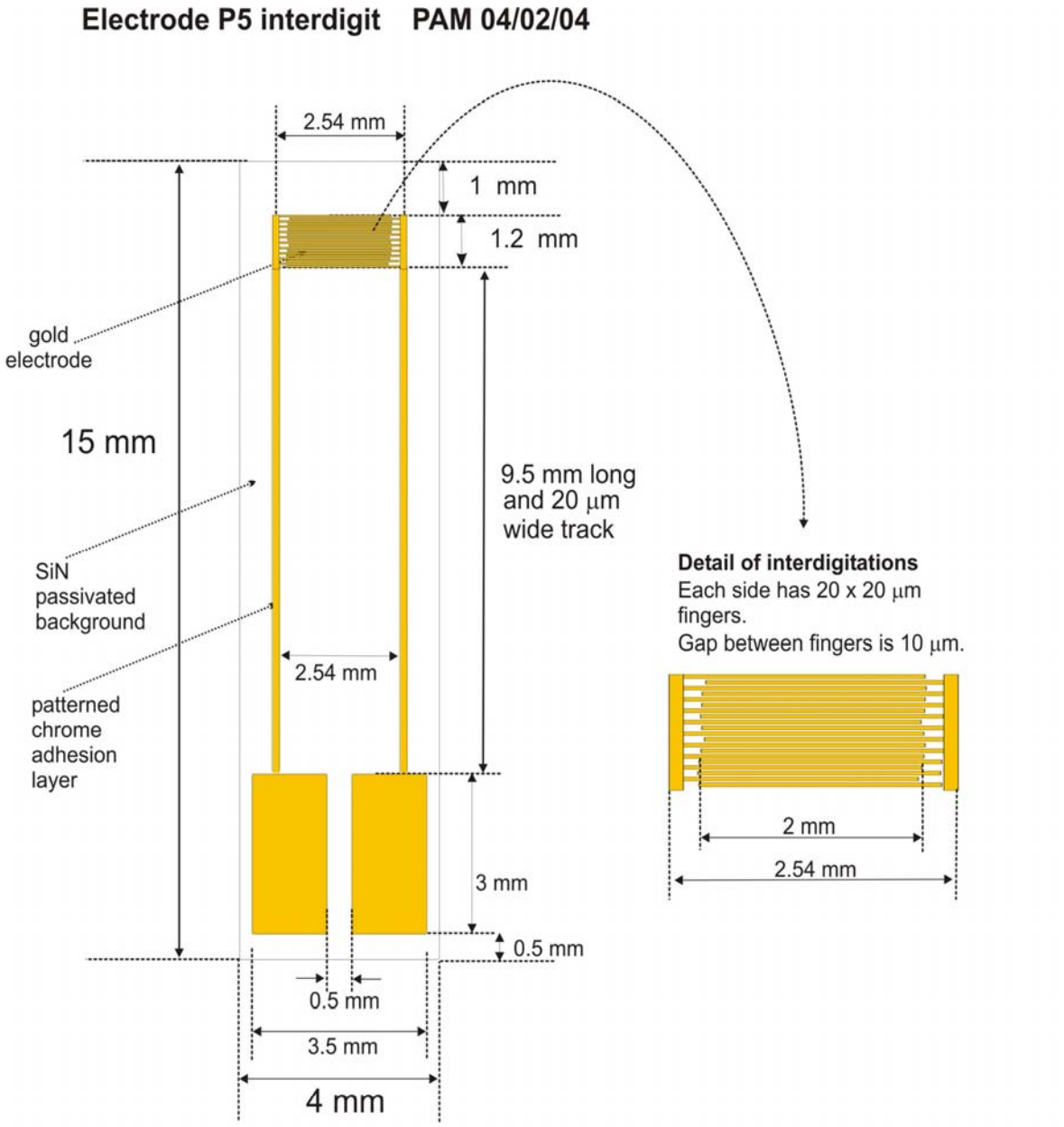

Substrate
Silicon/silicon oxide -suggest 800-1000nm SiO_2 then
adhesive layer - 50 nm Cr
electrode layer -100 -150 nm Au

Delivery
7 wafer run - wafers diced as single electrodes,
15 x 4 mm

Fig 3.10 P5 electrodes.

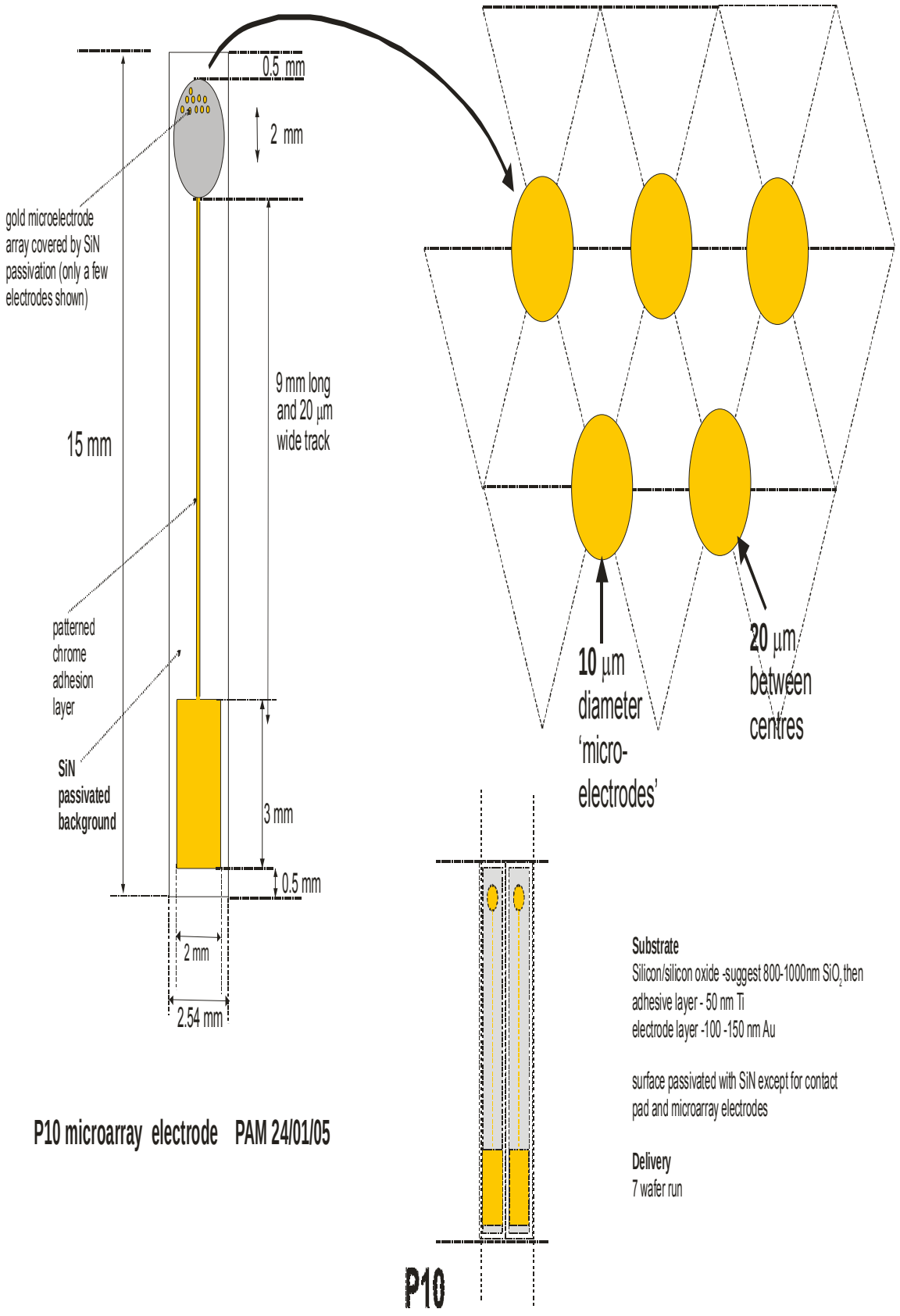

Fig 3.11 P10 electrodes.

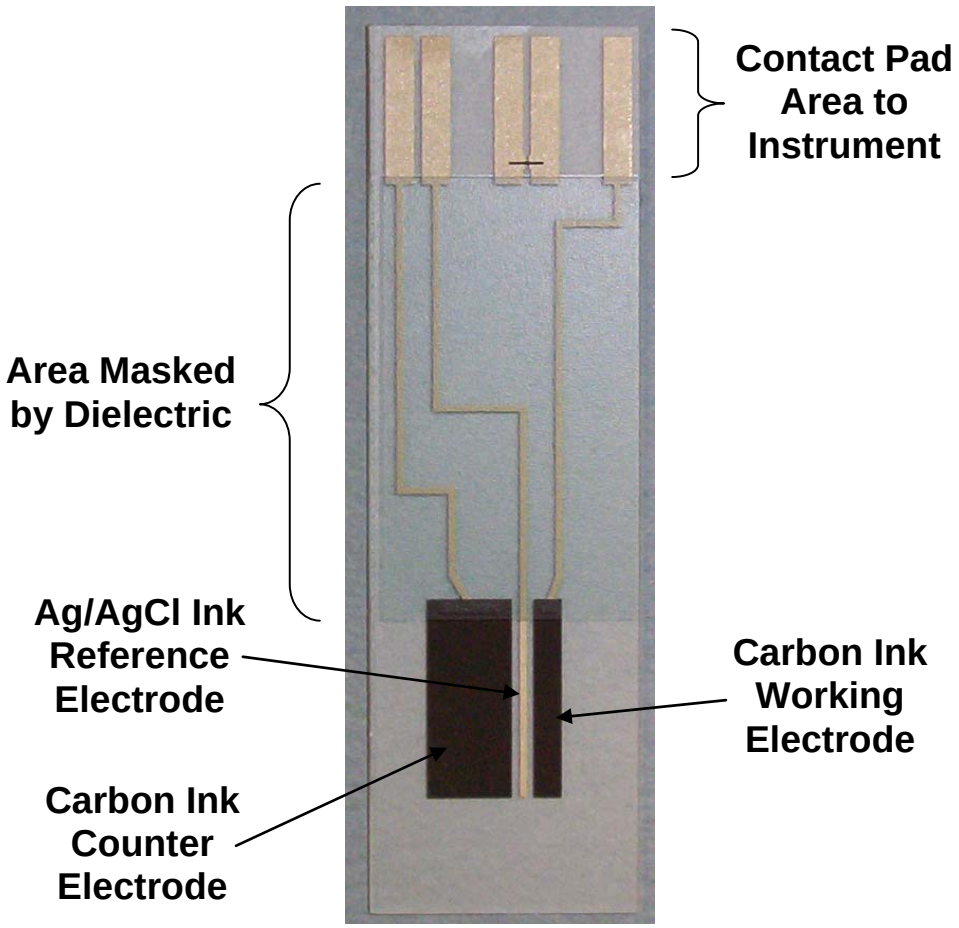

Fig 3.12 Screen-printed carbon sensor.

3.5 Experimental methodology

3.5.1 Ultra-thin polymer film coatings

• ***Preparation of poly-o-phenylenediamine (or polydiaminobenzene) films***

For the electrochemical characterization of gold sputtered glass electrodes, project specific electrodes and carbon ink electrodes prior to and following deposition of insulating *o*-phenylenediamine a 5mM *o*-phenylenediamine solution was prepared in pH 7.4 phosphate buffer. A three electrode system (working, counter and reference electrode) was used. In the case of glass and project specific electrodes an external reference electrode was employed. For carbon electrodes, the counter, working and reference electrodes were incorporated onto the same polycarbonate substrate.

Homogeneous insulation of the working electrode surface was achieved by sequentially scanning the working electrode potential from 0mV through to +900mV (vs. Ag/AgCl) and back to the starting potential at a scan rate of $50mVs^{-1}$ for 100 sweeps. Film growth was terminated at 0mV vs Ag/AgCl. Excess monomer was washed off with deionised water and the electrode was left to dry in air.

Studies towards the optimization of electrodeposition of *o*-phenylenediamine were subsequently carried out by adjusting the potential scan range. The working electrode potential was scanned from 0mV through to +900mV vs. Ag/AgCl and back to the starting potential at a scan rate of $50mVs^{-1}$ for 100 sweeps. Film growth was once again terminated at 0mV vs Ag/AgCl.

The electrochemical behaviour of the working electrode was recorded prior to and following *o*-phenylenediamine deposition via one cyclic potential sweep between -1000 and +1000mV vs Ag/AgCl at a scan rate of $50mVs^{-1}$ using the same three electrode arrangement as for the deposition. A potential scanning range between -200 and +600mV vs Ag/AgCl at a scan rate of $50mVs^{-1}$ was also employed. The electrochemical characterization was carried out in a ferrocene carboxylic acid (FCA) solution in PBS 7.4 buffer, which was prepared as described in Section 3.3.

• ***Preparation of polyaniline films***

For the fabrication of immunosensor platforms a conducting film of polyaniline was deposited on the surface of the screen-printed carbon electrodes. In order to optimise the conditions under which aniline is deposited on the surface of the working electrode a number of different pH buffers were used to prepare a 0.2M aniline solution, namely an acetate buffer pH5.0, a pH2.7 buffer and a pH1.0 buffer as detailed in Section 3.3.

Cyclic voltammetry was performed from -200mV to +600mV and back to the starting potential at a scan rate of $50mVs^{-1}$. A linear sweep from -200mV to +600mV vs. Ag/AgCl at $50mVs^{-1}$ was performed at the end of cyclic voltammetry to leave the polyaniline in its conductive emeraldine salt form. Excess monomer was washed off with de-ionised water and the electrodes were left to dry in air.

The number of potential sweeps used to deposit aniline monomer on the surface of the working electrode was also altered in the quest to optimise deposition conditions. Aniline was deposited by cycling the potential for 5, 20, 25, 30 or 100 cycles.

The electrochemical behaviour of the working electrode was recorded prior to and following aniline deposition after 5, 20, 25, 30 or 100 potential cycles via one cyclic potential sweep between -200 and +600mV vs Ag/AgCl at a scan rate of $50mVs^{-1}$ using the same three electrode arrangement as for the monomer deposition. The electrochemical characterization was carried out in a ferrocene carboxylic acid (FCA) solution in PBS 7.4 buffer.

3.5.2 Microelectrode array fabrication

Screen printed carbon electrodes were coated with an insulating film of *o*-phenylenediamine as described in section 3.5.1. The polymer modified electrodes were suspended in the centre of the sonication tank (Section 3.4.4), attached to a plastic support. A mechanical movement system was custom made to rotate the suspended electrodes throughout the sonication period so as to achieve an evenly distributed proportion of cavitation across the electrode surface (Fig. 3.13). This

minimised variability of the fabricated microelectrode sensors and also helped to remove any standing wave effects (i.e. node and anti-node regions) (Mills, 2005).

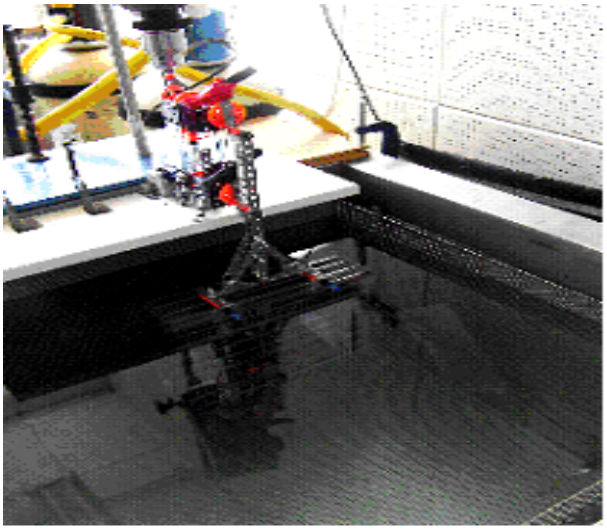

Fig 3.13 Rotating device for the movement of sensor sheets in the sonication tank.

The water in the tank was subjected to rigorous cleaning regimes. Organics and ions were removed through a two-stage ion exchange resin filter cartridge system and thermostated at 25°C. The internal tank pulse degassing system was used for 30 minutes prior to sonication to remove air bubbles in the liquid medium.

Sonochemical ablation optimization studies were performed by adjusting the sonication time, tank power and electrode positioning in the tank independently and in conjunction with each other. In order to achieve the desired population density and size of microelectrode templates, the duration of the sonochemical ablation was varied from 10 to 60 seconds while the power employed was increased from 50% up to 100% of the maximum intensity available.

The electrochemical behaviour of the microelectrode arrays fabricated by sonochemically ablating the polymer modified surface of the carbon electrodes was recorded prior to and following sonication by one cyclic potential sweep between -200 and +600mV vs Ag/AgCl at a scan rate of $50mVs^{-1}$. The electrochemical characterization was carried out in a ferrocene carboxylic acid (FCA) solution in PBS 7.4 buffer.

3.5.3 Immunosensor fabrication

Immunosensor platforms were fabricated in two different ways. The first one, used for the majority of the antibody-antigen pairs under investigation, employed the biotin-avidin technology to site-specifically immobilise biotinylated antibodies on the surface of the polymer modified electrodes. The second one was employed only in the fabrication of an immunosensor for CA-125 and took advantage of the antibody binding properties of aniline boronic acid.

3.5.3.1 Antibody immobilization using the avidin-biotin technology

Immunosensor fabrication using the avidin-biotin technology involves five distinct steps as described below, following the standard protocol of the kit.

Step 1. Antibody Biotinylation

Antibody biotinylation was performed prior to all other sensor fabrication steps and the biotinylated bioreceptors were stored frozen in working aliquots of approximately 1mg ml^{-1} at -20ºC. To remove sodium azide preservative, the antibody was subject to gel-filtration using a Sephadex (G25) gel-filtration column. Sodium azide can have adverse effects on the biotinylation of antibodies.

With the Sigma ImmunoProbe Kit used, biotinylation is performed with BAC-SulfoNHS. This derivative is soluble in water and biotinylation proceeds at near neutral pH values. The reagent is particularly useful when mild reaction conditions are required for the biotinylation of sensitive biomolecules such as antibodies, enzymes and cell surface proteins

Protein Labeling:

A sodium phosphate buffer sachet was reconstituted with 5ml of deionised water to 0.1M.

The IgG (anti-PSA, anti-ciprofloxacin, anti-MBP, anti-CA-125) for biotinylation was prepared at 1mg ml^{-1} in 0.1M sodium phosphate buffer. The A_{280} of an IgG solution at 1mg ml^{-1} is 1.4 (1.0cm path length).

30µl of DMSO were used to dissolve 5mg of BAC-SulfoNHS. 0.1M sodium phosphate buffer was then added to a final volume of 0.5ml and the solution vortexed well. The resulting concentration of BAC-SulfoNHS solution was 10mg ml^{-1}.

19µl of the BAC-SulfoNHS was immediately added to 1ml of the IgG solution with gentle stirring. The reaction mixture solution was incubated with gentle stirring for a further 30 minutes at room temperature or for 2 hours at 2-8ºC.

Isolation of labeled protein:

1 litre of 0.01M PBS was prepared for the fast gel-filtration step whereby the conjugate is separated from the reactants.

The gel filtration column was supported over a 100ml beaker.

The cap was removed from the top of the column. The lower tip of the column was cut open and the excess liquid was allowed to flow through.

The column, provided with the kit, was equilibrated with 30ml of PBS (6 x 5ml).

The reaction mixture (IgG with BAC-SulfoNHS) was applied to the column and the flow-through was collected as Fraction 1.

The column was then eluted with 9 x 1ml of PBS and the flow through was collected as Fractions 2-10. The gel-filtration column was then washed with a further 30 ml of PBS (6 x 5ml) and as such may then be regenerated up to five times.

The protein presence was monitored by measuring the absorbance at 280nm in the UV/visible spectrophotometer.

An elution profile was obtained and the fractions displaying a clear peak at 280nm (thus containing the protein) were pooled.

Working aliquots of 100µl were stored frozen at -20ºC until they were required during the latter stages of sensor fabrication utilizing the biological affinity attachment bridges for their specifically orientated immobilisation.

Determination of the Biotin/Protein ratio:

In order to determine the level of biotinylation in the proteins, it was necessary to measure the protein concentration (absorption at 280nm) and the biotin content (with the avidin-HABA assay).

0.1ml of the pooled biotinylated protein fraction was diluted to 1ml with PBS. The absorbance of this diluted sample was recorded at 280nm using the UV spectrophotometer. This sample was denoted as the 'Protein sample'.

Pronase was reconstituted in 1ml of de-ionised water.

10µl of pronase was added to another 0.1ml sample of the pooled biotinylated protein fraction and incubated overnight at room temperature. This sample was denoted as the 'Biotin sample'. The biotinylated IgG was digested with 0.1% pronase to prevent subsequent steric hindrance of biotin binding to avidin and nonspecific binding of the dye to the biotinylated protein when performing the avidin-HABA assay.

The avidin stock solution was reconstituted by dissolving the avidin in 19.4ml of deionised water.

A blank UV spectrophotometer trace was recorded at 500nm with PBS.

0.1ml of the 10mM HABA solution was added to 3.2ml of the avidin stock solution. The absorbance of the avidin-HABA solution at 500nm was 1.0 (1.0cm path length).

0.9ml of the avidin-HABA reagent was mixed with 0.1ml of PBS (HABA control).

0.9ml of the avidin-HABA reagent was mixed with 0.1ml of the pronase treated sample (Biotin sample).

The absorbance of the HABA control and Biotin sample were recorded at 500nm in 1.0cm path length cuvette allowing for the calculation of the ratio of biotin bound to protein. The pooled biotinylated antibody is then stored at -20ºC in working aliquots of 100µl.

Step 2. Biotinylation of polyaniline films

Polyaniline films were electrogenerated on the surface of the screen printed carbon electrodes as described in section 3.5.1. The polymer films were then exposed to 30µl of biotin 3-sulfo-N-hydroxysuccinimide (10 mg/ml in water) overnight. Biotin couples to the primary amines at the end of the polyaniline chains and secondary amines throughout the polymer. Unbound biotin was rinsed off with deionised water.

Step 3. Neutravidin

Neutravidin biotin-binding agent was prepared in de-ionised water at 10µg ml^{-1}. 30µl of neutravidin were added to the working electrodes of the biotinylated sensors for a 1 hour period. The sensors were then thoroughly flushed with deionised water to remove any non-specifically weakly adsorbed matter.

Step 4. Immobilisation of biotinylated antibody

Antibodies that were prepared as described in step 1 were defrosted and 30µl of the former were added to the neutravidin modified surface of the working electrode for a further 1 hour. Deionised water was once again used to remove any non-specifically bound antibodies. The following schematic is a representation of the assembly on the working electrode (Fig 3.14).

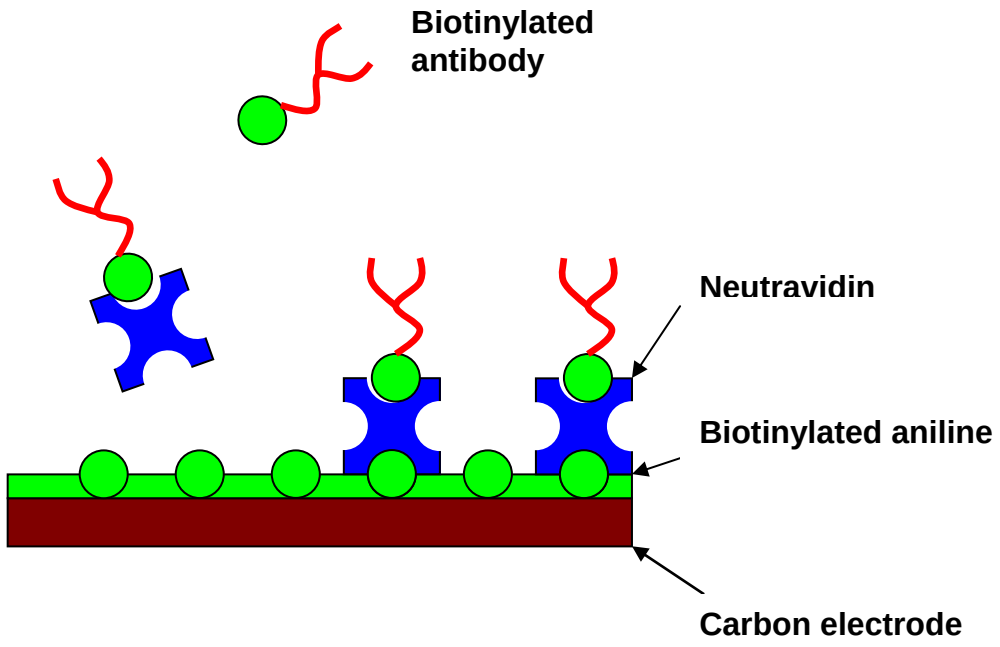

Fig 3.14 Site specific antibody immobilization on an aniline modified carbon electrode using neutravidin/biotin.

Step 5. Blocking with BSA

Bovine serum albumin was used to minimize the effect of non-specific binding of other biomolecules to the surface of the sensor. BSA blocking solution was prepared at a concentration of 10^{-6}M in deionised water. The working electrode of each sensor was exposed to 30µl of BSA for 1 hour before being thoroughly rinsed with deionised water to remove any excess BSA solution.

At this stage the immunosensor platforms were either used immediately in impedance measurements or stored overnight immersed in PBS 7.4 buffer at 4ºC.

3.5.3.2 Antibody immobilization on aniline boronic acid

An alternative approach for immobilising antibodies on the surface of the polymer modified electrode consisted of aniline boronic acid. The latter is a substituted form of aniline that can be electropolymerised on the surface of the working electrodes in the presence of fluoride forming a self-doped polymer layer (Nicolas, 2000). The substituted polymer has the ability to adsorb antibody entities, without the need of biotinylating the antibodies. This approach was employed for the fabrication of immunosensors for CA-125.

Aniline boronic acid was deposited on the electrode surface by cyclic voltammetry between -300 and +1000mV vs Ag/AgCl at $50mVs^{-1}$ for 20 progressive cycles followed by one linear sweep between -300 and +1000mV vs Ag/AgCl at $50mVs^{-1}$. The polymer modified electrode surface was left to air dry and then flushed with deionised water.

30µl of CA-125 in PBS Ph7.4 were added to the modified electrode surface and left to be adsorbed for 1 hour. The sensors were then exposed to 30µl of BSA blocking solution and rinsed with copious amounts of deionised water before being used for the impedance measurements.

3.5.4 Quartz Crystal Microbalance sensor fabrication validation

A quartz crystal microbalance was used to monitor each of the sensor fabrication steps on the surface of a quartz crystal that acted as the working electrode in the system. A thorough flushing regime using distilled de-ionised water was used in between each fabrication step. In all cases sufficient time was allowed as a stabilisation period. The crystal was attached to a crystal holder and the latter was in turn connected to an instrument that provides measurements for crystal frequency and crystal resistance thus relating deposition time in minutes of material on the surface of the quartz crystal to a quantifiable signal.

3.5.5 AC Impedance analysis

AC impedance measurements were performed with a Gill AC DSP Frequency Response Analyser performing both Faradaic and non-Faradaic electrochemical impedance spectroscopy (EIS). Impedance measurements were performed in the frequency range of 10,000Hz to 1Hz, 100 data points at 25 points per decade. A sinusoidal potential modulation (+/-5mV amplitude) was superimposed on the formal potential of the redox couple of $[Fe(CN)_6]^{4-}$ / $[Fe(CN)_6]^{3-}$ (+0.22V vs. Ag/AgCl).

A protocol was established for the impedimetric evaluation of the immobilised antibody sensor platforms upon exposure to complementary antigen, along with a series of control experiments devised to validate and verify the specificity of any responses.

Following the immobilisation of antibody receptor molecules, a baseline impedance trace was recorded in a buffer solution alone. This buffer solution contained 10mM $K_4[Fe(CN)_6]$ + 10mM $K_3[Fe(CN)_6]$ as a redox couple in PBS pH 7.4 and no antigen.

Antibody-loaded sensors were then exposed for 30 minute time periods to increasing concentrations of complementary antigen suspended in a PBS pH7.4 buffer solution. After 30 minutes exposure to a single concentration, the working electrode was removed from the antigen solution and flushed with 50ml PBS pH7.4 solution to remove any non-specifically adsorbed or weakly-bound matter. The impedance trace was then recorded in the buffer solution containing 10mM $K_4[Fe(CN)_6]$ + 10mM $K_3[Fe(CN)_6]$ in PBS pH 7.4. This process was then repeated for the full range of antigen concentrations, following exposure to the antibody-loaded sensors.

Simultaneous experiments were also performed for each antigen under investigation using polyclonal IgG serum antibody receptors instead of the specific antibody. The IgG antibody is immobilised at the electrode in an identical manner to the specific sensor under investigation and subject to an identical experimental interrogation protocol. To determine the resultant specific response of the sensors, the IgG sensor response was subtracted from the MAb sensor response.

Results and Discussion

Chapter 4

Electrochemical characterization of the electrodes

4.1 Introduction

As discussed in Chapter 1, an ultimate goal of this research was the fabrication of an immunosensor prototype for the detection of a range of different biomarkers that will be commercially available at a low cost. It follows therefore that an equally cost-effective base electrode material needs to be sought without compromising on the reproducibility and the sensitivity of the final prototype sensor. Towards this end, a wide range of inks and substrate materials may be used for screen printing and mass production of low cost sensor strips

One of the approaches investigated was to utilise screen printed gold, platinum and carbon inks for the fabrication of both planar electrodes and microelectrodes. Gold sputtered glass slides were custom made and were initially used due to their low unit cost and large surface area which rendered them easy to handle. Project specific electrodes provided by the Tyndall Institute in Cork, Ireland were employed afterwards and comprised of gold and platinum screen printed planar electrodes and microelectrodes on a silicon substrate. Finally there has been some attempts of screen printing our own carbon electrodes, however at the end we resolved in purchasing the latter from Microarray Ltd.

An alternative approach involved the fabrication of microelectrodes through the sonochemical ablation of the polymer modified electrode surface. By insulating the electrode surface with a polymer and then blasting it with ultrasound in a sonication tank, numerous cavities are created in the polymer layer, which act as a microelectrode array, providing an inexpensive way of constructing microelectrodes when compared to screen printing technologies and lithographic techniques. This procedure is discussed in detail in the following chapter.

Carbon or metal (such as platinum and gold) inks are commonly used for printing working electrodes. Carbon inks are particularly attractive for sensing applications because they are relatively inexpensive and exhibit lower background currents over a wider potential window than metal electrodes (Niwa and Tabei, 1994). Moreover they

exist in a variety of forms such as glassy carbon, carbon fibres or carbon (graphite) inks (Gilmartin and Hart, 1995).

Such heterogeneity in the surface topography and composition of the various inks strongly affects the electrode kinetics and overall analytical performance of the sensors. It is crucial therefore to investigate and electrochemically characterise the performance and reproducibility of the available sensors at the onset of this research project in the quest for the most suitable one for the impedimetric measurements that were to be carried out. Due to the nature of the latter, the behaviour of the electrodes should be highly reproducible. This is because impedimetric measurements are extremely sensitive and therefore deviations in the electrochemical behaviour of the electrodes or irreproducibility issues in between them could significantly alter the results obtained and hence lead to erroneous conclusions.

Towards this goal, cyclic voltammetry in the presence of ferrocence carboxylic acid was employed on bare electrodes as well as polymer modified electrodes. Polymer deposition on the surface of electrodes served a double purpose. On the one hand, it provided invaluable information on the kinetics on the electrode surface and lead to conclusions on the reliability and reproducibility of each of the electrode types employed. On the other hand, deposition of an insulating polymer film was the first step in the sonochemical fabrication of microelectrode arrays and therefore crucial in its own right, as further discussed in the following chapter.

The insulating polymer used throughout this research project was poly-*o*-phenelynediamine, referred to herein as P*o*PD. The *o*-phenylenediamine monomer (*o*PD) is an aromatic diamine (Fig 4.1) which can be synthesised by nitration and reduction processes involving benzene.

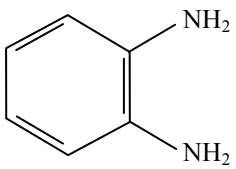

Fig 4.1 *o*-Phenylenediamine monomer (oPD).

Despite the attention P*o*PD has received, there is relative uncertainty as to the precise structure of the polymer. Various analytical methods have been employed to elucidate its nature, including electrochemical techniques (Yano, 1995), quartz-crystal microbalance studies (Dai *et al*, 1998), Raman and UV-Vis spectroscopies (Wu *et al*, 1996; Losito *et al*, 2001), radiometry (Martinusz *et al*, 1995) and scanning tunnelling microscopy (Ogura *et al*, 1995).

Two principal structures of P*o*PD have been suggested (Mederos *et al*, 1999). Oyama and co-workers proposed phenazine as a model compound, comparing the IR absorption spectra of P*o*PD with that of phenazine in KBr pellets (Chiba *et al*, 1987). They found that the IR spectrum of P*o*PD was similar to that of phenazine, and that the absorption peak, indicated at 805 cm^{-1}, could be attributed to the skeletal vibrations of the phenazine rings.

In contrast Yano found that electropolymerised P*o*PD films were soluble in common organic solvents and that a cast film of P*o*PD exhibited reversible redox behaviour, which was accompanied by electrochromism, just as it did before being dissolved. This indicated that the polymer structure remained more or less unchanged and allowed a representative elemental analysis to be carried out via H FT NMR spectra. The polymeric backbone proposed by Yano was a 1, 4-substituted benzoid-quinoid structure (Yano, 1995).

Figs 4.2 and 4.3 illustrate these two suggested polymer configurations for polymerisation at a pH1-7 range (Wu *et al*, 1996; Losito *et al*, 2001).

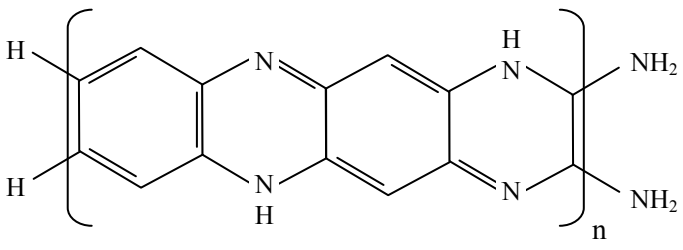

Fig 4.2 Phenazine type structure.

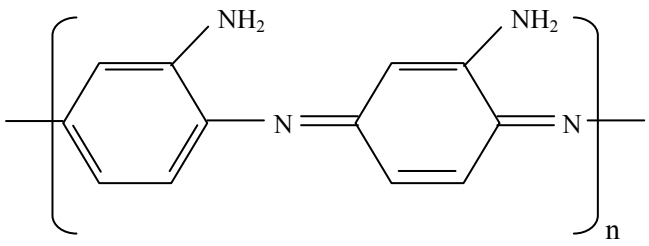

Fig 4.3 1, 4-substituted benzoid-quinoid structure.

Recent studies by Losito and coworkers have shown that the pH value of the solution in which P*o*PD is being formed greatly affects the final structure of the polymer. At acidic pH values the oligomer formation favours phenazine-like subunits, whereas in more basic solutions 1, 4-benzoquinonediimine forming processes are preferred (Locito et al, 2003). P*o*PD films resulting from the latter are less conjugated than the ones formed by phenazine subunits. The degree of conjugation, as further discussed in chapter 2, greatly influences the conductivity of the polymer film.

Much research has been carried out into the possible uses of P*o*PD that has included for example sensor modification for the permselectivity against blood interferents such as ascorbic acid (Garjonte and Malinaukas, 1999), and to H^+ ions for the application of pH sensing (Cheek *et al*, 1983). Other applications reported, include the protection against metal corrosion (D'Elia *et al*, 2001), electrochromic properties (Oyama *et al*, 1988), humidity sensing (Ogura *et al*, 1996), biomimetic molecularly imprinted polymers (Malitesta *et al*, 1999), as well as numerous applications in biosensors (Ekinci *et al*, 2001; Pritchard *et al*, 2004).

Conclusions drawn from the electrochemical characterization prior to and following P*o*PD deposition on the various electrode substrates under different polymerization protocols will not only determine the most suitable substrate material for the fabrication of the immunosensors, but also the optimum electropolymerisation conditions for P*o*PD films.

4.2 Investigation of the reproducibility of different electrodes

4.2.1 Gold sputtered glass slides

Initial investigations into the electrodeposition of insulating films of P*o*PD utilised gold sputter-coated ground glass slide electrodes. The scanning potential was cycled 100 times between 0 and +900 mV vs. Ag/AgCl at a scan rate of 50 mVs^{-1} in a 5mM solution of *o*PD in pH 7.4 phosphate buffer (PBS) (cyclic voltammogram illustrated in Fig 4.5).

As illustrated in Fig 4.5, the monomer can be polymerised to form an insulating film of P*o*PD at the gold coated glass surface. This can be deduced by the large drop in anodic current after completion of each progressive potential sweep and the lack of oxidation peaks following the first potential cycle. Two anodic peaks are exhibited on the first sweep, at 317mV and 550mV (vs. Ag/AgCl), although they are not very pronounced. As further insulating monomer is laid on the surface of the electrode, the electrode becomes progressively passivated and it is apparent that even after the first few cycles the electrode is almost entirely insulated.

The first oxidation peak results from the anodic oxidation of the monomer to form a corresponding cation, which in turn initiates polymerisation via the conventional cationic polymerisation mechanism (Fig 4.4). The lack of any peaks in the cathodic waveform indicates that the process is completely irreversible in nature (Jang *et al*, 1995).

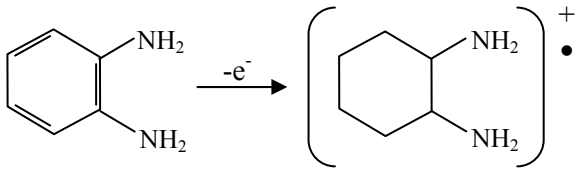

Fig 4.4 Initial oxidation of the oPD monomer to form a radical monocation.

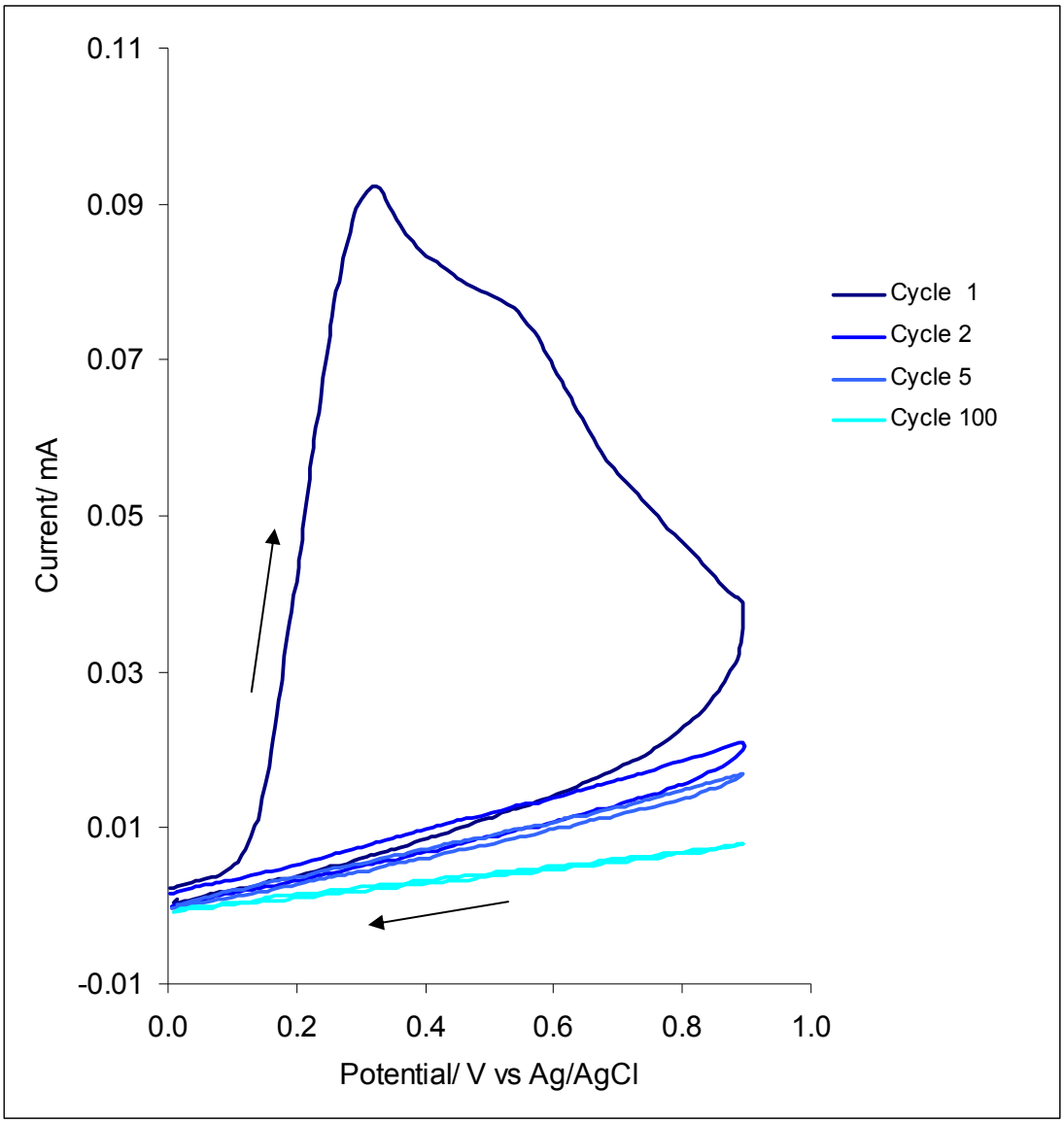

Fig 4.5 Cyclic voltammogram for the electropolymerization of 5mM *o*PD at a gold sputtered glass slide electrode.

[Supporting electrolyte: PBS pH 7.4, Scan rate: 50 mVs^{-1}]

The radical monocation immediately combines via radical coupling with another *o*PD monomer to form one of three possible dimers: the tail-to-tail, the head-to head and the head-to-tail (Fig 4.6). The head-to-tail dimer configuration has been shown to form preferentially in an aqueous solution, since bonding of carbon to nitrogen is dominant for the anodic oxidation of aromatic amines such as *o*PD (Volkov *et al*, 1980; Deng and Van Berkel, 1999).

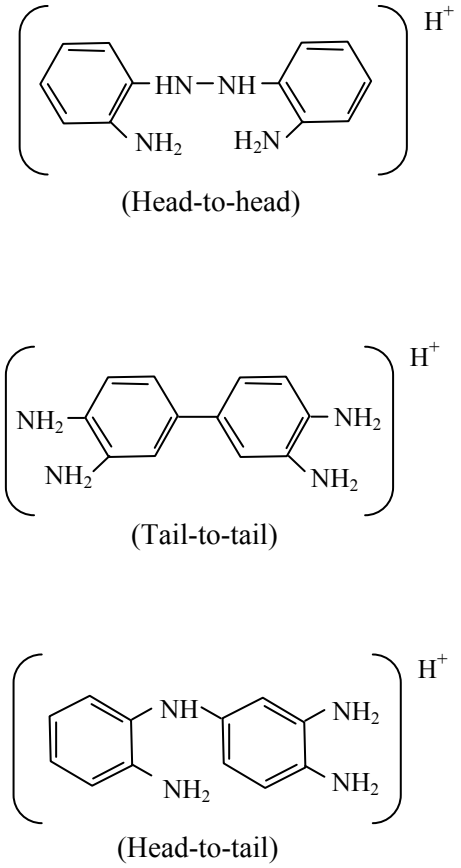

Fig 4.6 Possible dimers of oPD following oxidation.

Additional monomers can be added to this dimer, thus promoting elongation of the forming polymer (Fig 4.7).

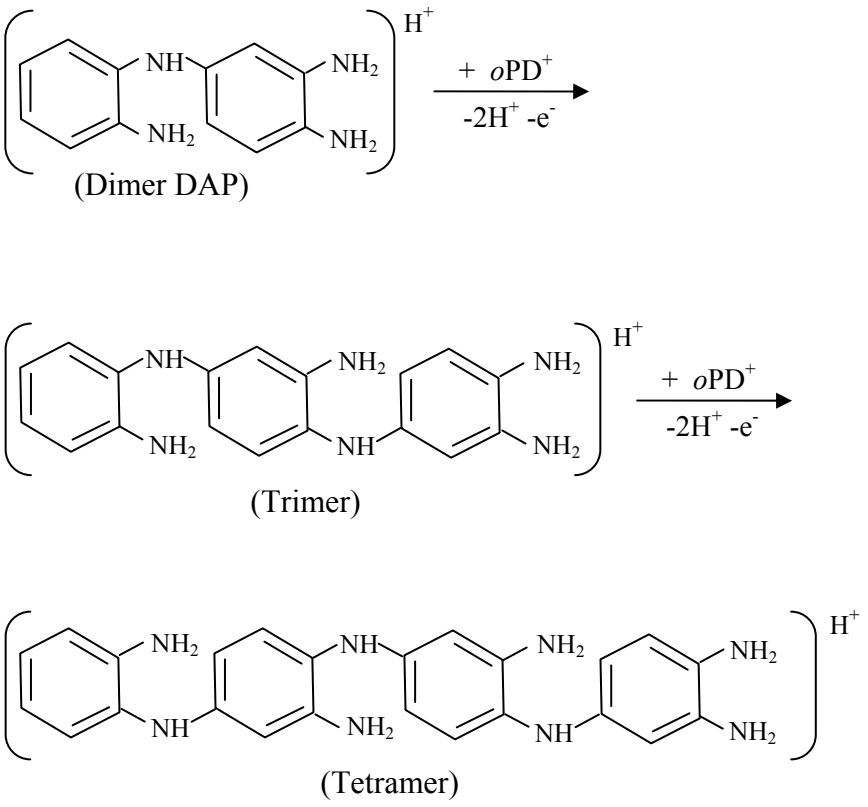

Fig 4.7 Chain propagation following dimerisation of *o*PD.

According to Locito and his team's detailed work on the species of dimeric, trimeric and tetrameric P*o*PD using electrospray ionization ion trap sequential mass spectrometry (ESI-ITMS), chain propagation beyond tetramer length occurs only when the applied potential is increased by about 200mV (vs. Ag/AgCl), giving rise to the second anodic peak (Locito *et al*, 2003).

At this point, more complex, pH-sensitive reactions take place, where competition exists between oxidative coupling (leading to chain propagation), and intramolecular oxidations with cyclisation. Oxidative coupling leads to the incorporation of phenazine and 1, 4 benzoquinonediimine into the polymeric structure. In acidic conditions, the oligomer formation favours phenazine-like subunits, whereas in more basic solutions, 1, 4-benzoquinonediimine forming processes are preferred and this results in a less conjugated polymer structure (Fig 4.8).

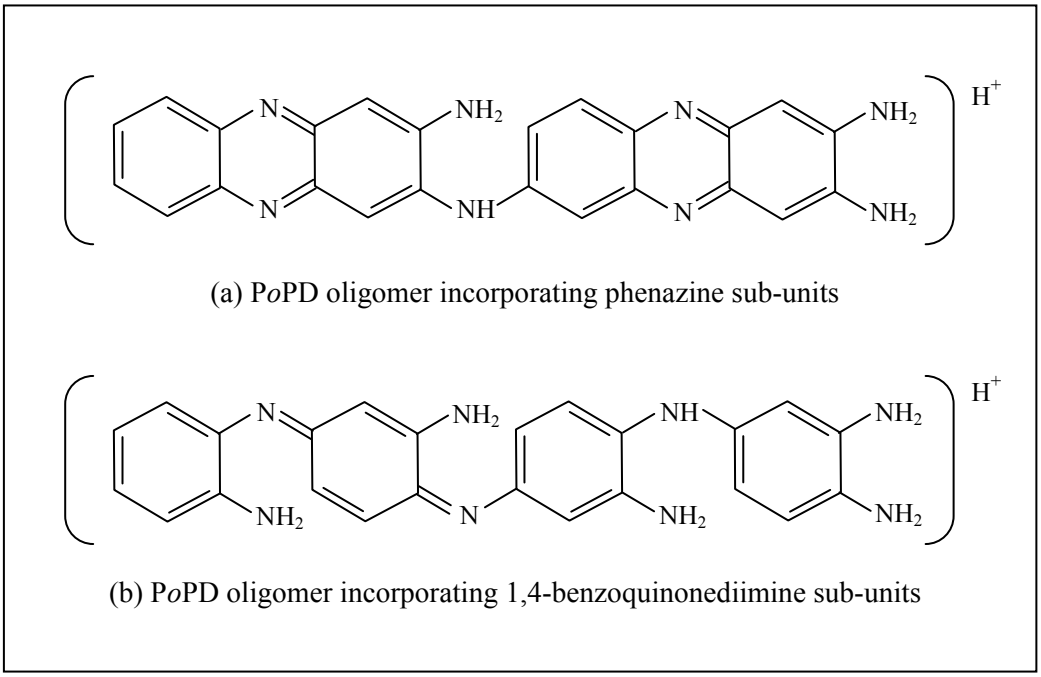

Fig 4.8 P*o*PD oligomers formed in acidic (a) and basic (b) conditions.

P*o*PD films resulting from the latter are less conjugated than the ones formed by phenazine subunits. The degree of conjugation as further discussed in chapter 2 greatly influences the conductivity of the polymer film and for this reason the P*o*PD films formed in the PBS buffer pH 7.4 are non conducting (Martinusz K *et al*., 1994).

In Fig 4.5, the oxidation currents fall sharply between subsequent scans and even after the first few potential cycles a current plateau is reached. This is in agreement with observations by Wu and Chang (Wu and Chang, 2004), who showed that for the same electrodeposition conditions, 96.5% of the charge had passed after 7 scans. It is the deposition (adsorption) of the insoluble, higher oligomers onto the electrode surface which results in electrode-passivation with an ultra-thin film of P*o*PD.

In contrast with aniline, described later on in the report, the formation of P*o*PD is not an auto catalytic reaction and the polymerisation occurs at low potentials, during the negative-going cycle. Furthermore, P*o*PD films are colorless in their reduced form and red in their oxidized form (Martinusz *et. al*., 1994).

The behaviour of the polymer modified sensors was studied asymmetrically in a solution of 1mM ferrocene carboxylic acid (FCA) in PBS pH7.4 buffer prior to and following the deposition of the polymer (Fig 4.9). The voltammograms depicted in

this picture were obtained by sweeping the potential from -1000mV to +1000mV vs. Ag/AgCl at 50mVs^{-1} at a P*o*PD coated and a bare gold sputtered glass slide electrode.

As the voltage becomes more positive (oxidizing), a value is reached where ferrocene carboxylic acid (reduced form) is converted to the oxidized underpricing species according to equation 4.1.

$$Fe^{(III)}(C_{11}H_{10}O_2) - e^- \leftrightarrow Fe^{(II)}(C_{11}H_{10}O_2) \qquad \textit{Eqn. 4.1}$$

The current produced was measured as a function of the applied potential. The transport of electroactive species to and from the electrode surface is subject to diffusion mass transport and for this reason the peak anodic and cathodic currents do not occur at the same applied potential. According to the Nernst equation (Eqn 2.10) a peak separation of 59mV should be expected for an ideal reversible diffusion controlled system. In this instance, the peak separation observed was ~230mV (vs. Ag/AgCl), which suggests a departure from non-ideal behaviour. It is likely that this discrepancy can be attributed to solution resistance and surface topography leading to non-idealist.

Non-ideality is also suggested by the fact that the ratio of i_{pc} and i_{pa} is not equal to one as expected from a reversible, diffusion-controlled single electron transfer reaction such as the one described in Eqn 4.1. This phenomenon can also be accounted for from the charge bias in favor of reduction. Since the solution consisted mainly of ferrocene carboxylic acid, the reaction product from the cathodic sweep experiences a diffusion gradient away from the electrode, thus causing it to move out of the diffusion layer.

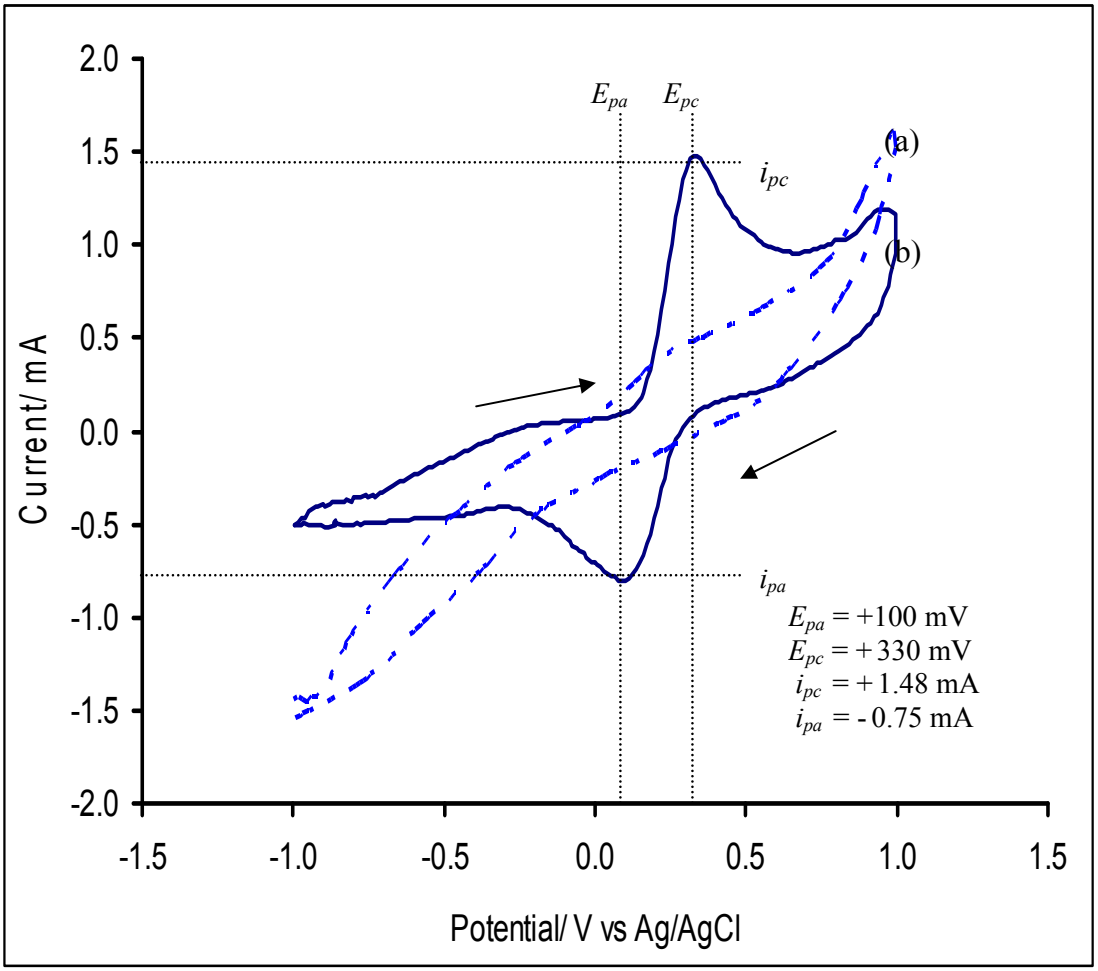

Fig 4.9 Cyclic voltammogram of 1mM FCA solution at a (a) PoPD coated gold sputtered glass slide electrode and (b) a bare gold sputtered glass slide electrode

[Supporting electrolyte: PBS pH 7.4, Scan rate: 50 mVs^{-1}]

It can be seen in Fig 4.9 that the insulation of the electrodes was not complete. Although no peaks appear in neither the anodic nor the cathodic potential sweeps, a small residual current is recorded, indicating that the transfer of electrons between the electrode surface and the redox couple still occurs. For this reason more electrodes were prepared and interrogated in the same fashion and a similar incomplete insulation of the working electrode was observed. It was concluded that the problem, most probably lies in inconsistencies in the fabrication procedure of this type of electrodes, rather than the procedure itself. For this reason the glass electrodes were not used again in this research.

One further phenomenon that can be observed in the cyclic mammograms in Fig 4.9 is the effect the double layer charging effect has on the measured current. Because of the applied potential, negatively and positively charged ions segregate creating a discontinuity at the electrode/solution interface which starts behaving as a capacitor. It follows that higher applied potential values will create an even greater segregation of ions and hence additional current will be measured across the electrode surface. This is the reason that increased current appears at the extremities of the potential range in the voltammograms of Fig 4.9.

This phenomenon can seriously affect the results and their interpretation as illustrated in Fig 4.10. In the latter the same polymer modified electrode has been swept from -700mV to +700mV and from -1000mV to +1000mV vs. Ag/AgCl at $50mVs^{-1}$.The resulting voltammograms are, however, startlingly different.

In order to minimize the discrepancies caused by the double layer charging effect when electrochemically investigating the electrodes in the presence of a redox couple, a narrower potential window was chosen. In all subsequent interrogations the potential was swept from -200 and +600mV vs. Ag/AgCl. This potential window is sufficiently wide to observe the redox processes on FCA which occur between 0mV and 500mV as seen in Fig 4.9, but narrow enough to minimize the effect of double layer charging effect on the extremities of the cyclic voltammograms.

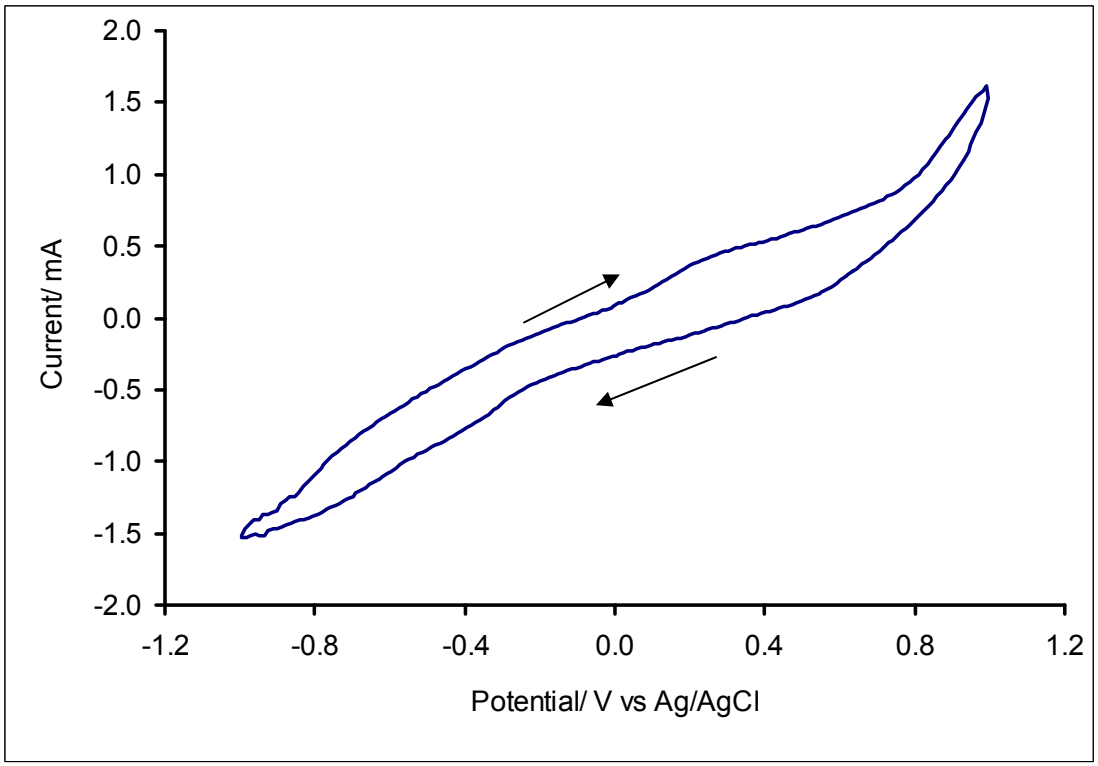

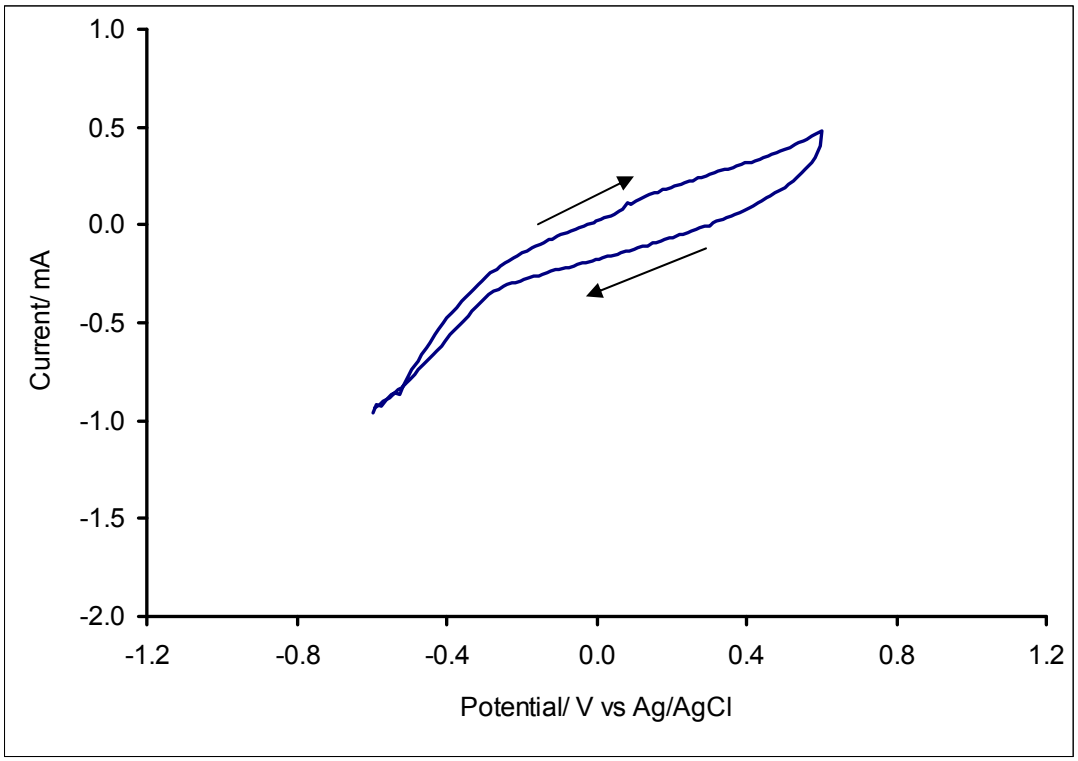

Fig 4.10 Cyclic voltammogram of 1mM FCA solution between -1000 and +1000mV vs. Ag/AgCl (top)) and 700 and +700mV vs Ag/AgCl (bottom) at a P*o*PD coated gold sputtered glass slide electrode.

[Supporting electrolyte: PBS pH 7.4, Scan rate: 50 mVs^{-1}]

According to the Randles – Sevcik equation (Equation 2.35), the peak current observed at a cyclic voltammogram is proportional to the square root of the scan rate. Therefore, by reducing the scan rate from $50mVs^{-1}$ to $25mVs^{-1}$ or even $10mVs^{-1}$, the current passed through the electrode is minimized and in this way the double layer charging effect can be minimised. Reducing the scan rate, however, results in the reduction of the peak anodic and cathodic currents observed, so in all the following electrochemical interrogations the scan rate was not altered.

Another way to address the effects of the double layer charging could be to increase the salt concentration of the PBS pH7.4 buffer in which FCA is dissolved, since the salt content of the buffer solution and the extent of the double layer charging effect are inversely related (Nurok et al, 2003).

4.2.2 Gold on a silicon substrate planar electrodes and microelectrodes

Following the initial investigations on gold sputtered glass electrodes, screen printed gold electrodes were electrochemically interrogated to determine their stability and sensitivity for biosensor applications. These electrodes were provided by the Tyndall Institute in Cork, Ireland which was a member of the ELISHA consortium.

Gold on a silicon substrate electrodes were electrochemically characterized in a solution of 1mM ferrocene carboxylic acid (FCA) in PBS pH7.4 buffer. The potential was swept from -200mV to +600mV vs. Ag/AgCl at $50mVs^{-1}$. The three electrode system comprised of two P3 gold electrodes as working and counter electrodes and an external Ag/AgCl reference electrode (Fig 4.11)

The anodic peak observed corresponds to the oxidation of ferrocene carboxylic acid. The subsequent reduction of the produced ferricinium species is demonstrated by the appearance of a cathodic peak when the potential is scanned in the reverse. The peak separation observed is 83mV (vs. Ag/AgCl), a value that does not depart considerably from the 59mV value anticipated by the Nernst equation for a completely reversible one electron transfer reaction.

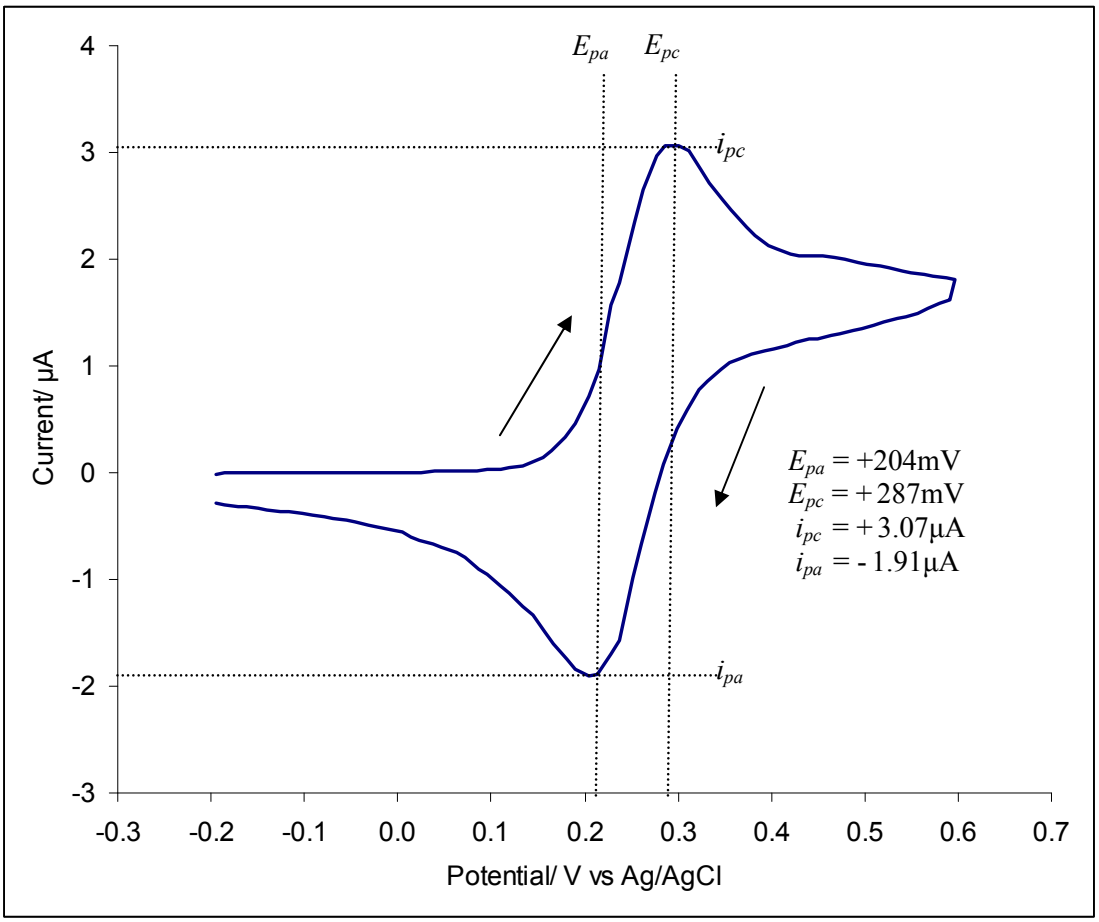

Fig 4.11 Cyclic voltammogram of 1mM FCA solution at a screen printed gold on a silicon substrate electrode (P3)

[Supporting electrolyte: PBS pH 7.4, Scan rate: 50 mVs^{-1}]

This deviation from the ideal peak separations, though, along with the ratio of the peak anodic and cathodic currents not being equal to one, indicates non ideal electrode kinetics. Solution resistance may be one of the factors affecting the peak potential and current values. However, the surface topography of the gold electrodes used, as well as inconsistencies in their screen printing are most probably the reasons for the discrepancies recorded. Nevertheless, it should be noted that the ΔE_P and i_{pa}/i_{pc} values obtained for these electrodes are far closer to the optimal values of 59mV separation and a ratio of 1, than the ones obtained for the gold sputter coated glass slides indicating an overall improvement in the electrode kinetics.

The current produced in response to the applied potential is in the region of microampers, due to the much smaller size of the working electrode surface compared to the gold coated glass slides used in earlier experiments. The exact dimensions of the gold sputter coated electrodes and the gold on a silicon substrate electrodes are listed in chapter 3.

The P10 electrodes were also characterized. P10 electrodes were microelectrode arrays whose manufacturing standards and surface topography can be found in chapter 3. The closed circuit system used comprised of a P10 working electrode, a P3 counter electrode and an external Ag/AgCl reference electrode. A sufficiently larger surface counter electrode was employed so as to not limit the current. The electrodes were characterized electrochemically in a 1mM ferrocene carboxylic acid (FCA) in PBS pH7.4 buffer. The polarizing potential was swept from -200mV to +600mV vs. Ag/AgCl at $50mVs^{-1}$ (Fig 4.12).

From the cyclic voltammogram in Fig 4.12, it can be seen that the electrochemical behaviour of this specific P10 electrode departs significantly from the behaviour of a typical microelectrode array (Fig. 2.20). The obtained cyclic voltammogram is similar to the cyclic voltammograms of planar electrodes and does not display a sigmoidal shape indicating that hemispherical diffusion is not occurring on the electrode surface and that the current recorded is limited by the mass transport of the reactant ferrocene species.

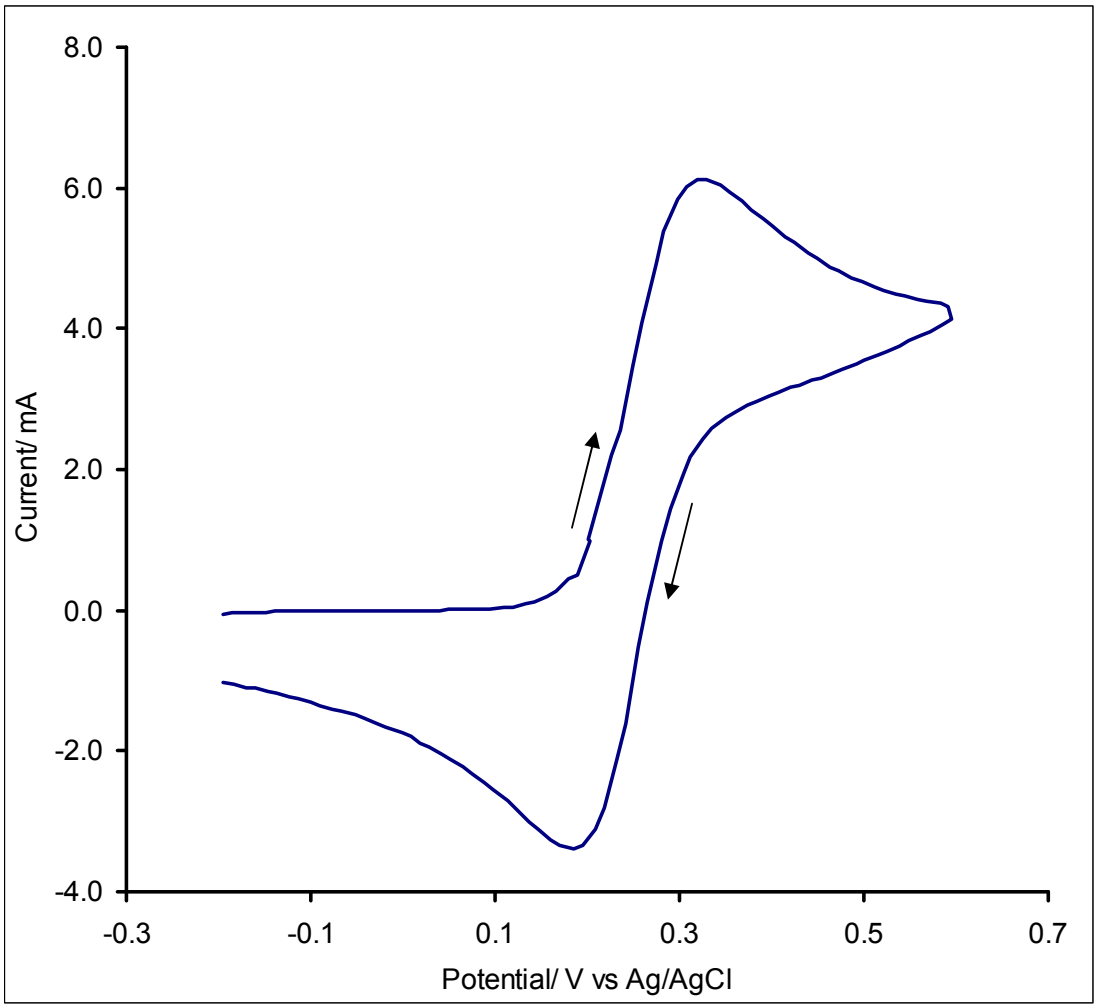

Fig 4.12 Cyclic voltammogram of 1mM FCA solution at a screen printed gold on a silicon substrate microelectrode (P10)

[Supporting electrolyte: PBS pH 7.4, Scan rate: 50 mVs^{-1}]

Subsequent electrochemical investigation of other P10 gold microelectrodes revealed once again a departure from the microelectrode behaviour. Fig 4.13 shows that none of the cyclic voltammograms obtained for the three P10 gold microelectrodes from the same batch resembles the typical sigmoidal shape and in addition reveals inconsistencies in the reproducibility between the electrodes themselves. Subsequent electrochemical characterization of a large number of gold on a silicon substrate electrodes revealed that these discrepancies in the reproducibility and electrochemical behaviour were not confined solely in that particular batch of P10 gold microelectrodes but rather represented a generalized problem. For this reason they were not used in the fabrication of the immunosensor platforms, since they would considerably hinder the evaluation of the results obtained.

The effect of the scan rate on the peak current was also investigated. Fig 4.14 shows the cyclic voltammogram of the same P10 gold electrode. The polarizing potential was swept from -200mV to +600mV vs. Ag/AgCl at $50mVs^{-1}$ and $10mVs^{-1}$. When the scan rate is increased the peak redox currents are also increased.

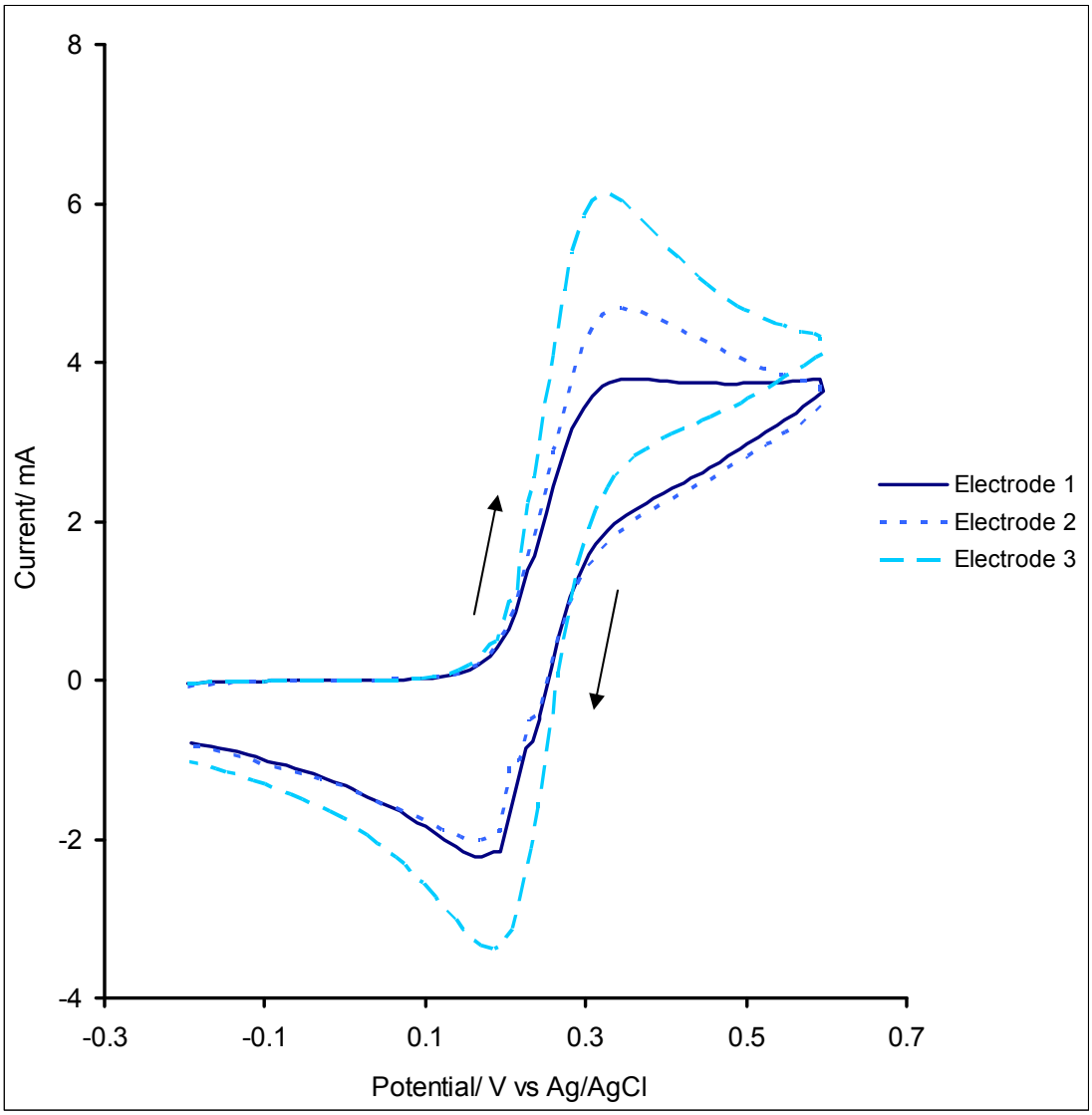

Fig 4.13 Cyclic voltammogram of 1mM FCA solution at three screen printed gold on a silicon substrate microelectrodes (P10) from the same batch

[Supporting electrolyte: PBS pH 7.4, Scan rate: 50 mVs^{-1}]

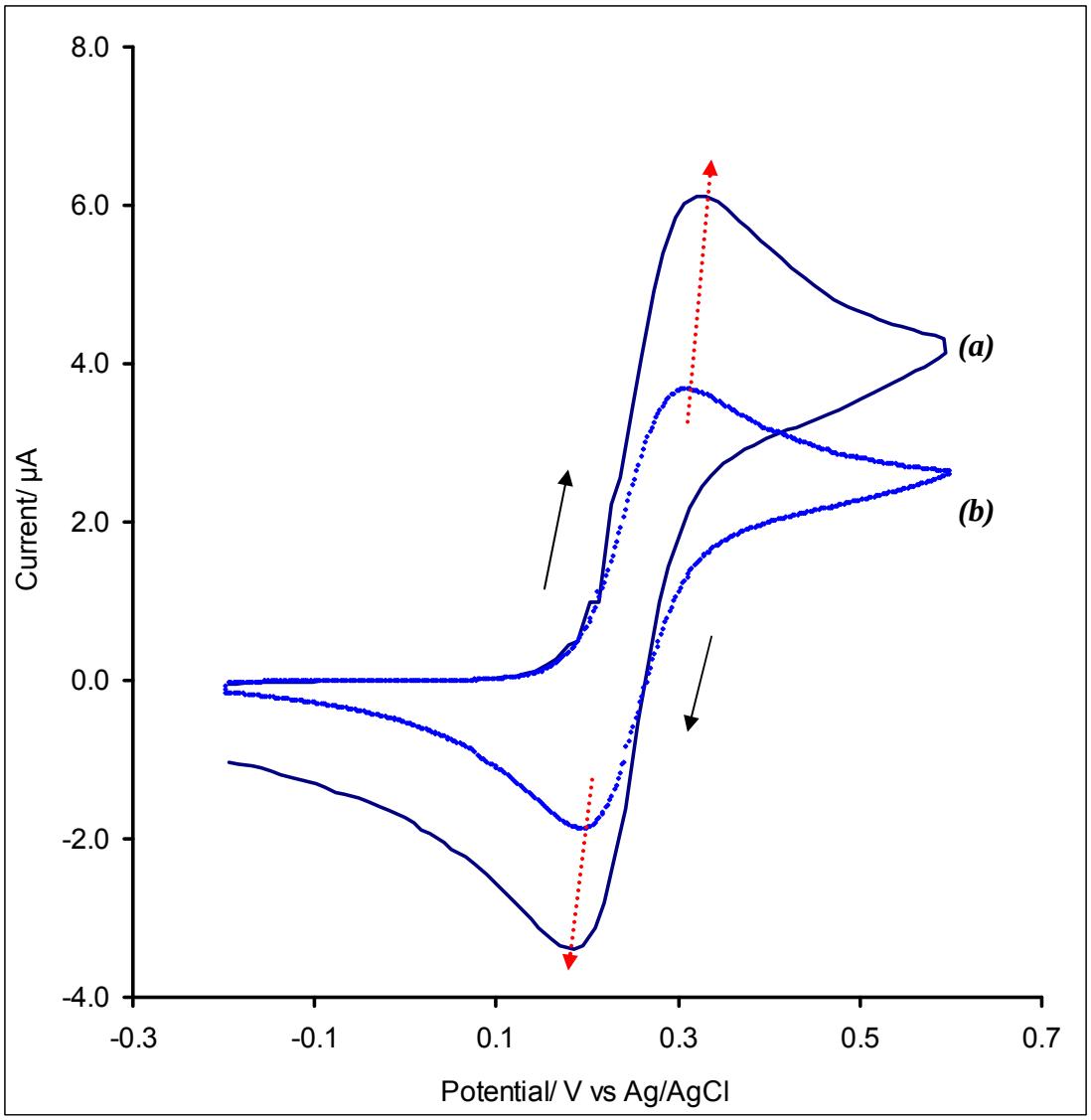

Fig 4.14 Cyclic voltammogram of 1mM FCA solution at a screen printed gold on a silicon substrate microelectrode (P10) at a scan rate of (a) 50 and (b) 10 mVs^{-1}

[Supporting electrolyte: PBS pH 7.4]

4.2.3 Carbon electrodes

Single disposable carbon ink electrodes were subjected to the same electropolymerisation regime used for gold substrate electrodes. These electrodes comprised of a working and a counter carbon ink electrode as well as an Ag/AgCl reference electrode, all of which were screen-printed on the same polycarbonate surface. The tracks were covered with a dielectric to insulate the former from contact with the buffer solution (Fig. 3.12). Polymerisation of *o*PD onto the working electrode was achieved by repeatedly cycling the electrode potential between 0 and +900mV vs. Ag/AgCl at $50mVs^{-1}$ for 100 progressive potential sweeps in a solution of 5 mM *o*PD in PBS pH 7.4 buffer (Fig 4.15).

The first anodic scan demonstrates the same features as those observed for *o*PD oxidation on gold electrodes, ie. the current intensity of the peak decreases upon cycling, suggesting the deposition of an insulating film of P*o*PD on the electrode surface (Fig 4.15). However in this case only one maximum is seen in the anodic direction with its peak occurring at approximately 680mV (vs. Ag/AgCl). Furthermore, the potential at which the anodic current starts to rise is also shifted to a more positive potential (+200mV compared to +100mV vs. Ag/AgCl for deposition on gold electrodes). The differences observed are due to the different electrode kinetics because of the electrode material. Gold is much more conductive when compared to carbon, resulting in the observed shifts in the peak current. The existence of two anodic peaks when using gold as the electrode raw material, in contrast with a single one as is the case with the carbon electrodes may be due to the two separate polymerization steps of *o*PD on gold (Gornall, 2001).

The polymer modified sensors were voltammetrically investigated in a solution of 1mM ferrocene carboxylic acid (FCA) in PBS pH7.4 buffer prior to and following the deposition of the monomer. The potential was swept from -200mV to +600mV vs. Ag/AgCl at $50mVs^{-1}$ (Fig 4.16).

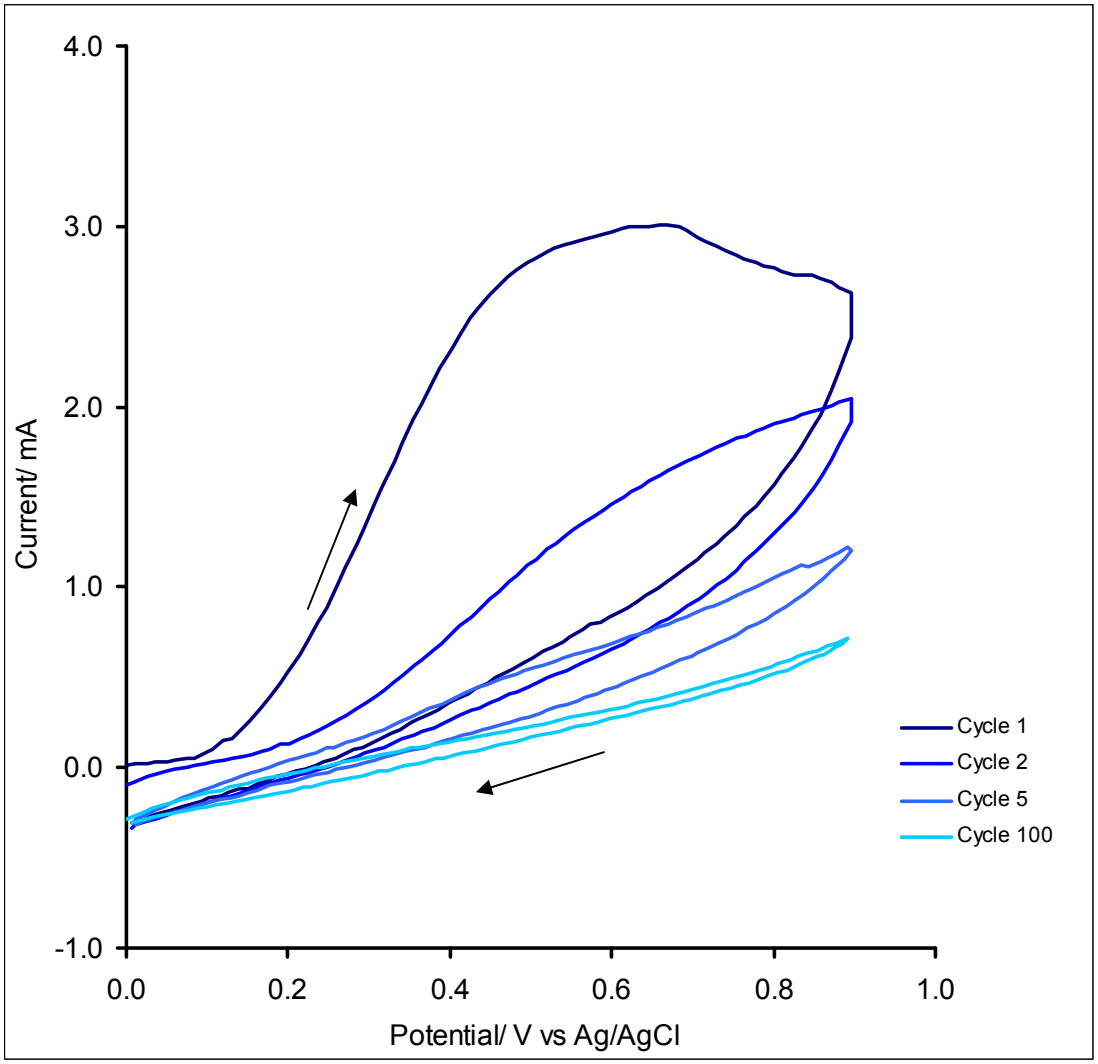

Fig 4.15 Cyclic voltammogram for the electropolymerization of 5mM *o*PD at a carbon screen printed electrode.

[Supporting electrolyte: PBS pH 7.4, Scan rate: 50 mVs^{-1}]

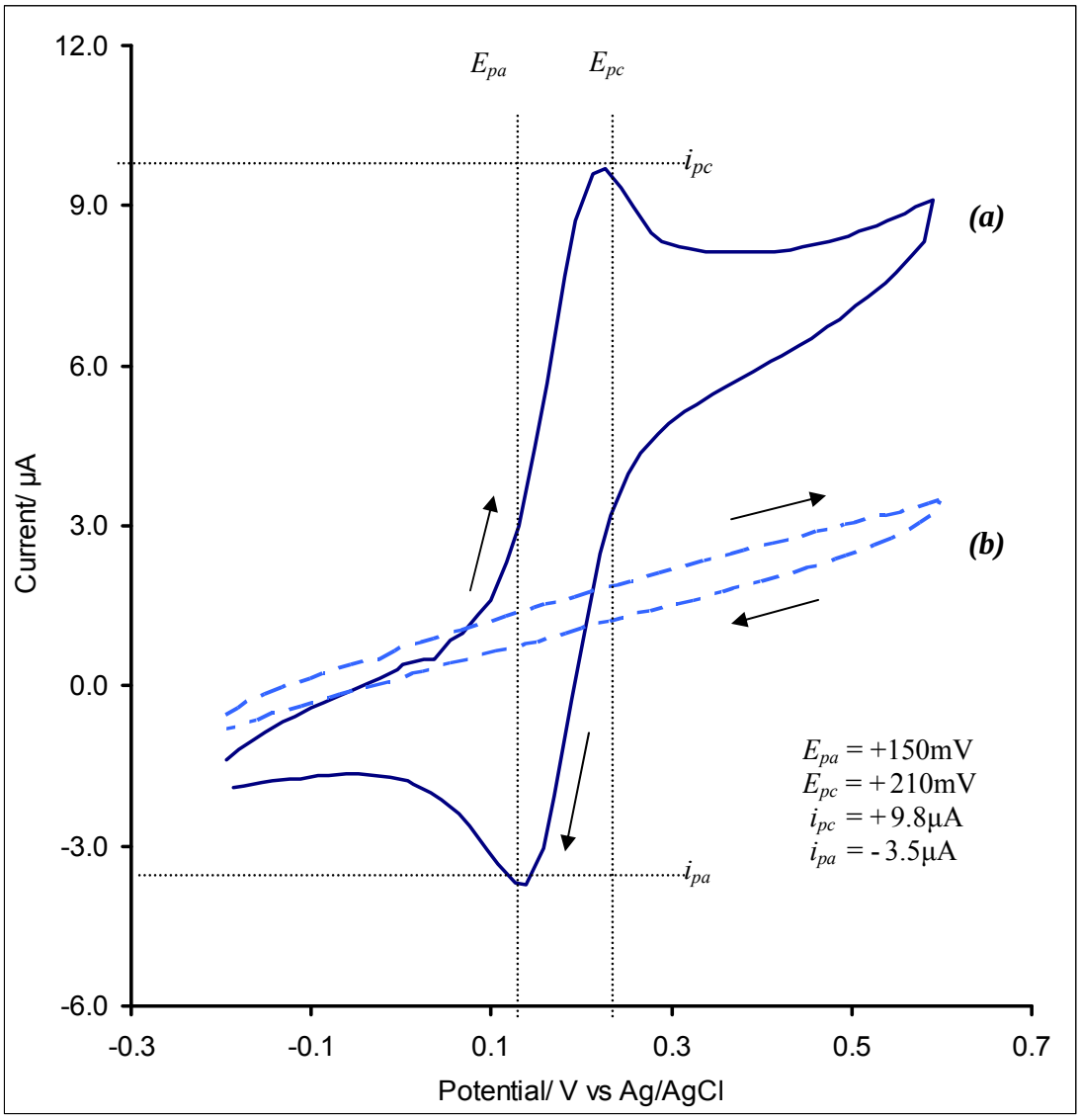

Fig 4.16 Cyclic voltammogram of 1mM FCA solution at a (a) carbon screen printed electrode and (b) PoPD coated carbon screen printed electrode.

[Supporting electrolyte: PBS pH 7.4, Scan rate: 50 mVs^{-1}]

In contrast with the polymerization of *o*-phenylenediamine on gold coated glass slide electrodes, the carbon electrode surface was insulated more completely. Complete passivation of the electrode surface can never be achieved due to cross-linking reactions taking place within the film, which even when 'insulating' still possesses a finite conductivity, especially when hydrated (Centonze *et al*, 1994).

The measured current produced in response to the applied potential is significantly lower than the one reported previously for the gold sputtered electrodes. However, when the former is compared to the peak current observed for the screen printed gold electrodes, it is increased. This is due to the surface area of the gold sputtered glass slides being larger than that of the carbon electrodes whose surface is in turn larger than the screen printed gold electrodes' surface. The peak separation observed of ~60mV (vs. Ag/AgCl) agrees with the behaviour of a completely reversible couple in which the electron transfer reaction is dictated by the Nernst equation (Eqn 2.10). However the ratio of the peak currents is not equal to one, indicating non ideal electrode kinetics most probably caused by the surface morphology and composition of the carbon ink layer.

Carbon electrodes exist in a variety of forms such as glassy carbon, carbon fibres, graphite pastes and carbon films (Gilmartin and Hart, 1995). Screen-printed carbon inks, such as the one used for the production of the carbon electrodes used, typically consist of a mixture of graphite powder, a polymeric binder (vinyl or epoxy based) and other chemical additive to aid dispersion and printing (Grennan *et al*, 2001). The resultant ink is a composite of randomly oriented graphite particles, suspended in matrix of insulating polymeric binder. Conductivity is provided by points of physical contact between graphite particles (Švancara *et al*, 2001). By careful optimization and control of production conditions, more reactive and reproducible screen printed carbon ink electrodes can be produced. Increasing the curing temperature, for example, results in the enhanced electroanalytical performance of the electrodes (Grennan *et al*, 2001).

4.3 Conclusions

This chapter has described the electropolymerisation and optimization of P*o*PD films on different conductive surfaces. P*o*PD films were deposited on the surface of the electrodes by cyclic voltammetry for 100 progressive cycles until the latter became fully insulated. Cyclic voltammograms relating to the electrodeposition of the film revealed the electropolymerisation as being a self-regulating and thus highly reproducible process, since diminishing peak currents were observed as the electrode became progressively passivated.

Proposed mechanisms relating to both the growth of the P*o*PD films across the electrode surfaces and the polymerization of the *o*PD itself, have been shown to agree with the experimental data collected and explain the redox peaks observed.

The electropolymerisation of *o*PD onto gold sputter-coated ground glass slide electrodes was initially characterised in neutral conditions to show a two electron transfer mechanism for the formation of a non-conducting, ultrathin film. This was then applied to screen printed gold on a silicon substrate electrodes and screen printed carbon electrodes in a manner analogous to the one employed for the gold sputtered glass slides.

Confirmation of the electrode insulation in all cases was obtained by the lack of any electroactivity in the presence of a redox couple by cyclic voltammetry prior to and following deposition of P*o*PD films.

The cyclic voltammograms obtained for the gold sputtered glass slides revealed inconsistencies in the fabrication procedure resulting in incomplete passivation of the electrodes following polymer deposition as well as non ideal electrode kinetics even on bare electrodes.

The screen printed gold electrodes, on the other hand, proved to be much more reliable since their electrochemical behaviour did not depart significantly from the behaviour of an ideal system under the same conditions. Nevertheless, these electrodes

were not employed in subsequent experimental investigations, since it was found that there is considerable irreproducibility in between them when cyclic voltammograms from a large number of these electrodes were compared.

Finally, screen printed carbon electrodes proved to be reproducible enough so as to be employed in the fabrication of immunosensor platforms and hence all the subsequent sensing applications were carried out employing only this type of electrodes.

Moreover, carbon ink electrodes were preferred to both the screen printed and sputter coated gold electrodes because they are far more affordable than both the latter. Bearing in mind, therefore, the low cost unit of the final immunosensor platform to be constructed, carbon ink is the most cost effective electrode material out of the ones investigated in this project. Additional attractive features include a wide anodic potential range, low electrical resistance and low residual current (Ricci *et al*, 2003). The only drawback is its low conductivity compared to gold and platinum.

Chapter 5

Microelectrode fabrication

5.1 Introduction

As discussed in chapter 2, microelectrodes possess a number of advantages when compared to planar electrodes. They experience unique hemispherical diffusion profiles, and can impart stir-independent characteristics to electrochemical sensors, while also offering lowered limits of detection. However, one major drawback is that they generate very small total current responses. One approach to overcoming this problem, without sacrificing on the benefits of microelectrodes is by the use of microelectrode arrays.

Microelectrode arrays can be manufactured in a number of ways, photolithography (Fofonoff *et al*, 2004) and laser ablation (Cunningham *et al*, 2001) being the most popular. These techniques, though, have proved cost prohibitive for the mass production of disposable sensor strips. This is the reason that despite the attractive properties of microelectrode arrays, there have been no commercial sensors based on them to date.

Previous work within this research group reported the production of microelectrode array sensors via the ultrasonic ablation of P*o*PD passivated gold sputter-coated ground glass slide electrodes (Myler, 2000) as well as screen printed carbon electrodes (Gornall, 2004). Investigations, in this research project, on the fabrication of individual microelectrode array sensors based on the developed protocol, employed the screen printed gold electrodes (P3), discussed in section 4.2.2. This simplified manufacturing approach lends itself well to rapid, large scale, and importantly low-cost fabrication of disposable microelectrode array sensors.

The method takes advantage of acoustic cavitation. As discussed in the literature review, ultrasonic agitation of a liquid medium such as water will result in the formation of cavities within the medium due to the expansion of molecular spacing. An implosion of any of these cavitation nuclei may generate temperatures of up to 5000°C and pressures of approximately 2000 atmospheres. The areas where the bubbles collapse are referred to as hot spots (Suslick *et al*, 1986). When these hot spots are close to a solid surface then the liquid trying to fill the burst cavity will be

hindered from that side (Blake, 1986). The majority of the liquid medium will enter the void from the other side, creating in this way a jet targeted towards the solid surface at speeds of several hundreds of metres per second (Chahine, 1982). The elevated temperatures and pressures associated with the collapse of cavitation voids along with the jet of liquid generated in the process were exploited to ablate the polymer modified surface of the sensors.

One of the most attractive characteristics associated with using electropolymerisable non-conducting polymers such as P*o*PD, is their ability to produce self-insulating coatings, which cover the entire electrode surface irrespective of electrode topography. The extent of the surface ablation caused by exposure to ultrasound is sufficient to cause perforations in the uniform soft P*o*PD film through to the harder underlying conductive electrode surface (Fig. 5.1).

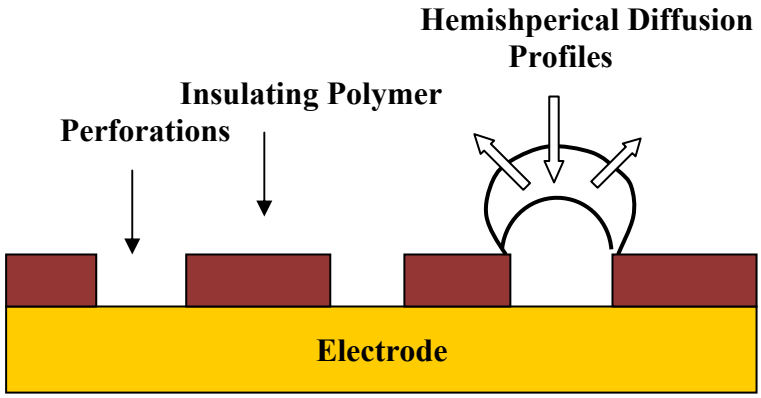

Fig 5.1 Scematical representation of a sonochemically fabricated microelectrode.

Not all of the formed perforations are of the same diameter. Different ablation conditions will give rise to different sized perforations. If the latter are too wide, then the microelectrode behaviour is lost, whereas if they are too small then the electrode will remain coated with the insulating polymer and hence passivated.

Furthermore, since the ablation process exposes a single, continuous piece of conductive material, each perforation forms part of a microelectrode array construction.

For the production of sound waves a bench top ultrasonic bath as well as a custom made sonication tank were used, whose dimensions and specifications are described in chapter 3. The distribution of the localised pressure fields, i.e. nodes and anti-nodes of the produced sonic waves within the tank as well as the effect they have on the ablated surfaces have been extensively characterized in previous work of our research group with the use of numerous mapping strategies such as sonolumiscence (Gornall, 2004; Mills, 2005).

An inherent spatial inhomogeneity of cavitational intensity exists due to the presence of standing waves with their associated pressure gradients. These regions of consistently high acoustic amplitude (focal antinodes) host more pronounced cavitational activity than pressure nodes. It has been shown that to achieve homogeneous cavitational distribution throughout the tank, an internal ultrasonic baffling system must be introduced (Fig 3.6) (Mills, 2005). The numerous, regularly spaced perforations of the baffle act as point sources of acoustic emission and since their diameter is smaller than the range of incident wavelengths the homogeneity of node and anti node positions is increased. Furthermore, a mounting device for the polymer modified sensors was employed to shield the sensors on the outer edges from preferential nucleation of transient cavitational bubbles.

This chapter is therefore focused towards the fabrication and characterisation of sonochemically formed microelectrode arrays using screen printed carbon electrodes. A number of different parameters will be investigated such as the intensity of the applied frequency, its duration and the positioning of the electrodes in the sonication tank, all of which have been shown to greatly affect the cavitational phenomena on the surface of the polymer film and hence the formation of indentations.

5.2 Initial investigations into the ultrasonic fabrication of microelectrode arrays

Screen printed gold on a silicon substrate planar electrodes (P3) were insulated with a film of PoPD by cycling the potential between 0 and +900mV vs. Ag/AgCl at $50mVs^{-1}$ for 100 progressive potential sweeps, as described in the previous chapter.

Their electrochemical behaviour prior to and following polymer deposition was recorded in a solution of 1mM ferrocene carboxylic acid in PBS pH7.4 buffer (Fig 5.3). The voltammograms depicted in this figure were obtained by sweeping the potential from -200mV to +600mV vs. Ag/AgCl at $50mVs^{-1}$ and indicate the complete passivation of the electrode surface following P*o*PD electrodeposition.

Initial investigations into the ultrasonic fabrication of microelectrode arrays were subsequently carried out using a small bench top 25kHz Transsonic T460 ultrasonic bath containing de-gassed, distilled, deionised water. The passivated electrodes were suspended vertically in the centre of the ultrasonic bath right above the single transducer as illustrated in Fig 5.2.

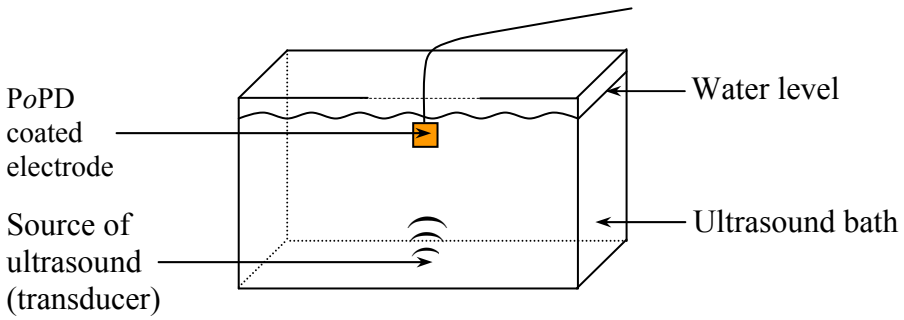

Fig 5.2 Schematic representation of small scale microelectrode fabrication using an ultrasonic bath.

The polymer modified electrodes were then sonochemically ablated for 20 seconds. Electrochemical characterisation of the sonicated electrodes was carried out via cyclic voltammetric interrogation of a 1mM FCA in PBS pH7.4 buffer. The cyclic voltammogram obtained was compared to the cyclic voltammogram of the same polymer modified electrode prior to sonication (Fig 5.4).

Fig 5.4 shows that for the P*o*PD coated electrode, electrochemical responses of FCA are barely discerned, indicating that the electrochemical reactions are suppressed by the presence of the film on the electrode surface. Contrastingly, the cyclic voltammogram obtained at the sonochemically fabricated microelectrode array, hints at a sigmoidal shape, although a clear steady state response is absent.

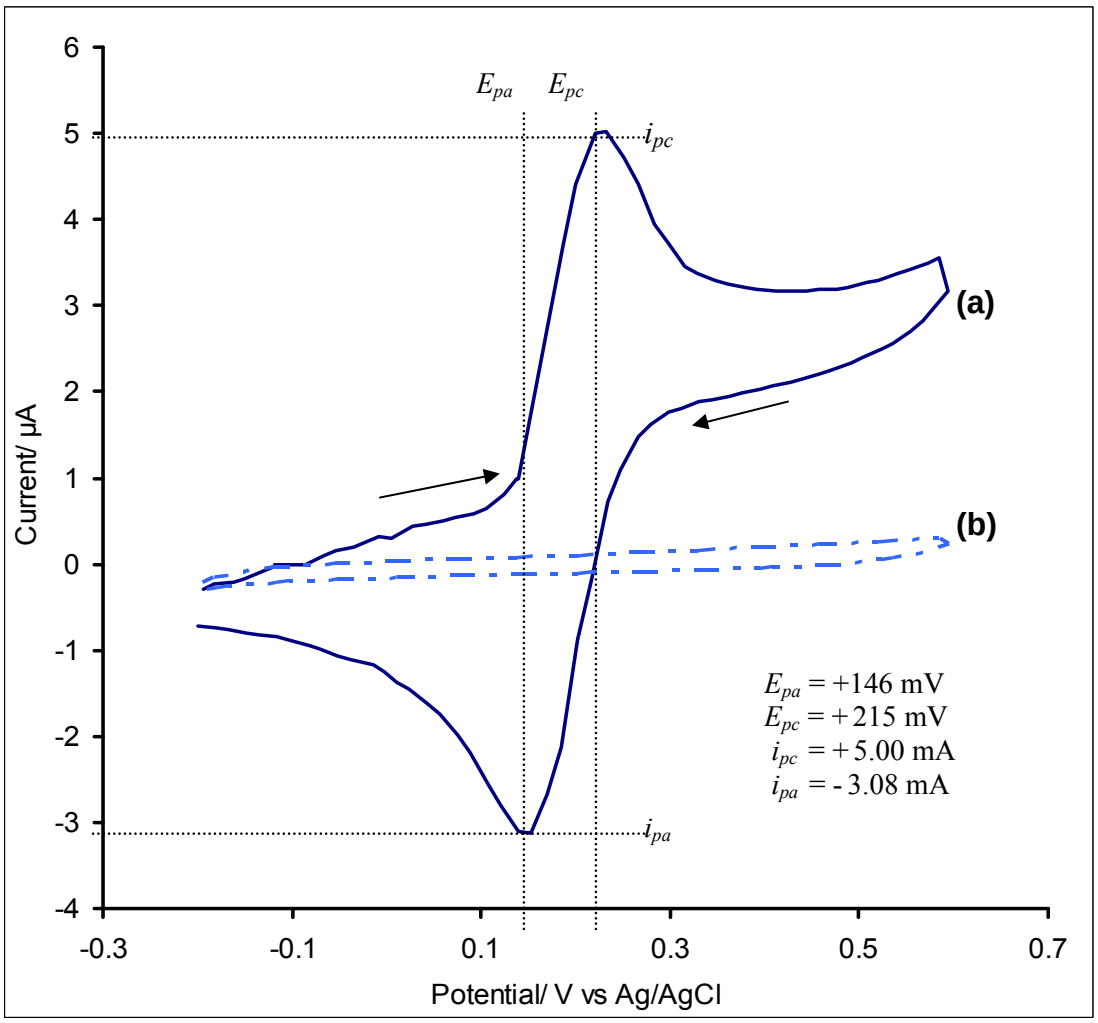

Fig 5.3 Cyclic voltammograms of 1mM FCA solution at a (a) bare screen printed gold electrode and a (b) PoPD coated screen printed gold electrode.

[Supporting electrolyte: PBS pH 7.4, Scan rate: 50 mVs^{-1}]

The duration of sonochemical ablation was therefore not adequate to create enough perforations in the polymer layer and thus create a microelectrode array.

To determine the optimal duration of sonication required to produce enough indentations in the polymer film without completely stripping it off from the electrode surface, four identical P3 electrodes were insulated with P*o*PD and sonochemically ablated in the ultrasonic bath for 10, 20, 45 and 60 second respectively. Their electrochemical behaviour was investigated in a solution of 1mM FCA in PBS pH7.4 buffer (Fig 5.5).

It appears that 10 seconds are not adequate to create enough perforations through the polymer layer and the electrode remains passivated. After 30 seconds of sonochemical ablation the electrochemical response recorded reaches a maximum value, even greater than the response recorded after 20 seconds of sonication. The response, though, obtained following 45 and 60 seconds of sonochemical ablation does not indicate any significant increase and is even reduced when compared to the response recorded after 30 seconds of sonication. This is probably due to the actual stripping off of the polymer film from the electrode surface and the damage caused to the underlying gold layer. Therefore, the optimal duration of sonochemical ablation of the polymer modified electrodes using the bench top ultrasonic bath is 30 seconds.

The shape of the cyclic voltammograms in Fig 5.5 indicates that a steady-state condition, where non-linear diffusion occurs, has not been reached under none of the sonication protocols employed. The hemispherical diffusion profile of microelectrodes allows for a substantially increased flux of electroactive species to the electrode- as compared to the linear diffusion typical of macroelectrodes- which gives rise to ‘sigmoidal’ voltammograms rather than the usual peak-shaped responses of planar electrodes.

Furthermore, microelectrode theory predicts that for an ideal microelectrode, the oxidative and reductive sweeps will overlay perfectly, however in Fig 5.5 it can be seen that there is some separation of the forward and reverse sweeps. This is a consequence of the chaotic nature of the cavitation process, whereby microelectrode pores are positioned randomly across the sensor surface.

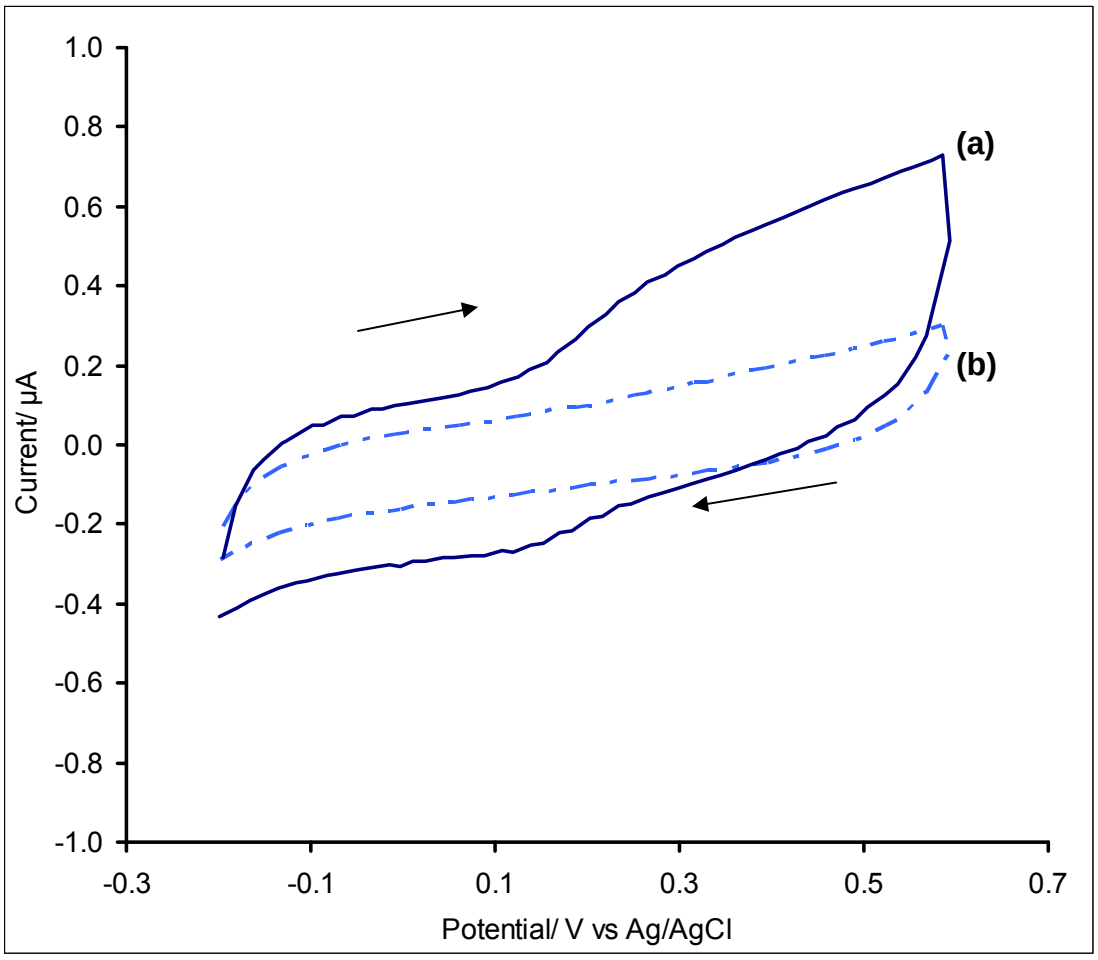

Fig 5.4 Cyclic voltammograms of 1mM FCA solution at a (a) sonochemically ablated polymer modified electrode and a (b) P*o*PD coated electrode.

[Supporting electrolyte: PBS pH 7.4, Scan rate: 50 mVs^{-1}]

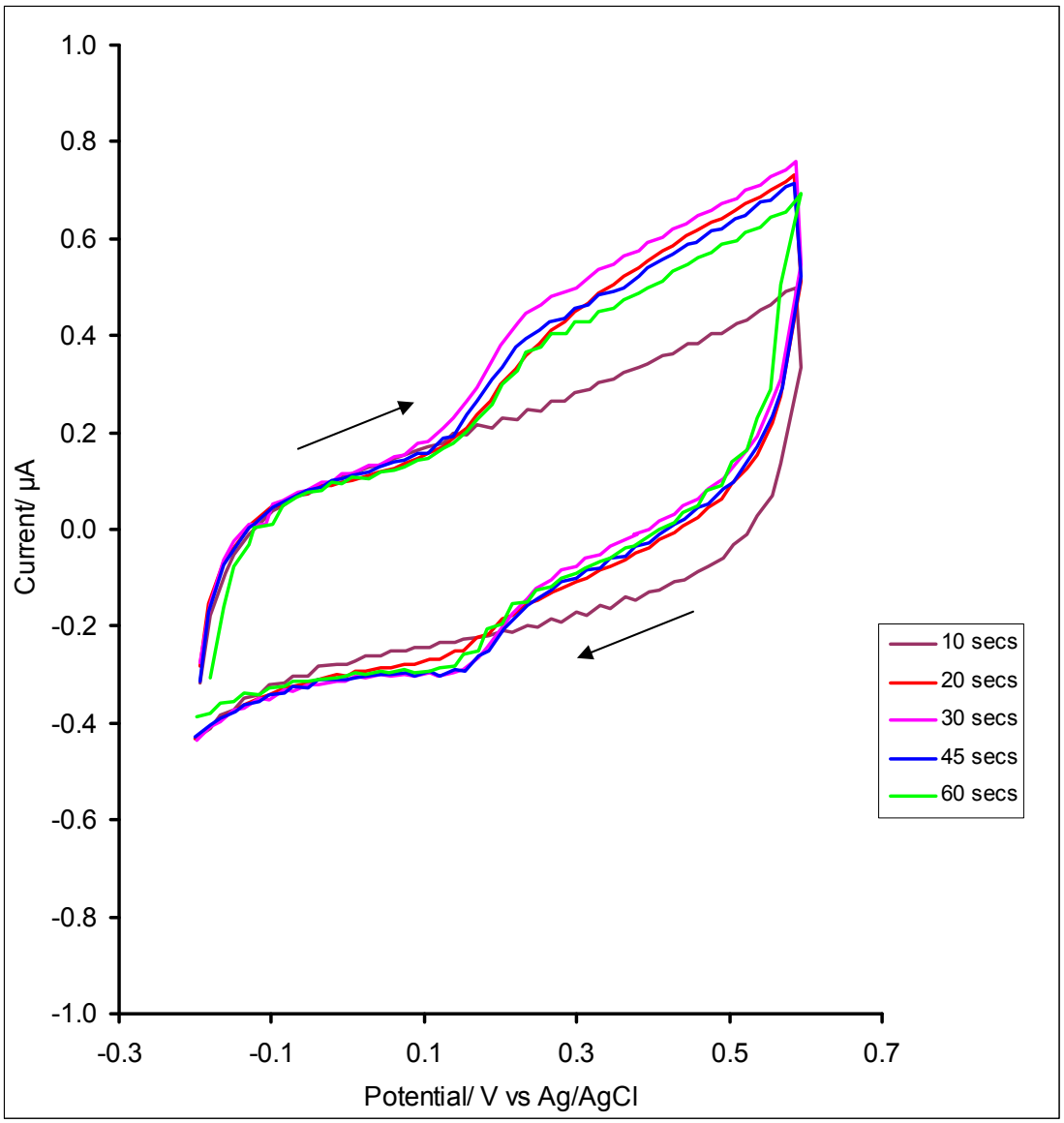

Fig 5.5 Cyclic voltammograms of 1mM FCA solution at a sonochemically ablated polymer modified electrode for 10, 20, 30, 45 and 60 seconds.

[Supporting electrolyte: PBS pH 7.4, Scan rate: 50 mVs^{-1}]

Inevitably some of the microelectrodes formed will be in such close proximity that there will be an overlap of the diffuse parts of their double layers resulting in a charging capacitance.

The lack of or non-ideal microelectrode behaviour displayed by the sonochemically ablated polymer-modified electrodes using the ultrasonic bath indicates that the sonication conditions have not been sufficiently optimized. Further work towards the optimization of the sonication protocols for the ultrasonic bath was not carried out. A sonication tank was used instead, whose size allowed for the sonochemical fabrication of microelectrode arrays on a scale larger than that of a research laboratory. Sonication protocols were thus optimized for this tank and not for the ultrasonic bath (Section 5.3).

5.3 Optimisation of ultrasound conditions to facilitate the mass fabrication of microelectrode arrays

For the scale up of the sonochemical fabrication of microelectrode arrays further considerations should be taken into account. A crucial issue that needs to be addressed is whether it is possible to achieve a uniform sonication profile throughout a large sonication tank with multiple transducers. A number of groups have been involved in solving such issues for the purposes of ultrasonic cleaning at an industrial scale (Mason & Berlan, 1992). Furthermore, previous members of our research group have extensively worked on optimizing the conditions of sonochemical ablation of polymer-modified electrodes for microelectrode array fabrication (Gornall, 2004). We set out to optimize the sonication protocols for our own screen printed gold electrodes, taking into consideration all the previous studies.

The industrial sized ultrasound tank used was custom built in conjunction with Ultrawave Limited (Cardiff, Wales). The dimensions of the tank were 0.75m x 0.75m x 0.6m whilst it possessed 10 transducers attached at the bottom to permit even spread of acoustic energy throughout the volume of water contained. The transducers were powered by an external amplifier, generating a 2kW, 25.1 kHz frequency signal. A heating system was included to maintain the temperature of the water at 25ºC ± 1ºC

since temperature can affect the energy of the cavitational phenomena. Software incorporated within the power generation system allowed for the power to be varied between 50 and 100%, and the sonication time to be varied between 1 and 99 seconds (Fig 3.4).

The following chapters examine the effect of different parameters on sonication, namely the duration of sonication (Chapter 5.3.1) and the power of the sonication in association with the positioning of the electrodes in the tank (Chapter 5.3.2).

For all experimental set ups described in the following sections, the electrodes were attached to the mounting device described in section 5.1. The electrodes were placed at the centre of the mounting device unless otherwise stated.

5.3.1 Effects of the duration of sonication upon electrode performances

As discussed in section 5.2, the optimum period of exposure to sonication in a bench-top ultrasonic bath is 30 seconds. The situation in a large sonication tank could be completely different and the time required to obtain optimal results less or in fact more than 30 seconds. For this reason, a similar experimental set up was followed as for the ultrasonic bath, to establish the sonication time required to obtain microelectrode arrays in the sonication tank.

PoPD electrodeposition on the electrode surface was performed for 100 cycles as described in Section 5.2. The polymer modified electrodes were then sonochemically ablated for 10, 30, 60, 100 and 120 seconds respectively. Electrochemical characterization of the sonicated electrodes was carried out via cyclic voltammetric interrogation of a 1mM FCA in PBS pH7.4 buffer (Fig 5.6)

As for the ultrasonic bath, the cyclic voltammograms in Fig 5.6 show that 30 seconds is the optimum period of sonication to obtain maximum response to FCA. If the duration of the polymer film ablation is less than 30 seconds, the electrode remains passivated, while for longer exposure periods the response is lowered indicating physical damage to the polymer film and/or the electrode surface.

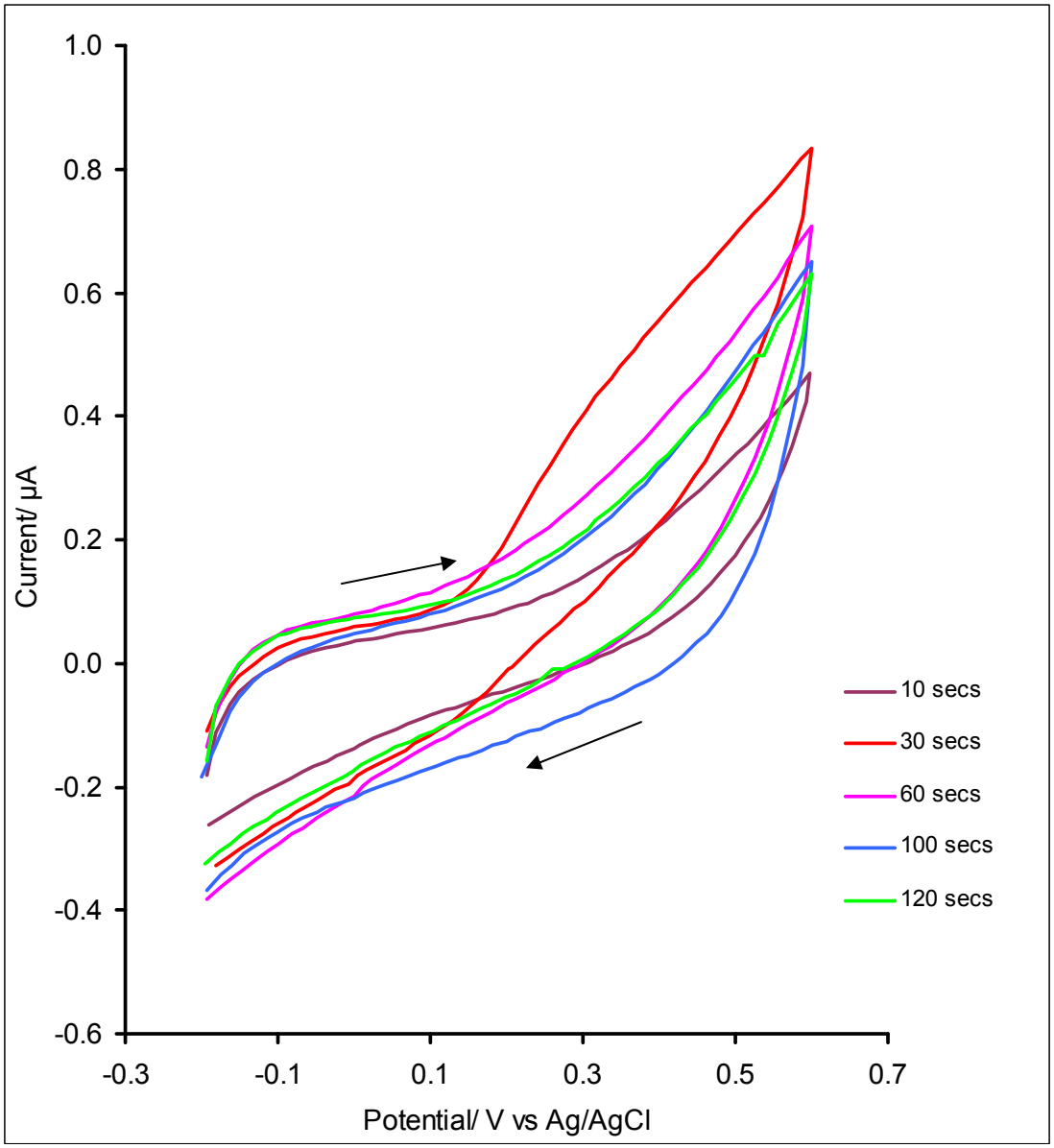

Fig 5.6 Cyclic voltammograms of 1mM FCA solution at sonochemically ablated polymer modified electrodes for 10, 30, 60, 100 and 120 seconds respectively.

[Supporting electrolyte: PBS pH 7.4, Scan rate: 50 mVs^{-1}]

5.3.2 Effects of the power of sonication in association with the positioning of the electrodes upon electrode performance

Having established that the optimum duration of sonication is 30 seconds, P*o*PD modified electrodes were consequently sonicated at 50, 75 and 100% power at five different positions on the mounting device.

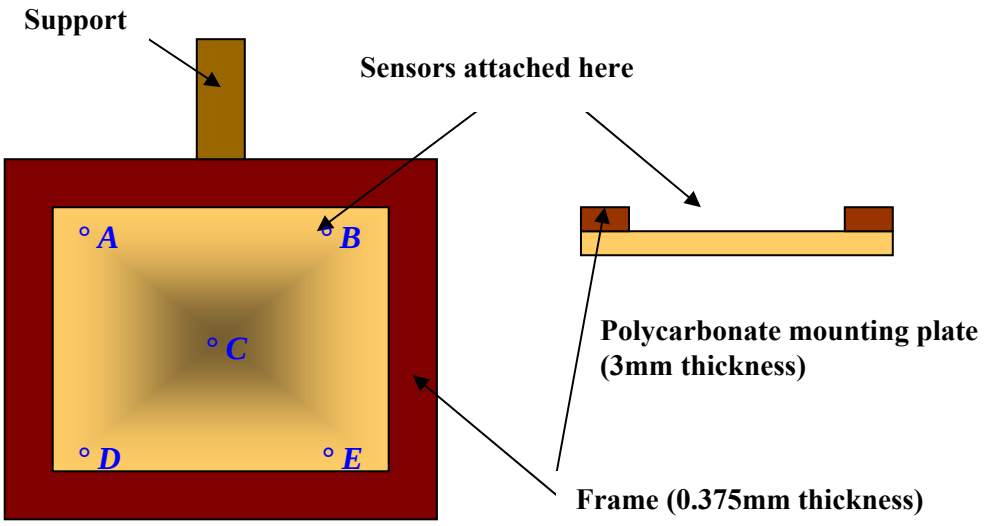

Fig 5.7 Positioning of the electrodes on the mounting device.

Two electrodes were placed at the top left and right corners of the polycarbonate mounting plate (Positions A and B) and another two at the bottom left and right corners (Positions D and E). One electrode was positioned at the centre of the plate in position C (Fig 5.7).

The resultant cyclic voltammograms (Figs 5.8-10) clearly demonstrate that there is no general optimum power setting since the response of each electrode upon electrochemical interrogation in an FCA solution greatly depends on its positioning in the sonication tank. For example, although an electrode in position C will remain virtually passivated following sonication at 50% and 75% power settings it will give a response, albeit not one associated with a microelectrode, at 100%.

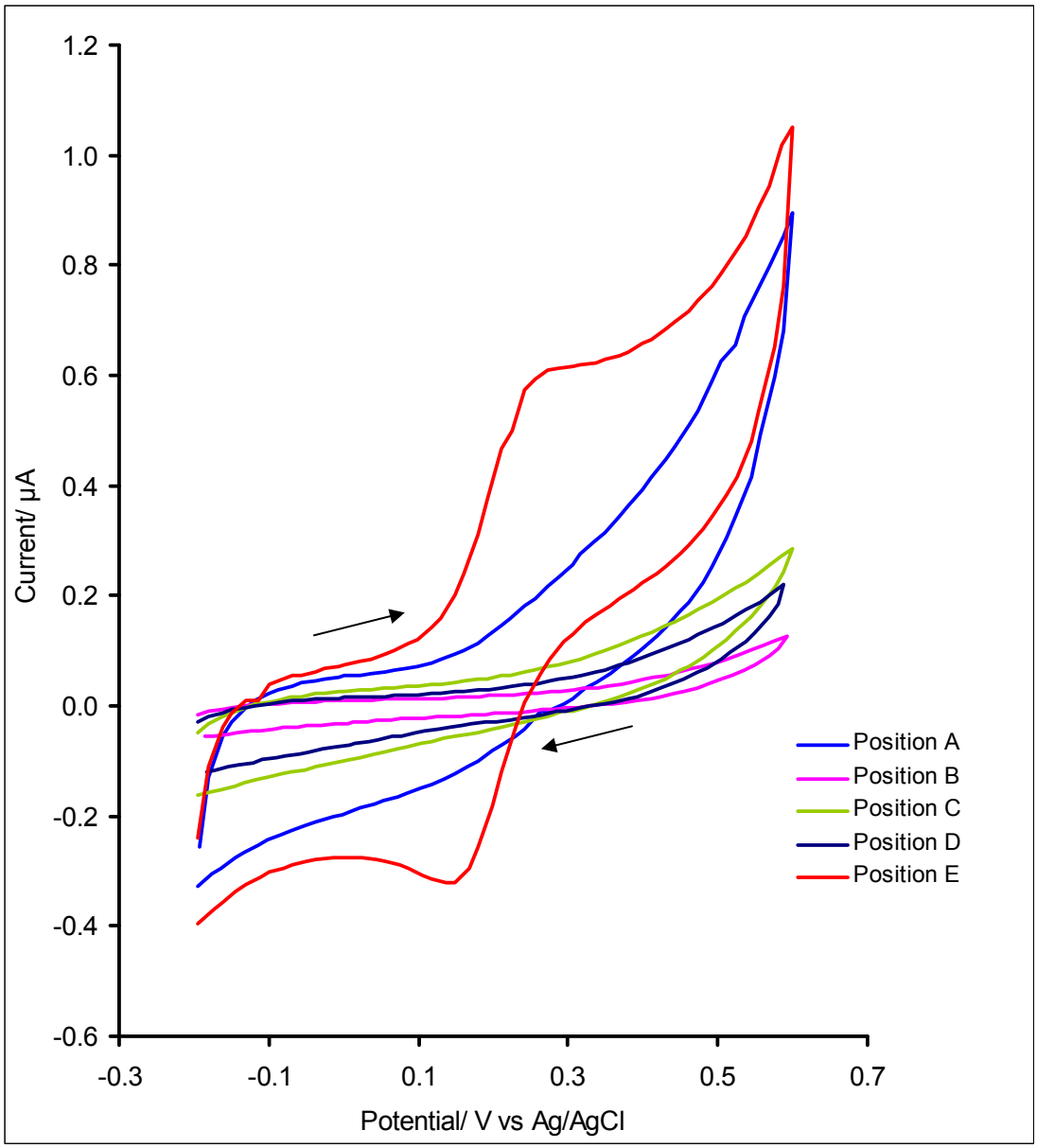

Fig 5.8 Cyclic voltammograms of 1mM FCA solution at sonochemically ablated polymer modified electrodes at 50% power for 30 seconds in five different positions.

[Supporting electrolyte: PBS pH 7.4, Scan rate: 50 mVs^{-1}]

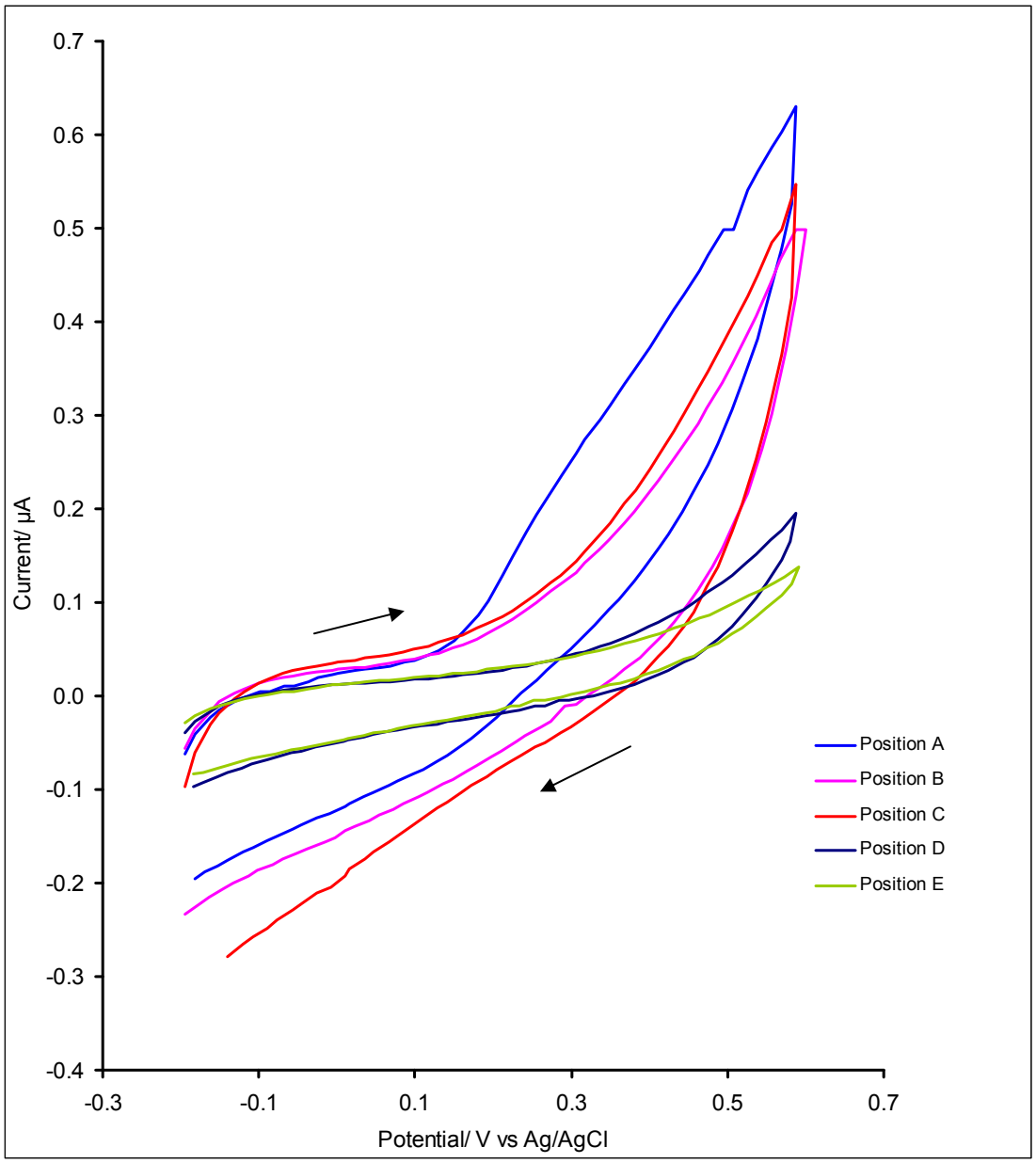

Fig 5.9 Cyclic voltammograms of 1mM FCA solution at sonochemically ablated polymer modified electrodes at 75% power for 30 seconds in five different positions.

[Supporting electrolyte: PBS pH 7.4, Scan rate: 50 mVs^{-1}]

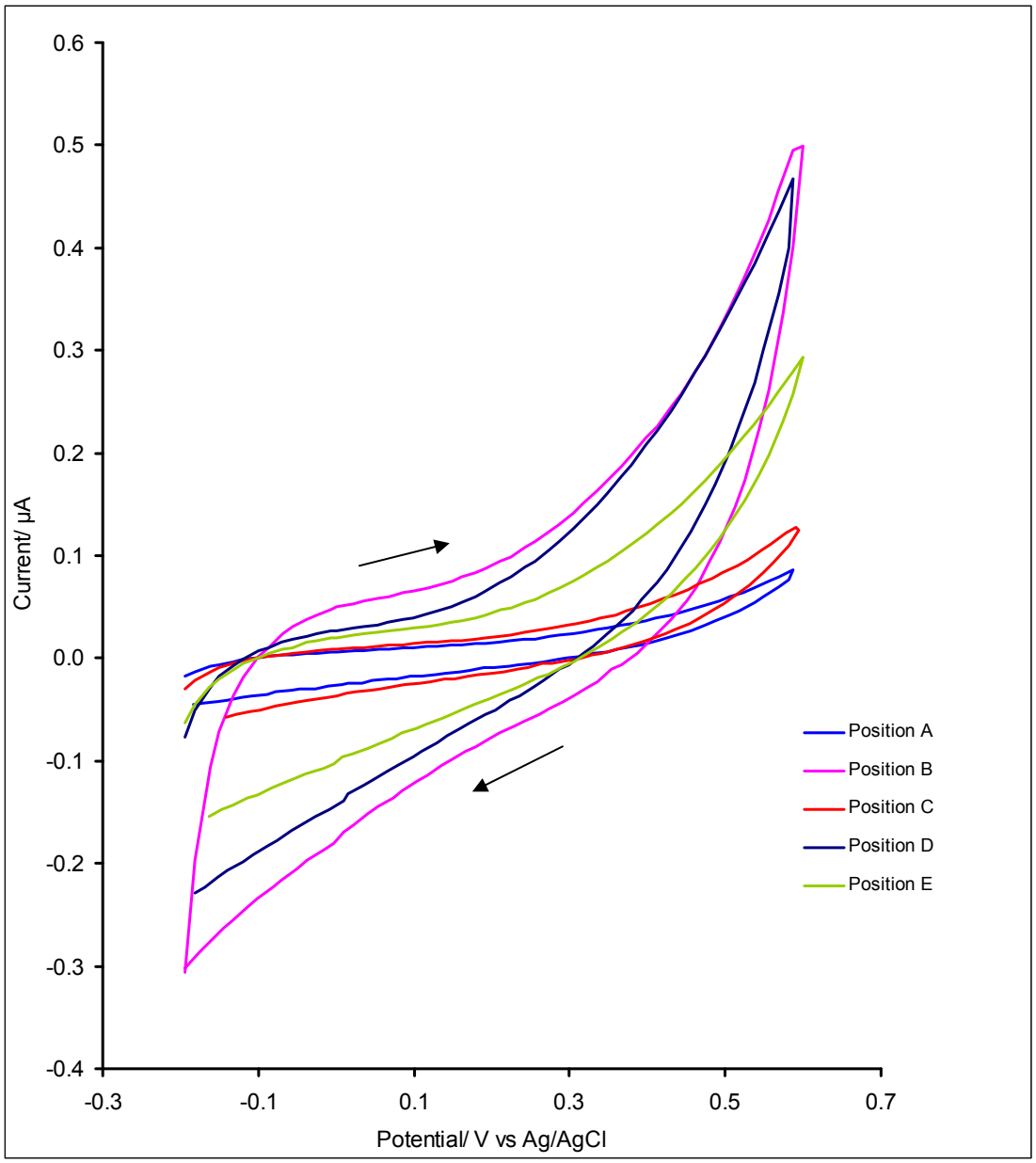

Fig 5.10 Cyclic voltammograms of 1mM FCA solution at sonochemically ablated polymer modified electrodes at 100% power for 30 seconds in five different positions.

[Supporting electrolyte: PBS pH 7.4, Scan rate: 50 mVs^{-1}]

It can also be noted that although for some electrodes there appears to be an electrochemical response at 50% or even 75% power settings, none or little response is recorded at 100% power at the same position on the mounting device. The electrodes in position A for example give an electrochemical response at 50 and 75 % power but show no response at 100% power. This is due to the physical damage caused on the underlying gold surface.

The need to account for the inhomogeneity of the cavitation phenomena becomes therefore apparent. One obvious solution would be to increase the homogeneity of the ultrasound within the tank. This would involve introducing further measures to the baffle and the mounting device, to spread more evenly the sonic waves and minimize the effect of the standing waves. A simpler solution would be to modify the sonication protocol to account for the various regions of different cavitation intensity. The latter solution was adopted by our research group since it does not involve costly alterations of the existing equipment and is described in the following section.

5.3.3 Introduction of a rotating mechanism

The electrochemical interrogation of the ablated polymer-modified electrodes in the previous section demonstrated the need to account for the inhomogeneity of the ultrasound within the sonication tank. The applied sonic wave is a series of nodes and anti-nodes whose distance has be determined to be around 3cm by previous members of our research group (Gornall, 2004; Mills, 2005). This separation is close to the natural variation of acoustic amplitude experienced in the vertical plane which results from antinodal positions in a 25.1 kHz standing wave field.

Bearing in mind that cavities in the polymer film take time to form and grow, it becomes apparent that if the sonic waves blasting the polymeric surface are not uniform, then the cavities formed will not be uniform either. The surface area of the electrode complicates matters even more because it is actually even smaller than the length between a node and anti-node of the applied wave. Therefore, at any given time, one electrode may be blasted constantly resulting in damaging the electrode surface whilst another one may not be affected by any sonic wave whatsoever.

A rotating device was therefore custom-built (Fig 5.11). The robotic device constructed permitted the movement in a circular vertical plane of 3cm radius. In this way, the sensors could be moved through the nodes and anti-nodes both vertically and horizontally and hence experience both the intense and moderate cavitation regions within the tank.

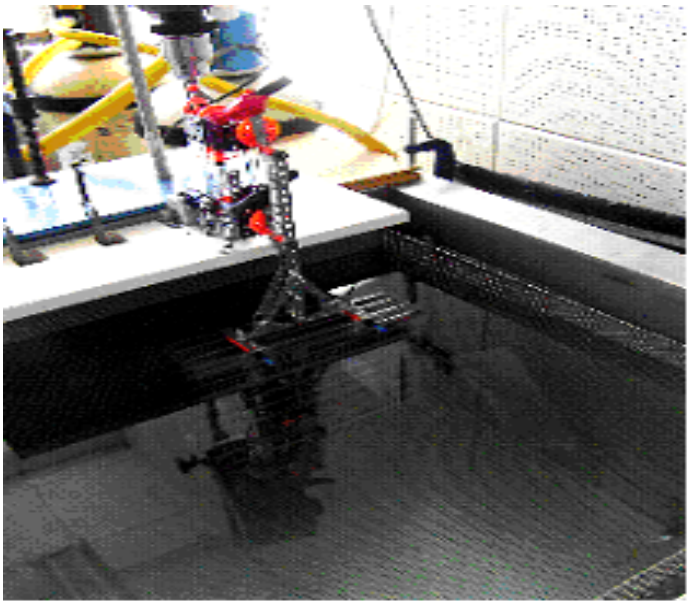

Fig 5.11 Rotating device for the movement of the sensor mounting device (not shown)

From the information ascertained from the cyclic voltammograms in Figs 5.8, 5.9 and 5.10, it appears that only the polymer modified electrodes in position E give a microelectrode-like behaviour when blasted at 50% power. This is the reason this position was chosen to test the effect of the introduction of the rotating device on the electrochemical behaviour of the sonochemically ablated electrode.

Sonochemically ablated electrodes were tested as described in the previous section in a solution of 1mM FCA in PBS pH7.4 buffer. Voltammograms of unmodified (planar) electrodes were compared to both P*o*PD insulated, and microelectrode array sensors fabricated by sonochemical ablation at 50% power, in Position E, with the use of the rotating device. (Fig 5.12).

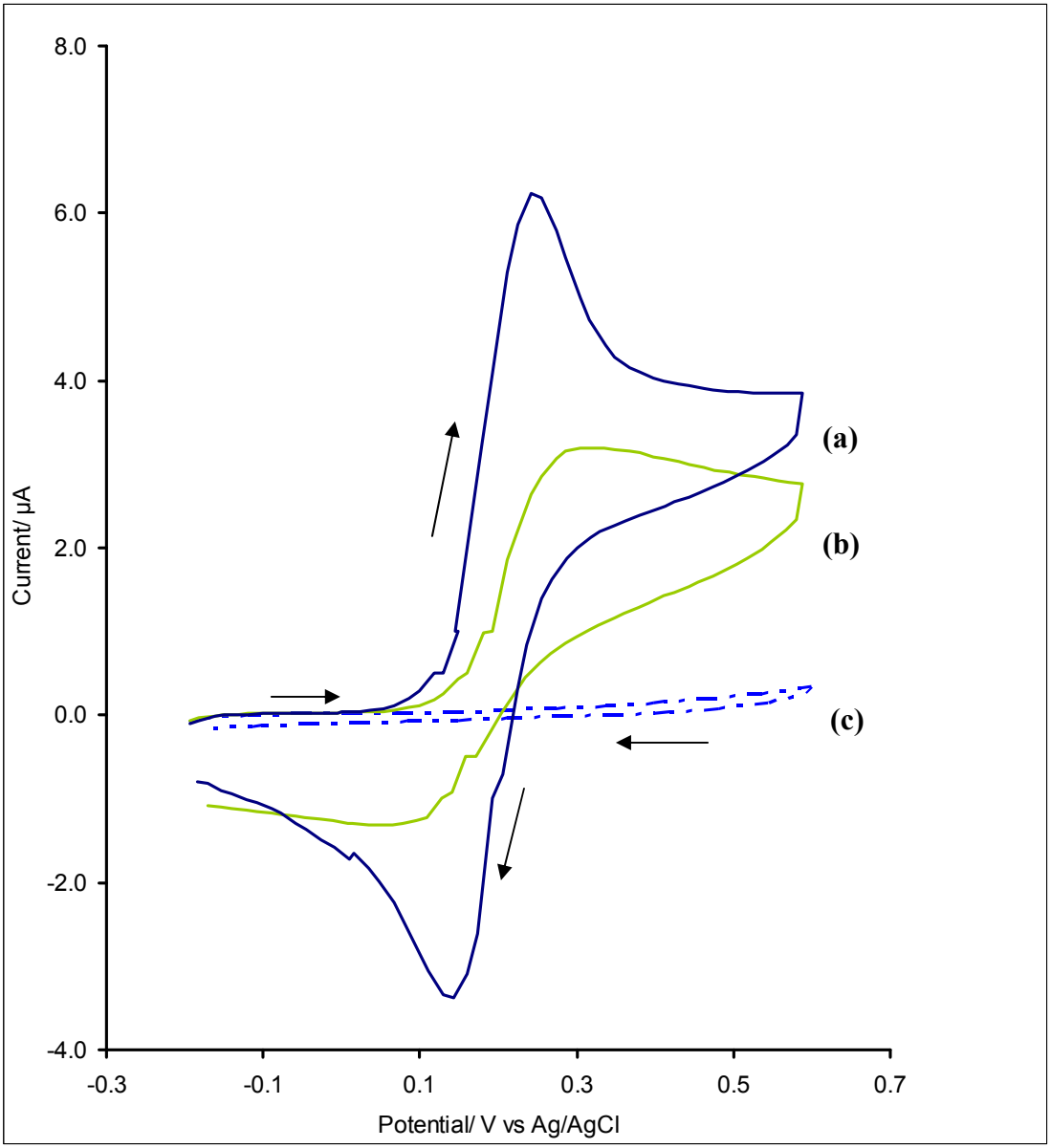

Fig 5.12 Cyclic voltammograms of 1mM FCA solution at a (a) bare screen printed gold electrode, an (c) ablated electrode at 50% power for 30 seconds with the use of the rotating device (position E) and a (b) PoPD coated screen printed gold electrode.

[Supporting electrolyte: PBS pH 7.4, Scan rate: 50 mVs^{-1}]

The voltammogram corresponding to the planar (uncoated) electrodes indicates a Nernstian peak separation of approximately 59 mV, as would be expected for a reversible, diffusion controlled single electron transfer process. In contrast, very little faradaic response is observed for the unsonicated, P*o*PD coated electrode, confirming the presence of a pristine, insulating polymeric layer.

Interrogation of the ultrasonically ablated microelectrode array sensors revealed a sigmoidal response, suggesting a non-linear (hemispherical) diffusion profile typically associated with microelectrode constructions. In both the forward, oxidative and the reverse, reductive current transients there is a characteristic plateau in which diffusion no longer acts as the rate limiting step but instead the electrode is now under kinetic control.

5.4 Conclusions

Initial attempts of producing microelectrode array assemblies were made by sonochemically ablating P*o*PD modified screen printed gold electrodes (P3) provided by the Tyndall Insitute, Cork, Ireland using a laboratory ultrasonic bath. The duration of the applied ultrasound was varied to optimise the fabricated arrays. The electrochemical behaviour of the sensors was determined using cyclic voltammetry in a ferri/ferrocene carboxylic acid redox couple. It has been shown that near microelectrode behaviour can be achieved after 30 seconds of exposure to ultrasonic waves in the ultrasonic bath.

Investigations into the mass production of gold microelectrode arrays based sensors were then performed in a large industrial-sized ultrasonic tank. The sonication parameters were optimised in terms of power and duration in order to obtain microelectrode arrays that possess sigmoidal voltammetric behaviour. These parameters were determined once again via cyclic voltrammetric interrogation of the fabricated arrays.

The sonication protocol was further enhanced via the use of a custom built mechanical system which rotated the electrodes attached to the mounting device in a radius that was sufficient to expose each individual electrode to approximately the same intensity

of cavitation, irrespectively of their positioning in the sonication tank. The introduction of the rotating device along with the use of a baffle to diffract the applied ultrasound and of a sensor mounting device to avoid variations in electrode responses caused by exposure to regions of acoustic turbulence and streaming, have permitted the fabrication of microelectrode arrays which show sigmoidal behaviour and offer good microelectrode array performance.

However, as highlighted in chapter 4, reproducibility is a key consideration in the development of immunosensors for biomedical applications. Exhaustive studies on the reproducibility of the fabricated microelectrode arrays, involving numerous P3 electrodes from the same or different batches, have demonstrated large deviations from the expected behaviour. This is probably due to the inhomogeneity observed within the ultrasound tank. Despite the improvements introduced to the sonication protocols, inhomogeneity issues have not been completely accounted for. Furthermore, as noted in chapter 4, inconsistencies of the electrochemical response towards FCA observed on bare P3 electrodes could also contribute to the irreproducible results obtained with the fabricated microelectrode arrays. For this reason, sonochemically fabricated microelectrode arrays were not employed in subsequent experimental set ups.

Chapter 6

Optimisation of the immunosensor fabrication protocol

6.1 Introduction

Most polymeric materials are poor electrical conductors because of the unavailability of large numbers of free electrons to participate in the conduction process. *O*-phenynediamine for example, used in the electrode characterisation experimental set-ups described previously, is a widely used polymer, which is insulating when electrodeposited at neutral pH values. However, there exist a number of polymers that permit some electrical conductivity in at least one redox state following their deposition on the electrode surface. These polymers are usually synthesised and possess electrical conductivities at least on par and in some cases better than semi-conductors. The polymer backbone itself is conducting, although they can be further doped with impurities to increase conductivity, resulting in the formation of either *n*-type (free radical dominant) or *p*-type (hole dominant) polymers. Unlike semiconductors, the dopant atoms do not replace or substitute for any of the polymer atoms (Roncali, 1992).

Conducting polymers can be exploited for the manufacture of planar electrode sensors in two ways; either by entrapping biomolecules during electrodeposition or by immobilizing biomolecules to their surface, following their electrodeposition. Furthermore, owing to their conductivity, the thickness of the polymer films can be easily varied and is not confined to very thin films, in comparison to those formed by insulating polymers.

The conductive polymer used for the fabrication of immunosensor platforms throughout this research project was polyaniline, referred to herein as PANI. PANI was the polymer of choice due to its ease of polymerisation, low cost, high conductivity and its high chemical durability against oxygen and moisture (Li *et al*, 2002). PANI is a conductive polymer of the semi-flexible rod polymer family, members of which are poly (*p*-phenylene oxide) and poly (*p*-phenylene sulfide) (Genies *et al*, 1990).

Aniline, also known as phenylamine or aminobenzene ($C_6H_5NH_2$) is a primary aromatic amine consisting of a benzene ring and an amino group. It is oily and, although colourless, it can be slowly oxidized in air to form impurities, which can

give rise to a red-brown tint. Chemically, aniline is a weak base. Aromatic amines such as aniline are generally much weaker bases than aliphatic amines.

Aniline undergoes oxidation at positive potentials to form PANI. The mechanism of polymer growth at carbon electrodes was first proposed by Yasui (Yasui, 1935). The polymerisation is initiated by the formation of an aniline radical cation, which is the rate-determining step (Fig 6.1).

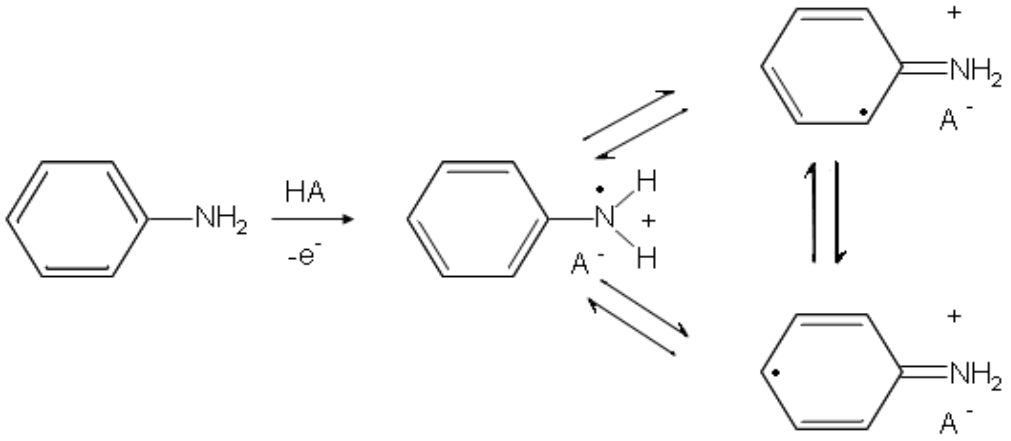

Fig 6.1 Formation of an aniline radical cation (Genies *et al*, 1985; Genies *et al*, 1988).

The monomer units are then connected in a head-to-tail fashion, i.e. a carbon atom bonds to a nitrogen atom. Dimerisation is accompanied with the simultaneous elimination of two protons (Fig 6.2).

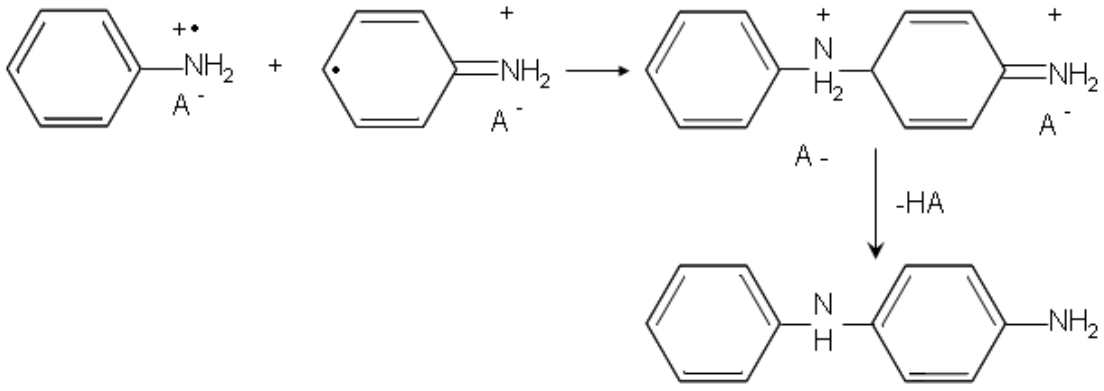

Fig 6.2 Radical coupling and dimerisation (Genies *et al*, 1985; Genies *et al*, 1988).

Subsequent oxidation of the formed dimers and trimers results in chain propagation (Mu *et al*, 1997). The formed polymer is doped by the acid (HA) present in solution (Fig 6.3). This is why PANI is one of the so-called doped polymers, in which conductivity results from a process of partial oxidation or reduction. PANI compounds can be designed to achieve the required conductivity for a given application. The resultant blends can be as conductive as silicon and germanium or as insulating as glass.

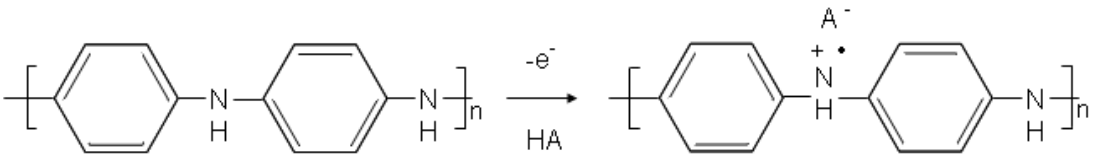

Fig 6.3 Polymer doping (Genies *et al*, 1985; Genies *et al*, 1988).

PANI may exist in three distinct redox states depending on the value of the pH when it is being formed: leucoemeraldine, emeraldine and pernigraniline.

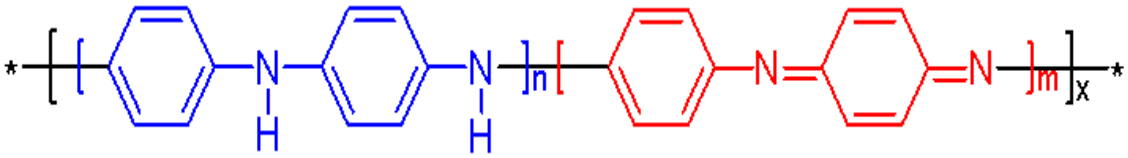

Fig 6.4 Generalised polyaniline structure.

In Fig 6.4, x equals half the degree of polymerization (DP); n represents an amine group and m an imine group. Leucoemeraldine with n = 1, m = 0 is the fully reduced state of PANI. Pernigraniline is the fully oxidized state (n = 0, m = 1) with imine links instead of amine links. In the emeraldine form of polyaniline, often referred to as emeraldine base (EB), the ratio of amine to imine groups is ~0.5, hence EB is neutral.

Emeraldine base is regarded as the most useful form of polyaniline due to its high stability at room temperature, compared to the easily oxidized leucoemeraldine and the easily degraded pernigraniline. Emeraldine salt, which is conductive, can be formed by doping of the emeraldine base with the acid present within the solution.

PANI was electrodeposited on the electrode to form a matrix on which antibodies could be attached through the affinity interactions between biotin and neutravidin (Section 2.8.3). This chapter deals with the optimization of PANI deposition on the screen printed carbon electrodes. Towards this goal, efforts were made to maintain the conductive state of the film so as to facilitate electron transfer between the antibody/antigen complexes and the electrode. As the conductivity of PANI decreases, as the pH of the buffer solution increases, polymerization solutions of three different pH values were tested. Deposition of PANI on the electrodes' surface was tested with the use of a quartz crystal microbalance.

6.2 Optimisation of aniline electrodepositon on carbon electrodes

6.2.1 Polymerisation of aniline in a pH 5.0 acetate buffer

A solution of 0.2M aniline in acetate buffer pH 5.0 was electrodeposited at the surface of screen printed carbon electrodes by cyclic voltammetry. The potential was cycled between -200 and +800 mV vs. Ag/AgCl at a scan rate of 50 mVs^{-1} for a 100 progressive potential cycles.

In Fig 6.5, the first scan exhibits a discernable and irreversible anodic peak due to monomer oxidation at 650mV (vs. Ag/AgCl). As cycling continues, this peak diminishes. No cathodic peak can be observed. The anodic peak corresponds to the oxidation of aniline to the corresponding radical cation and then its dimerisation.

The absence of a cathodic peak indicates a fast consumption of the electrogenerated monocation and dication radicals by subsequent chemical reactions that result in the elongation of the forming PANI film on the electrode - as discussed in the previous section.

The current recorded, decreases with each progressive potential cycle. This is due to the deposition of emeraldine base on the electrode surface. This is due to the pH value of the buffer not being sufficiently acidic to produce a doped polymer film. The polymer film deposited is hence effectively insulating.

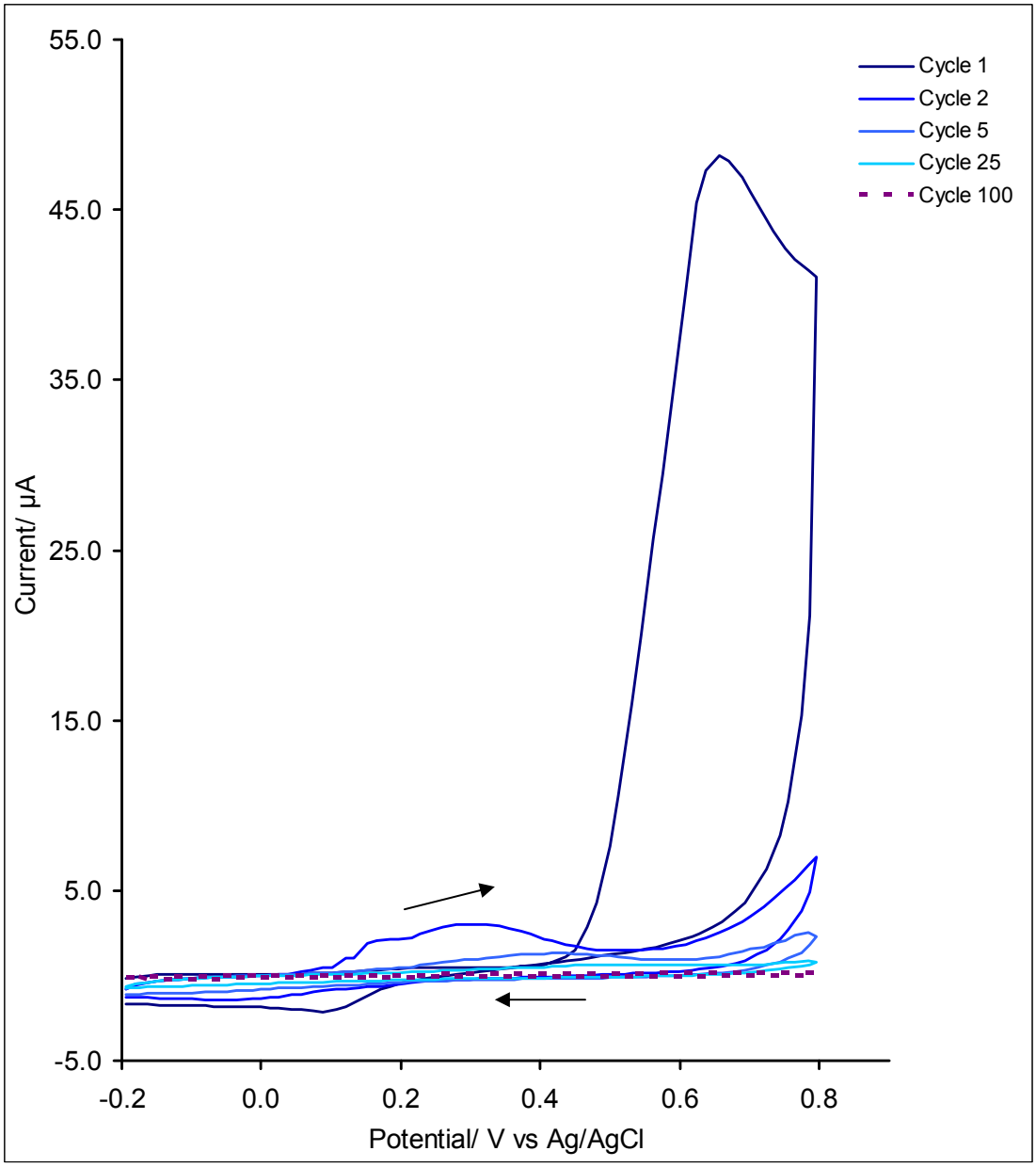

Fig 6.5 Cyclic voltammogram for the electropolymerization of 2M aniline at a screen printed carbon electrode (Cycles 1, 2, 5, 25 and 100 are shown).

[Supporting electrolyte: pH 5.0 acetate buffer, Scan rate: 50 mVs^{-1}]

The behaviour of the polymer modified sensors was studied voltammetrically in a solution of 1mM ferrocene carboxylic acid (FCA) in PBS pH7.4 buffer prior to and following the polymer deposition (Fig 6.6). The potential was swept from -200mV to +600mV vs. Ag/AgCl at $50mVs^{-1}$.

In Fig 6.6, the complete passivation of the electrode surface following deposition of PANI is observed, since no peaks appear in either the anodic or cathodic direction. The peak separation observed of 68mV (vs. Ag/AgCl) is approximately in line with the behaviour of a completely reversible one electron transfer reaction as dictated by the Nernst equation (Eqn 2.10).

Nevertheless, the aim of polyaniline electrodeposition on the carbon electrodes was not to produce an insulating film but a conductive matrix upon which to immobilise the antibodies in order to fabricate an immunosensor platform. For this reason, the electrodeposition of PANI, dissolved in buffers of lower pH values, was investigated.

6.2.2 Polymerisation of aniline in a pH 2.7 solution

It is known that the more acidic the pH value of the buffer in which aniline is dissolved, the more conductive the electrodeposited polymer film will be. Due to the insulating properties of the polymer film in a pH 5.0 acetate buffer observed in the previous section, a more acidic buffer (pH 2.7) was investigated, whose composition can be found in chapter 3.

A solution of 0.2M aniline in a pH 2.7 buffer was electrodeposited on the surface of screen printed carbon electrodes by cyclic voltammetry. The potential was cycled between -200 and +800 mV vs. Ag/AgCl at a scan rate of 50 mVs^{-1} for a 100 progressive potential cycles.

In Fig 6.7, the first potential cycle exhibits a similar irreversible anodic peak as the one observed for the electrodeposition of polyaniline in a pH 5.0 acetate buffer (Fig 6.5). This peak is due to monomer oxidation and occurs at 790mV (vs. Ag/AgCl).

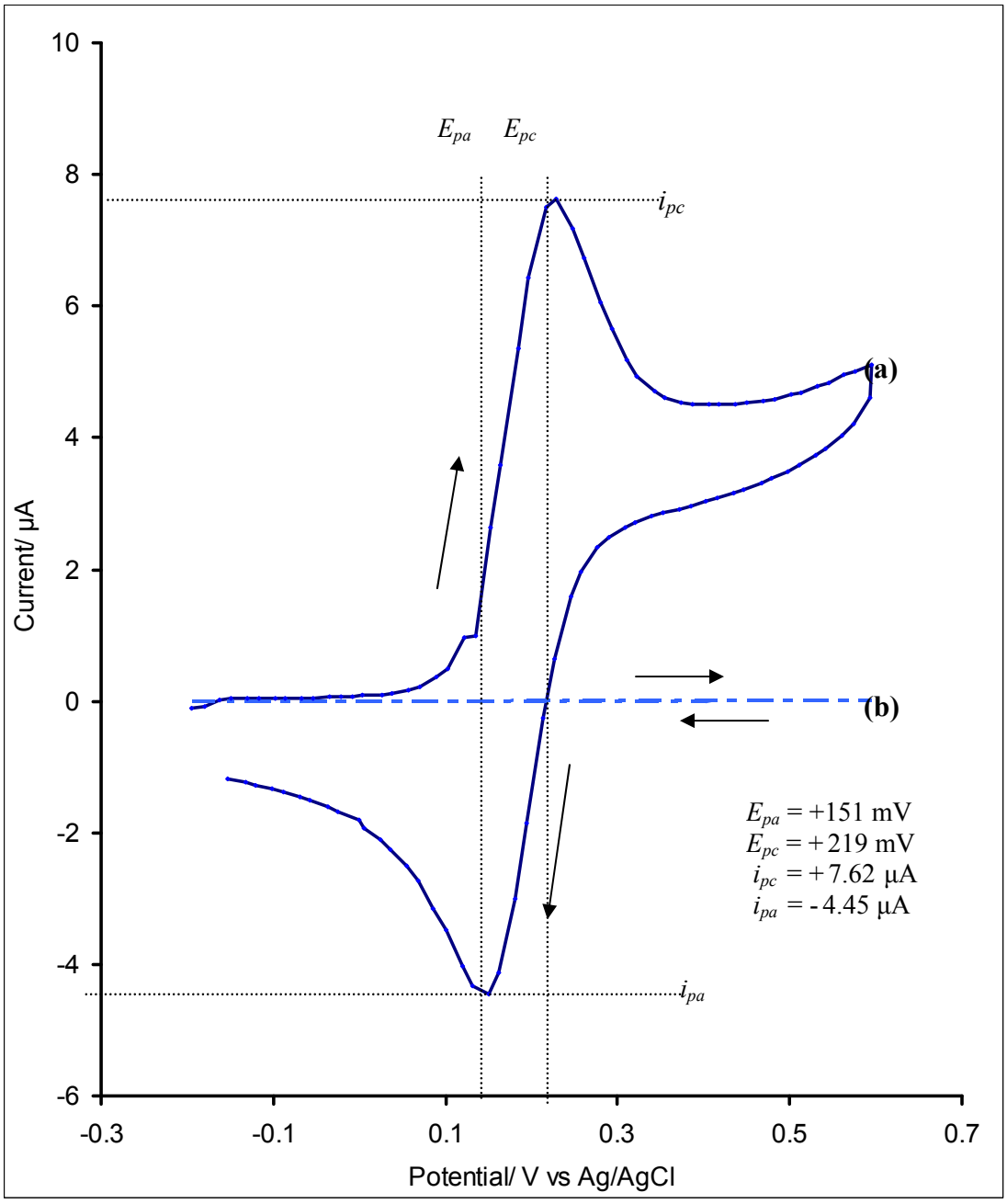

Fig 6.6 Cyclic voltammogram of a 1mM FCA solution at a (a) polyaniline coated screen printed carbon electrode in a pH 5.0 acetate buffer and (b) the same bare screen printed carbon electrode.

[Supporting electrolyte: PBS pH 7.4, Scan rate: 50 mVs^{-1}]

As cycling continues this peak decreases. Furthermore, no cathodic peak can be observed. In the second scan, one redox system at +322mV (anodic)/ +239mV (cathodic) (vs. Ag/AgCl) appears. The currents on the anodic and cathodic waves of this system increase steadily with each progressive potential cycle, reflecting the growth of the conductive PANI film.

The irreversible anodic peak corresponds to the oxidation of aniline to its radical cation and subsequently of this radical cation oxidation to form a dication. The absence of a cathodic peak indicates a fast consumption of the electrogenerated radical monocations and dications by subsequent chemical reactions to form the electroactive polyaniline film on the electrode. The appearance of the new redox peaks at less positive potentials illustrates the latter and it is the result of doping reactions on the forming PANI film.

At this point, it is worth noting that the magnitude of the peak redox currents recorded following 25 and 100 cycles is almost identical. This shows that there exists a point after which further deposition of PANI does not result in increased conductivity. Investigations into the number of potential cycles required to achieve optimum conductivity of the deposited polyaniline film, showed that 25 potential cycles produce the most conductive film (Fig 6.8). The current response obtained after 25 cycles of PANI deposition in a solution of 1mM FCA in PBS pH 7.4 buffer was compared to that of the same bare electrode. The increase in conductivity can be easily observed (Fig 6.9).

6.2.3 Polymerisation of aniline in a pH 1.0 solution

Following electrodeposition of PANI films in a pH 2.7 buffer, polymerization conditions were further optimized by shifting the pH of the buffer to even more acidic values. A solution of 0.2M aniline in a pH 1.0 buffer was electrodeposited on the surface of screen printed carbon electrodes by cyclic voltammetry. The potential was cycled between -200 and +800 mV vs. Ag/AgCl at a scan rate of 50 mVs^{-1} for 20 potential cycles and terminated at +800 mV vs. Ag/AgCl.

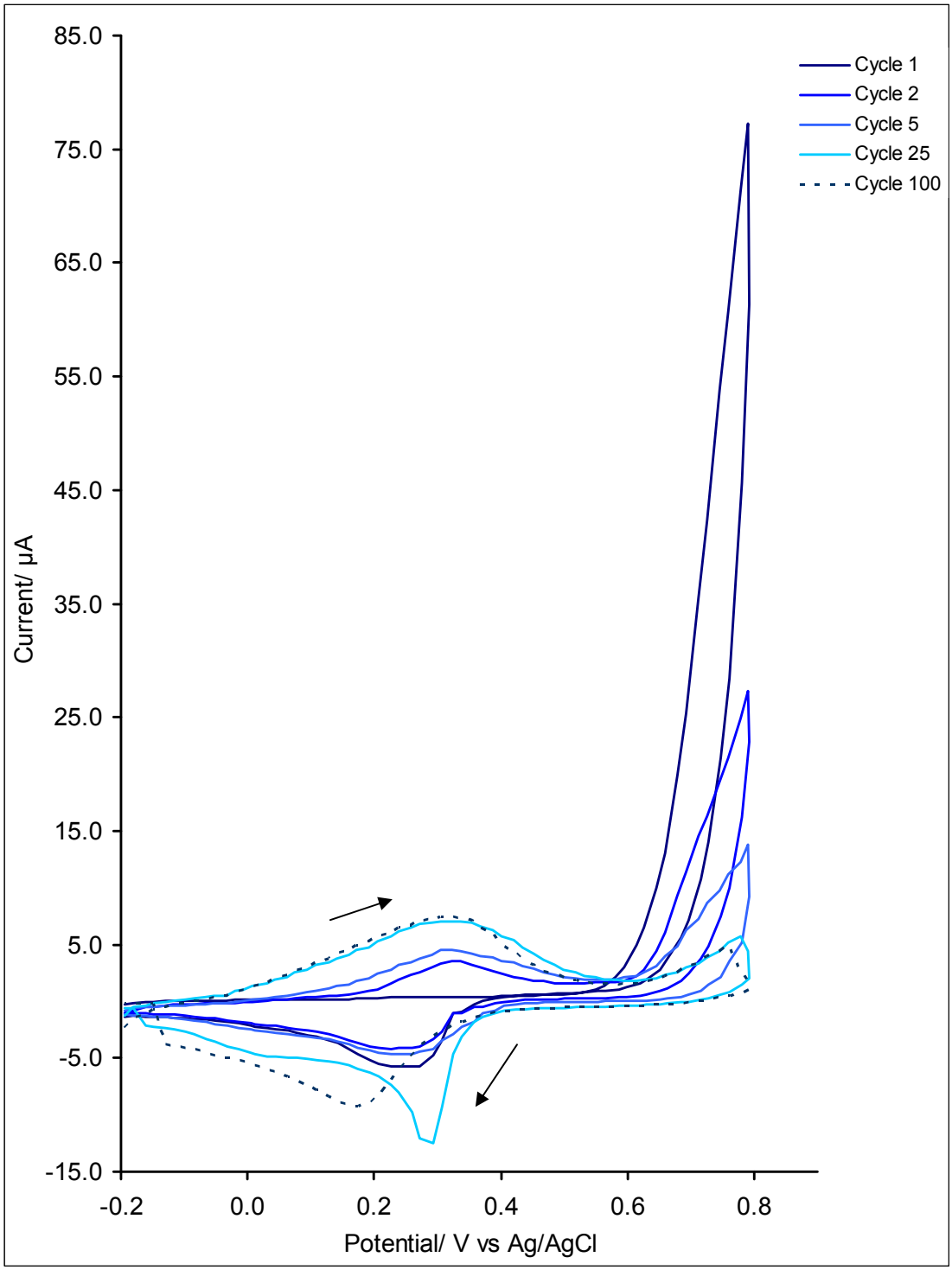

Fig 6.7 Cyclic voltammogram for the electropolymerization of 2M aniline at a screen printed carbon electrode in (Cycles 1, 2, 5, 25 and 100 are shown).

[Supporting electrolyte: pH 2.7 buffer, Scan rate: 50 mVs^{-1}]

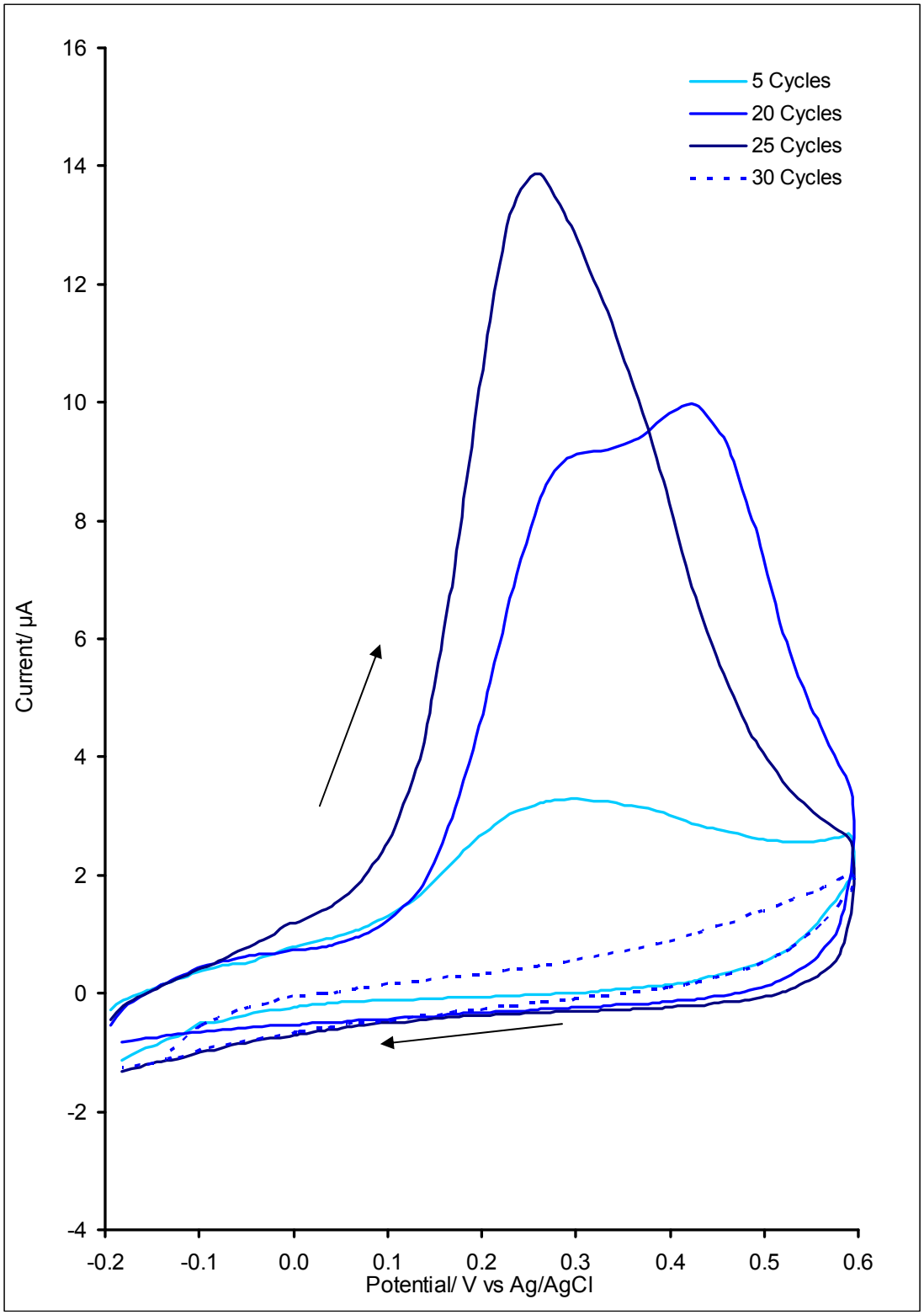

Fig 6.8 Cyclic voltammogram of a 1mM FCA solution after 5, 20, 25 and 30 potential cycles of polyaniline electrodepositon in a pH 2.7 buffer.

[Supporting electrolyte: PBS pH 7.4, Scan rate: 50 mVs^{-1}]

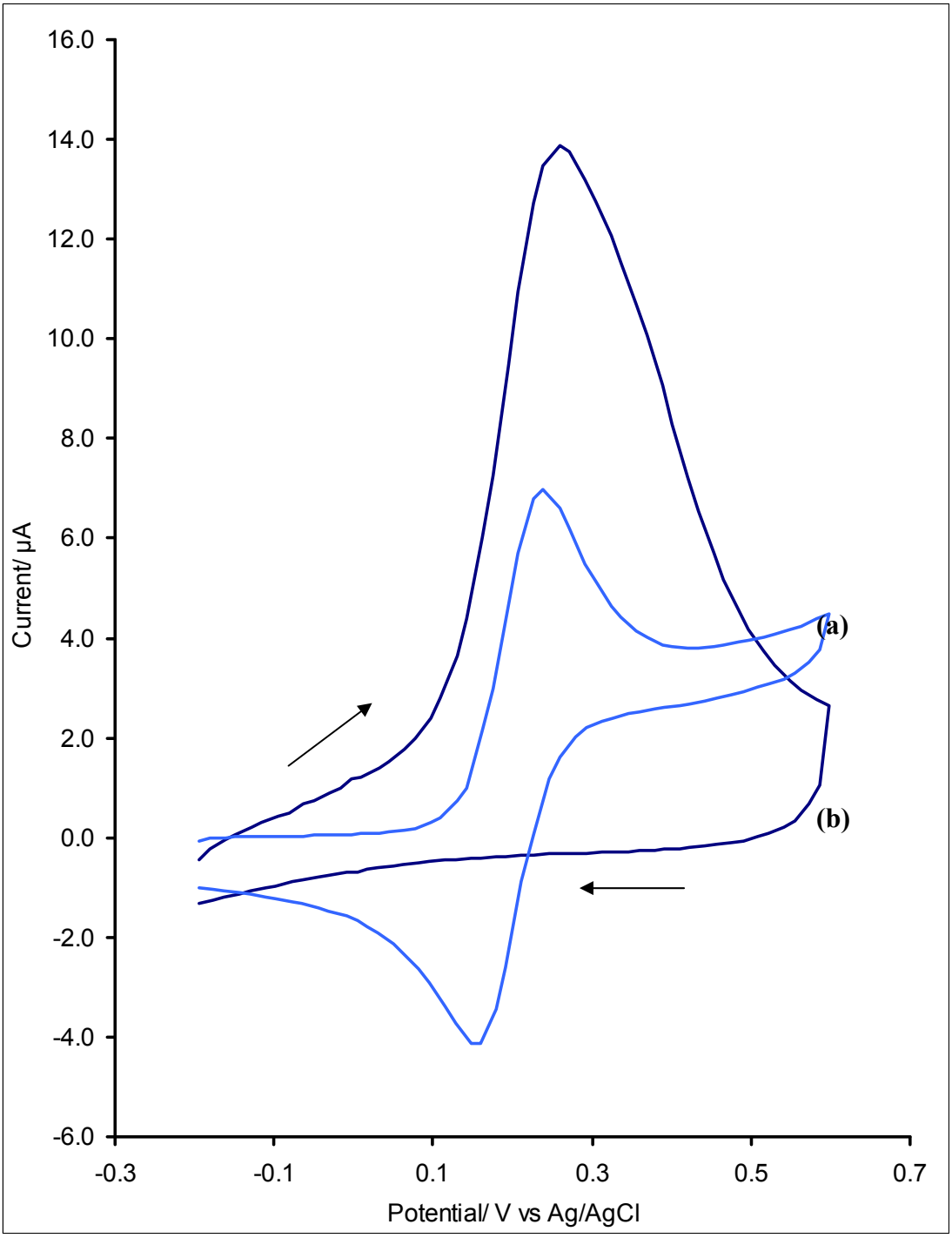

Fig 6.9 Cyclic voltammogram of a 1mM FCA solution at a (a) bare screen printed carbon electrode and (b) the same polyaniline coated screen printed carbon electrode in a pH 2.7 buffer.

[Supporting electrolyte: PBS pH 7.4, Scan rate: 50 mVs^{-1}]

The number of potential cycles was decreased since, as shown in Fig 6.10, at this pH value, PANI electrodeposition is no longer a self-limiting process. Furthermore, the polymer film deposited in a pH 1.0 buffer following 20 potential cycles exhibits an 8-fold increase in conductivity compared to the polymer film deposited after the same number of potential cycles in pH 2.7 buffer, hence less potential cycles are required to coat the electrode with highly conductive PANI films. The potential cycling was terminated at +800 mV vs. Ag/AgCl due to emeraldine salt being deposited during the positive direction of potential sweeping.

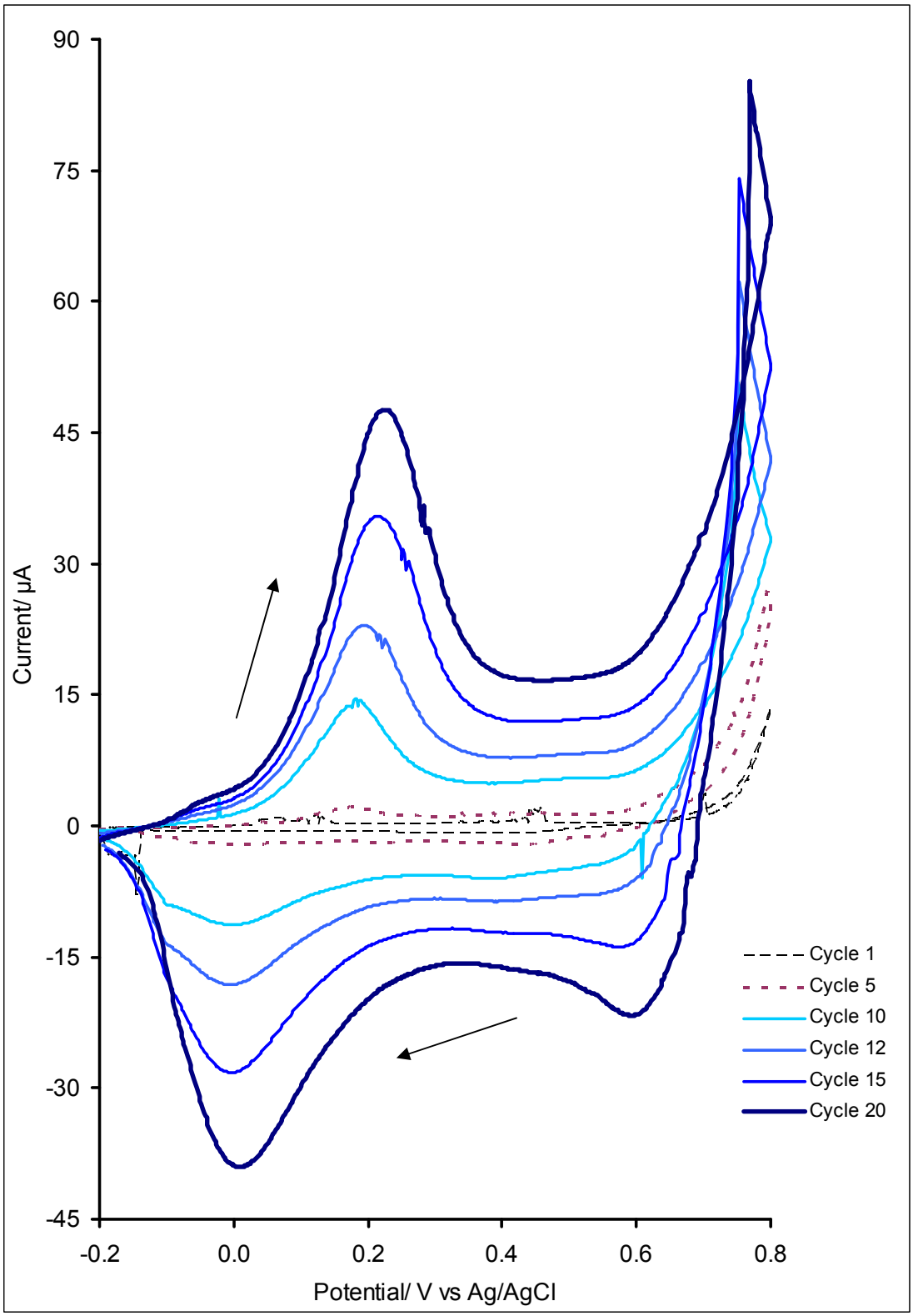

Fig 6.10 Cyclic voltammograms for the electropolymerization of 2M aniline at a screen printed carbon electrode (Cycles 1, 5, 10, 12, 15 and 20 are shown).

[Supporting electrolyte: pH 1.0 buffer, Scan rate: 50 mVs^{-1}]

6.3 Quartz Crystal Microbalance PANI deposition validation

The deposition of PANI films on the surface of gold-coated quartz crystal chips was monitored with the use of a QCM (Fig 6.11). The sensitivity of the QCM is approximately 100 times higher than an electronic fine balance with a sensitivity of 0.1μg. This means that QCMs are capable of measuring mass changes as small as a fraction of a monolayer or single layer of atoms.

PANI electrodeposition was performed following the same protocol as for its deposition on screen printed carbon electrodes in a pH 1.0 buffer. Fig 6.11 illustrates the cyclic mass change for the electrogeneration of a PANI film on a QCM chip after 20 cyclic depositions and 1 linear sweep to +800mV. The frequency shift related to mass increase at the surface by the Sauerbrey equation equates to approximately 6μg cm^{-1} of PANI growth (Eqn 2.44).

The electrochromic phenomenon of PANI was also observed throughout the electrodeposition as PANI transitions from colourless leucoemeraldine (-200mV) to its protonated green emeraldine salt (+800mV). The deprotonated form of emeraldine salt, emeraldine base is blue.

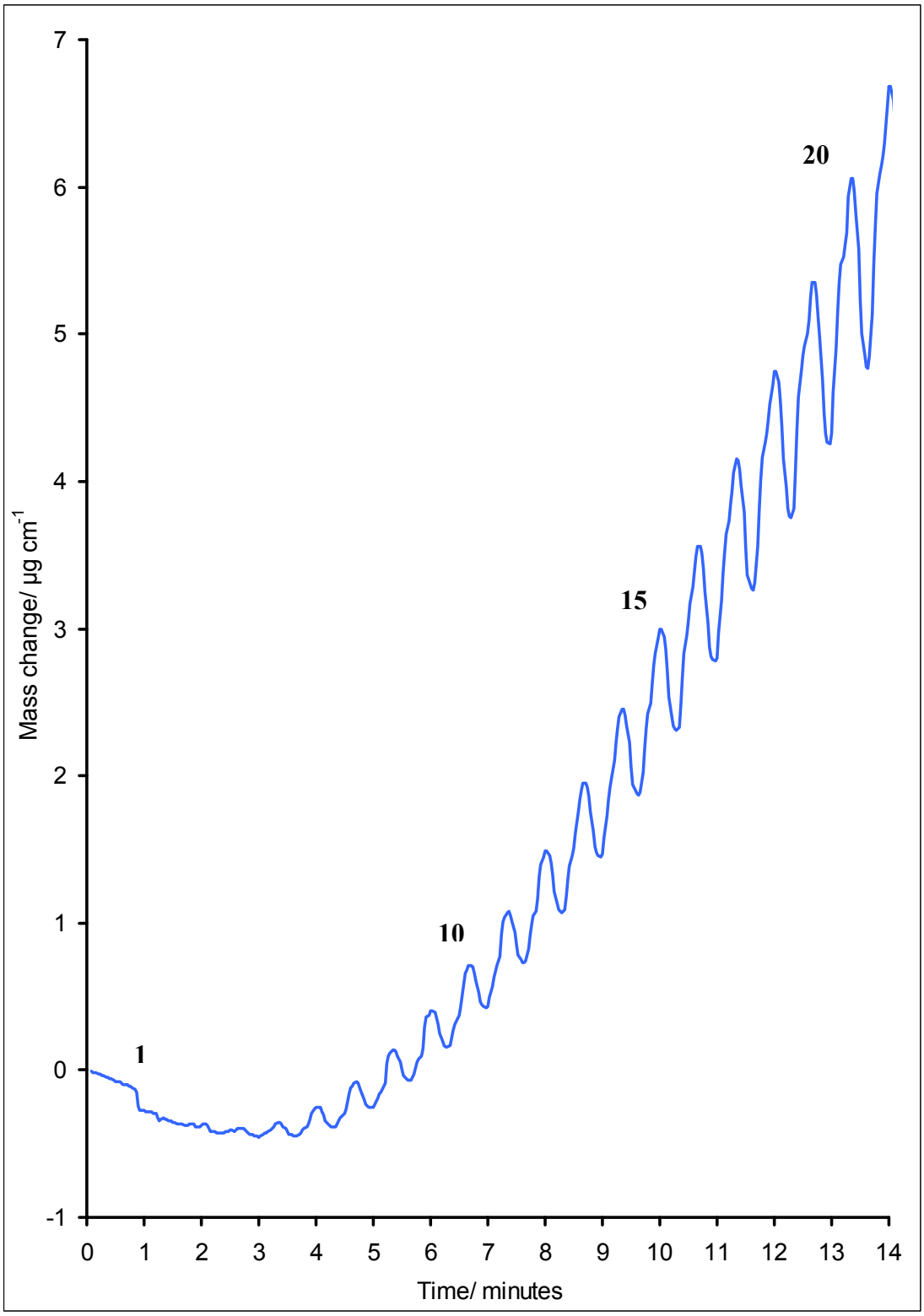

Fig 6.11 QCM data showing the electrodeposition of PANI on a QCM chip.

6.4 Immobilisation of antibodies following PANI deposition on the electrode surfaces

The stable immobilisation of biomolecules on conductive surfaces with complete retention of their biological recognition properties is a crucial problem for the commercial development of miniaturised biosensors. Effectively most of the conventional procedures of biomolecule immobilisation such as cross-linking, covalent binding and entrapment in gels or membranes suffer from low reproducibility and a poor spatially controlled deposition.

Within this work, the use of an affinity-based immobilisation system is reported to specifically orientate a monolayer of antibody receptors on electrodeposited PANI films thus forming an immunosensor. Such a system could take advantage of Protein A/Protein G or avidin/biotin interactions, as already discussed in Section 2.7.3.

Due to the high affinity constant of the avidin-biotin interaction (association constant $K_a = 10^{15}$ M^{-1}) (Wilchek & Bayer, 1998), this coupling system has been used for protein immobilisation on biotinylated polymer films. To be more precise, a deglycosylated form of avidin was used, neutravidin, for the reasons mentioned in Section 2.7.3. The attachment of antibodies is achieved via the simple formation of two neutravidin-biotin bridges between a molecule of neutravidin and biotinylated PANI and the same molecule of neutravidin and biotinylated antibodies. The avidin-biotin interaction is the strongest known biochemical (non-covalent) bond (Vermette *et al*, 2003).

The protocol relating to the biotinylation of PANI films and antibodies as well as to the affinity immobilization of the latter on the former via the use of neutravidin can be found in Section 3.5.3.1. A similar protocol was followed by Ouerghi and his team, to fabricate immunosensors by using avidin-biotin bridges between electropolymerised biotinylated polypyrrole films and biotinylated antibodies (Ouerghi *et al*, 2002).

6.5 Conclusions

This chapter has described the investigations into the coating of electrodes with a conductive film of polyaniline as the first step towards the construction of immunosensor platforms.

The presented results have allowed an enhanced understanding of the oxidation reactions of aniline occurring at the electrode/solution interface resulting in the coating of the latter with PANI. It has been shown that the optimum conductive PANI films can be obtained by employing a very acidic buffer of pH 1.0.

In contrast, the usage of a pH 5.0 acetate buffer yielded films with insulating properties. The deposition of PANI in a pH 2.7 buffer results in a conductive film, however it is a self-limiting process since after 25 potential cycles the current recorded on the polymer coated electrodes does not increase any further.

The number of potential cycles required to deposit a sufficiently conductive PANI film in a pH 1.0 buffer is, however, less. 20 potential cycles will be used in all subsequent experimental set-ups.

The deposition of PANI on the screen printed carbon electrodes was validated with a quartz crystal microbalance, which allowed for the detection of minute mass changes caused by polymer deposition on the quartz crystal chips.

Having therefore established the optimum conditions of aniline deposition we then proceeded in the immobilization of antibodies. This was performed according to the protocol described in Chapter 3, which involved a sophisticated and elegant strategy of non-covalent affinity attachment whereby the orientation of the receptor biomolecules can be controlled to a greater extent to facilitate antibody-antigen interactions. The polymer-coated surface was biotinylated and then exposed to neutravidin. The biotinylated antibodies were allowed to bind to the PANI-biotin-neutravidin complex on the electrode surface. As a final step, the surface of the sensors was blocked with a BSA solution to minimise non-specific binding upon exposure to the antigen solutions.

At this stage, the immunosensor platforms were ready to be employed in the subsequent impedimetric interrogations described in the following chapters. Chapter 7 is dedicated to studies relating to the fabrication of an immunosensor for the detection of ciprofloxacin. Chapter 8 describes an immunosensor for sensing Myelin Basic Protein. Finally, Chapter 9 is concerned with the construction of an immunosensor for Cancer Antigen 125.

Chapter 7

Electrochemical Impedance Studies on ciprofloxacin immunosensors

7.1 Introduction

Potentiometric immunoassays have been of great interest since the 70s. These are based on the premise that proteins in solution are polyelectrolytes and hence, as an antibody is a protein, its electrical charge will be affected upon binding with an antigen. The potential difference between an electrode to which an antibody has been immobilised, and a reference electrode, will depend on the concentration of the bound antigen, assuming that the antibody-binding site is free to participate in the interaction with the antigen. Although the immobilization of enzymes on the surface of electrochemical sensors has been reported as early as 1962 (Clark and Lyons, 1962), the incorporation of antibodies into conducting polymer films was first demonstrated in 1991. Anti-human serum albumin (anti-HSA) was incorporated into a polypyrrole film, which was galvanostatically polymerised onto a platinum wire substrate. When the pyrrole anti-HSA electrode was exposed to 50μg ml^{-1} HSA for ten minutes, a new reduction peak was observed at a potential of approximately +600mV vs. Ag/AgCl. This peak increased in magnitude after a further thirty minutes in the same solution and it was suggested this could be due to an antibody/antigen interaction with the polymer. Further work by the same group gave rise to reports of a reversible real-time immunosensor (John *et al*., 1991). Other early work utilized a pulsed amperometric detection technique for other analytes, including *p*-cresol (Barnett *et al*., 1994), thaumatin (Sadik *et al*., 1994), and polychlorinated biphenyls (Bender and Sadik, 1994). Since then, there has been a huge increase in the development of electrochemical immunosensors as detailed in several recent reviews (Diaz-Gonzalez *et al*., 2005).

More recently, impedance spectroscopy has become a rapidly developing electrochemical technique for the characterisation of biomaterial-functionalised electrodes and biocatalytic transformations at electrode surfaces, as well as specifically for the transduction of biosensing events at electrodes (Sargent and Sadik, 1999; Bardea *et al*, 2000; Berggren *et al*, 2000; Kharitonov *et* al, 2000; Alfonta *et al*, 2001; Katz *et al*, 2001; Kharitonov *et al*, 2000; Ouerghi *et* al, 2002; Katz & Willner, 2003; Guan *et al*, 2004; Tang *et al*, 2004; Wang *et al*, 2004; Wu *et al*, 2005). The immobilisation of biomaterials, in this case antibodies, alters the capacitance and interfacial electron transfer resistance of the conductive surface. Impedance

spectroscopy allows analysis of interfacial changes such as differing redox states of the polymer, faradaic charge transfers and also capacitive transduction events originating from bio-recognition events at electrode surfaces. The recognition complex formed between the sensing biomaterial and the analyte alters the capacitance and resistance at the modified surface-electrolyte interface. These two components can be measured as separate entities using impedance spectroscopy.

A small-amplitude sinusoidal voltage or current perturbation is applied to the system at various frequencies, and then the response is monitored. The amplitude signals are typically 5mV or smaller, since the current-potential relationship is then approximately linear rather than exponential. The results are often interpreted in terms of equivalent electrical circuits, that is, via networks of resistors and capacitors, and sometimes other types of components. Another way of presenting the results is by monitoring the impedance as a function of frequency. In a Bode plot, the total impedance is plotted against the logarithm of the frequency. In a Nyquist plot, Z'' (imaginary component), is plotted against Z' (real component).

This study has chosen the use of electrochemical impedance spectroscopy (EIS) because it allows for the resolution of both the kinetic and/or mass transport processes occurring within a system at various applied potentials and frequencies, using only minimal alternating current perturbations. By contrast, characterization of antibody-antigen interactions by means of thermodynamic concepts has failed to describe adequately their non-equilibrium kinetics at conducting polymer surfaces.

This chapter investigates the antibody – antigen (Ab-Ag) interactions at screen printed carbon electrodes, modified with conducting PANI, utilising electrochemical impedance spectroscopy techniques. Immunosensors interrogated in this chapter were successfully fabricated via a step-wise protocol to ensure orientation specific immobilisation of antibodies utilising neutravidin-biotin non-covalent affinity technologies as detailed in section 3.5.3.1.

In all cases, the sensors were blocked with a bovine serum albumin (BSA) solution prior to exposure to antigen solutions so as to minimize non-specific binding. This has been proven to be of great importance in previous studies, since material absorbs on

the surface of the sensors, which can alter the obtained impedance spectra, which in turn can lead to erroneous results.

Following the immobilisation of antibody receptor molecules at the surface of conducting emeraldine PANI films, the immunosensor assemblies were exposed to increasing concentrations of complementary antigen in buffered test solution - and subjected to electrochemical impedance spectroscopy. For every specific sensor assembly analysed a matched control sensor was also interrogated to allow for a corrected non-specific response. In this case the antibody immobilised was non-specific to the target analyte. Three replicate sensors were used for all experimental set ups and the results shown are the mean values obtained.

The specific aim of the investigation was to develop an analytical test for the labeless detection of ciprofloxacin. The quinolones are a family of broad-spectrum antibiotics with the majority of quinolones in clinical use being fluoroquinolones, which have a fluoro group attached to the central ring system. They are widely used within adult patients because of excellent tissue penetration, which makes them extremely effective against bacteria that grow intracellularly such as salmonella (Gendrei *et al.*, 2003). Ciprofloxacin, a member of the fluoroquinolones (Fig 7.1), is a broad-spectrum antibiotic active against many bacteria including anthrax (Torriero et al. 2006). Many of these fluoroquinolones are added to farm animal feed since they can lead to greater and more rapid weight gain. Unfortunately the effect of this is thought to have enabled the rise of resistant species of bacteria (Gendrei *et al*., 2003).

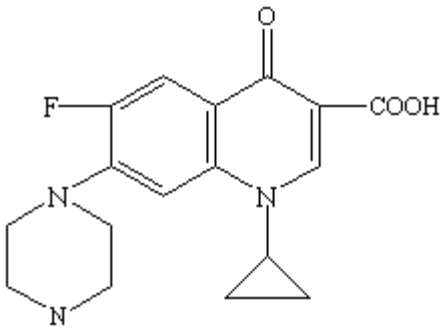

Fig 7.1 Structure of ciprofloxacin.

The monitoring of fluoroquinolones within both food and the environment is important since these antibiotics have potential health and environmental damaging effects. Ciprofloxacin concentrations in hospital outflow water between 0.7-124.5 ng ml^{-1} were measured using high performance liquid chromatography (HPLC) and shown to display genotoxicity at levels as low as 5.2 ng ml^{-1} (Hartmann *et al*., 1999). Similar work (Batt *et al*., 2006) measured wastewater ciprofloxacin using liquid chromatography/mass spectrometry/mass spectrometry (LC/MS/MS) and found levels between 0.031-5.6 ng ml^{-1} (even after treatment) with a limit of detection of 0.030 ng ml^{-1}. Levels *in vivo* have also been widely studied with the therapeutic ranges typically being between 0.57-2.30 μg ml^{-1} in serum and 1.26-4.03 μg g^{-1} in tissue (Licitra *et al*., 1987).

A recent publication (Torriero *et al.*, 2006) details the use of a horseradish peroxidase based biosensor for the detection of ciprofloxacin due to its inhibition of the oxidation of catechol, however other piperazine based compounds could potentially interfere with this determination. Linear responses were obtained between 0.02-65 μM with the limit of detection being 0.4 nM.

The goal of this work was therefore to develop a labeless immunosensor for the detection of ciprofloxacin within the range of therapeutic/clinical significance.

7.2.1 Electrochemical impedance spectroscopy (EIS) studies on ciprofloxacin immunosensors: Specific sensors

Following immobilisation of anti-ciprofloxacin, according to section 3.5.3.1 impedance analyses were performed from 1Hz to 10,000Hz (+/- 5mV amplitude perturbation) in a pH 7.4 phosphate buffer, i.e. containing no antigen, as a baseline trace. This buffer solution did, however, contain a 50:50 mixture of $[KFe(CN)_6]^{3-/4-}$, at a concentration of 10mM as redox mediator so as to perform faradaic impedance spectroscopy. The potential of the electrochemical cell was offset to the formal potential of the redox probe (+0.4 V vs. Ag/AgCl). Subsequently, anti-ciprofloxacin doped sensors were exposed to a range of ciprofloxacin concentrations from 1ng to 10μg ml^{-1}. Stock ciprofloxacin had already been dissolved in pH 7.4 phosphate buffer at concentrations of 1ng, 5ng, 10ng, 20ng, 50ng, 100ng, 500ng, 1μg, 5 μg and 10μg per ml of PBS buffer. The experimental protocol developed and described in section

3.5.5 was followed for the electrochemical impedimetric interrogation of ciprofloxacin immunosensors.

Fig 7.2 shows one popular format for evaluating electrochemical impedance data, the Nyquist plot. This format is also known as a Cole-Cole plot or complex impedance plane plot. The imaginary impedance component (Z'') is plotted against the real impedance component (Z') at each excitation frequency.

For plot 7.2, the Z' component is seen to increase with decreasing frequency over the whole range of frequencies from 10,000Hz to 1Hz. The Z'' component, however, increases from 10,000Hz up to the characteristic frequency, ω, (the frequency at which the Z'' value is at its maximum) before decreasing to the final applied frequency (1Hz). The impedance spectrum is indicative of a surface-modified electrode system where the electron transfer is slow (Katz and Willner, 2003). All subsequent traces follow this general form.

A slow electron-transfer step results in a large semicircle region that is not accompanied by a straight line. The semicircle portion corresponds to the electron-transfer-limited process, whereas the linear part represents the diffusion limited electrochemical process. In the case of very fast electron transfer processes, the impedance spectrum could include only the linear part.

The electron transfer kinetics and diffusion characteristics can be extracted from the spectra. The semicircle diameter (extrapolated) is equal to the electron transfer resistance, R_{et}. The intercept of the semicircle with the Z' axis at high frequencies is equal to the solution resistance; R_s. Extrapolation of the semicircle to lower frequencies yields an intercept corresponding to $R_s + R_{et}$.

The electron transfer resistance, R_{et}, controls the electron transfer kinetics of the redox probe at the electrode interface. Ciprofloxacin recognition by the immobilized antibodies enhances the interfacial electron transfer kinetics and hence decreases the electron transfer resistance.

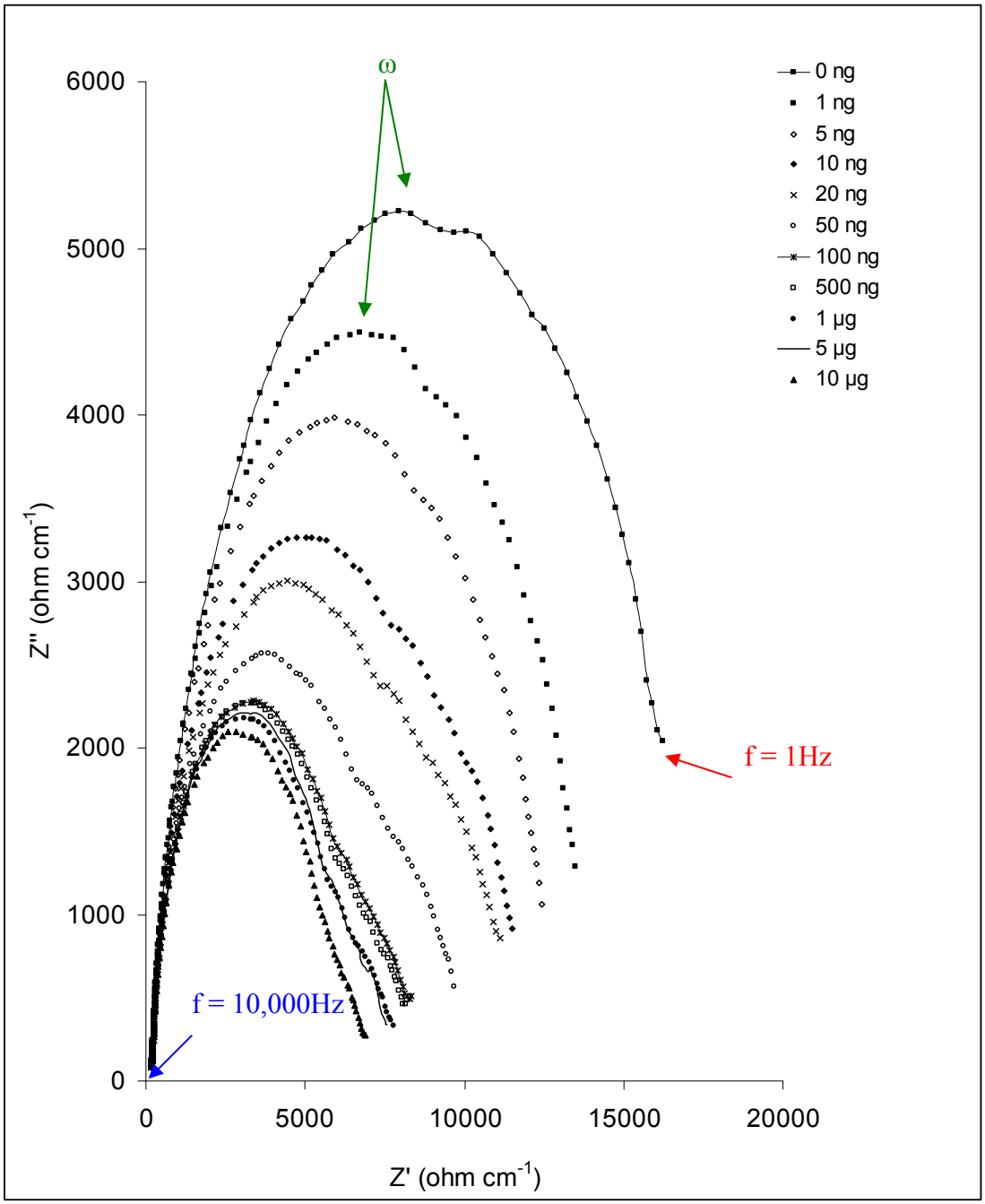

Fig 7.2 Nyquist plot for an anti-ciprofloxacin-doped PANI immunosensor following exposure to the full range of ciprofloxacin concentrations in PBS pH 7.4.

The electron transfer resistance at the electrode is the sum of the constant electron transfer resistance of the unmodified carbon electrode *(*R_c) and the variable electron transfer resistance introduced by the modifier (R_{mod}).

All electronic characteristics of the equivalent circuit and the corresponding physical parameters of the real electrochemical system can be extracted from an electrochemical impedance analysis. Since the variable parameters of the system represent the functions of the modifying layer and its composition, they can be used to quantitatively characterise the layer. Analysis of the Z' and Z'' values observed at different frequencies allows the calculation of the following important parameters: a) the double-layer capacitance, C_{dl} and its variable component C_{mod}; b) the electron transfer resistance, R_{et}, and its variable component R_{mod} and c) the electron transfer rate constant, k_{et}, for the applied redox probe derived from the electron transfer resistance, R_{et}. Thus, impedance spectroscopy represents not only a suitable transduction technique to follow the interfacial interactions of biomolecules, but it also provides a very powerful method for the characterisation of the structural features of the sensing interface and for explaining mechanisms of chemical processes occurring at the electrode/solution interface (Janata, 2002).

An approximate decrease in electron transfer resistance of ~ 3kΩ to ~10kΩ was observed for the anti-ciprofloxacin doped immunosensors upon antigen binding. The solution resistance was constant for all of the traces recorded and equal to ~150Ω. The intercept of the semicircle region of the baseline trace had a value of ~18kΩ. The electron transfer resistance was thus approximately equal to 17.85kΩ. In the same manner, the electron transfer resistance of the sensor upon exposure to 1ng of ciprofloxacin was calculated to be ~13.85kΩ. Hence, the decrease in electron transfer resistance of the immunosensor associated with the exposure of the latter to 1ng of antigen was 4kΩ. The total impedance decreases in magnitude as the sensors are exposed to increasing antigen concentrations, eventually reaching a plateau, indicating that the sensor's surface is saturated.

One of the most important parameters governing the technique of faradaic impedance spectroscopy is the applied frequency. At low frequencies (f < 1 mHz) the impedance value is basically determined by the DC-conductivity of the electrolyte solution. At

very high frequencies (f > 100 kHz) inductance of the electrochemical cell and connecting leads can contribute to the impedance spectra. Thus, the analytically meaningful impedance spectra are usually recorded at frequencies where they are mainly controlled by the interfacial properties of the modified electrodes (10 mHz < f < 100kHz). This is best illustrated in a Bode plot, where the total impedance of the anti-ciprofloxacin loaded sensors is plotted as a function of the $\log_{10}$ of the applied frequency as illustrated in Fig 7.3.

Previous work by our group showed that while both the imaginary and real components change due to the formation of antibody-antigen complexes on the surface of the sensors, the change from the baseline trace in the real component dominated the total change in the impedance (Grant *et al*., 2005). In this case, changes in both real and imaginary components are visible and again the real component is the major contributor to total impedance. It was also found that the real component offers far greater reproducibility in comparison to the imaginary contribution. Faradaic impedance spectroscopy is generally regarded to be more sensitive to changes on the electrode surface upon antigen binding to the antibody-functionalised electrode surfaces.

For these reasons, the real component of the impedance at 1Hz was used to plot a calibration curve of the of percentage changes from the baseline trace of the electron transfer resistance across the $\log_{10}$ of a range of antigen concentrations (Fig 7.4). As can be seen, there is a steady decrease in impedance as antigen concentration increases up to a concentration of about 100 ng ml^{-1}, above which concentration there is a tend towards a plateau, possibly indicating saturation of the specific binding sites. Between a concentration range of 1-100 ng ml^{-1}, there is a near linear correlation of the impedance change with the $\log_{10}$ of concentration (R^2=0.96) (Fig 7.5). This concentration range corresponds with the range of therapeutic and clinical significance for ciprofloxacin.

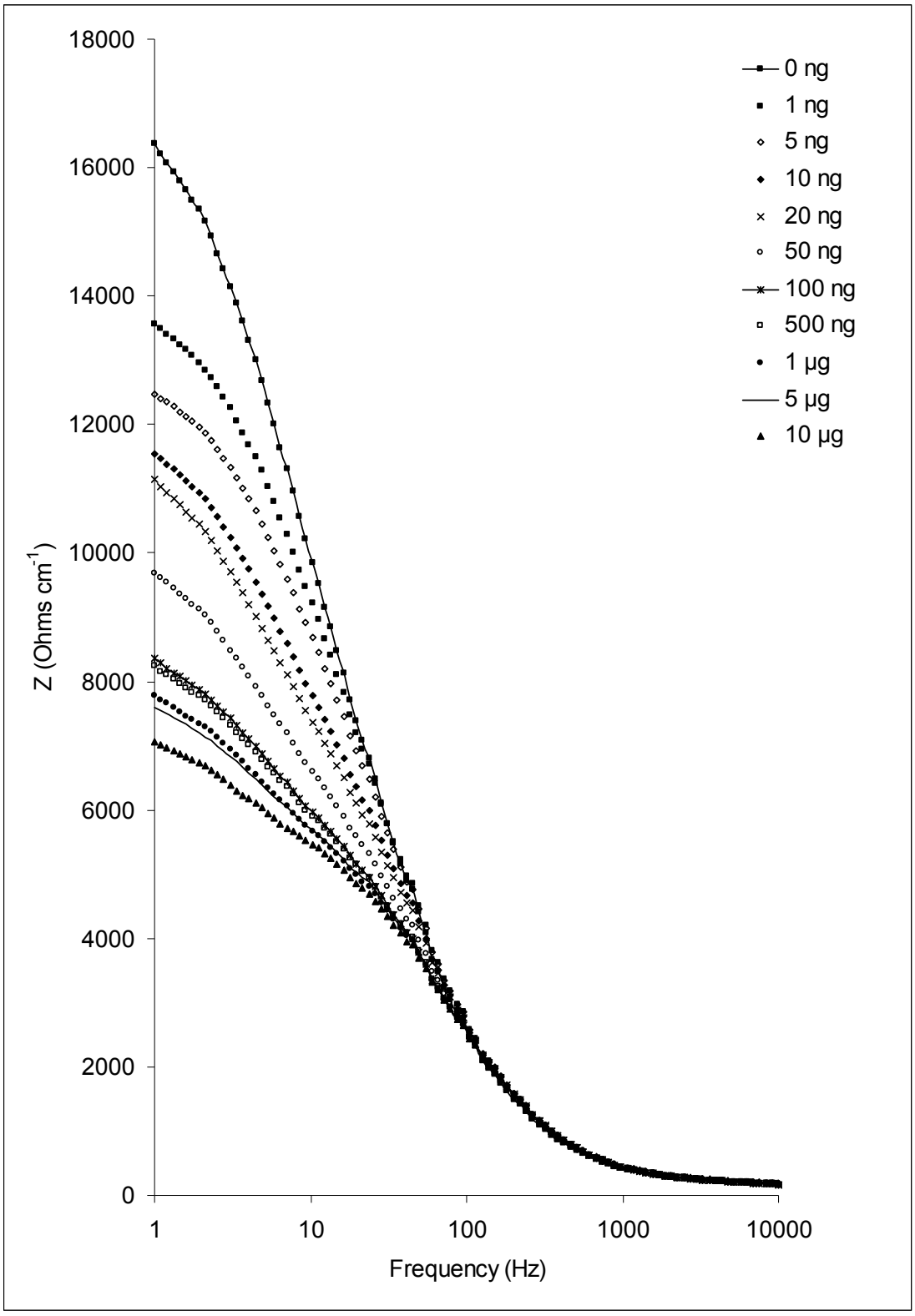

Fig 7.3 Bode plot for an anti-ciprofloxacin-doped PANI immunosensor following exposure to the full range of ciprofloxacin concentrations in PBS pH 7.4.

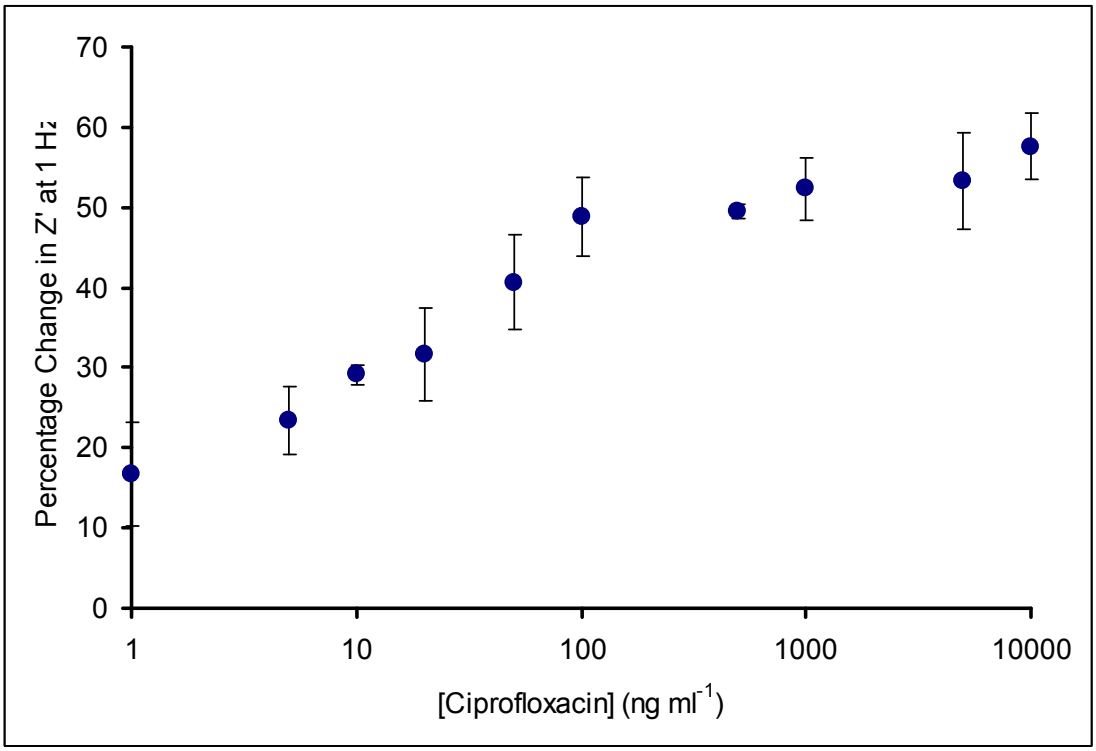

Fig 7.4 Calibration curve of the change in electron transfer resistance from the baseline response for anti-ciprofloxacin modified electrodes upon exposure to the $\log_{10}$ of the full range of ciprofloxacin concentrations in PBS pH 7.4.

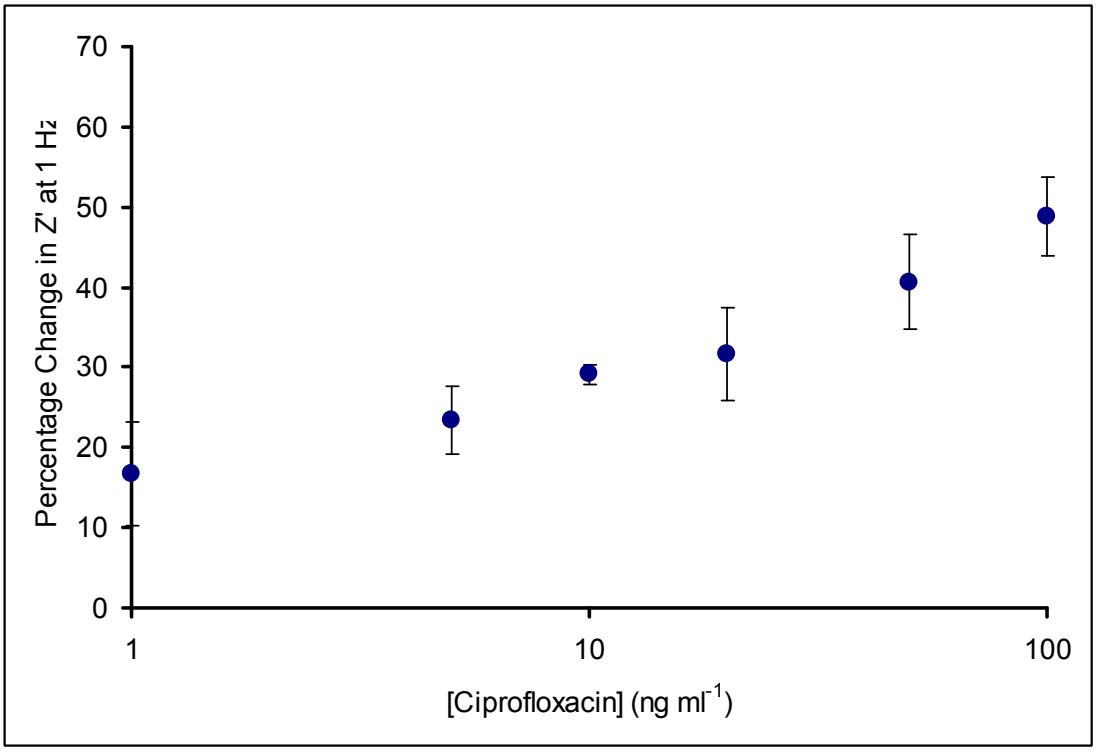

Fig 7.5 Calibration curve of the change in electron transfer resistance from the baseline response for anti-ciprofloxacin modified electrodes upon exposure to the $\log_{10}$ of the full range of ciprofloxacin concentrations in PBS pH 7.4 (only linear section is shown).

7.2.2 Electrochemical impedance spectroscopy (EIS) studies on ciprofloxacin immunosensors: Non-Specific sensors and Corrected Calibration Profile

In order to validate the specificity of the observed response for the anti-ciprofloxacin modified sensor assembly, control experiments were performed to gauge non-specific events that may be occurring. A generic IgG antibody was immobilized following the same fabrication protocol as for the specific anti-ciprofloxacin doped sensors. In every other sense the matched sensors were identical and they were interrogated simultaneously following exposure to antigen solutions. The results obtained permit an overall assessment of the contribution of non-specific effects to the changes encountered in Figs 7.2 and 7.3.

All impedimetric spectral traces obtained follow a similar general form to those obtained in section 7.2.1 for the specific sensors (Fig 7.6). The Z' component is again seen to increase with decreasing frequency for the entire range of applied frequencies whereas the Z component is seen to increase up to the characteristic frequency of each trace (the frequency at which the Z'' value is at its maximum) before decreasing to the final applied frequency (1Hz). The impedance spectrum is indicative of a surface-modified electrode system where the electron transfer is slow.

A striking difference between the spectral traces in Figs 7.2 and 7.6 is that exposure to ciprofloxacin and formation of antibody-antigen complexes on the surface of the IgG modified sensors results in an increase in the total impedance. Recognition of the antigen does not result therefore in enhanced electron transfer kinetics but rather hinders this process. Therefore, it could be said, that ciprofloxacin, in the case of the non-specific sensors, acts as an insulator.

The values of the individual components of impedance as well the value of the total impedance should also be noted. These values are in the case of non-specific sensors significantly increased and in addition it can be seen that the greater differences from the baseline trace are displayed in the imaginary, capacitive component of impedance in contrast with the specific sensors where the real component has the greatest contribution to the changes in the total impedance of the system.

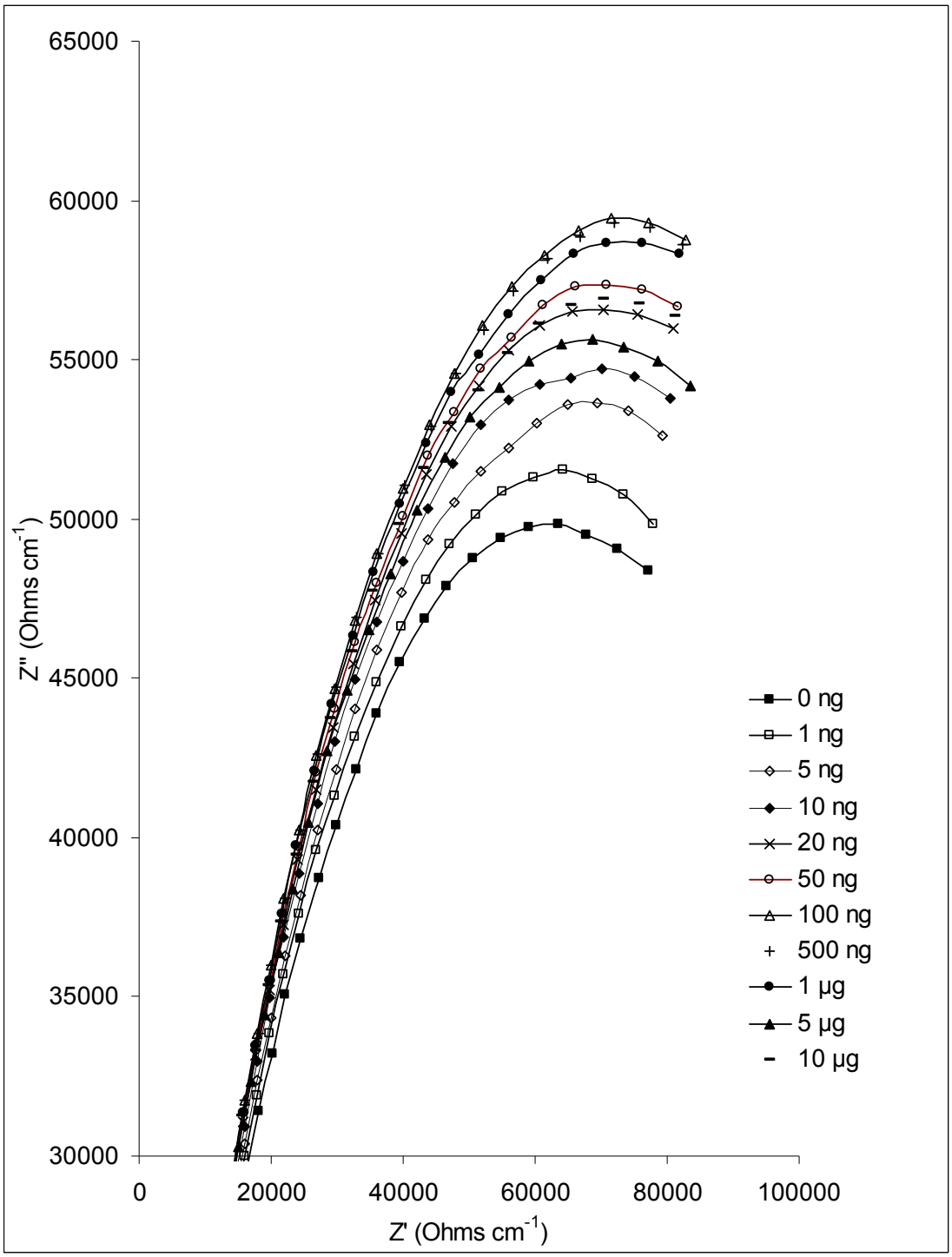

Fig 7.6 Nyquist plot for a generic IgG-doped PANI immunosensor following exposure to the full range of ciprofloxacin concentrations in PBS pH 7.4. For clarity, only Z'' values greater than 30kΩ are shown.

Once again, maximum changes from the baseline trace upon exposure to antigen were observed at low frequencies, a fact clearly illustrated in the Bode plot in Fig 7.7.

The real component of the impedance at 1Hz was used to plot a calibration curve of the percentage change of the electron transfer resistance across the $\log_{10}$ of a range of antigen concentrations (Fig 7.8). The same values on the x and y axis were employed as for the calibration curve plotted for the specific sensors (Fig 7.4). Upon comparison of Fig 7.8 with Fig7.4, it is apparent that approximately 16% of the changes in the electron transfer resistance encountered with the anti-ciprofloxacin modified sensors are, in fact, non-specific. However, there is a much lower response for the non-specific sensors, showing that although there are non-specific interactions, they comprise a minor component of the detected response.

The non-specific response observed could arise from factors such as non-specifically adsorbed matter not being removed via the flushing regime and thus remaining at the sensor surface and / or weakly bound matter, polymer swelling, proton doping and transitional changes of the polyaniline at the neutral test pH, i.e. becoming less conductive.

A correction can be made to acquire the true specific anti-ciprofloxacin immunosensor response by subtracting the non-specific sensor response at each antigen concentration from the specific sensor response (Fig 7.9). In Fig 7.9, there is a steady increase in the real component of the impedance as antigen concentration increases up to a concentration of about 100 ng ml^{-1}, above which concentration the sensor becomes saturated. Between a concentration range of 1-100 ng ml^{-1}, as for the non corrected calibration profile, there is a near linear correlation of the impedance change with the $\log_{10}$ of concentration (R^2=0.95) (Fig 7.10).

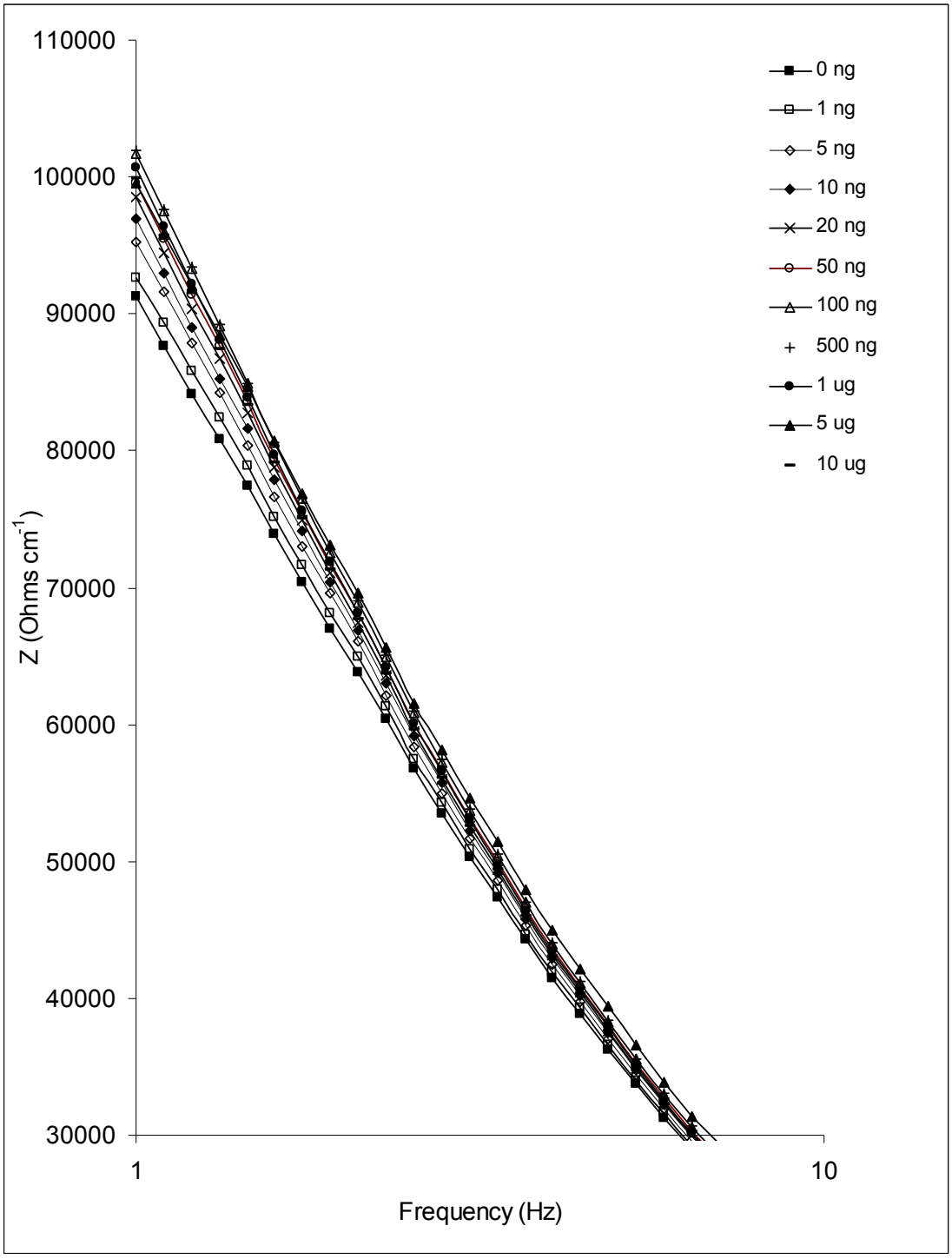

Fig 7.7 Bode plot for a generic IgG-doped PANI immunosensor following exposure to the full range of ciprofloxacin concentrations in PBS pH 7.4. For clarity, only Z values greater than 30kΩ and frequency values from $\log_{10}$ 1 to 10 Hz are shown.

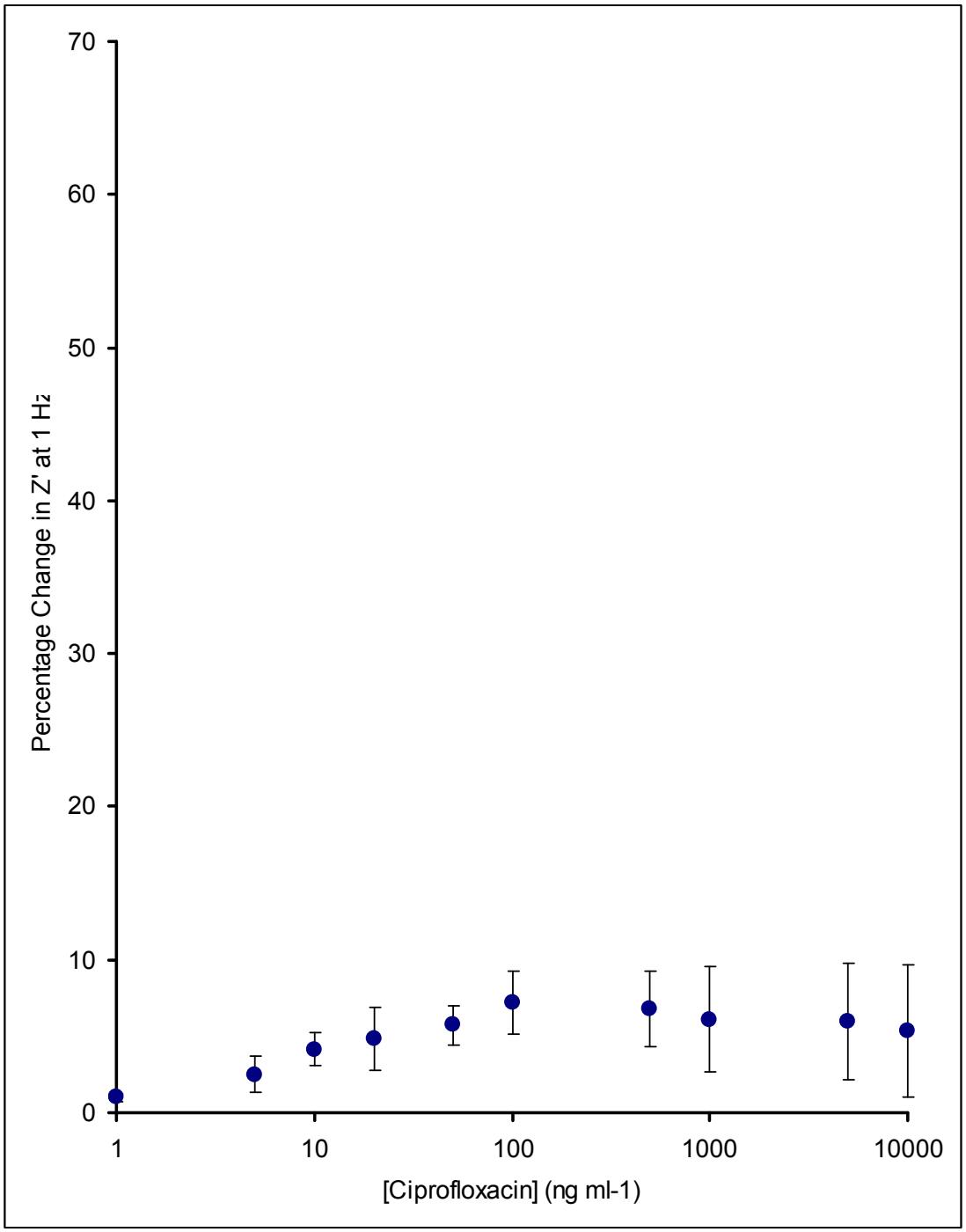

Fig 7.8 Calibration curve the change in electron transfer resistance from the baseline response for IgG modified electrodes upon exposure to the $\log_{10}$ of the full range of ciprofloxacin concentrations in PBS pH 7.4.

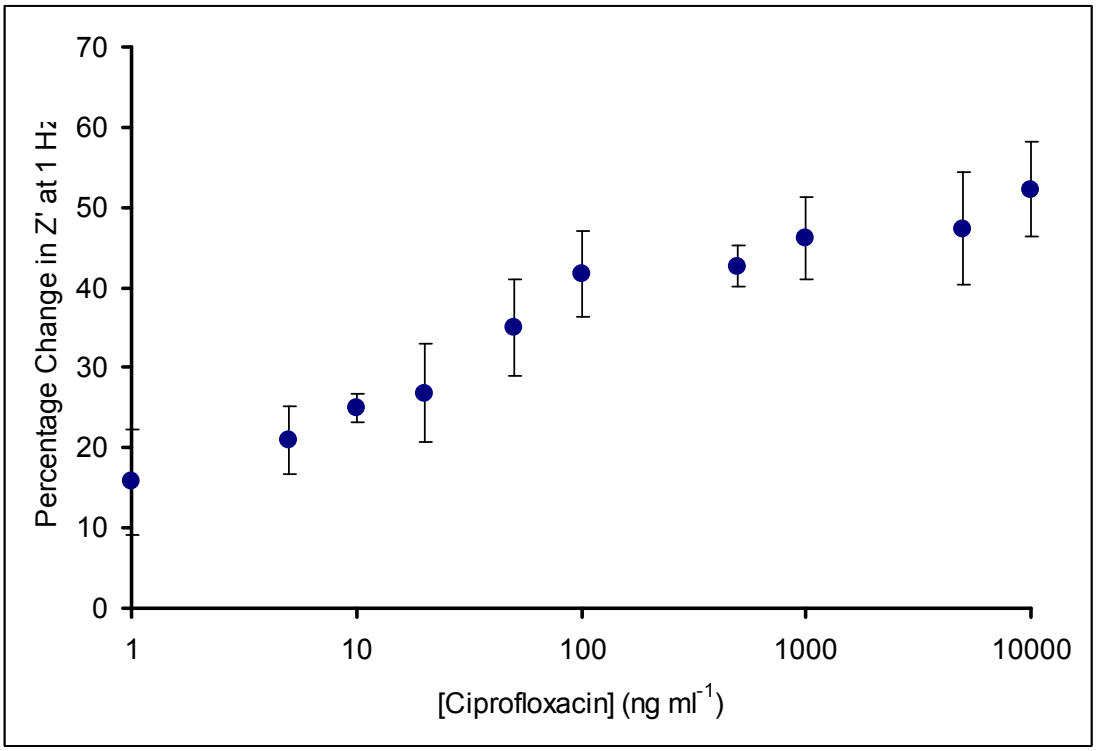

Fig 7.9 Calibration curve of the 'corrected' change in electron transfer resistance from the baseline response for the $\log_{10}$ of the full range of ciprofloxacin concentrations in PBS pH 7.4.

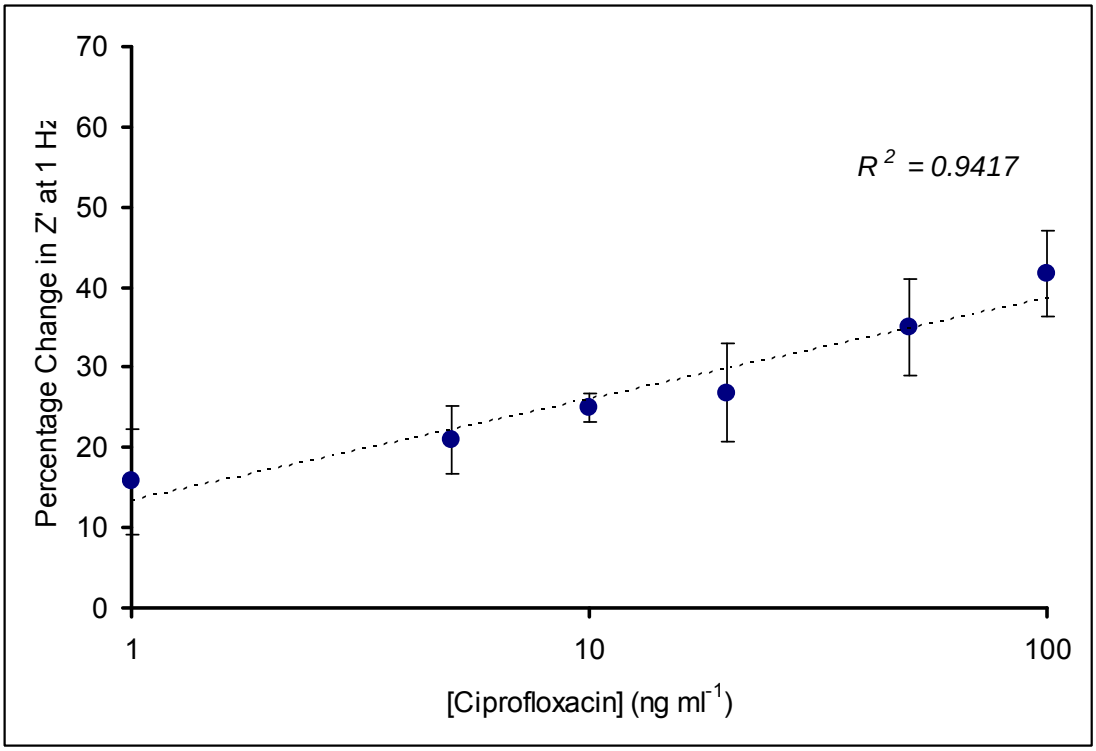

Fig 7.10 Calibration curve for the 'corrected' change in electron transfer resistance from the baseline response for the $\log_{10}$ of a range of ciprofloxacin concentrations in PBS pH 7.4 (only linear part is shown).

7.2.3 Electrochemical impedance spectroscopy (EIS) studies on ciprofloxacin immunosensors in milk: Specific sensors

For an immunosensor to be of practical use it must be capable of detecting its antigen within a wide range of matrices. Since there is a wide use of fluoroquinonolones within the animal industry, it was decided to investigate whether ciprofloxacin can be detected in milk. The European Union has set a maximum residue limit of 100 ng ml^{-1} for enrofloxacin plus ciprofloxacin in milk (Hassouan *et al.,* 2007). Previous studies have utilised techniques such as HPLC to detect various fluoroquinolones in bovine milk with a detection limit of 3 ng ml^{-1} for ciprofloxacin (Hassouan *et al.,* 2007) and liquid chromatography with luminescence detection to measure ciprofloxacin in milk with a linear range of 8-3500 ng ml^{-1} and a detection limit of 3 ng ml^{-1} (Rodriguez-Diaz *et al*., 2006). A number of ELISA based tests have also been developed to detect fluoroquinolones in milk with detection limits of several ng ml^{-1} (Bucknall *et al*., 2006; Duan and Yuan, 2001). Recent work has also described the construction of a DNA based sensor which combined with a surface plasmon resonance method allows quantification of enrofloxacin between 3-20 μg ml^{-1} in milk (Cao *et al.,* 2007). An immunosensor for ciprofloxacin based on polypyrrole films combined with an AC impedance technique has also been described with sensitivities as low as 10 pg ml^{-1} (Ionescu et al., 2007).

Following immobilisation of anti-ciprofloxacin, according to section 3.5.3.1 impedance analyses were performed from 1Hz to 10,000Hz (+/- 5mV amplitude perturbation) in milk alone, i.e. containing no antigen, as a baseline trace. The potential of the electrochemical cell was DC offset to +400 mV against Ag/AgCl. The same experimental protocol as the one used for the ciprofloxacin immunosensors in PBS described in the previous section was applied for the electrochemical impedimetric interrogation of the immunosensors in milk.

Antigen solutions were prepared by initially dissolving ciprofloxacin in PBS, then diluting to the required concentration of antigen in 30ml of milk. A range of concentrations were employed; 0.1ng, 1ng, 10ng, 100ng, 1μg and 10μg per ml of milk. The results obtained were presented as Nyquist plots of the imaginary versus the real component of impedance (Fig 7.11).

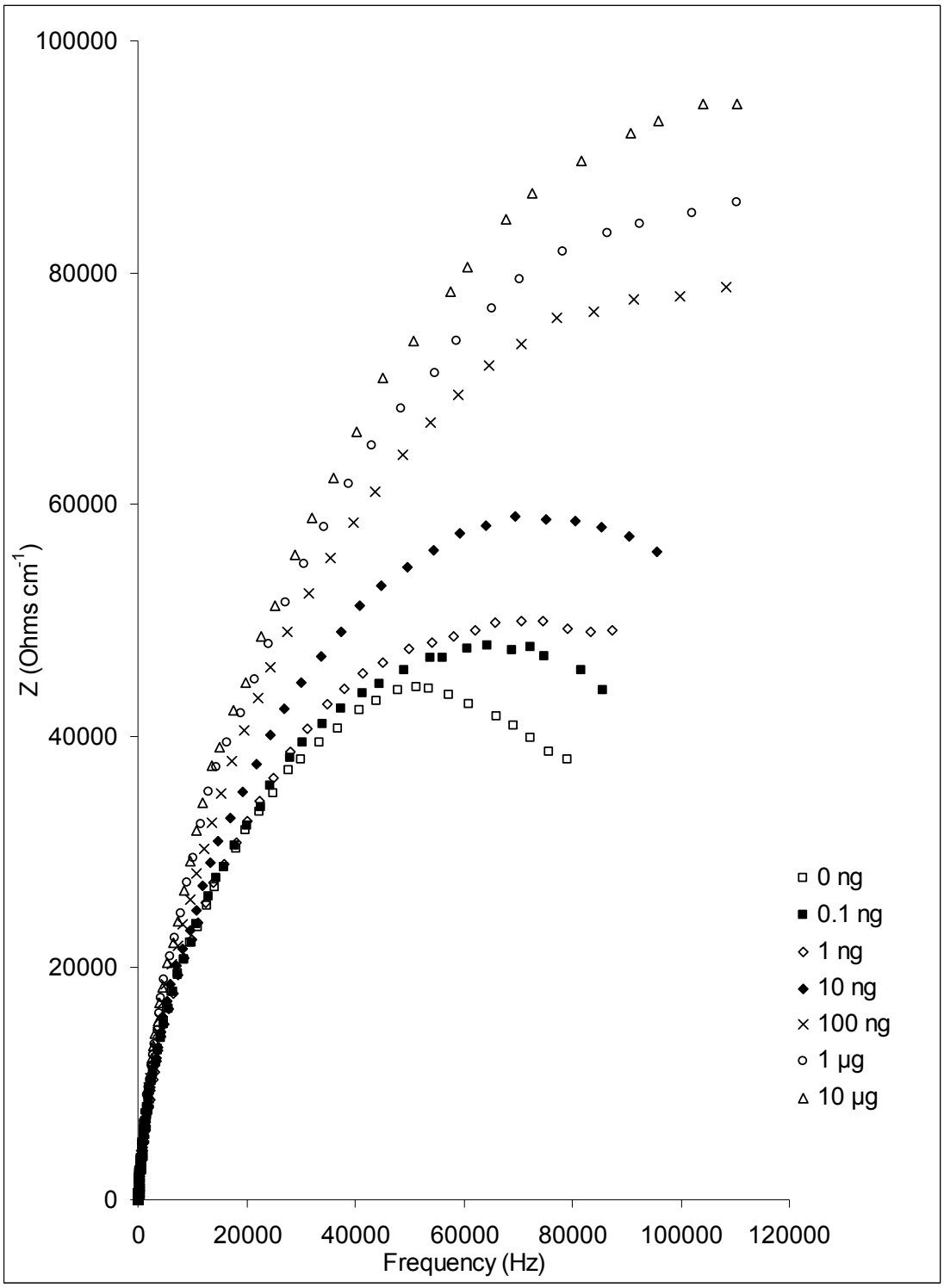

Fig 7.11 Nyquist plot for an anti-ciprofloxacin-doped PANI immunosensor following exposure to the full range of ciprofloxacin concentrations in milk.

For plot 7.11, the Z' component is seen to increase with decreasing frequency over the whole range of frequencies from 10,000Hz to 1Hz. The Z'' component, however, increases from 10,000Hz up to the characteristic frequency, ω, (the frequency at which the Z'' value is at its maximum) before decreasing to the final applied frequency (1Hz). The latter can not be clearly observed for spectral traces recorded following exposure to large concentrations of antigen due to the frequency range used to interrogate the sensors. The impedance spectrum is indicative of a surface-modified electrode system where the electron transfer is slow (Katz and Willner, 2003). All subsequent traces follow this general form.

Once again, maximal changes from the baseline trace upon exposure to antigen were observed at low frequencies, a fact clearly illustrated in the Bode plot in Fig 7.12. What came as a surprise was the fact that the impedance of the sensors did not decrease as was the case in PBS pH 7.4. Instead, the total impedance of the sensors increased following exposure to increasing antigen concentrations. This indicates that the antigen-antibody complexes forming on the sensor surface hinder electron transfer kinetics and encourage double layer charging, thus increasing the capacitance of the sensors.

It has been reported that in the presence of calcium ions, many fluoroquinolone antibiotics, including ciprofloxacin readily form calcium chelate complexes (Upadhyay *et al.*, 2006; Toyoguchi *et al.*, 2005). These complexes are usually dimeric in nature with two ciprofloxacin units complexed to a single calcium ion. It appears from the results presented in this and the previous section that the antibody is capable of binding ciprofloxacin in either its free or chelated form over similar concentration ranges, as shown by responses compared to control samples. However the great structural differences between the free and complexed forms of the antigen leads to different effects on the AC impedance results.

The effects of adsorption of various moieties on the AC impedance behaviour are highly complex and not well understood. For example in previous work by our group on DNA based sensors, adsorption of complementary DNA stands has been shown to lead to drops in the AC impedance of our electrodes whereas adsorption of non-complementary DNA leads to an increase (Davis *et al.*, 2004; Davis *et al.*, 2007).

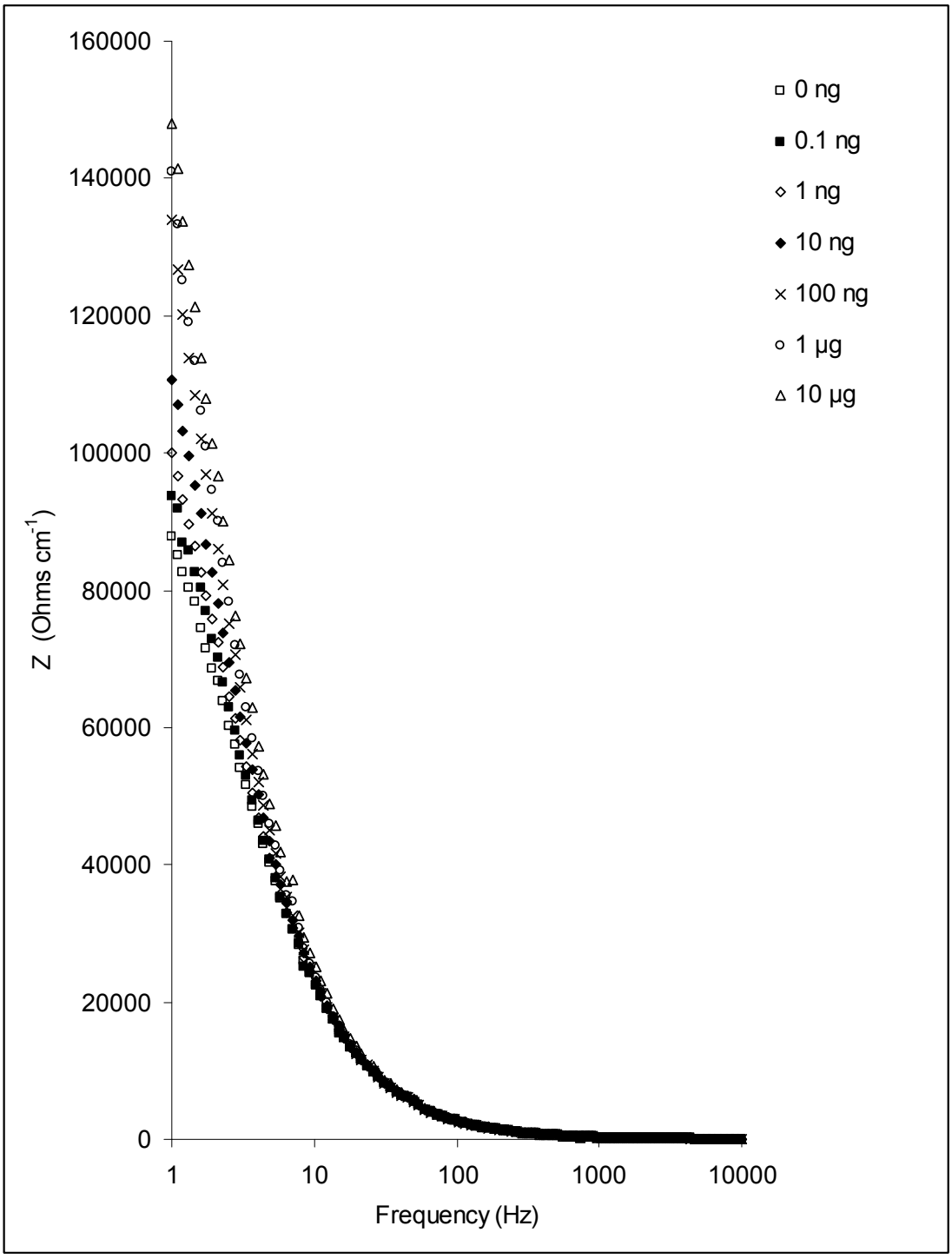

Fig 7.12 Bode plot for an anti-ciprofloxacin-doped PANI immunosensor following exposure to the full range of ciprofloxacin concentrations in milk.

This means that it is possible to differentiate between complexed and free ciprofloxacin. This is of interest since the FDA recommend that ciprofloxacin is not taken with dairy products, calcium fortified juices or calcium containing antacids as they may reduce adsorption of the drug (U.S. FDA, 2008)

Furthermore, it is worth noting the differences in the value of the total impedance of the ciprofloxacin immunosensors in milk and PBS. Whereas in PBS the total impedance of the sensors at 1 Hz is in between 7 and 17kΩ for the given antigen concentrations, in milk total impedance values are significantly larger (~90-150kΩ). This again can be accounted for due to the formation of chelation complexes between ciprofloxacin and calcium ions.

The real component of the impedance at 1Hz was used to plot a calibration curve of the percentage change of the electron transfer resistance across the $\log_{10}$ of a range of antigen concentrations (Fig 7.13). As can be seen, there is a steady increase in impedance as antigen concentration increases up to a concentration of about 100 ng ml^{-1}, above which concentration there is a tend towards a plateau, possibly indicating saturation of the specific binding sites. It is possible that any further changes in impedance beyond this level could simply be due to non-specific interactions. Between a concentration range of 1-100 ng ml^{-1}, there is a near linear correlation of the impedance change with the $\log_{10}$ of concentration ($R^2 = 0.97$) (Fig 7.14)

7.2.4 Electrochemical impedance spectroscopy (EIS) studies on ciprofloxacin immunosensors in milk: Non-Specific IgG sensors

In order to evaluate the specificity of the observed response for the anti-ciprofloxacin modified sensor assembly, control experiments were performed to determine non-specific events that may be occurring. A generic IgG antibody was immobilized following the same fabrication protocol as for the specific anti-ciprofloxacin doped sensors. In every other sense, the matched sensors were identical and were interrogated simultaneously in milk following exposure to antigen solutions.

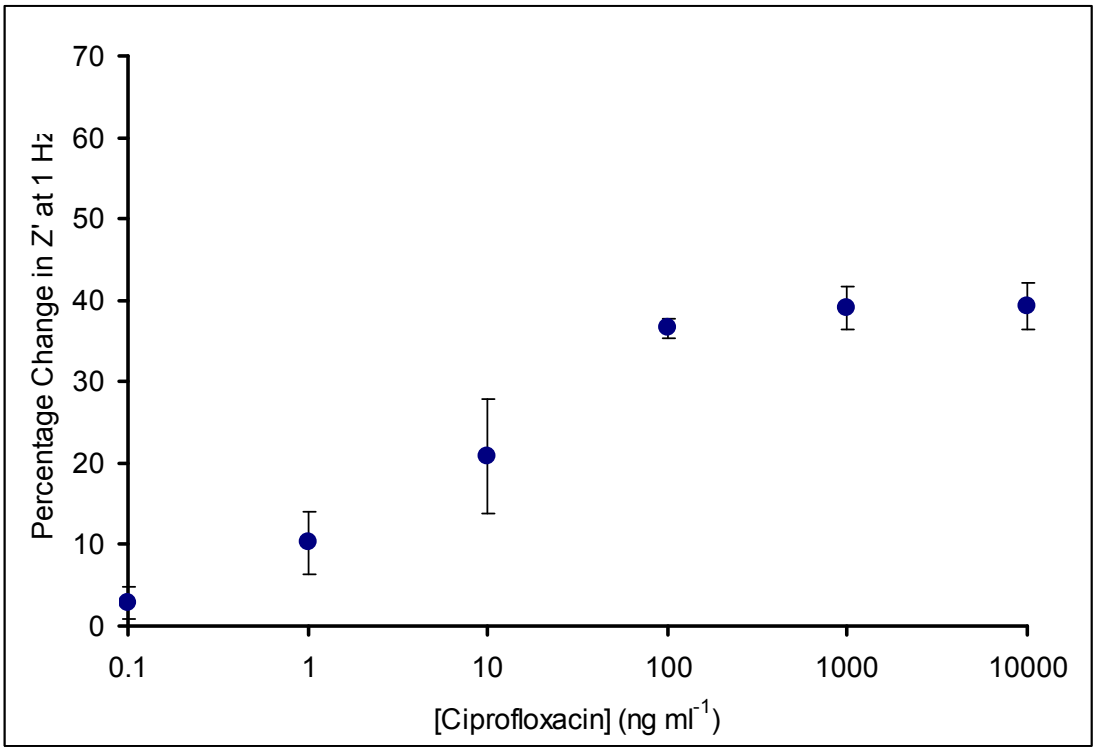

Fig 7.13 Calibration curve of the change in electron transfer resistance from the baseline response for anti-ciprofloxacin modified electrodes upon exposure to the $\log_{10}$ of the full range of antigen concentrations in milk.

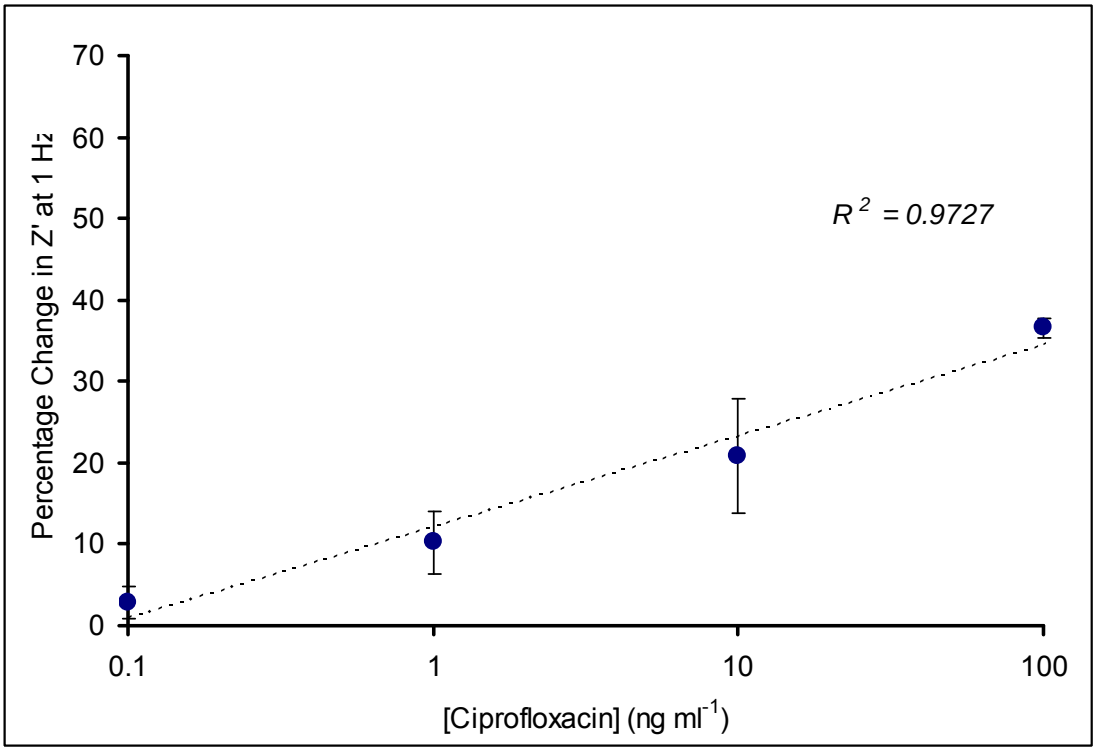

Fig 7.14 Calibration curve of the change in electron transfer resistance from the baseline response for anti-ciprofloxacin modified electrodes upon exposure to a range of antigen concentrations in milk (only linear part is shown).

Nyquist and Bode plots (not included in the thesis) for the recorded spectral traces, show that there is a very high decrease in impedance upon antigen recognition by the generic IgG doped sensors. This contrasts with the observed increase to the impedance for the non-specific sensors in PBS following exposure to increasing antigen concentrations (Section 7.2.2).

Further experiments showed that these results are a function of the time of exposure rather than ciprofloxacin concentration. The explanation for this is that since milk is such a complex mixture of components in comparison to phosphate buffer, some of the latter specifically bind to the generic IgG loaded sensors. Therefore, IgG doped sensors cannot be used to examine non-specific binding events.

The real component of the impedance at 1Hz was used to plot a calibration curve of the absolute values of percentage change in the electron transfer resistance across the $\log_{10}$ of a range of antigen concentrations (Fig 7.15). The same values on the x and y axis were employed as for the previous calibration curves (Figs 7.4 and 7.8). Upon comparison of the calibration curve in Fig 7.15 with the calibration curve for the specific, anti-ciprofloxacin sensors in milk (Fig 7.13), the unsuitability of these sensors to measure non-specific responses becomes apparent. The changes in the electron transfer resistance encountered with the IgG-modified non-specific sensors are almost equal to the changes in the real component of impedance measured with the specific sensors.

7.2.5 Electrochemical impedance spectroscopy (EIS) studies on ciprofloxacin immunosensors in milk: Non-Specific anti-PSA sensors

As mentioned in the previous chapter, the large decrease in electron transfer resistance recorded with the IgG doped sensors was due to binding of biomolecules present in milk over sufficient exposure time. In order to test this theory, another set of control electrodes was utilised, where instead of non-specific IgG antibody, a specific antibody against an antigen not found in milk was utilised.

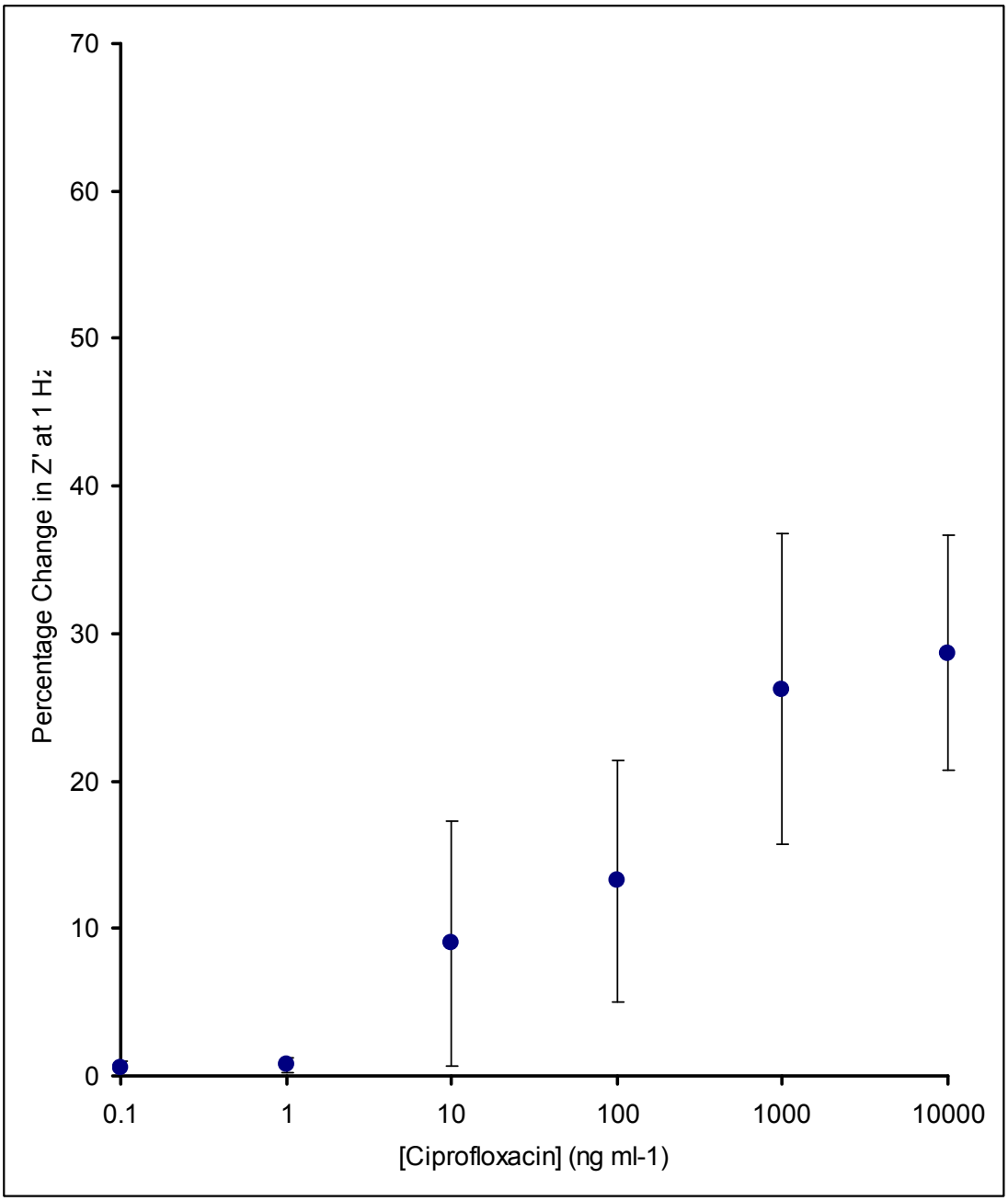

Fig 7.15 Calibration curve of the change in electron transfer resistance from the baseline response for IgG modified electrodes upon exposure to the $\log_{10}$ of the full range of ciprofloxacin concentrations in milk.

Anti-prostate specific antigen (anti-PSA) was used for this purpose. The results obtained were presented as Nyquist plots of the imaginary versus the real component of impedance (Fig 7.16).

For plot 7.16, the Z' component is seen to increase with decreasing frequency over the whole range of frequencies from 10,000Hz to 1Hz. The Z'' component, however, increases from 10,000Hz up to the characteristic frequency, ω, (the frequency at which the Z'' value is at its maximum) before decreasing to the final applied frequency (1Hz). The latter can not be clearly observed for spectral traces recorded following exposure to large concentrations of antigen due to the frequency range used to interrogate the sensors. The impedance spectrum is indicative of a surface-modified electrode system where the electron transfer is slow (Katz and Willner, 2003).

The results obtained support the theoretical assumption made in the previous section. A generic IgG loaded sensor cannot be used to estimate non-specific interactions due to the specific interactions of molecules found in milk with IgG antibodies. The PSA doped immunosensor, on the other hand, showed an increase in impedance similar to the one observed for the IgG-loaded sensors interrogated in PBS (Section 7.2.2). Recognition of the antigen does not result therefore in enhanced electron transfer kinetics but rather hinders this process.

The real component of the impedance at 1Hz was used to plot a calibration curve of the percentage change of the electron transfer resistance across the $\log_{10}$ of a range of antigen concentrations (Fig 7.17). The same values on the x and y axis were employed as for the calibration curve plotted for the specific anti-ciprofloxacin sensors impedimetrically interrogated in milk (Fig 7.13). Upon comparison of Fig 7.17 with Fig 7.13, it is apparent that approximately 30% of the changes in the electron transfer resistance encountered with the anti-ciprofloxacin modified sensors are, in fact, non-specific. However, there is a much lower response for the non-specific sensors, showing that although there are non-specific interactions, they comprise a minor component of the detected response.

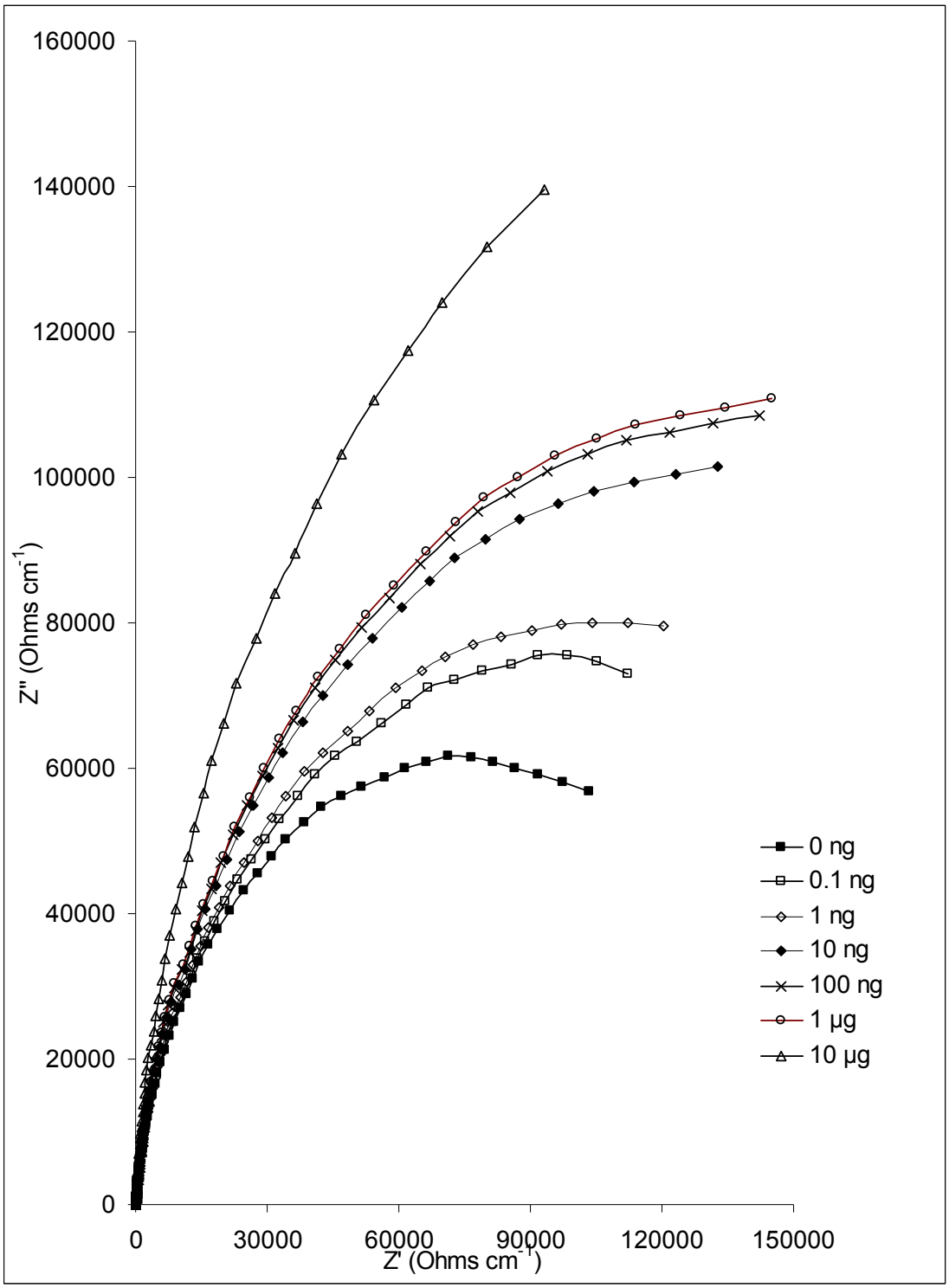

Fig 7.16 Nyquist plot for an anti-PSA doped PANI immunosensor following exposure to the full range of ciprofloxacin concentrations in milk.

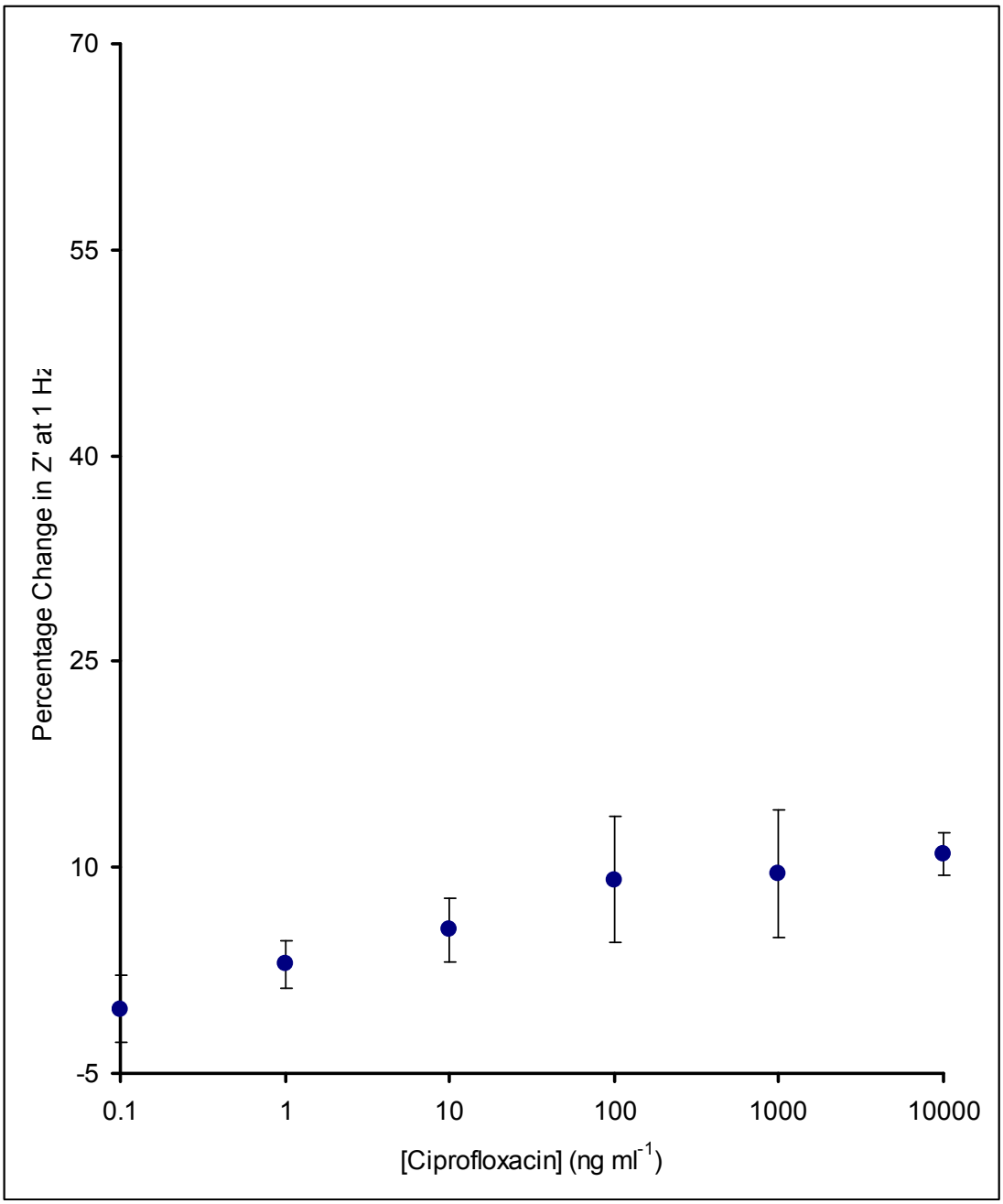

Fig 7.17 Calibration curve of the change in electron transfer resistance from the baseline response for anti-PSA modified electrodes upon exposure to the $\log_{10}$ of the full range of ciprofloxacin concentrations in milk.

7.2.6 Electrochemical impedance spectroscopy (EIS) studies on ciprofloxacin immunosensors in milk: Corrected Calibration Profile

To obtain a calibration profile, in terms of 'corrected' percentage impedance change for an anti-ciprofloxacin immunosensor in milk, accounting for any non-specific responses, the changes obtained in Fig 7.17 (non-specific) were subtracted from those obtained in Fig 7.13 (specific) over the entire analytical concentration range. Fig 7.18 shows the subtracted responses. As can be seen, there is a steady increase in impedance as antigen concentration increases up to a concentration of about 100 ng ml^{-1}, above which concentration there is a tend towards a plateau, possibly indicating saturation of the specific binding sites. It is possible that any further changes in impedance beyond this level could simply be due to non-specific interactions. Between a concentration range of 1-100 ng ml^{-1}, there is a near linear correlation of the impedance change with the $\log_{10}$ of concentration ($R^2 = 0.96$) (Fig 7.19).

Fig 7.20 also displays our earlier results for ciprofloxacin in PBS overlaid over those for milk. As can be seen, the results are very similar in that they give linear ranges with very similar gradients in the region 0-100 ng ml^{-1} and above 100 ng ml^{-1} appear to be saturated. However they are of opposite nature; adsorption of ciprofloxacin from milk gives an increase in the real component of impedance whereas from PBS a decrease is observed. As already analysed previously, this is due to the chelation phenomena between calcium ions and ciprofloxacin molecules in milk.

.

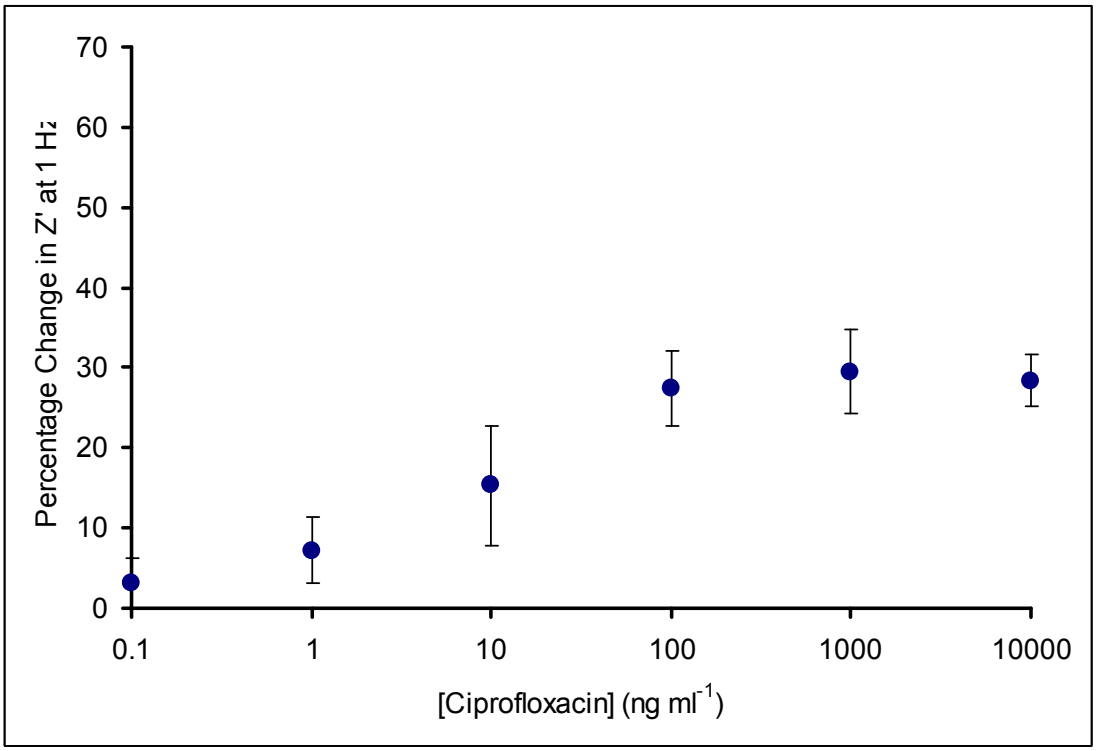

Fig 7.18 Calibration curve for the 'corrected' change in electron transfer resistance from the baseline response for the $\log_{10}$ of the full range of ciprofloxacin concentrations in milk.

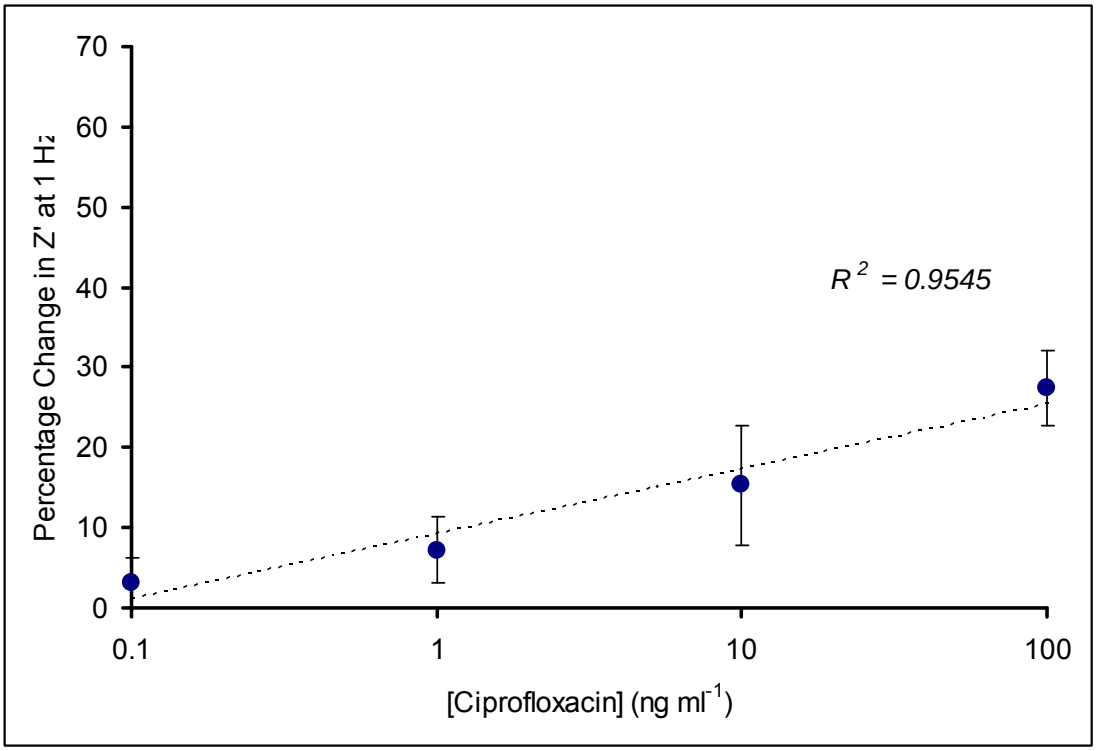

Fig 7.19 Calibration curve for the 'corrected' change in electron transfer resistance from the baseline response for the $\log_{10}$ of a range of ciprofloxacin concentrations in milk (only linear part is shown).

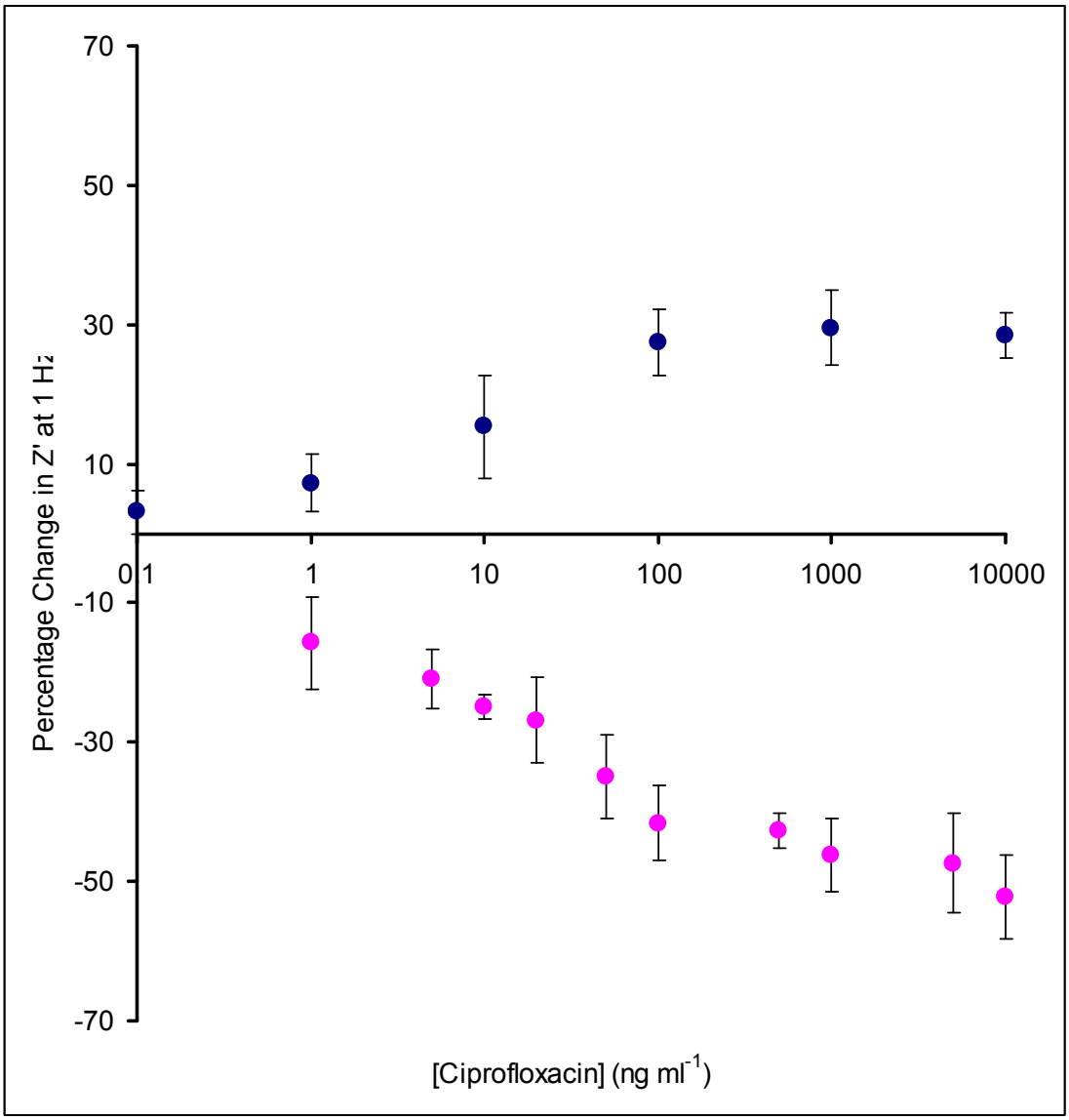

Fig 7.20 Calibration curve for the 'corrected' change in electron transfer resistance from the baseline response for the $\log_{10}$ of the full range of ciprofloxacin concentrations in milk (blue) and in PBS pH 7.4 (pink).

7.3 Conclusions

We have demonstrated the construction of an immunosensor for the antibiotic ciprofloxacin using a combination of screen-printed carbon electrodes coated with conducting polyaniline and immobilised antibodies against ciprofloxacin via the neutravidin/biotin affinity interactions. Interrogation of these sensors by AC impedance in a phosphate buffer (PBS pH 7.4) demonstrated the detection of ciprofloxacin

The higher the ciprofloxacin concentration in the test solution the greater the number of stable antibody-antigen complexes formed at the sensor surface. The complex formation was shown to enhance electron transfer of the redox couple within the test solution at the formal redox potential and hence the electron transfer resistance extracted from the spectra obtained decreased accordingly with the antigen concentration. At concentrations of analyte above 100 ng ml^{-1}, the response began to plateau as the sensor saturated, with the recognition entities becoming occupied with analyte and active sites for further antigen binding being no longer available.

Non-specific interactions were accounted for by the simultaneous interrogation of sensors loaded with a generic IgG in PBS pH 7.4. It was found that 16% of the response obtained from the specific sensors was due to non-specific binding events. A calibration curve of the corrected changes in the electron transfer resistance was plotted across the range of antigen concentrations. Linear correlation of the impedance change with the log of concentration (R^2=0.95) was observed between 1-100 ng ml^{-1}.

The fabrication of an immunosensor for the detection of ciprofloxacin in a buffer solution has been published in Analytical Letters (Garifallou *et al*, 2007). A copy of the paper is attached in the Appendix at the back of this thesis.

The electrodes were then exposed to antigen solutions in milk. Interrogation of the electrodes by AC impedance demonstrated the detection of the antigen. Linear increases of the impedance change with the log_{10} of concentration (R^2=0.97) were observed between concentrations of 0.1-100 ng ml^{-1}. The increase in electron transfer

resistance observed was due to the formation of chelation complexes between calcium ions in milk and ciprofloxacin and contrasted with the decrease observed upon antigen exposure of the sensors in PBS. The sensors therefore not only bound the antigen from PBS or milk, but also proved capable of distinguishing from which matrix the ciprofloxacin was adsorbed.

Non-specific interactions were once again estimated with the use of a generic IgG loaded immunosensor exposed to the same concentrations of antigen in milk as the specific sensor. It was shown, that the use of IgG in the fabrication of non-specific sensors gave erroneous results due to the specific binding of molecules found in milk over sufficient exposure time. For this reason, non-specific sensors were prepared loaded with anti-PSA whose complementary antigen is not found in milk. The changes in electron transfer resistance recorded in this case constituted only a minor component of the total changes in response recorded with the specific sensors in milk.

A calibration curve of the corrected changes in the electron transfer resistance was plotted across the range of antigen concentrations. Linear correlation of the impedance change with the log of concentration (R^2=0.96) was observed between 1-100 ng ml^{-1}.

The fabrication of an immunosensor for the detection of ciprofloxacin in milk has been submitted for publication in Analytical Chemistry. The submitted manuscript is also attached in the Appendix.

Chapter 8

Electrochemical Impedance Studies on Myelin Basic Protein immunosensors

8.1 Introduction

This chapter deals with the fabrication of immunosensors for the detection of Myelin Basic Protein, referred to herein as MBP. The protocol used to construct the antibody-doped polymer-modified carbon electrodes is identical to the one used for the ciprofloxacin immunosensors described in the previous chapter (Chapter 7) and was designed to ensure orientation specific immobilisation of antibodies utilising neutravidin-biotin non-covalent affinity technologies as detailed in section 3.5.3.1. In all cases, the sensors were blocked with a bovine serum albumin (BSA) solution prior to exposure to antigen solutions so as to minimize non-specific binding.

Following the immobilisation of antibody receptor molecules at the surface of conducting emeraldine polyaniline films, the immunosensor assemblies were exposed to increasing concentrations of complementary antigen in buffered test solution within the required physiological range. For every specific sensor assembly analysed a matched control sensor was also interrogated to measure the effects of non-specific binding and to allow the subtraction of these unspecific interactions from the specific binding of MBP. This will help to increase the reliability of these sensors when applied to clinical samples. Three replicate sensors were used for all experimental arrangements. The presented results are in all cases the mean values obtained for the three replicate sensors.

Electrochemical impedance spectroscopy (EIS) was chosen to interrogate the fabricated immunosensors, because it allows for the resolution of both the kinetic and/or mass transport processes occurring within a system at various applied potentials and frequencies, using only minimal alternating current perturbations. The experimental protocol described in section 3.5.5 was followed for the electrochemical impedimetric interrogation of MBP immunosensors, which is identical to the protocol used for the interrogation of the ciprofloxacin immunosensors previously.

The obtained results were presented in a series of Bode and Nyquist plots. In a Bode plot, the total impedance is plotted against the logarithm of the frequency. In a Nyquist plot, Z'' (imaginary component), is plotted against Z' (real component).

Myelin forms a sheath around axons in vertebrate species (Arroyo and Scherer, 2000). It is the most abundant membrane structure within the vertebrate nervous system, allowing the fast conduction of nerve impulses through the nerve fibres due to its high resistance and low capacitance (Baumann and Pham-Dinh, 2001). Myelin basic protein is a cytoplasmic protein important in the process of myelination of nerves in the central nervous system since it comprises the bulk of the main line of compact myelin and up to 30% of the protein content of myelin overall (Baumann and Pham-Dinh, 2001).

A demyelinating disease is any disease of the nervous system in which the myelin sheath of neurons becomes damaged. This impairs the conduction of signals in the affected nerves, causing impairment in sensation, movement, cognition, or other functions depending on which nerves are involved. Multiple sclerosis (MS) which is a chronic and inflammatory disease of the central nervous system is an example of a demyelinating disease. Multiple sclerosis affects neurons, the cells of the brain and spinal cord that carry information, create thought and perception, and allow the brain to control the body. The name multiple sclerosis is derived from the multiple scars (or scleroses) that can be observed on the myelin sheaths. Multiple sclerosis currently does not have a cure, though several treatments are available that may slow the appearance of new symptoms.

Multiple sclerosis is often diagnosed following occurrence of MS type symptoms. Magnetic resonance imaging (MRI) may be used to evaluate patients who display these symptoms. MRI is capable of imaging areas where demyelination is occurring. Cerebrospinal fluid can also be utilised in the diagnosis of MS since the presence of immunoglobins can be detected in the majority of MS sufferers. However other conditions can also lead to the presence of these species (Rudick and Whitaker, 1987).

Other demyelinating diseases include transverse myelitis, Guillain-Barré syndrome, and progressive multifocal leukoencephalopathy. There are various causes of demyelination, including autoimmune reactions (Ercolini and Miller, 2006), infectious agents (Wingerchuk, 2006), genetic conditions (Kilfoyle *et al.,* 2006) and also exposure to compounds such as carbamate pesticides that have been identified as potential causes (Santinelli, 2006).

The presence of antibodies against myelin proteins such as MBP can be a predictor of multiple sclerosis (Berger, 2003). Clinical studies of 103 patients suffering from MS demonstrated that the presence of antibodies for MBP and myelin oligodendrocyte glycoprotein within serum could be correlated with a greatly increased level of relapse compared to patients without these antibodies. Other demyelinating conditions also lead to elevated levels of MBP in cerebrospinal fluid (Manzo *et al.,* 1996; Lamers *et al.*, 2003), for example in cases of closed head trauma (Mukherjee *et al.,* 1985) or acquired immunodeficiency syndrome (AIDS) dementia complex (ADC) (Liuzzi *et al.,* 1992). A significant correlation has also been determined between the clinical stage of the childhood-onset cerebral form of adrenoleukodystrophy and cerebrospinal fluid myelin basic protein levels (Phillips *et al.*, 1994). MBP levels between 4 and 8 ng ml^{-1} in cerebrospinal fluid may indicate a chronic breakdown of myelin, or recovery from an acute episode. MBP levels greater than 9 ng ml^{-1} indicate that active demyelination may be occurring. Normally there should be less than 4 ng ml^{-1} of myelin basic protein in the cerebral spinal fluid.

Increased myelin basic protein levels can also occur as a result of a stroke. A stroke, also known as cerebrovascular accident (CVA), is an acute neurological injury in which blood supply to a part of the brain is interrupted. That is, stroke involves sudden loss of neuronal function due to arterial or even venous disturbance in cerebral perfusion. The part of the brain with disturbed perfusion no longer receives adequate oxygen. This imitates the ischemic cascade, which causes brain cells to die or be seriously damaged, impairing local brain function. An indirect result of stroke is active myelin breakdown or demyelination and therefore the levels of myelin basic protein in cerebral spinal fluid (CSF) can act as markers for stroke.

There exist commercial ELISA tests for myelin basic protein, for example Diagnostic Systems Laboratories (Texas) manufacture an ELISA which can measure levels of MBP in cerebrospinal fluid in four hours. Our aim was to fabricate an immunosensor that would allow the fast, label-less detection of MBP within the physiological range of antigen concentrations at a low unit cost.

8.2.1 Electrochemical impedance spectroscopy (EIS) studies on MBP immunosensors: Specific sensors

Following immobilisation of anti-MBP, according to section 3.5.3.1, impedance analyses were performed from 1Hz to 10,000Hz (+/- 5mV amplitude perturbation) in a pH 7.4 phosphate buffer, i.e. containing no antigen, as a baseline trace. This buffer solution did, however, contain a 50:50 mixture of $[KFe(CN)_6]^{3-/4-}$, at a concentration of 10mM as a redox mediator so as to perform faradaic impedance spectroscopy. The potential of the electrochemical cell was offset to the formal potential of the redox probe (+0.4 V vs. Ag/AgCl). Subsequently, anti-MBP doped sensors were exposed to pre-prepared analyte concentrations of 1ng, 2ng, 4ng, 6ng, 8ng, 10ng, 15ng, 100ng, 500ng and 1μg per ml of PBS pH 7.4 buffer. The experimental protocol described in section 3.5.5 was followed for the electrochemical impedimetric interrogation of MBP immunosensors. A consistent sensor was used for all analytical concentrations and changes encountered were compared to the initial baseline trace (0 ng ml^{-1} MBP).

Results are presented in the form of Nyquist plots depicting the faradaic (Z') and capacitive (Z'') components of impedance and their variation throughout the recording of the AC impedance spectra (Fig 8.1). For the baseline trace, the Z' component is seen to increase with decreasing frequency for the entire range of applied frequencies whereas the Z'' component is seen to increase up to the characteristic frequency ω of each trace (the frequency at which the Z'' value is at its maximum) before decreasing to the lower applied frequencies (~1Hz). In general, the impedance spectrum is indicative of a surface-modified electrode system where the electron transfer is slow and the impedance is controlled by the interfacial electron transfer (Katz and Willner, 2003). All subsequent traces following antigen exposure also follow this general form.

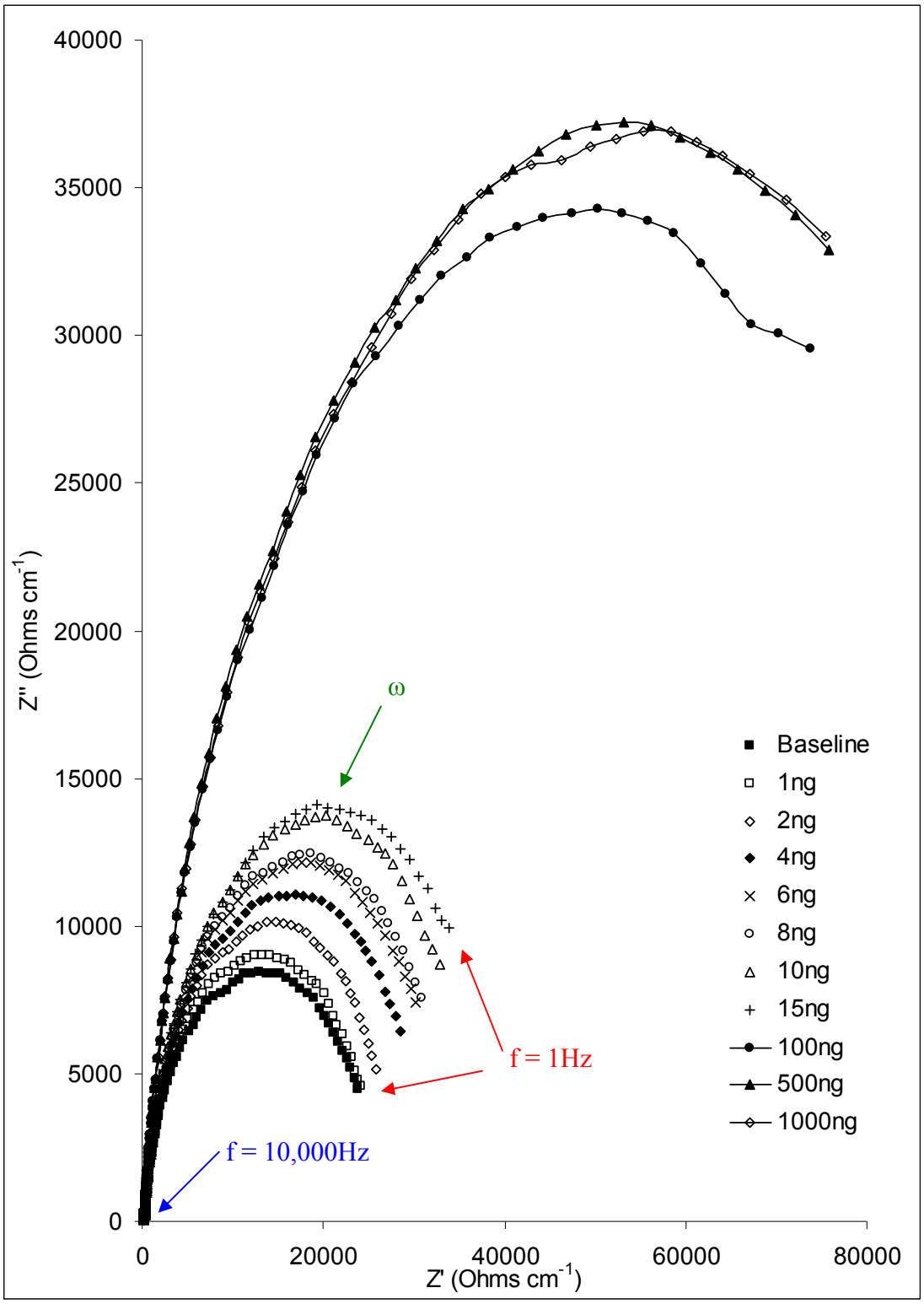

Fig 8.1 Nyquist plot for an anti-MBP doped PANI immunosensor following exposure to the full range of MBP concentrations in PBS pH 7.4.

As can be seen, exposure of the anti-MBP doped sensors to increasing antigen concentrations resulted in the increase of the total impedance of the sensors. It was concluded, therefore, that the formation of antibody-antigen complexes on the polymer modified surface hindered electron transfer kinetics and encouraged double layer charging phenomena, thus increasing the capacitance of the sensors.

The intercept of the semicircle region of the impedemetric traces with the Z' axis at high frequencies is equal to the solution resistance, R_s. The latter was constant for all of the traces recorded and equal to ~150Ω. As expected, this value agrees with the solution resistance value obtained for the ciprofloxacin immunosensors, since both immunosensors were interrogated in the same buffer solution. Extrapolation of the semicircle to lower frequencies yields an intercept corresponding to $R_s + R_{et}$. For the baseline trace, this intercept had a value of ~27kΩ. The electron transfer resistance was thus approximately equal to 16.85kΩ. Exposure of the sensors to 1ng of MBP resulted in the increase of the electron transfer resistance by roughly 1 kΩ. In the same manner, changes from the baseline trace upon exposure to various antigen concentrations can be calculated.

Analytically meaningful impedance spectra are usually recorded at frequencies where they are mainly controlled by the interfacial properties of the modified electrodes (10 mHz < f < 100kHz). This is best illustrated in a Bode plot, where the total impedance of the anti-MBP loaded sensors was plotted as a function of the $\log_{10}$ of the applied frequency as illustrated in Fig 8.2.

Previous work by our group showed that while both the imaginary and real components change due to the formation of antibody-antigen complexes on the surface of the sensors, the change from the baseline trace in the real component dominated the total change in the impedance (Grant *et al*., 2005, Garifallou *et al.*, 2007). In this case, changes in both real and imaginary components are visible and again the real component is the major contributor to total impedance. It was also found that the real component offers far greater reproducibility in comparison to the imaginary contribution. Faradaic impedance spectroscopy is generally regarded to be more sensitive to changes on the electrode surface upon antigen binding to the antibody-functionalised electrode surfaces.

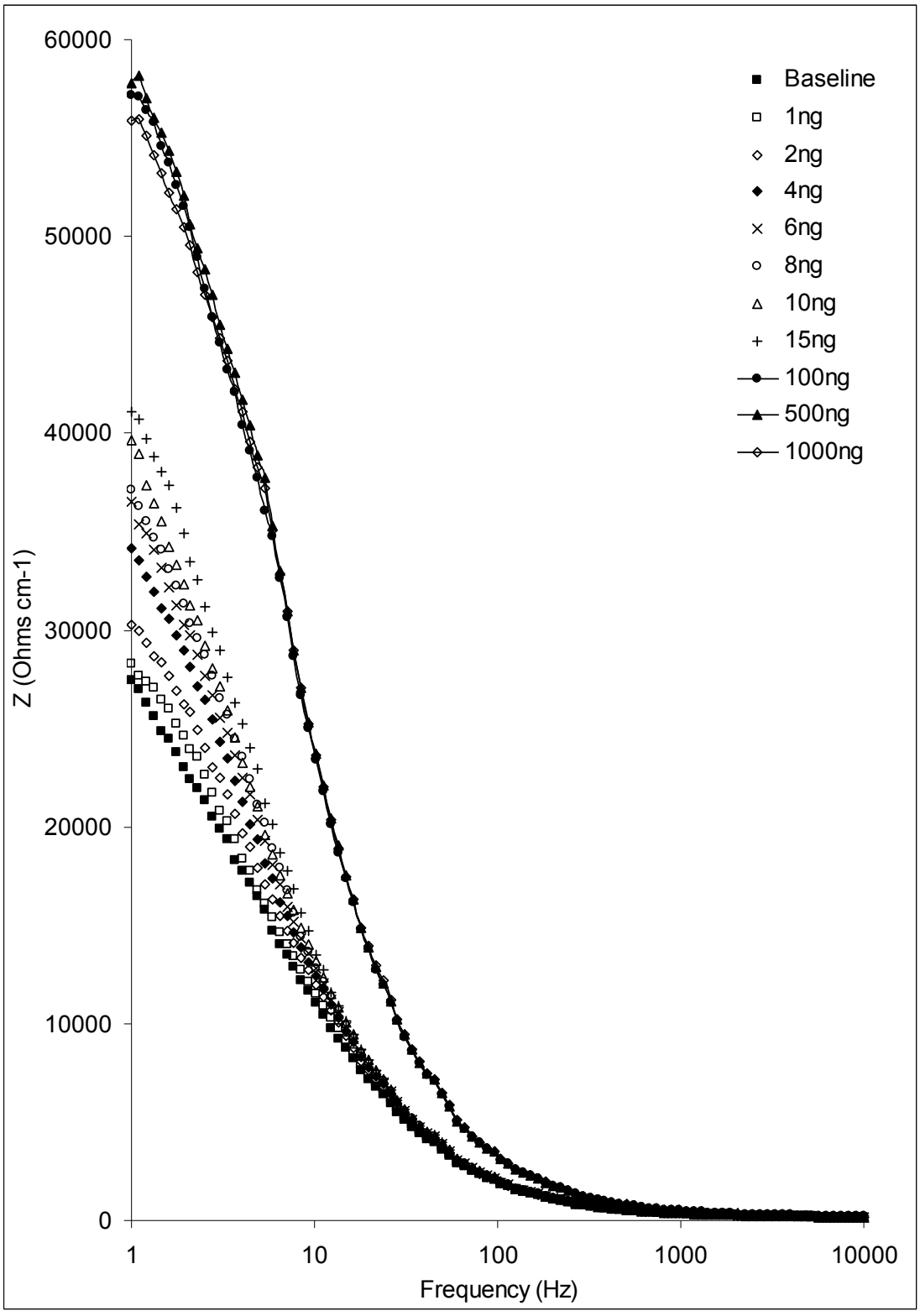

Fig 8.2 Bode plot for an anti-MBP doped PANI immunosensor following exposure to the full range of ciprofloxacin concentrations in PBS pH 7.4.

This is why the real component of the impedance at 1Hz was used to plot a calibration curve of the percentage change from the baseline trace of the electron transfer resistance across the $\log_{10}$ of a range of antigen concentrations (Fig 8.3). As can be seen, there is a steady increase in impedance as antigen concentration increases up to a concentration of about 100 ng ml^{-1}above which concentration there is a tend towards a plateau, possibly indicating saturation of the specific binding sites. It is possible that any further changes in impedance beyond this level could simply be due to non-specific interactions. Between a concentration range of 1-100 ng ml^{-1}, there is a near linear correlation of the impedance change with the $\log_{10}$ of concentration (R^2=0.965) (Fig 8.4). This concentration range corresponds with the range of physiological/clinical significance for MBP.

8.2.2 Electrochemical impedance spectroscopy (EIS) studies on MBP immunosensors: Non-Specific sensors and Corrected Calibration Profile

In order to validate the specificity of the observed response for the anti-MBP modified sensor assembly, control experiments were performed to investigate non-specific events that may be occuring. A generic IgG antibody was immobilized following the same fabrication protocol as for the specific anti-MBP doped sensors. In every other sense the matched sensors were identical and were interrogated simultaneously with their specific counterparts over the same antigen concentration range. The results obtained permit an overall assessment of the contribution of non-specific effects to the changes encountered in Figs 8.1 and 8.2. A correction can therefore be made to the electron transfer resistance changes from the baseline response at each concentration to acquire the true specific anti-MBP immunosensor system response.

The obtained impedimetric spectral traces are presented as Nyquist plots in Fig 8.5. They follow a similar general form to those obtained in section 8.2.1 for the specific sensors (Fig 8.1). The Z' component is again seen to increase with decreasing frequency for the entire range of applied frequencies whereas the Z component is seen to increase up to the characteristic frequency of each trace (the frequency at which the Z'' value is at its maximum) before decreasing to the final applied frequency (1Hz).

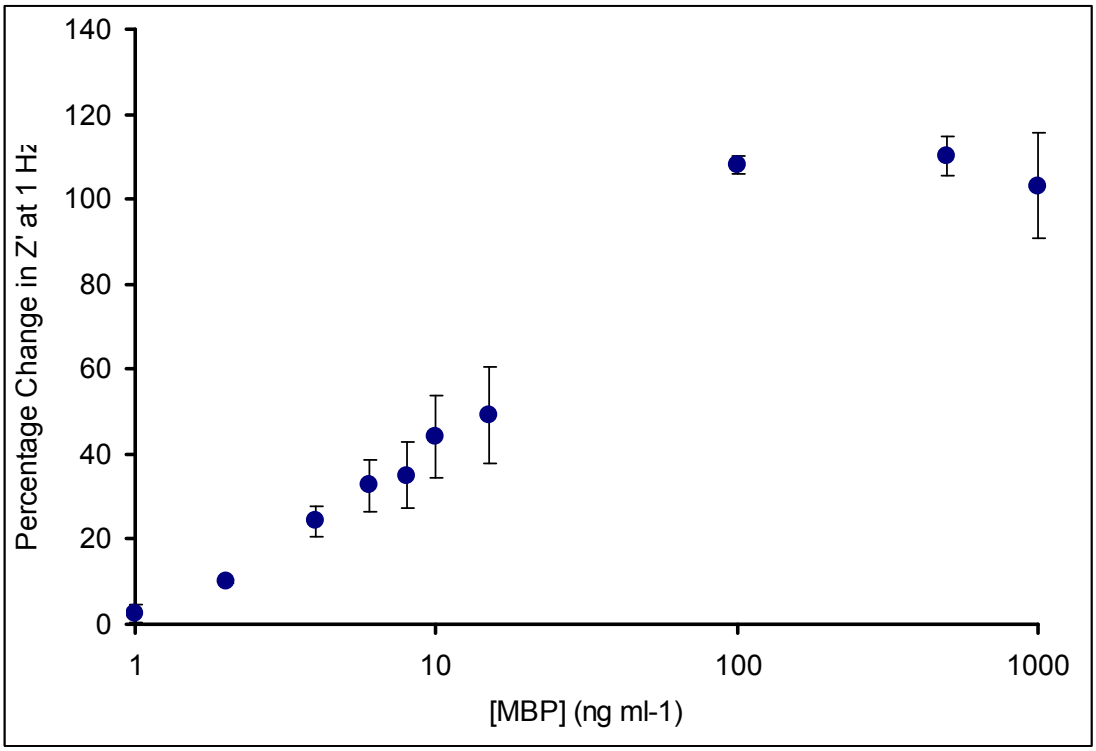

Fig 8.3 Calibration curve of the change in electron transfer resistance from the baseline response for anti-MBP modified electrodes upon exposure to the $\log_{10}$ of the full range of MBP concentrations in PBS pH 7.4.

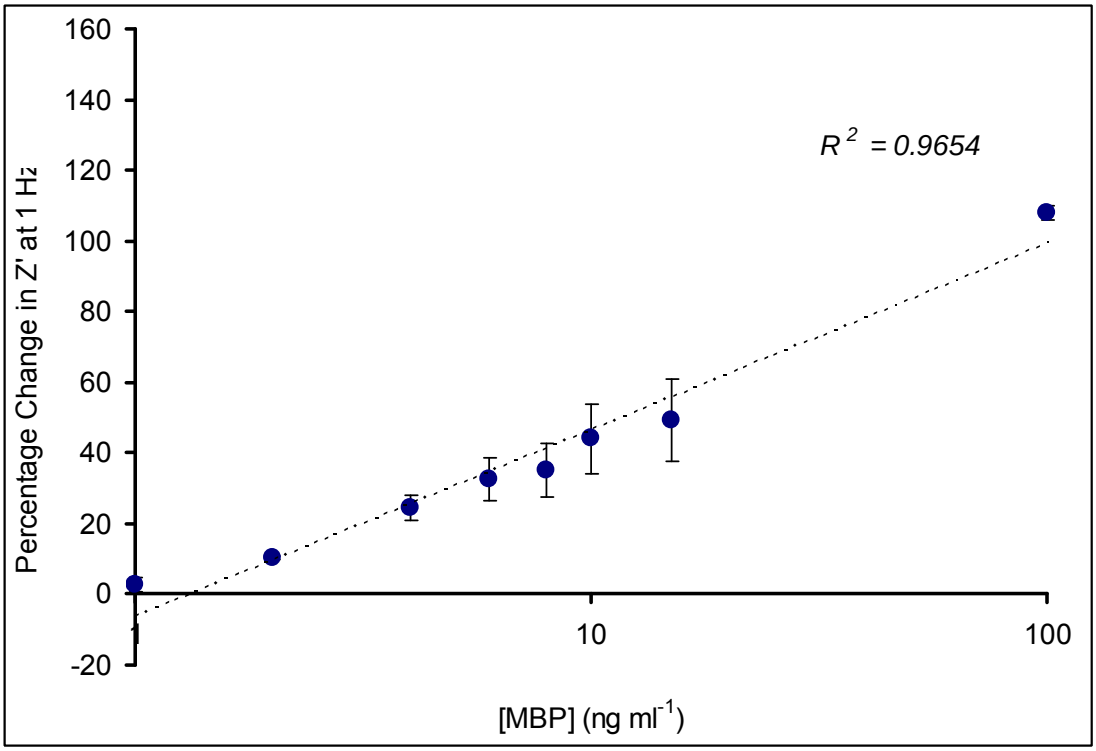

Fig 8.4 Calibration curve of the change in electron transfer resistance from the baseline response for anti-MBP modified electrodes upon exposure to the $\log_{10}$ of the full range of MBP concentrations in PBS pH 7.4 (only linear part is shown).

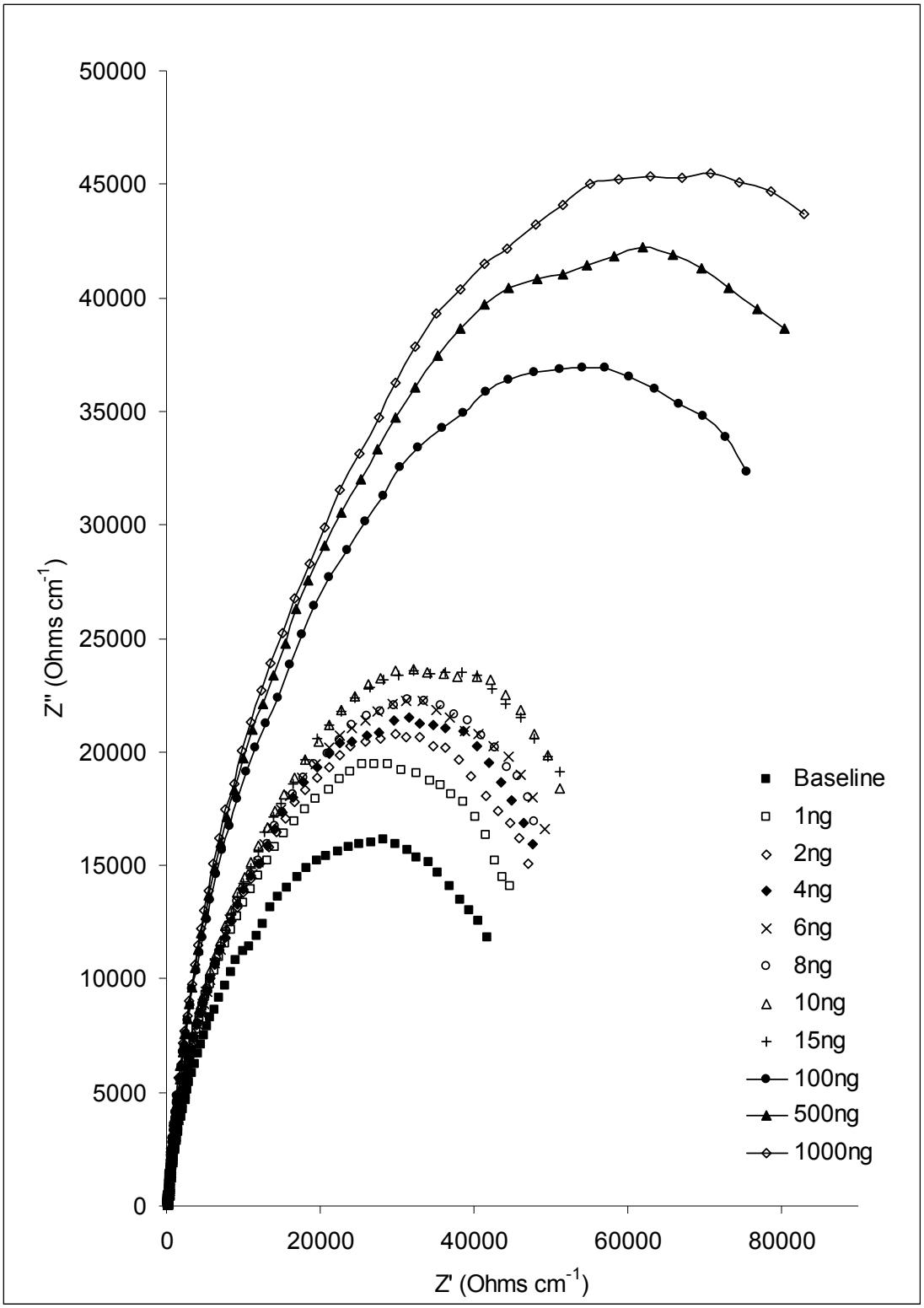

Fig 8.5 Nyquist plot for a generic IgG-doped PANI immunosensor following exposure to the full range of MBP concentrations in PBS pH 7.4.

Once again, maximum changes from the baseline trace upon exposure to antigen were observed at low frequencies, a fact clearly illustrated in the Bode plot in Fig 8.6.

Exposure of the IgG modified sensors to increasing MBP concentrations resulted in the increase of impedance of the sensors due to the formation of antibody-antigen complexes. The major contributor of the changes incurred in the total impedance of the system was once again the real component. The latter can be seen to increase with increasing antigen concentrations in Fig 8.5. The capacitance of the sensors also increases across the range of antigen concentrations however changes in recorded in the imaginary component are less pronounced than the changes recorded in the real component.

For the aforementioned reasons and as discussed in the previous section, the real component of the impedance at 1Hz was used to plot a calibration curve of the percentage change of the electron transfer resistance across the $\log_{10}$ of a range of antigen concentrations (Fig 8.7). The calibration curve plotted for the specific sensors across the same antigen concentration was also included. Upon comparison of the two calibration curves in Fig 8.7, it is apparent that approximately 25% of the changes in the electron transfer resistance encountered with the anti-ciprofloxacin modified sensors are, in fact, non-specific. However, there is a much lower response for the non-specific sensors, showing that although there are non-specific interactions, they comprise a minor component of the detected response

The non-specific response observed could arise from factors such as non-specifically adsorbed matter not being removed via the flushing regime and thus remaining at the sensor surface and / or weakly bound matter, polymer swelling, proton doping and transitional changes of the polyaniline at the neutral test pH, i.e. becoming less conductive.

A correction can be made to acquire the true specific anti-MBP immunosensor response by subtracting the non-specific sensor response at each antigen concentration from the specific sensor response (Fig 8.8).

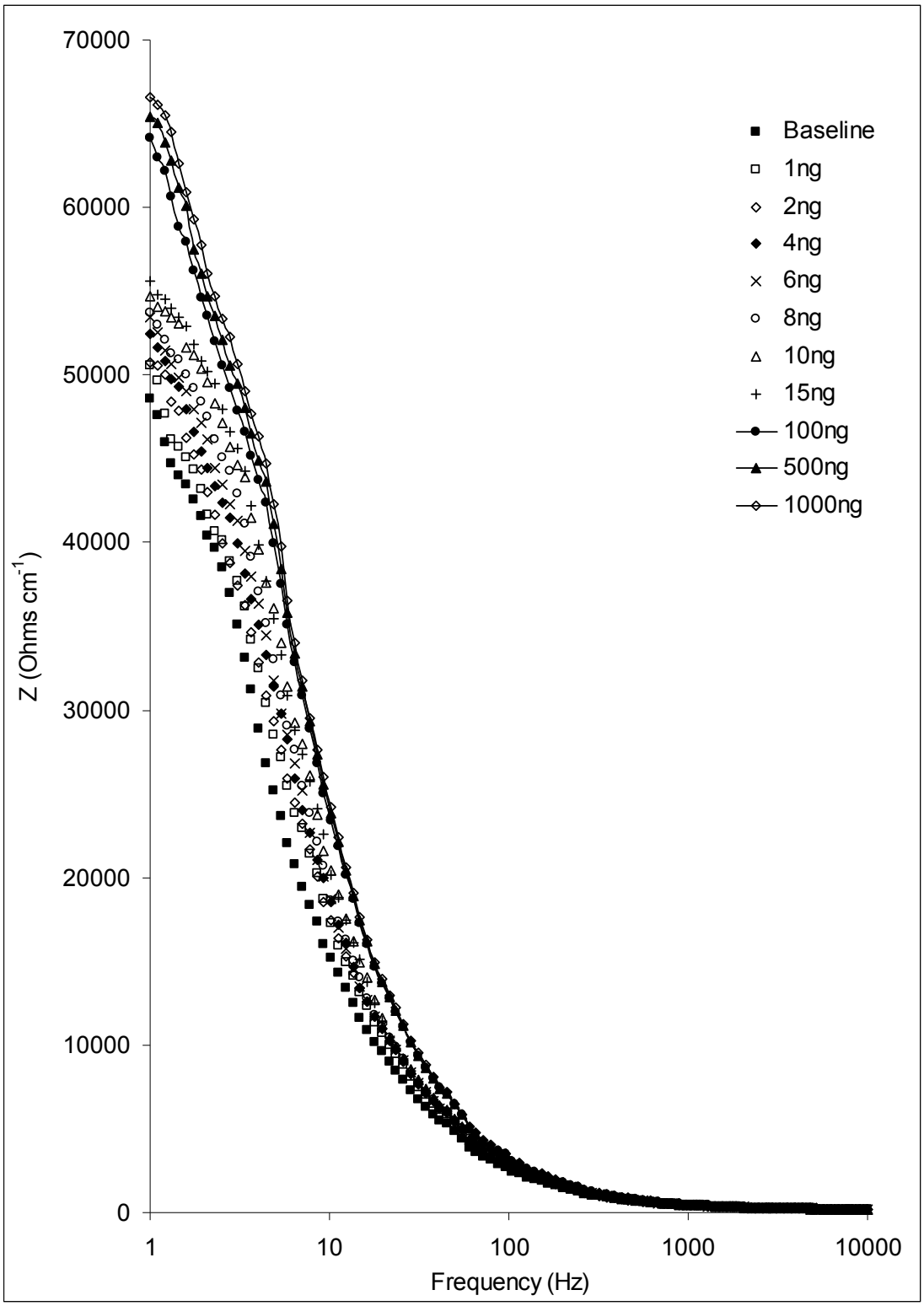

Fig 8.6 Bode plot for a generic IgG-doped PANI immunosensor following exposure to the full range of MBP concentrations in PBS pH 7.4.

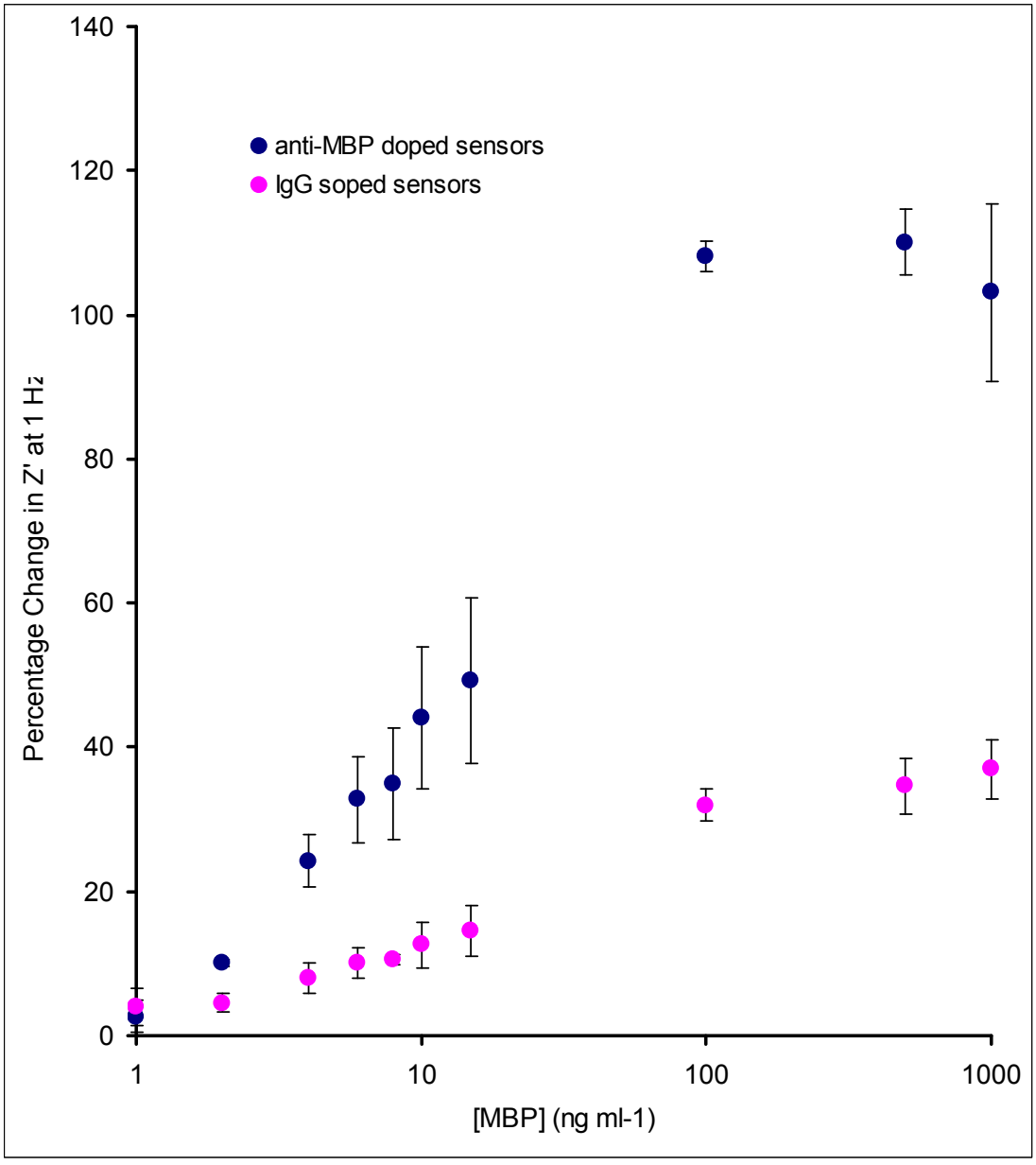

Fig 8.7 Calibration curve of the change in electron transfer resistance from the baseline response for IgG and anti-MBP modified electrodes upon exposure to the $\log_{10}$ of the full range of MBP concentrations in PBS pH 7.4.

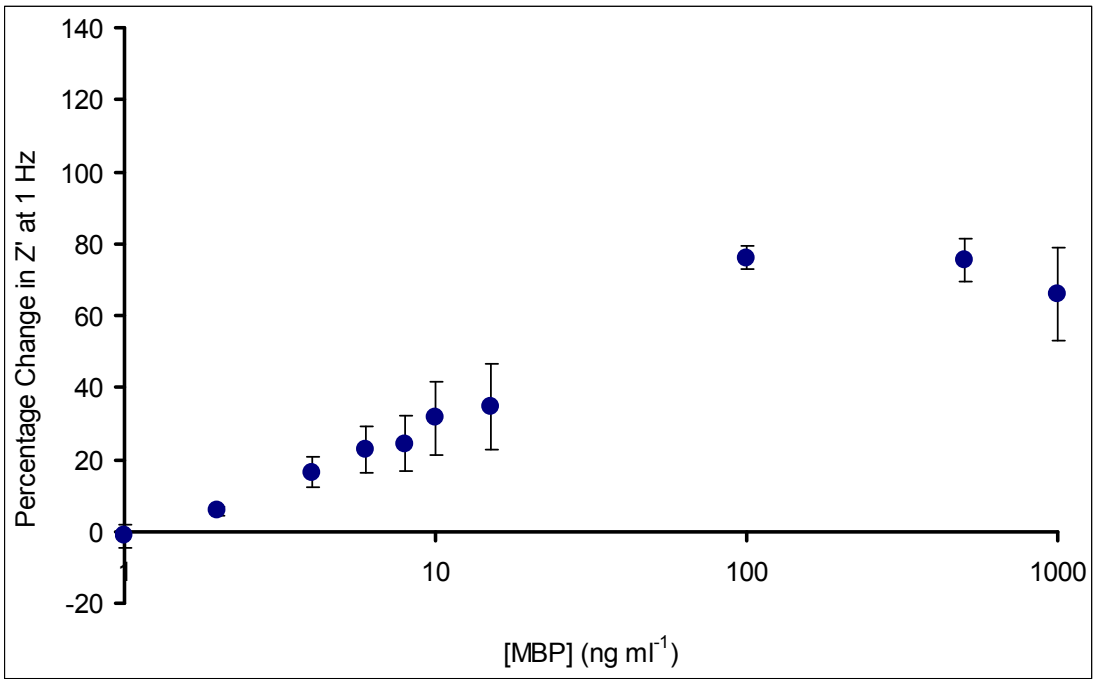

Fig 8.8 Calibration curve of the 'corrected' change in electron transfer resistance from the baseline response for the $\log_{10}$ of the full range of MBP concentrations in PBS pH 7.4.

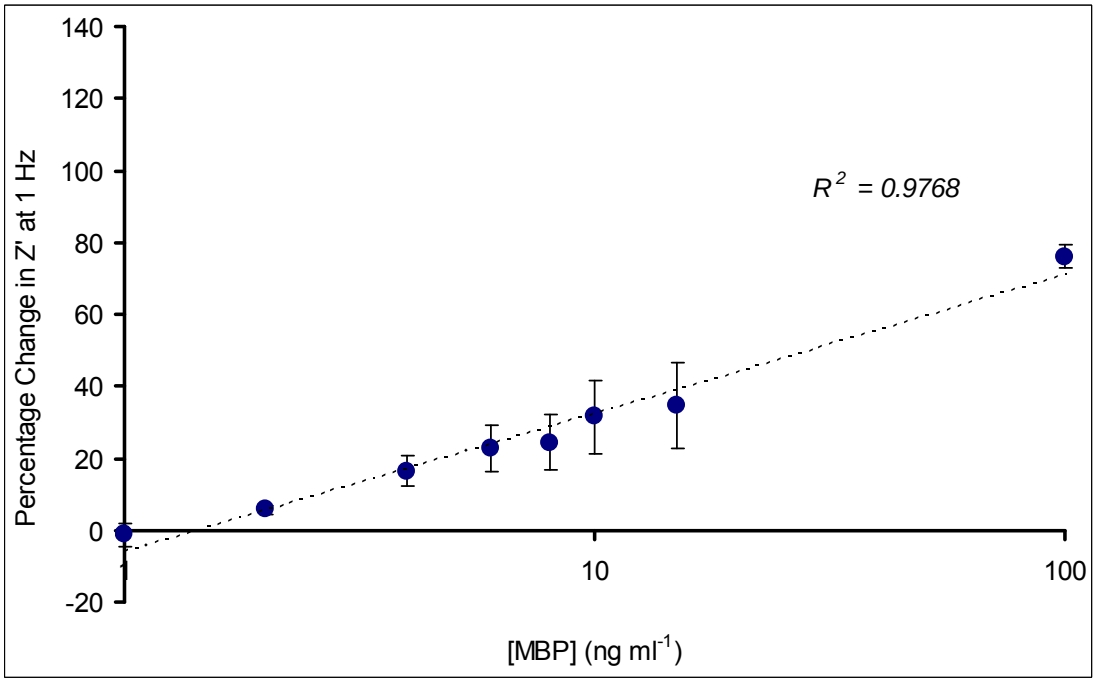

Fig 8.9 Calibration curve of the 'corrected' change in electron transfer resistance from the baseline response for the $\log_{10}$ of the full range of MBP concentrations in PBS pH 7.4.

In Fig 8.8, there is a steady increase in the real component of the impedance as antigen concentration increases up to a concentration of about 100 ng ml^{-1}, above which concentration the sensor becomes saturated. Between a concentration range of 1-100 ng ml^{-1}, as for the non corrected calibration profile, there is a near linear correlation of the impedance change with the log_{10} of concentration (R^2=0.98) (Fig 8.9).

8.3 Conclusions

We have demonstrated the construction of an immunosensor for Myelin Basic Protein using a combination of screen-printed carbon electrodes coated with conducting polyaniline and immobilised antibodies against MBP via the neutravidin/biotin affinity interactions. Interrogation of the electrodes by AC impedance demonstrated the detection of the antigen.

It can be summarised than the higher the MBP concentration in the test solution the greater the number of stable antibody-antigen complexes formed at the sensor surface. Complex formation was shown to hinder electron transfer of the redox couple within the test solution at the formal redox potential and hence the electron transfer resistance increased with increasing antigen concentrations. At concentrations of analyte above 100 ng ml^{-1}, the response began to plateau as the sensor saturated, with the recognition entities becoming occupied with analyte and active sites for further antigen binding being no longer available.

Non-specific interactions were accounted for by the simultaneous interrogation of sensors loaded with a generic IgG in PBS pH 7.4. It was found that ~25% of the response obtained from the specific sensors was due to non-specific binding events. A calibration curve of the corrected changes in the electron transfer resistance was plotted across the range of antigen concentrations. Linear correlation of the change in the electron transfer resistance with the log_{10} of concentration (R^2=0.977) was observed between concentrations of 1-100 ng ml^{-1}.

Further work utilising samples of cerebrospinal fluid with various levels of MBP need to be undertaken, however the use of a dual antibody (specific and non-specific)

electrode system should allow subtraction of any non-specific binding events and allow the detection of MBP levels in "real" samples.

Work described in this chapter as well as the results obtained with the MBP immunosensors have been published in Analytical Chemistry (Tsekenis *et al.*, 2008). A copy of the paper is attached in the Appendix at the back of this thesis.

Chapter 9

Electrochemical Impedance Studies on Cancer Antigen 125 immunosensors

9.1 Introduction

Ovarian cancer is the fifth leading cause of cancer deaths in women, the leading cause of death from gyneacological malignancy, and the second most commonly diagnosed gynecologic malignancy. The exact causes are usually unknown. The disease is more common in industrialized nations, with the exception of Japan. In the United States, females have a 1.4% to 2.5% (1 out of 40-60 women) lifetime chance of developing ovarian cancer. Older women are at highest risk. More than half of the deaths from ovarian cancer occur in women between 55 and 74 years of age and approximately one quarter of ovarian cancer deaths occur in women between 35 and 54 years of age. The risk of developing ovarian cancer appears to be affected by several factors, both epigenetic and hereditary in origin. The use of oral contraceptives, the number of children a woman gives birth to and the use of fertility medication, to name but a few, have been shown to affect the risk of developing ovarian cancer (Brinton *et al*., 2005; Franco, 2008). Hereditary predisposition to developing ovarian carcinoma has been established at carriers of certain mutations of the BRCA1 or the BRCA2 gene as well as those that have a strong family history of uterine cancer, colon cancer, or other gastrointestinal cancers (Lachine *et al*., 2004).

Ovarian cancer is classified according to the histology of the tumours, obtained in a pathology report, into surface epithelial-stromal tumours, sex cord-stromal tumours, germ cell tumours and mixed tumours. It can also be the metastatic result of breast or gastrointestinal tumours and hence a secondary cancer. By far the most common forms of ovarian carcinomas are the epithelial malignancies, which account for more than 80 percent of the reported cases (Hart, 1992). Histology dictates many aspects of clinical treatment, management and prognosis.

Although effective treatment of ovarian cancer is possible when diagnosed at an early stage, ovarian cancer at its early stages (I/II) is notoriously difficult to diagnose until it spreads and advances to later stages (III/IV). This is due to the fact that most of the common symptoms are non-specific. Since there is no accurate screening test, an exploratory surgical procedure called laparotomy is generally required for the

definitive diagnosis of ovarian cancer. During this procedure, cysts or other suspicious areas must be removed and biopsied.

Current research is looking at ways to combine tumour marker proteomics along with other indicators of disease (i.e. radiology and/or symptoms) to improve accuracy. The challenge in such an approach is that the very low population prevalence of ovarian cancer means that even testing with very high sensitivity and specificity will still lead to a number of false positive results. It is of paramount importance therefore to identify a highly specific biomarker or a combination of biomarkers that can be applied towards the screening detection of ovarian cancer.

Of the biomarkers described in ovarian cancer Cancer Antigen 125, referred to herein as CA-125, has been the most extensively studied. It is a mucinous glycoprotein and the product of the MUC16 gene. Mucins are a large family of heavily glycosylated proteins. Some mucins are membrane-bound due to the presence of a hydrophobic membrane-spanning domain that favors retention in the plasma membrane, while others are secreted on mucosal surfaces, blood and saliva. Increased mucin production occurs in many adenocarcinomas, including cancer of the pancreas, lung, breast, ovary, colon, etc (Beatrice *et al*, 2002).

For use as a screening tool in an immunosensor platform, several observations are relevant. CA-125 levels have been shown to be elevated prior to the clinical development of primary and recurrent ovarian cancer. In those patients with early-stage cancer, however, CA-125 is elevated in less than half of the cases. Furthermore, in premenopausal cases, several benign conditions are associated with elevated levels of CA-125, such as endometriosis, pelvic inflammatory disease and even pregnancy. Finally, raised CA-125 values have been observed in lung, breast, colon, cervix, pancreas and endometrium cancers (Teneriello and Park, 1995).

It becomes apparent therefore that the use of CA-125 alone as a screening tool is not adequate to positively discriminate between different cancer types or even between a malignant or benign tumour. A combination of biomarkers is probably the solution, although up until now the use of other markers for detection screening of ovarian

cancer has been limited. Recently, simultaneous investigations of several biomarkers have been evaluated to determine whether sensitivity and specificity can be improved. Visintin and his team described a blood biomarker test, that combined six markers of ovarian carcinoma with an improved sensitivity of 95.3% and specificity of 99.4% (Visintin *et al*., 2008) while Wu and his group fabricated an immunosensor chip for the fast simultaneous detection of CA 19-9 and CA-125 (Wu *et al*., 2007). Wilson and Nie described an electrochemical immunosensor for performing multianalyte measurements of tumour markers that was used to measure the concentrations of seven important tumour markers simultaneously: AFP, ferritin, CEA, hCG-beta, CA 15-3, CA 125, and CA 19-9 (Wilson and Nie, 2006).

This chapter deals with the development of a label free immunosensor for the detection of CA-125 using the same protocol as previously described for the ciprofloxacin and Myelin Basic Protein immunosensors in Chapter 7 and 8 respectively. Dai and his team in 2003 reported the fabrication of an amperometric immunosensor for the detection of CA-125. This immunosensor, however, was not labeless since antigen recognition by the antibody was quantified through direct electrochemistry on horseradish peroxidase (Dai *et al.*, 2003).

CA-125 serum levels have been shown to directly correlate with the onset of primary tumour or tumour recurrence. Although, CA-125 levels cannot provide a definitive answer on their own they can be used in conjunction with a physical examination or jointly with the detection of other biomarkers in serum to diagnose ovarian cancer or monitor its post-treatment behaviour. For example, in patients with a history of ovarian cancer, three progressively rising serum CA-125 values in the normal range (< 35 U/ml) at 1- to 3-month intervals are associated with a high likelihood of tumor recurrence. Patients with such a pattern should undergo immediate investigation to rule out and/or identify recurrent cancer (Wilder *et al.*, 2003). It is widely accepted that CA-125 values greater than 35U/ml are a cause for concern.

The protocol used to construct the antibody-doped polymer-modified carbon electrodes is identical to the one used for the ciprofloxacin and Myelin Basic protein immunosensors described in the previous chapters and was designed to ensure orientation specific immobilisation of antibodies utilising neutravidin-biotin

non-covalent affinity technologies as detailed in section 3.5.3.1. The experimental protocol described in section 3.5.5 was followed for the electrochemical impedimetric interrogation of CA-125 immunosensors.

An alternative approach to fabricating these immunosensors was also tested, which involved the direct immobilisation of the antibodies on the deposited polyaniline film. In this case the monomer was a modified aniline moiety with a boronic acid attached to it. This allowed for the direct binding of antibodies to the polymer surface without the need of biotinylation and addition of neutravidin.

For both fabrication protocols, the reported results were the mean valued of three replicate sensors and they were presented in a series of Bode and Nyquist plots. In a Bode plot, the total impedance is plotted against the logarithm of the frequency. In a Nyquist plot, Z'' (imaginary component), is plotted against Z' (real component). The real (Z') component of impedance refers to the resistance of the system where the impedance is in phase with the AC potential waveform. The imaginary (Z") component, on the other hand, refers to the capacitance of the system where the impedance is 180^{o} out of phase.

9.2.1 Electrochemical impedance spectroscopy (EIS) studies on CA-125 immunosensors: Specific sensors

Following immobilisation of anti-CA-125, according to section 3.5.3.1, impedance analyses were performed from 1Hz to 10,000Hz (+/- 5mV amplitude perturbation) in a pH 7.4 phosphate buffer, i.e. containing no antigen, as a baseline trace. This buffer solution did, however, contain a 50:50 mixture of $[KFe(CN)_6]^{3-/4-}$, at a concentration of 10mM as redox mediator so as to perform faradaic impedance spectroscopy. The potential of the electrochemical cell was offset to the formal potential of the redox probe (+0.4 V vs. Ag/AgCl). Subsequently, anti-MBP doped sensors were exposed to pre-prepared analyte concentrations of 1U, 5U, 10U, 20U, 30U, 40U, 50U and 100U per ml of PBS pH 7.4 buffer. The experimental protocol described in section 3.5.5 was then followed for the electrochemical impedimetric interrogation of CA-125 immunosensors. A consistent sensor was used for all analytical concentrations and changes encountered were compared to the initial baseline trace (0U ml^{-1} CA-125).

Results are presented in the form of Nyquist plots depicting the faradaic (Z') and capacitive (Z'') components of impedance and their variation throughout the recording of the AC impedance spectra (Fig 9.1). For the baseline trace, the Z' component is seen to increase with decreasing frequency for the entire range of applied frequencies whereas the Z'' component is seen to increase up to the characteristic frequency ω of each trace (the frequency at which the Z'' value is at its maximum) before decreasing to the lower applied frequencies (~1Hz). In general, the impedance spectrum is indicative of a surface-modified electrode system where the electron transfer is slow and the impedance is controlled by the interfacial electron transfer (Katz and Willner, 2003). All subsequent traces following antigen exposure also follow this general form.

As can be seen, exposure of the anti-CA-125 doped sensors to increasing antigen concentrations resulted in the increase of the total impedance of the sensors. It was concluded, therefore, that the formation of antibody-antigen complexes on the polymer modified surface hindered electron transfer kinetics and encouraged double layer charging phenomena, thus increasing the capacitance of the sensors.

Analytically meaningful impedance spectra are usually recorded at frequencies where they are mainly controlled by the interfacial properties of the modified electrodes (10 mHz < f < 100kHz). This is best illustrated in a Bode plot, where the total impedance of the anti-MBP loaded sensors was plotted as a function of the $\log_{10}$ of the applied frequency as illustrated in Fig 9.2. As can be seen in Fig 9.2, the greatest differences in the total impedance of the sensors are observed at 1Hz.

Previous work by our group showed that while both the imaginary and real components change due to the formation of antibody-antigen complexes on the surface of the sensors, the change from the baseline trace in the real component dominated the total change in the impedance (Grant *et al*., 2005, Garifallou *et al.*, 2007). In this case, changes in both real and imaginary components are visible and again the real component is the major contributor to total impedance. It was also found that the real component of impedance offers far greater reproducibility in comparison to the imaginary contribution.

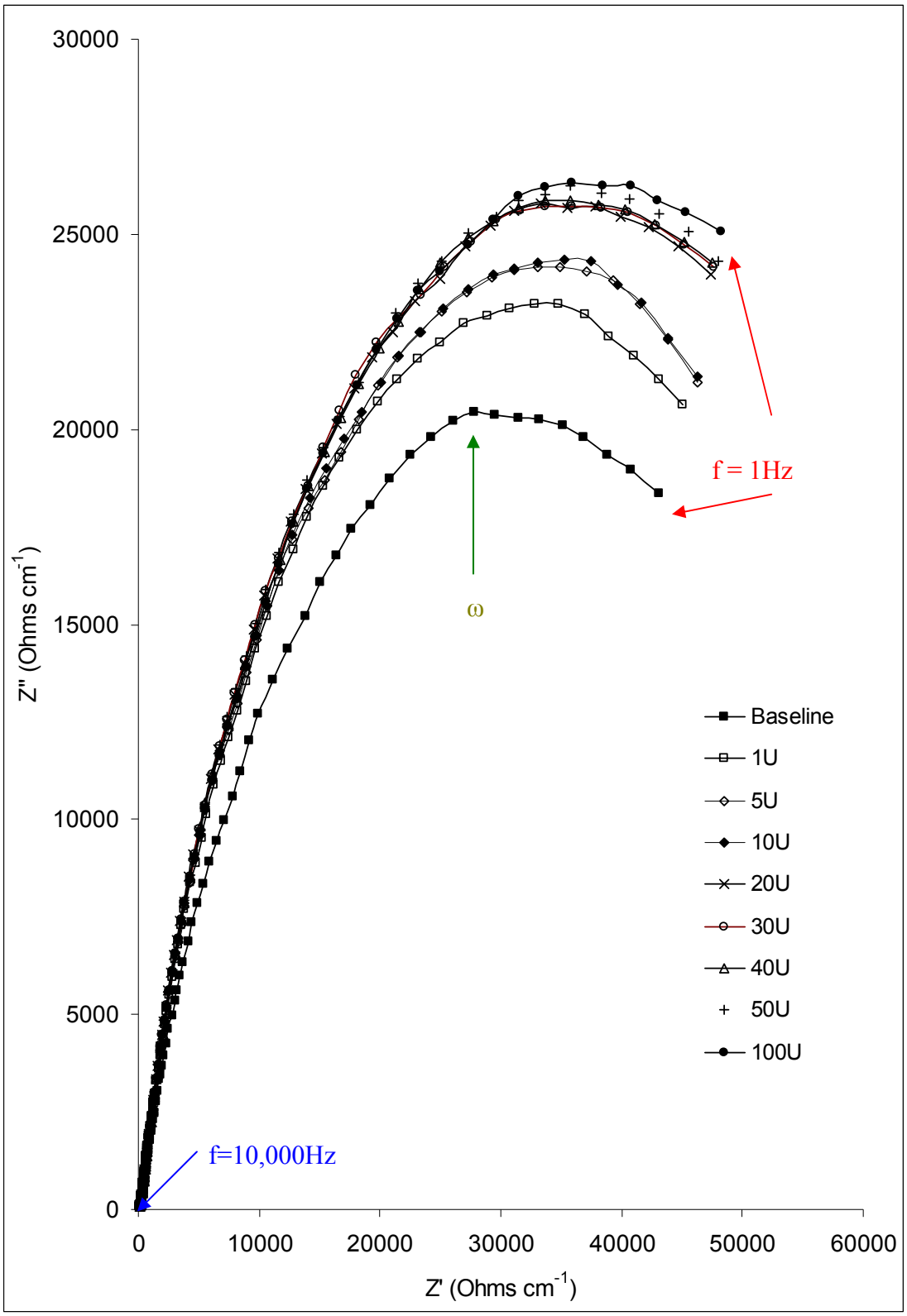

Fig 9.1 Nyquist plot for an anti-CA-125 doped PANI immunosensor following exposure to the full range of CA-125 concentrations in PBS pH 7.4.

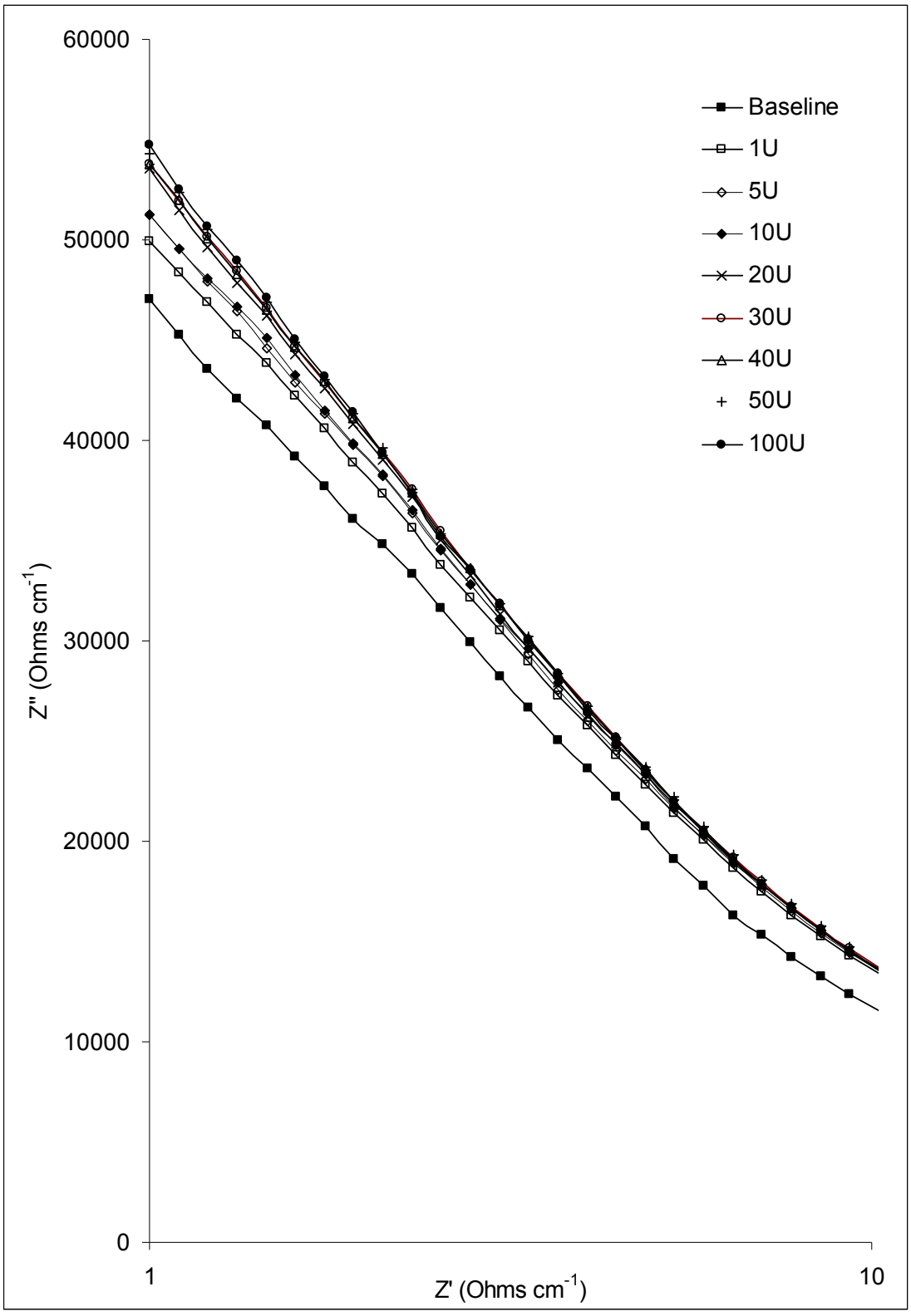

Fig 9.2 Bode plot for an anti-CA-125 doped PANI immunosensor following exposure to the full range of CA-125 concentrations in PBS pH 7.4. For clarity, only frequency values from $\log_{10}$ 1 to 10 Hz are shown.

Faradaic impedance spectroscopy is generally regarded to be more sensitive to changes on the electrode surface upon antigen binding to the antibody-functionalised electrode surfaces.

This is the reason the real component of the impedance at 1Hz was used to plot a calibration curve of the percentage change from the baseline trace of the electron transfer resistance across the $\log_{10}$ of the full range of antigen concentrations (Fig 9.3). As can be seen, there is a steady increase in impedance as antigen concentration increases up to a concentration of 100 Uml^{-1}. No saturation of the sensors is observed even following exposure to 100Uml^{-1}, indicated by the absence of a plateau in the calibration curve. This suggests that antigen binding sites on the electrode surface are not fully occupied. Furthermore, there is a linear correlation of the electron transfer resistance change with the $\log_{10}$ of antigen concentration across the clinically significant range (R^2=0.9716) (Fig 9.3).

9.2.2 Electrochemical impedance spectroscopy (EIS) studies on CA-125 immunosensors: Non-Specific IgG sensors

In order to validate the specificity of the observed response for the anti-CA-125 modified sensor assembly, control experiments were performed to gauge non-specific events that may be occurring. A generic IgG antibody was immobilized following the same fabrication protocol as for the specific anti-CA-125 doped sensors. In every other sense the matched sensors were identical and they were interrogated simultaneously following exposure to antigen solutions. The obtained results permit an overall assessment of the contribution of non-specific effects to the changes encountered in Figs 9.1 and 9.2.

All obtained impedimetric spectral traces follow a similar general form to those obtained in section 9.2.1 for the specific sensors (Fig 9.4). The Z' component is again seen to increase with decreasing frequency for the entire range of applied frequencies whereas the Z component is seen to increase up to the characteristic frequency of each trace (the frequency at which the Z'' value is at its maximum) before decreasing to the final applied frequency (1Hz). The impedance spectrum is indicative of a surface-modified electrode system where the electron transfer is slow.

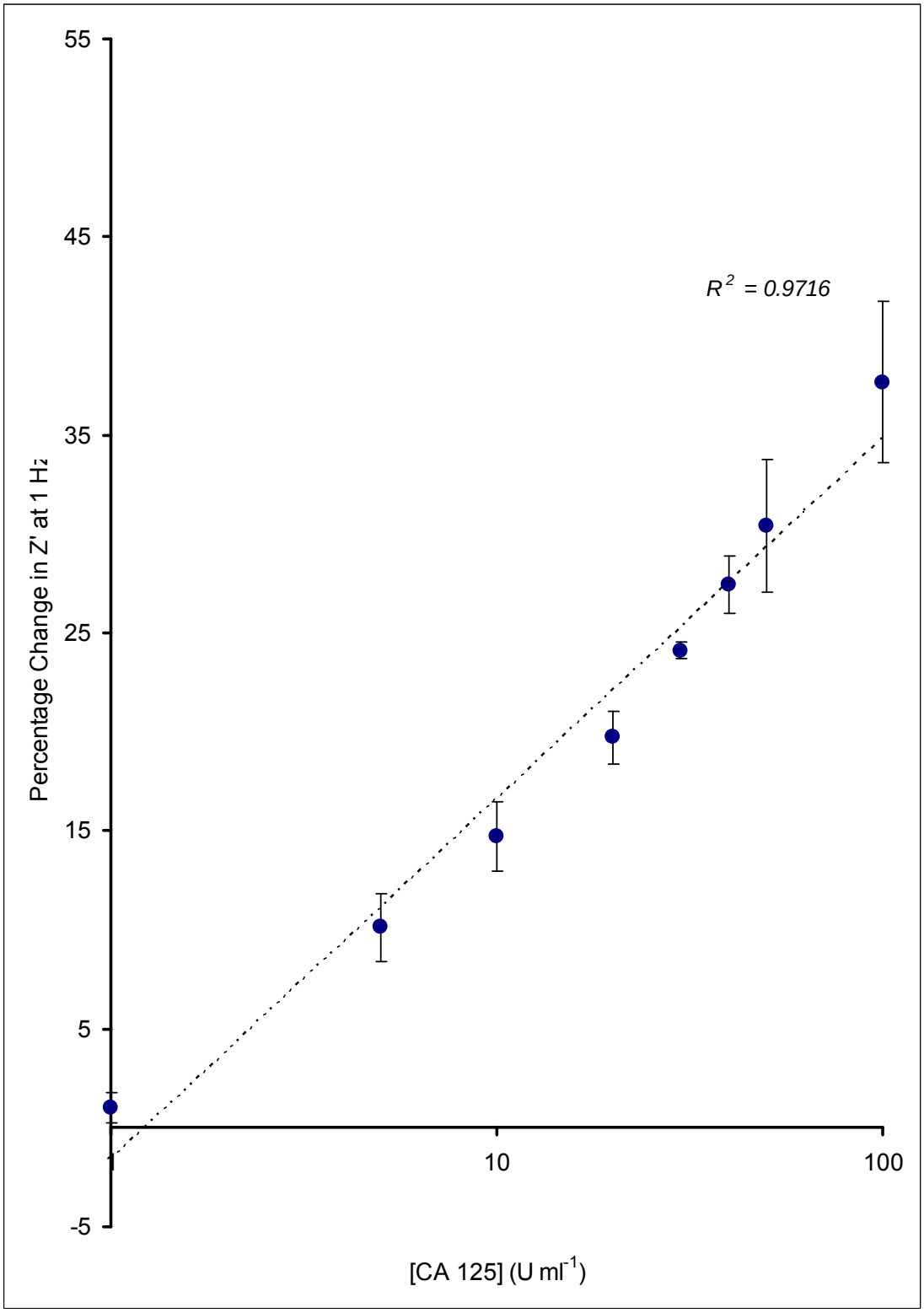

Fig 9.3 Calibration curve of the change in electron transfer resistance from the baseline response for anti-CA-125 dopes PANI immunosensors upon exposure to the $\log_{10}$ of the full range of ca-125 concentrations in PBS pH 7.4.

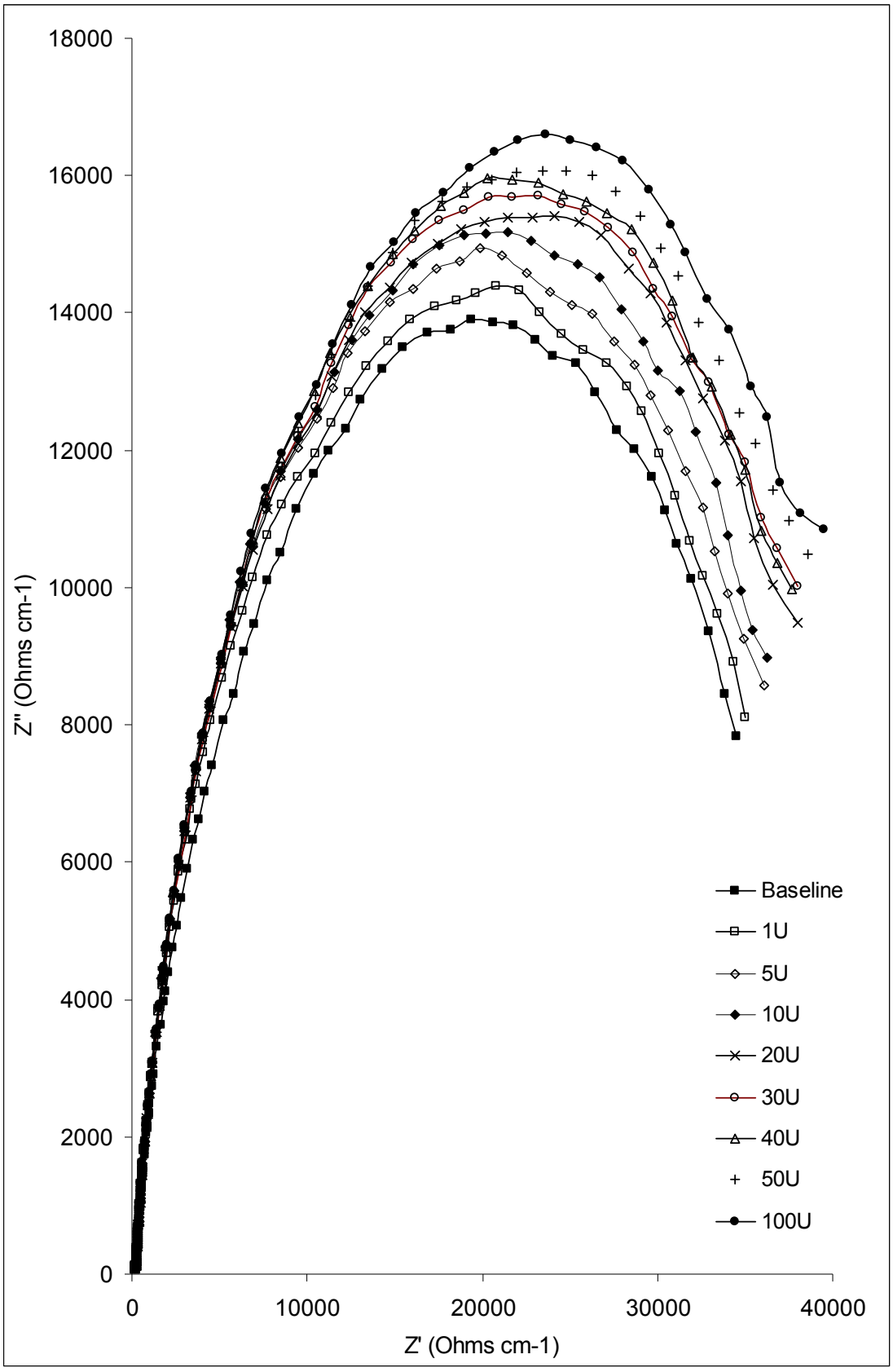

Fig 9.4 Nyquist plot for a generic IgG doped PANI immunosensor following exposure to the full range of CA-125 concentrations in PBS pH 7.4.

Once again, maximum changes from the baseline trace upon exposure to antigen were observed at low frequencies, a fact clearly illustrated in the Bode plot in Fig 9.5.

The real component of the impedance at 1Hz was used to plot a calibration curve of the percentage change of the electron transfer resistance across the $\log_{10}$ of the full range of antigen concentrations (Fig 9.6). The same values on the x and y axis were employed as for the calibration curve plotted for the specific sensors (Fig 9.3). The calibration curve plotted for the specific sensors across the same antigen concentration was also included. Upon comparison of the two calibration curves it is apparent that approximately 20 to 30% of the changes in the electron transfer resistance encountered with the anti-ciprofloxacin modified sensors are, in fact, non-specific. However, there is a much lower response for the non-specific sensors, showing that although there are non-specific interactions, they comprise a minor component of the detected response.

The non-specific response observed could arise from factors such as non-specifically adsorbed matter not being removed via the flushing regime and thus remaining at the sensor surface and / or weakly bound matter, polymer swelling, proton doping and transitional changes of the polyaniline at the neutral test pH, i.e. becoming less conductive.

A correction can be made to acquire the true specific anti-CA-125 immunosensor response by subtracting the non-specific sensor response at each antigen concentration from the specific sensor response (Fig 9.7). In Fig 9.7, there is a steady increase in the real component of the impedance as the concentrations of the antigen to which the sensors are exposed increase. There is a linear correlation between the change in the electron transfer resistance and the $\log_{10}$ of antigen concentrations (R^2=0.9745).

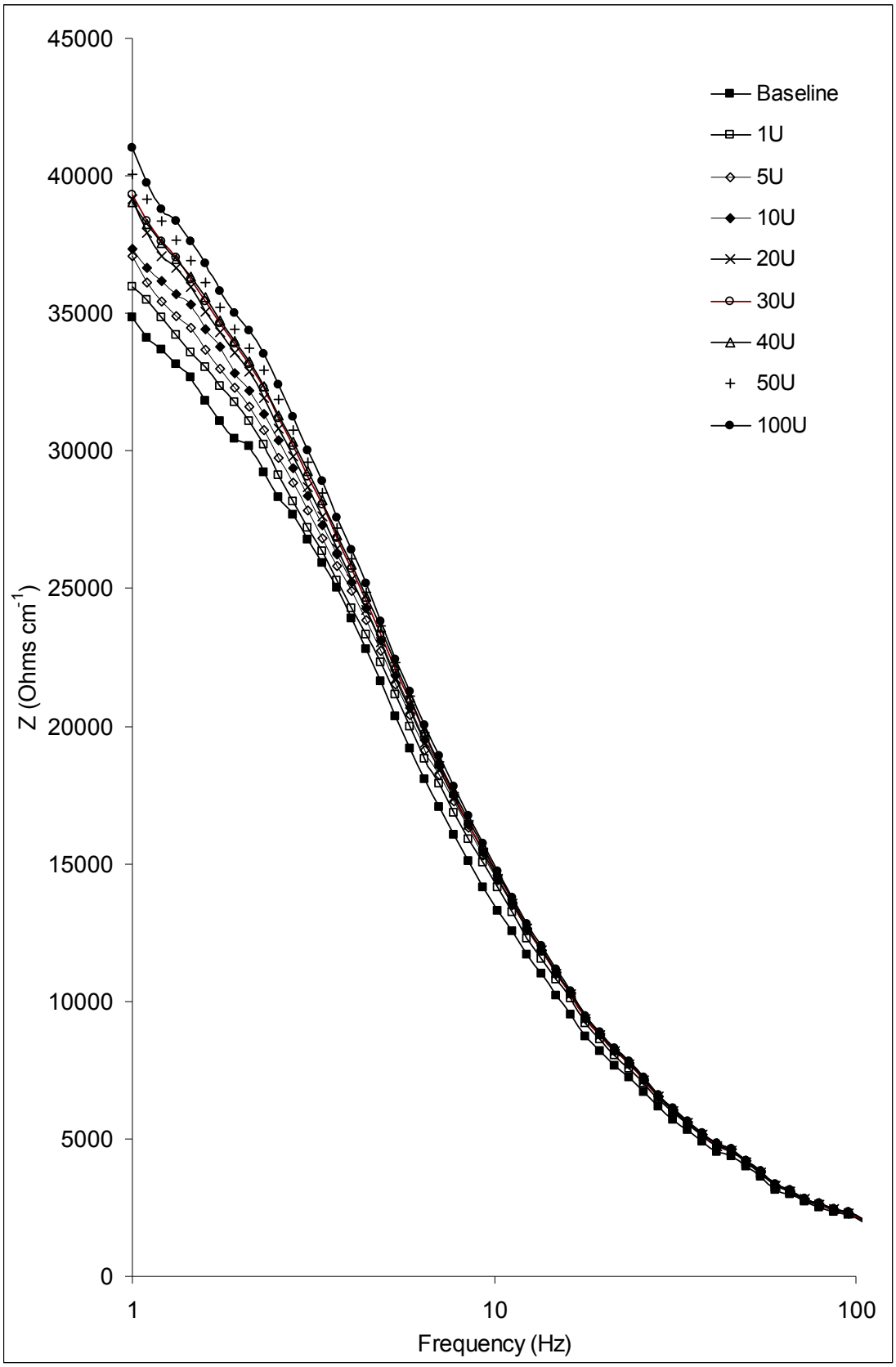

Fig 9.5 Bode plot for a generic IgG doped PANI immunosensor following exposure to the full range of CA-125 concentrations in PBS pH 7.4. For clarity, only frequency values from $\log_{10}$ 1 to 100 Hz are shown.

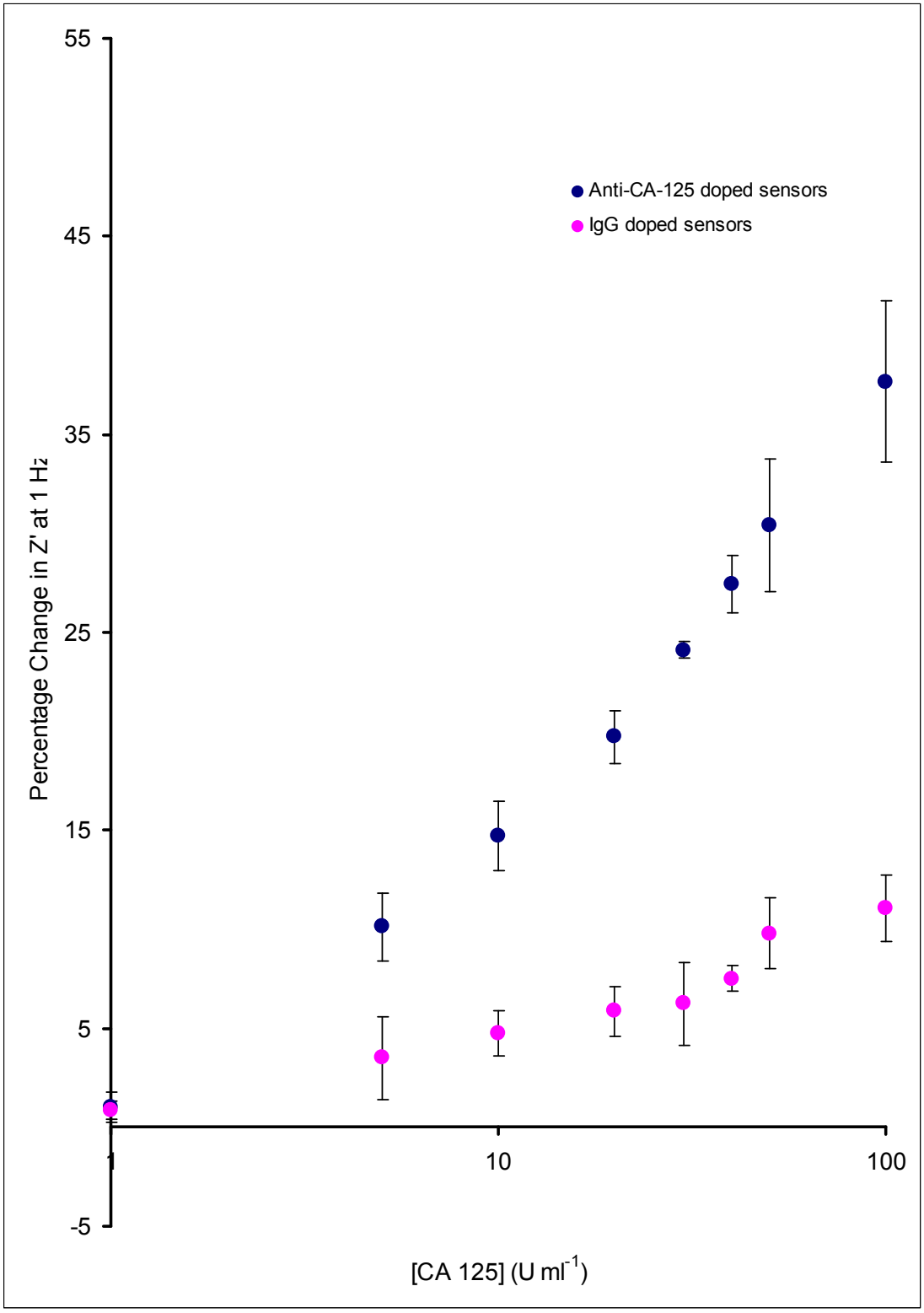

Fig 9.6 Calibration curve of the change in electron transfer resistance from the baseline response for IgG and anti-CA-125 modified electrodes upon exposure to the $\log_{10}$ of the full range of CA-125 concentrations in PBS pH 7.4.

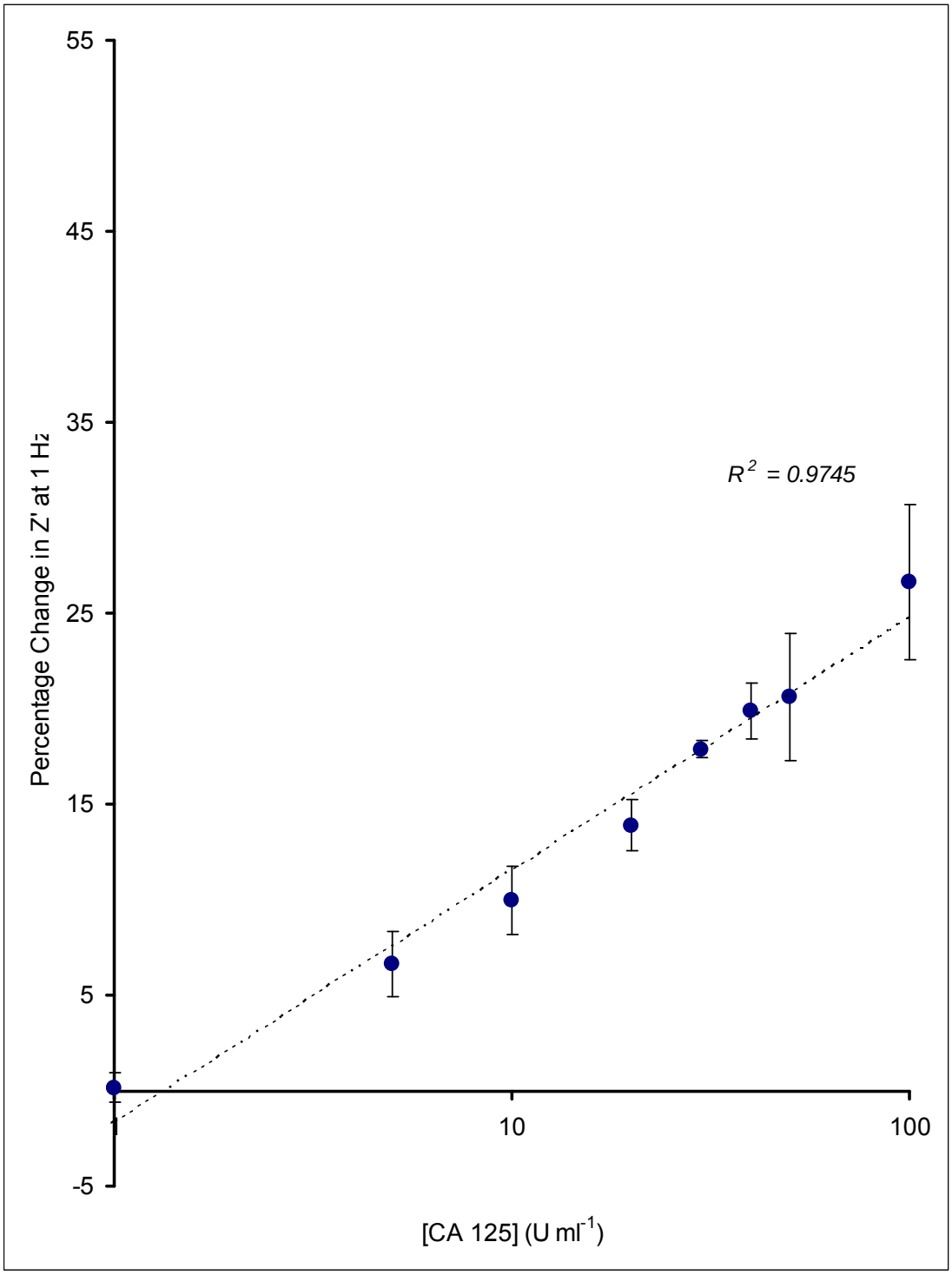

Fig 9.7 Calibration curve of the 'corrected' change in electron transfer resistance from the baseline response for polyaniline modified electrodes across the $\log_{10}$ of the full range of CA-125 concentrations in PBS pH 7.4.

9.3 Aniline Boronic Acid

Following the fabrication of immunosensors for the detection of ciprofloxacin, Myelin Basic Protein and CA-125 via the conventional protocol described in Section 3.5.3.1, an alternative approach which involved a substituted aniline monomer was investigated. The substituant of aniline used was boronic acid (Fig 9.8).

Boronic acid is an alkyl or aryl substituted boric acid containing a carbon to boron chemical bond that belongs to the larger class of organoboranes. Boronic acids act as Lewis acids. Their unique feature is that they are capable of forming reversible covalent complexes with sugars, amino acids, hydroxamic acids (Hall, 2005).

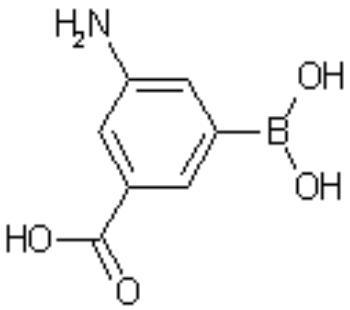

Fig 9.8 Aniline Boronic Acid

Aniline boronic acid has already been used extensively in sensing applications, especially for the non-enzymatic detection of saccharides, such as glucose via the direct binding of the boronic acid moiety with the diol group of saccharides. Shoji and Freund described such a sensor for the potentiometric detection of saccharides based on the pK(a) changes of poly(aniline boronic acid) (PABA) (Shoji and Freund, 2002). Huh *et al*. recently described a sensor for the detection of saccharides on the basis of UV-vis and IR spectrophotometry, and four-point probe conductivity measurements (Huh *et al*., 2007).

Another widely reported application of aniline boronic acid sensors has been the detection of dopamine. In 2003, Fabre and Taillebois described a conductimetric sensor for dopamine based on PABA (Fabre and Taillebois, 2003), while in 2007, Ali *et al*. described a non-oxidative sensor based on a self-doped polyaniline carbon

nanotube composite for sensitive and selective detection of the neurotransmitter dopamine (Ali *et al*. (a), 2007). The latter group in the same year showed an interference of ascorbic acid with dopamine detection using a similar sensor (Ali *et al*. (b), 2007). Finally, a novel layer-by-layer approach for the fabrication of conducting polymer/RNA multilayer films, where RNA was used both as a polyelectrolyte for multilayer formation as well as dopant for PABA, for controlled release of RNA under physiological conditions was described in 2006 (Rechsiedler *et al*., 2006).

In the case of the PABA sensors fabricated for this research project, their significant advantage was that they substantially reduced the required fabrication time. The direct complexion of PABA with the anti-CA-125 antibodies allowed for the omission of the biotin/neutravidin steps of the protocol described in section 3.5.3.1

9.3.1 PABA electrodeposition

Poly (aniline boronic acid) was deposited on the surface of the screen printed electrodes according to Section 3.5.3.2. The potential was cycled between -300 and +1000 mV vs. Ag/AgCl at $50mVs^{-1}$ for 20 progressive cycles followed by one linear sweep between -300 and +1000mV vs. Ag/AgCl at $50mVs^{-1}$(Fig 9.9).

In Fig 9.9, the first scan exhibits a discernable and irreversible anodic peak due to monomer oxidation at 1000mV (vs. Ag/AgCl). As potential cycling continues, this anodic peak increases in the first couple of potential sweeps and then steadily decreases. It is the result of the oxidation of aniline boronic acid to the corresponding radical cation and to the formation of dications.

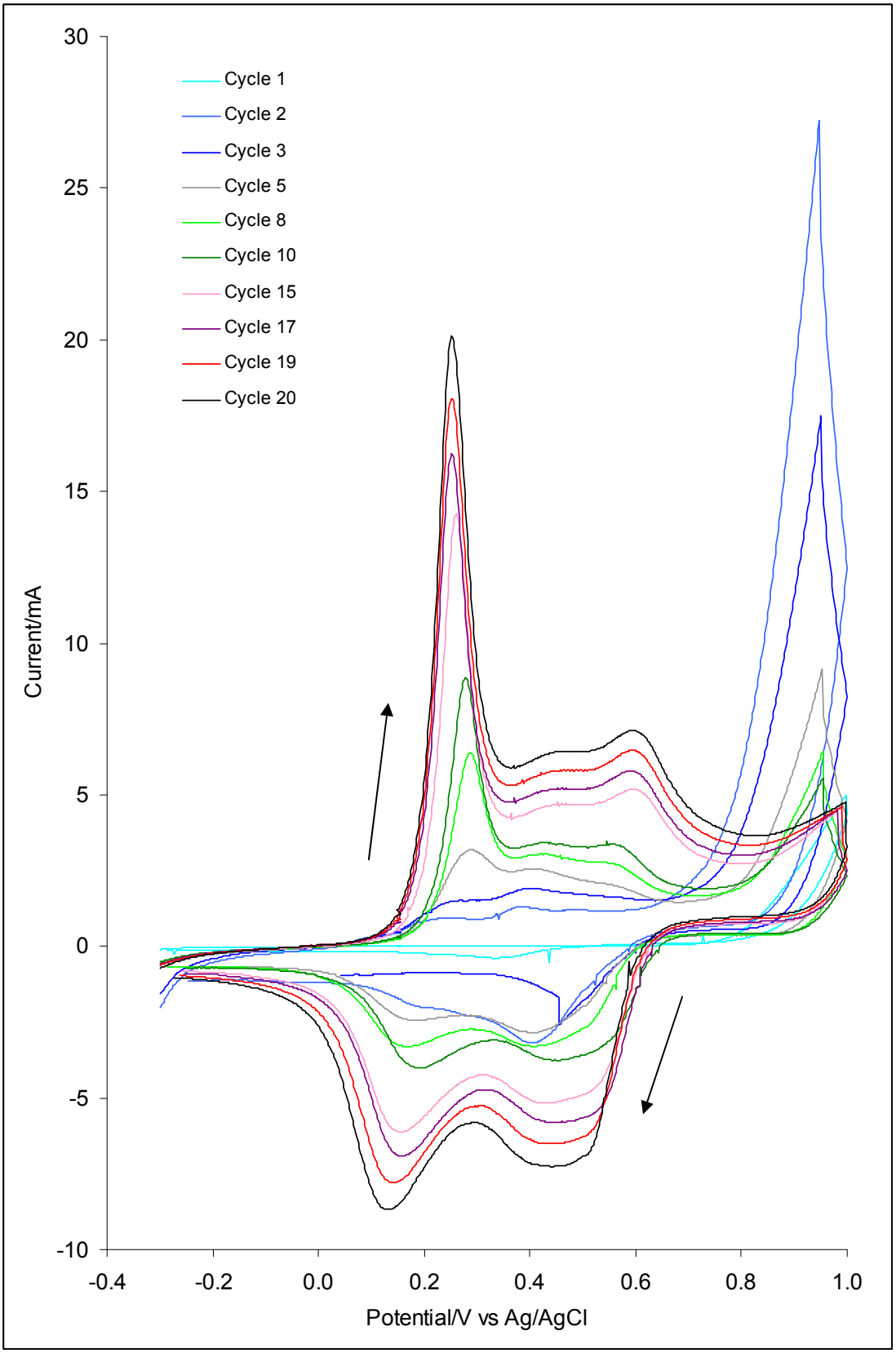

Fig 9.9 Cyclic voltammograms of the electropolymerization of aniline boronic acid at a screen printed carbon electrode (Cycles 1, 2, 3, 5, 8, 10, 15, 17, 19 and 20 are shown).

[Supporting electrolyte: pH 1.0 buffer, Scan rate: 50 mVs^{-1}]

The absence of a cathodic peak indicates a fast consumption of the electrogenerated monocation and dication radicals by subsequent chemical reactions that result in the elongation of the forming PABA film on the electrode.

In the second scan, one redox system at +600mV (anodic)/ +420mV (cathodic) (vs. Ag/AgCl) appears. The currents on the anodic and cathodic waves of this system increase steadily with each progressive potential cycle, reflecting the growth of the conductive PANI film.

After the fifth potential cycle, a second redox system appears at +300mV (anodic)/ +160mV (cathodic) (vs. Ag/AgCl). The appearance of the two redox systems is associated with the elongation of the forming polymer film and its subsequent doping.

By comparing the cyclic voltammograms obtained for PABA electrodeposition on the electrode surface to the relevant voltammograms for polyaniline synthesis (Fig 6.10), it can be seen that although the current increases with each progressive potential cycle in both cases, there is only one redox system in polyamine deposition. PABA synthesis on the other hand is associated with two redox systems that occur at different potential values than the one observed in polyaniline deposition.

9.3.2 Electrochemical impedance spectroscopy (EIS) studies on CA-125 PABA immunosensors: Specific sensors

Following immobilisation of anti-CA-125, according to section 3.5.3.2, impedance analyses were performed from 1Hz to 10,000Hz (+/- 5mV amplitude perturbation) in a pH 7.4 phosphate buffer, i.e. containing no antigen, as a baseline trace. This buffer solution did, however, contain a 50:50 mixture of $[KFe(CN)_6]^{3-/4-}$, at a concentration of 10mM as redox mediator so as to perform faradaic impedance spectroscopy. The potential of the electrochemical cell was offset to the formal potential of the redox probe (+0.4 V vs. Ag/AgCl). Subsequently, anti-CA-125 doped sensors were exposed to pre-prepared analyte concentrations of 1U, 5U, 10U, 20U, 30U, 40U, 50U and 100U per ml of PBS pH 7.4 buffer. The experimental protocol described in section 3.5.5 was followed for the electrochemical impedimetric interrogation of CA-125

immunosensors. The same sensor was used for all analytical concentrations and changes encountered were compared to the initial baseline trace (0U ml^{-1} CA-125).

Results are presented in the form of Nyquist plots depicting the real (Z') and imaginary (Z'') components of impedance and their variation throughout the recording of the AC impedance spectra (Fig 9.10). For the baseline trace, the Z' component is seen to increase with decreasing frequency for the entire range of applied frequencies, whereas the Z'' component is seen to increase up to the characteristic frequency ω of each trace (the frequency at which the Z'' value is at its maximum) before decreasing to the lower applied frequencies (~1Hz). In general, the impedance spectrum is indicative of a surface-modified electrode system where the electron transfer is slow and the impedance is controlled by the interfacial electron transfer (Katz and Willner, 2003).

Once again, maximum changes from the baseline trace upon exposure to antigen were observed at low frequencies, a fact clearly illustrated in the Bode plot in Fig 9.11.

Exposure of the IgG modified sensors to increasing CA-125 concentrations resulted in the increase of impedance of the sensors due to the formation of antibody-antigen complexes on the sensor surface. The major component of the changes incurred in the total impedance of the system was once again the real one or the electron transfer resistance. The latter can be seen to increase with increasing antigen concentrations in Fig 9.10. The capacitance of the sensors also increases across the range of antigen concentrations however changes in recorded in the imaginary component are less pronounced than the changes recorded in the real component.

For the aforementioned reasons and as discussed in section 9.2.1, the real component of the impedance at 1Hz was used to plot a calibration curve of the percentage change of the electron transfer resistance across the $\log_{10}$ of the full range of antigen concentrations (Fig 9.12). As can be seen, there is a steady increase in impedance as antigen concentration increases up to a concentration of 100 Uml^{-1}. No saturation of the sensors is observed even following exposure to 100Uml^{-1}. There is a linear correlation of the electron transfer resistance change with the $\log_{10}$ of antigen concentration across the clinically significant range (R^2=0.9455).

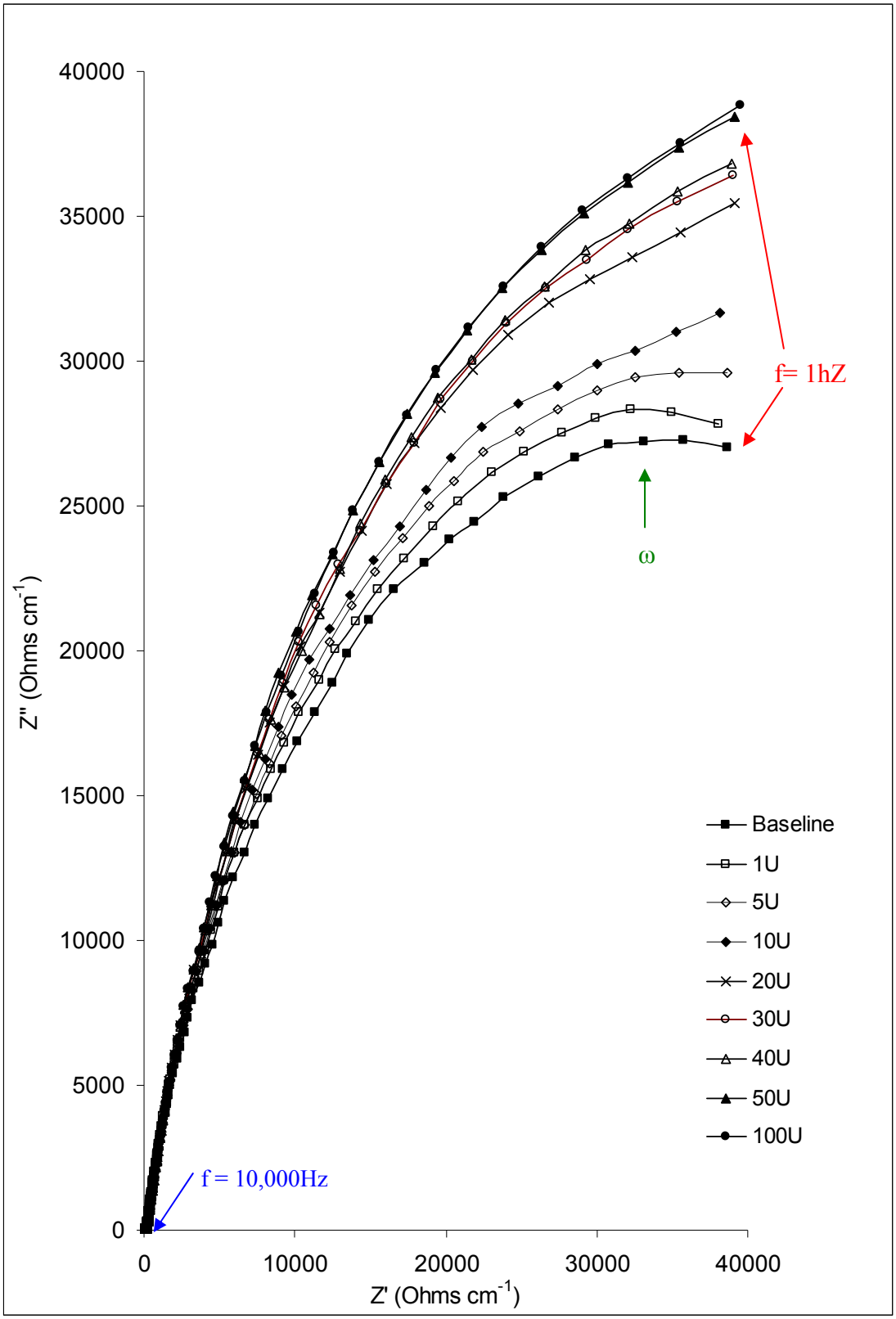

Fig 9.10 Nyquist plot for anti-CA-125 doped PABA immunosensors following exposure to the full range of CA-125 concentrations in PBS pH 7.4.

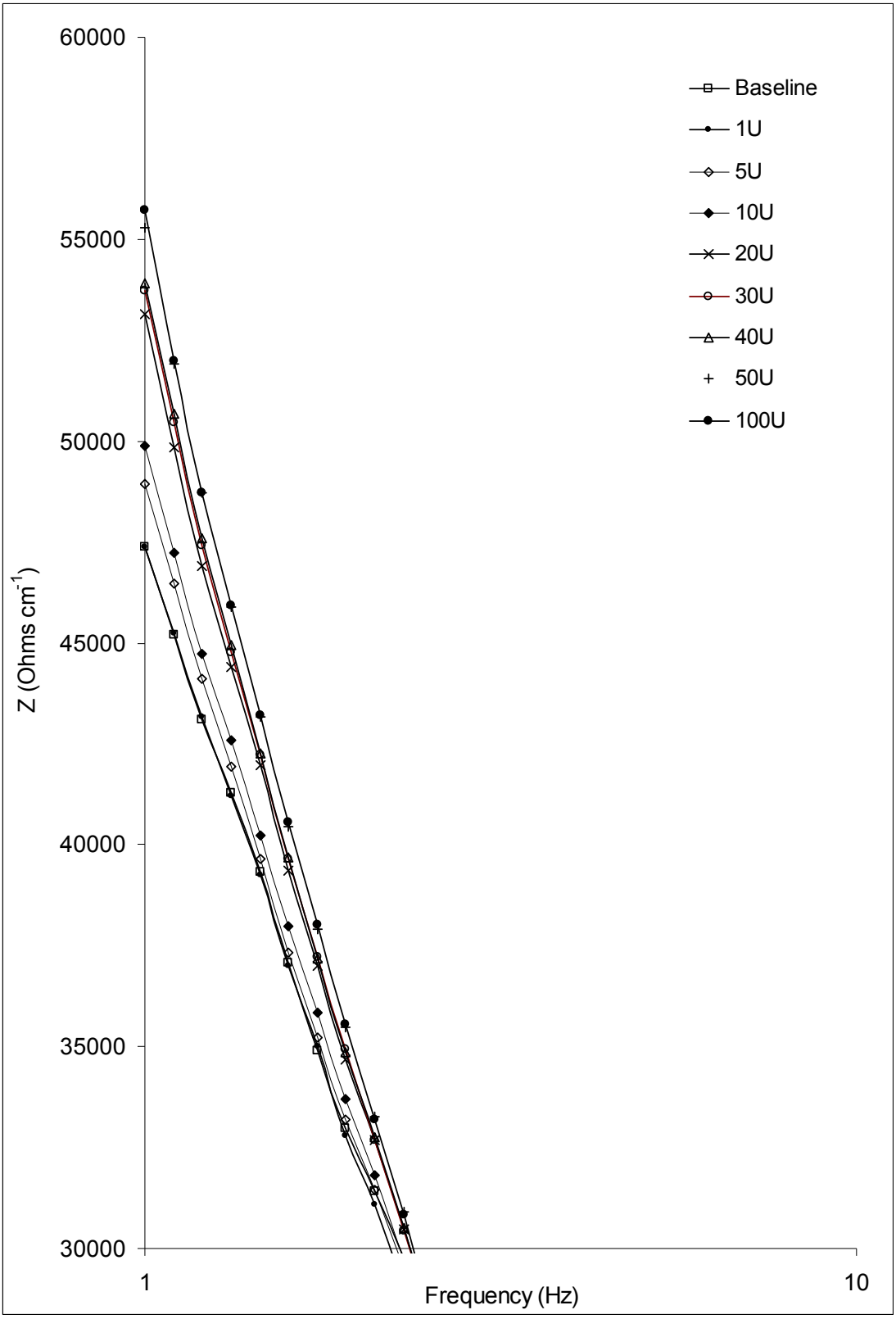

Fig 9.11 Bode plot for anti-CA-125 doped PABA immunosensors following exposure to the full range of CA-125 concentrations in PBS pH 7.4. For clarity, only Z values greater than 30kΩ and frequency values from $\log_{10}$ 1 to 10 Hz are shown.

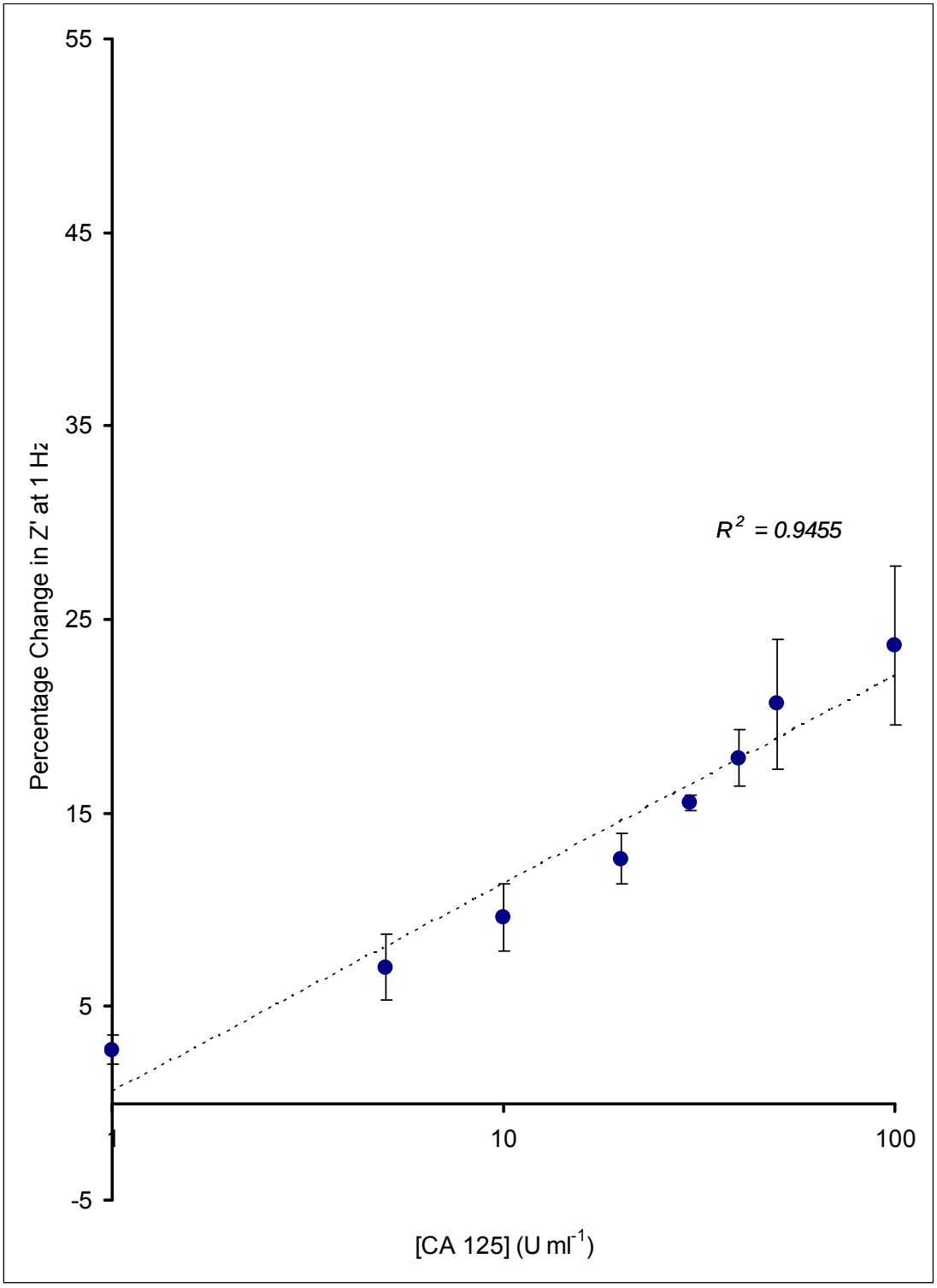

Fig 9.12 Calibration curve of the change in electron transfer resistance from the baseline response for anti-CA-125 modified PABA immunosensors upon exposure to the $\log_{10}$ of the full range of CA-125 concentrations in PBS pH 7.4.

9.3.3 Electrochemical impedance spectroscopy (EIS) studies on CA-125 PABA immunosensors: Non-Specific sensors

In order to evaluate the specificity of the observed response for the anti-CA-125 modified PABA sensors, control experiments were performed to determine non-specific events that may be occurring. A generic IgG antibody was immobilized following the same fabrication protocol as for the specific anti-CA-125 doped sensors. In every other sense, the matched sensors were identical and were interrogated simultaneously in PBS pH 7.4 following exposure to antigen solutions.

The results obtained were presented as Nyquist plots of the imaginary versus the real component of impedance (Fig 9.13). For the plot of Fig 9.13, the Z' component is seen to increase with decreasing frequency over the whole range of frequencies from 10,000Hz to 1Hz. The Z'' component, however, increases from 10,000Hz up to the characteristic frequency, ω, (the frequency at which the Z'' value is at its maximum) before decreasing to the final applied frequency (1Hz). The latter can not be clearly observed for spectral traces recorded following exposure to large concentrations of antigen due to the frequency range used to interrogate the sensors.

Once again, maximum changes from the baseline trace upon exposure to antigen were observed at low frequencies, a fact clearly illustrated in the Bode plot in Fig 9.14. Exposure of the IgG modified sensors to increasing CA-125 concentrations resulted in the increase of impedance of the sensors due to the formation of antibody-antigen complexes on the sensor surface. The major component of the changes incurred in the total impedance of the system was once again the real one or the electron transfer resistance. The latter can be seen to increase with increasing antigen concentrations in Fig 9.13. The capacitance of the sensors also increases across the range of antigen concentrations however changes in recorded in the imaginary component are less pronounced than the changes recorded in the real component.

The real component of the impedance at 1Hz was used to plot a calibration curve of the percentage change of the electron transfer resistance across the $\log_{10}$ of a range of antigen concentrations (Fig 9.15). The calibration curve plotted for the specific sensors across the same antigen concentration was also included.

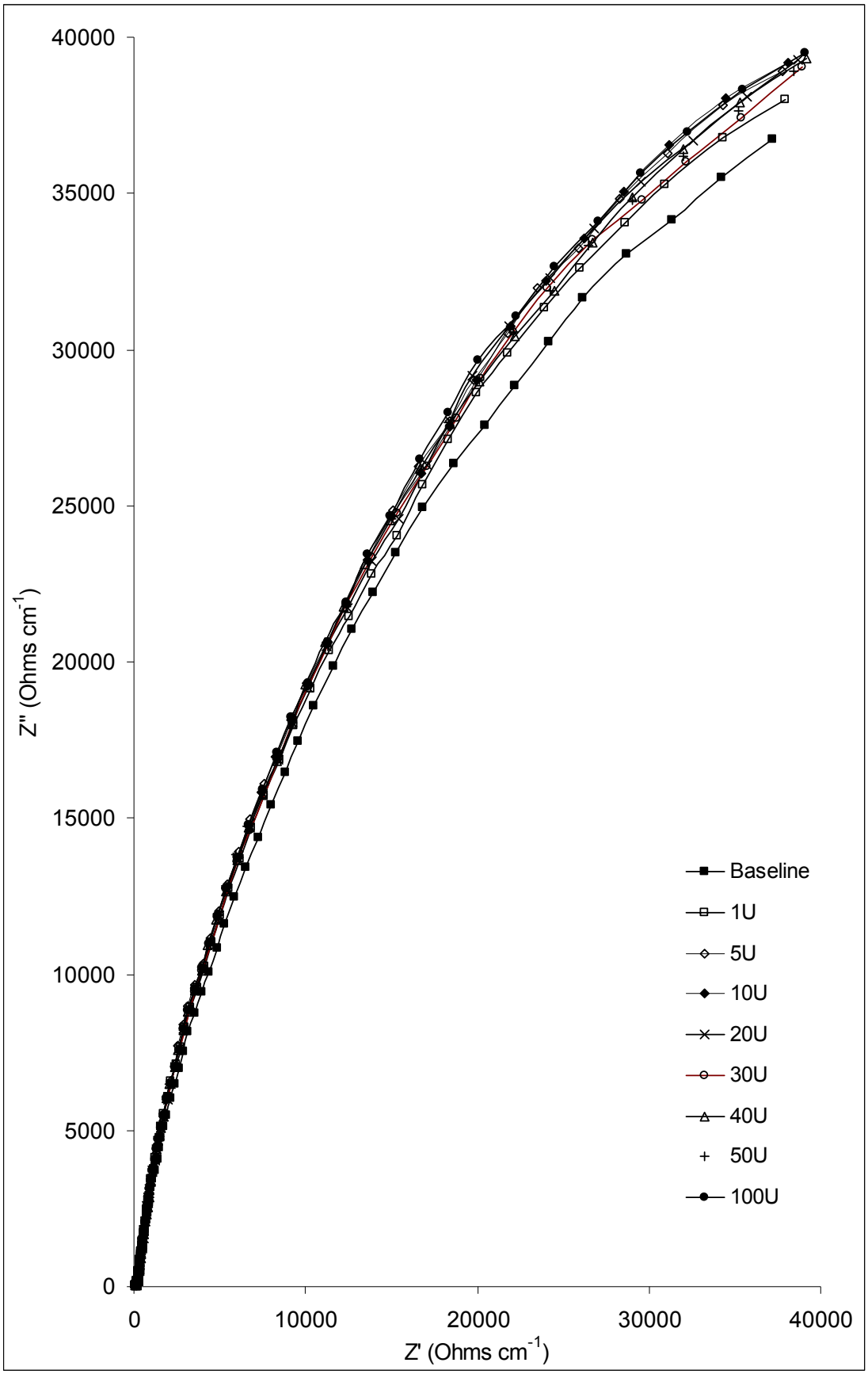

Fig 9.13 Nyquist plot for generic IgG doped PABA immunosensors following exposure to the full range of CA-125 concentrations in PBS pH 7.4.

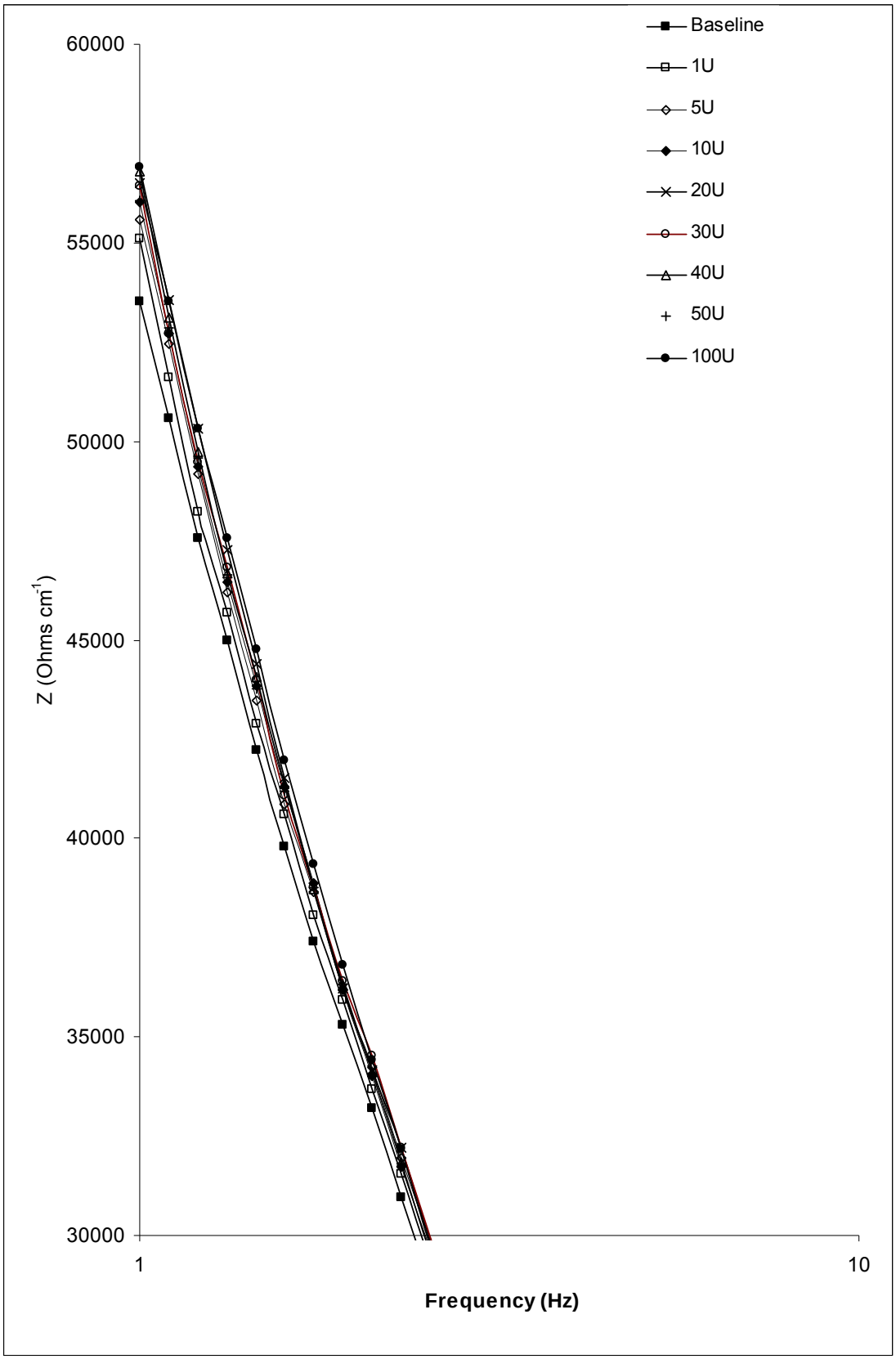

Fig 9.14 Bode plot for generic IgG doped PABA immunosensors following exposure to the full range of CA-125 concentrations in PBS pH 7.4. For clarity, only Z values greater than 30kΩ and frequency values from $\log_{10}$ 1 to 10 Hz are shown.

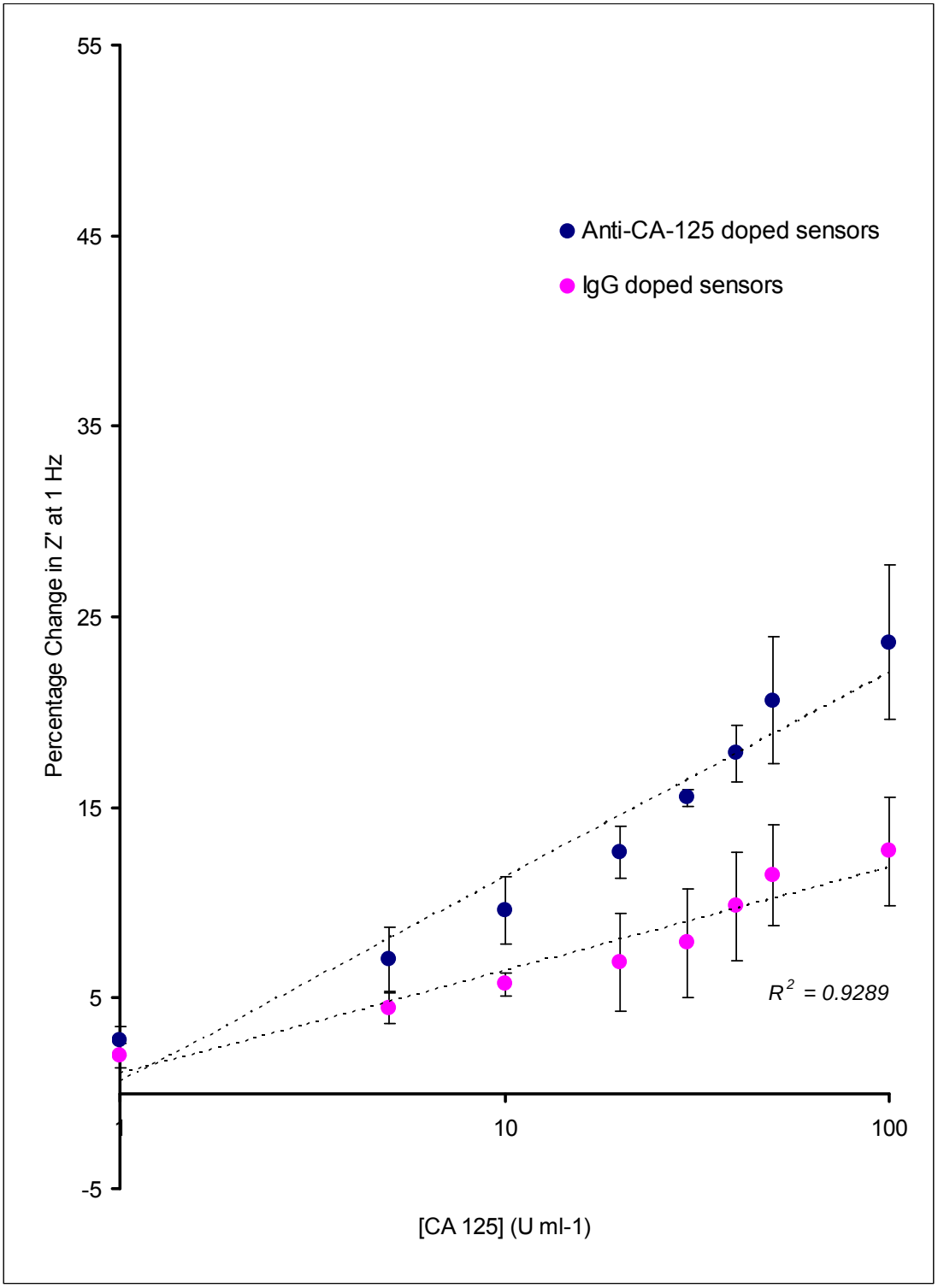

Fig 9.15 Calibration curve of the change in electron transfer resistance from the baseline response for IgG and anti-CA-125 modified PABA immunosensors upon exposure to the $\log_{10}$ of the full range of CA-125 concentrations in PBS pH 7.4.

For the calibration curve plotted for the generic IgG loaded sensors in Fig 9.15 there is a near linear correlation of the impedance change with the $\log_{10}$ of concentration (R^2=0.9289).

Upon comparison of the two calibration curves in Fig 9.15 it is apparent that approximately 50% of the changes in the electron transfer resistance encountered with the anti-CA-125 modified sensors are, in fact, non-specific.

9.3.4 Electrochemical impedance spectroscopy (EIS) studies on CA-125 PABA immunosensors: Corrected Calibration Profile

To obtain a calibration profile, in terms of 'corrected' percentage impedance change for an anti-CA-125 immunosensor, accounting for any non-specific responses, the changes obtained in Fig 9.15 (non-specific) were subtracted from those obtained in Fig 9.12 (specific) over the entire antigen concentration range. Fig 9.16 shows the subtracted responses. As can be seen, there is a steady increase in impedance as antigen concentration increases up to a concentration of 100 Uml^{-1}. No saturation of the sensors is observed even following exposure to 100Uml^{-1}, indicated by the absence of a plateau in the calibration curve. This suggests that antigen binding sites on the electrode surface are not fully occupied. Furthermore, there is a near linear correlation of the electron transfer resistance change with the $\log_{10}$ of antigen concentration across the clinically significant range (R^2=0.9475). A significant variation between the sensors can be observed as indicated by the large standard deviations for each antigen concentration in Fig 9.16.

Fig 9.20 shows the corrected calibration curve for the PABA modified sensors overlaid over the corrected profile for the PANI modified sensors across the same antigen concentration range. As can be seen, the recorded changes in the electron transfer resistance for the PABA modified sensors are less pronounced than the changes reported previously for the PANI modified sensors.

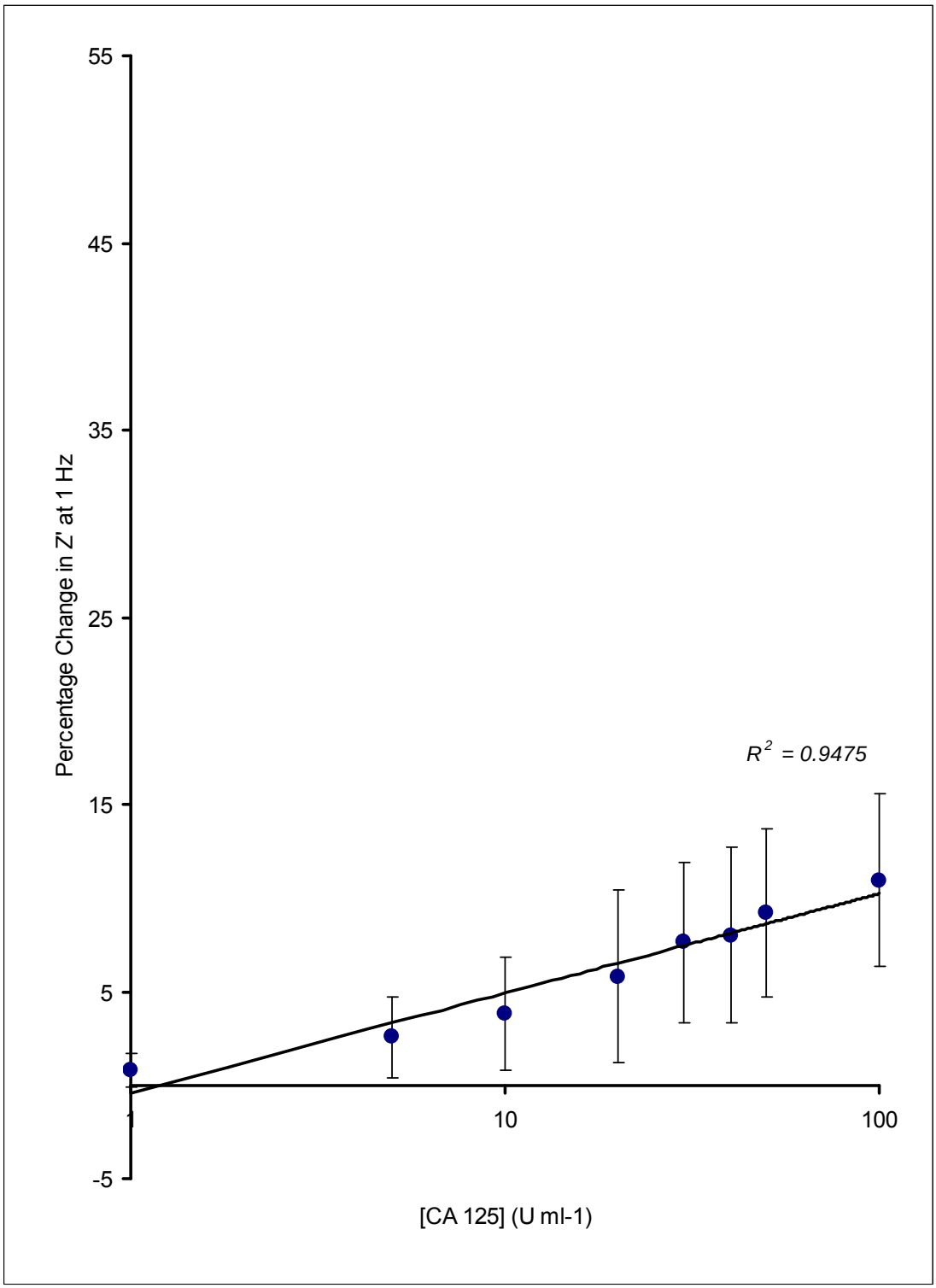

Fig 9.16 Calibration curve for the 'corrected' change in electron transfer resistance from the baseline response for PABA modified immunosensors across the $\log_{10}$ of the full range of CA-125 concentrations.

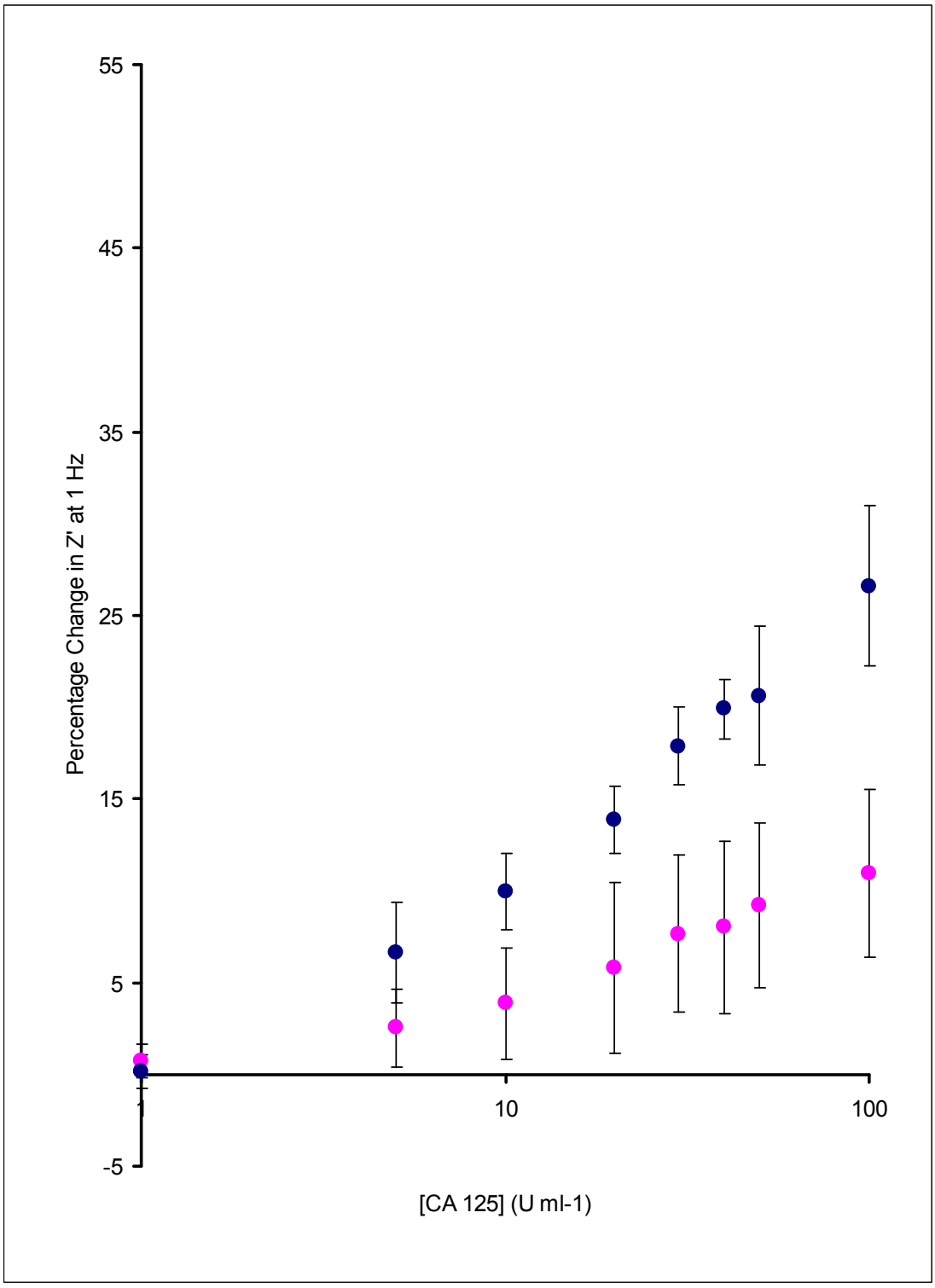

Fig 9.17 Calibration curve for the 'corrected' change in electron transfer resistance from the baseline response for PABA modified immunosensors (pink) and PANI modified immunosensors (blue) across the $\log_{10}$ of the full range of CA-125 concentrations.

9.4 Conclusions

We have demonstrated the construction of an immunosensor for the cancer biomarker CA-125 using a combination of screen-printed carbon electrodes coated with conducting polyaniline and immobilised antibodies against CA-125 via the neutravidin/biotin affinity interactions. Interrogation of these sensors by AC impedance in a phosphate buffer (PBS pH 7.4) demonstrated the detection of CA-125 across the clinically significant range.

The higher the CA-125 concentration in the test solution the greater the number of stable antibody-antigen complexes formed at the sensor surface. Complex formation was shown to hinder electron transfer of the redox couple within the test solution at the formal redox potential and hence the electron transfer resistance increased with increasing antigen concentrations. Saturation of the immunosensors was not observed as for the ciprofloxacin and Myelin Basic Protein sensors described in the previous two chapters.

Non-specific interactions were accounted for by the simultaneous interrogation of sensors loaded with a generic IgG in PBS pH 7.4. It was found that 30% of the response obtained from the specific sensors was due to non-specific binding events. A calibration curve of the corrected changes in the electron transfer resistance was plotted across the range of antigen concentrations. Linear correlation of the impedance change with the log of concentration (R^2=0.9745) was observed.

A novel immunosensor fabrication protocol was then developed. Aniline boronic acid was electrodeposited on the surface of the screen printed carbon electrodes. The rationale behind its use is that it has been shown to bind amino acids, however to date there have been no published papers describing immunosensor fabrication on poly (aniline boronic acid) modified electrodes. Interrogation of the electrodes by AC impedance demonstrated the detection of CA-125 across the same range as for the polyaniline modified sensors.

Simultaneous interrogation of sensors loaded with a generic IgG was performed to determine non-specific interactions between CA-125 and the immobilised antibodies. For both the specific and non-specific sensors, increasing antigen concentrations resulted in an increase of the impedance.

Changes in the electron transfer resistance for both the specific and non-specific sensors were plotted against the $\log_{10}$ of antigen concentrations. The calibration curves recorded were used to obtain a corrected calibration profile for antigen recognition by the PABA immunosensors. A near linear correlation of the changes in the real component of the impedance $\log_{10}$ of antigen concentrations (R^2=0.9475) was observed between.

By comparing the calibration profiles of the polyaniline and poly (aniline boronic acid) modified sensors it can be concluded that for the latter there is a much greater variability in between sensors. This is probably due to the sensors being less stable than the polyaniline modified sensors. In addition, the changes recorded upon antigen exposure were much more pronounced for the polyaniline modified sensors, resulting in a steeper, well-defined calibration curve. Therefore, although poly (aniline boronic acid) does offer a promising alternative approach to immunosensor fabrication, more research needs to be carried out into its use or sensing.

Chapter 10

General Conclusions

This thesis has described investigations towards the fabrication of labeless and reversible impedimetric immunosensors for the detection of biomarkers for biomedical applications. Focus has been drawn towards the detection of biomedical markers for the fluoroquinolone antibiotic, ciprofloxacin, the multiple sclerosis and stroke biomarker, Myelin Basic Protein and the cancer biomarker, CA-125.

The intermediary aims of this research programme were to optimise each of the stages involved in the fabrication of the immunosensor platforms. These included the characterisation of the electrochemical behaviour of various substrate electrodes, the optimisation of conditions for the deposition of conductive films on the electrode surfaces and the site-specific immobilisation of antibodies against the antigens of interest to this research project. Further to these, a protocol for the sonochemical fabrication of microelectrode arrays was employed.

Chapter 4 details initial investigations on the reproducibility of the various electrodes available at the onset of this research project. As a prerequisite to the production of immunosensors assemblies, the electrodes should exhibit highly reproducible electrochemical behaviour. This was tested in solutions of ferrocene carboxylic acid in PBS pH 7.4 prior to and following electrodeposition of an insulating polymer film.

The electropolymerisation of *o*-phenylenediamine onto gold sputter-coated ground glass slide electrodes was initially characterised in neutral conditions to show a two electron transfer mechanism for the formation of a non-conducting, ultrathin film. This was then applied to screen printed gold on silicon substrate electrodes and screen printed carbon electrodes in a manner analogous to the one employed for the gold sputtered glass slides.

The cyclic voltammograms obtained for the gold sputtered glass slides revealed inconsistencies in their fabrication procedure leading in non-homogeneous surfaces, which in turn resulted in the incomplete passivation of the electrodes following polymer deposition as well as non ideal electrode kinetics even on bare electrodes. The screen printed gold electrodes, on the other hand, proved much more reliable since their electrochemical behaviour did not depart significantly from the behaviour of an ideal system under the same conditions, as predicted by the Nernst equation. However, these electrodes were employed in subsequent experimental investigations

since it was found that there is considerable irreproducibility in between them when cyclic voltammograms from a large number of these electrodes were compared.

Screen printed carbon ink electrodes were used for all consequent experimental set ups, since they provided reproducible results in the presence of a redox couple when voltammetrically interrogated.

Cyclic voltammograms relating to the electrodeposition of the films revealed the electropolymerisation as being a self-regulating and thus highly reproducible process, since diminishing peak currents were observed as the electrode became progressively insulated by the poly (*o*-phenylenediamine) film.

Initial attempts to produce microelectrode array assemblies via the ultrasonic ablation of poly (*o*-phenylenediamine) modified screen printed gold electrodes (P3) in a bench-top ultrasonic bath were described in Chapter 5. It was shown that near microelectrode behaviour can be achieved after 30 seconds of exposure to ultrasound in the ultrasonic bath.

An industrial-scale ultrasonic tank was then procured to scale up the fabrication of microelectrode arrays. The sensors responses were found to be dependant upon their position within the tank, as well as the duration and the power of the applied ultrasound. Thus the sonication parameters were optimised. It was found that the optimum duration and power of ultrasound to which the sensors were subjected, greatly depended on their positioning and no single sonication protocol is sufficient.

The sonication protocol was further enhanced via the use of a custom built mechanical system which rotated the electrodes attached to the mounting device in a radius that was sufficient to expose each individual electrode to approximately the same intensity of cavitation, irrespectively of their positioning in the sonication tank. The introduction of the rotating device along with the use of a baffle to diffract the applied ultrasound and of a sensor mounting device to avoid variations in electrode responses caused by exposure to regions of acoustic turbulence and streaming, have permitted the fabrication of microelectrode arrays which show sigmoidal behaviour and offer good microelectrode array performance.

However, irreproducibility issues arose once again. It was found that the electrochemical behaviour of the fabricated microelectrode arrays in the presence of a redox couple differed between different or even the same batches. This is the reason the sonochemically fabricated microelectrodes were not used in the following investigations into the construction of immunosensors.

Chapter 6 focused on the deposition and optimisation of conductive polyaniline films on the surface of the screen-printed carbon electrodes. The formation of a conductive polyaniline film on the electrode surface was the first step towards the fabrication of the immunosensor platforms.

The presented results have allowed an enhanced understanding of the oxidation reactions of aniline occurring at the electrode/solution interface resulting in the coating of the latter with polyaniline. It has been shown that the optimum conductive polyaniline films can be obtained by employing a very acidic buffer of pH 1.0, whereas the use of more basic buffers, such as the pH 2.7 buffer or the pH 5.0 acetate buffer resulted in the electrodeposition of insulating or only partially conductive polyaniline films respectively. Validation of polyaniline deposition on the electrode surface was achieved via the use of a quartz crystal microbalance.

The bio recognition entity (antibody receptor) was subsequently immobilised at the modified electrode transducer, taking advantage of the neutravidin/biotin affinity technologies whereby the orientation of the immobilised antibody can be controlled to a great extent, to facilitate antibody-antigen interactions. In this manner, immunosensors for the detection of ciprofloxacin (Chapter 7), Myelin Basic Protein (Chapter 8) and CA-125 (Chapter 9) were constructed. All of them were impedimetrically interrogated using the same protocol, described in the Materials and Methods section.

In summary, the anti-ciprofloxacin immunosensor gave rise to a linear-type response from 1 to 100 ng ml^{-1} ciprofloxacin (R^2=0.95) when interrogated in a PBS pH 7.4 buffer. At concentrations of analyte above 100 ng ml^{-1}, the response began to plateau as the sensor saturated. The formation of antibody-antigen complexes was shown to enhance electron transfer of the redox couple within the test solution at the formal

redox potential and hence the electron transfer resistance extracted from the obtained spectra decreased with increasing antigen concentrations.

To obtain this corrected calibration profile the response obtained for non-specific, IgG loaded sensor was subtracted from the specific sensor response at each concentration. It was found that 16% of the response obtained from the specific sensors was due to non-specific binding events.

Identical specific and non-specific immunosensors were then simultaneously interrogated in milk using the same protocol. Milk was used as an example of a 'real' sample where ciprofloxacin concentrations need to be determined. An increase in electron transfer resistance was observed which was due to the formation of chelation complexes between calcium ions in milk and ciprofloxacin.

Changes in the electron transfer resistance due to non-specific interactions were once again determined with the use of generic IgG loaded immunosensors that were exposed to the same concentrations of antigen in milk as the specific sensors. However, specific binding of molecules found in milk with the immobilised IgG over sufficient exposure time gave an erroneous calibration profile. For this reason, non-specific sensors were prepared loaded with anti-PSA whose complementary antigen is not found in milk. The changes in electron transfer resistance recorded in this case constituted only a minor component of the total changes in response recorded with the specific sensors in milk.

A calibration curve of the corrected changes in the electron transfer resistance was plotted across the range of antigen concentrations. Linear correlation of the impedance change with the log of concentration (R^2=0.96) was observed between 1-100 ng ml^{-1} ciprofloxacin. Furthermore, the two corrected calibration profiles for the ciprofloxacin immunosensors in milk and in PBS pH 7.4 buffer were opposite in nature; adsorption of ciprofloxacin from milk gave an increase in the real component of impedance whereas from PBS a decrease was observed.

The work on the fabrication of immunosensors for the labeless detection of ciprofloxacin in PBS pH 7.4 has been published in Analytical Letters (Garifallou *et*

al, 2007). Its follow-up article on the work on the detection of ciprofloxacin in milk has been submitted for publication in Analytical Chemistry.

For the Myelin Basic Protein (MBP) immunosensors, impedimetric interrogation in a solution of PBS pH 7.4 gave rise to linear response from 1 to 100 ng ml^{-1} MBP, above which saturation was reached indicated by a plateau on the corrected calibration profile. For the linear part of the calibration profile the R^2 was equal to 0.977.

The higher the MBP concentration in the test solution the greater the number of stable antibody-antigen complexes formed at the sensor surface. Complex formation was shown to hinder electron transfer of the redox couple within the test solution at the formal redox potential and hence the electron transfer resistance increased with increasing antigen concentration. Non-specific interactions were accounted for by the simultaneous interrogation of sensors loaded with a generic IgG in PBS pH 7.4. It was found that ~25% of the response obtained from the specific sensors was due to non-specific binding events.

The studies towards the fabrication of an immunosensor for the detection of Myelin Basic Protein have been published in Analytical Chemistry (Tsekenis *et al.*, 2008).

Finally, in chapter 9 work on the fabrication of immunosensors for the detection of CA-125 following two different protocols was described. The first protocol took advantage of the neutravidin/biotin affinity technologies and was identical to the protocol followed for the fabrication of both the ciprofloxacin and MBP immunosensors.

The higher the CA-125 concentration in the test solution the greater the number of stable antibody-antigen complexes formed at the sensor surface. Complex formation was shown to hinder electron transfer of the redox couple within the test solution at the formal redox potential and hence the electron transfer resistance increased with increasing antigen concentrations.

Non-specific interactions were accounted for by the simultaneous interrogation of sensors loaded with a generic IgG in PBS pH 7.4. It was found that 30% of the response obtained from the specific sensors was due to non-specific binding events. A

calibration curve of the corrected changes in the electron transfer resistance was plotted across the range of antigen concentrations. Linear correlation of the impedance change with the log of concentration (R^2=0.9745) was observed.

The alternative fabrication protocol took advantage of the capability of aniline boronic acid to bind amino acids. Poly (aniline boronic acid) (PABA) immunosensors for the detection of CA-125 were thus fabricated omitting the neutravidin/biotin fabrication steps and thus cutting down the time required to produce the immunosensors. Interrogation of the electrodes by AC impedance demonstrated the detection of CA-125 across the same range as for the polyaniline modified sensors.

Simultaneous interrogation of sensors loaded with a generic IgG was performed to determine non-specific interactions between CA-125 and the immobilised antibodies. For both the specific and non-specific sensors, increasing antigen concentrations resulted in an increase of the impedance.

Changes in the electron transfer resistance for both the specific and non-specific sensors were plotted against the $\log_{10}$ of antigen concentrations. The calibration curves recorded were used to obtain a corrected calibration profile for antigen recognition by the PABA immunosensors. A near linear correlation of the changes in the real component of the impedance $\log_{10}$ of antigen concentrations (R^2=0.9475) was observed between.

Comparison of the results obtained using the two different fabrication protocols revealed that the PABA modified sensors were not as reproducible as the PANI sensors and furthermore, changes in the electron transfer resistance recorded with the latter were significantly more pronounced than the changes in response observed with the PABA modified sensors.

In conclusion, the successful fabrication of three different labeless immunosensors for the detection of ciprofloxacin, Myelin Basic Protein and CA 125 has been demonstrated. In addition, the academic aims of this research, set out in the beginning of this research project have been addressed.

The results presented within this thesis combined with the simplicity and low cost of the immunosensor fabrication protocol used, suggest that these sensors can have a wide spread applicability in the field of biomedical diagnosis as prognostic and diagnostic tools as well as for the monitoring of various diseases following treatment.

Chapter 11

Suggestions for further work

This thesis has described the development of generically applicable, disposable immunosensors via exploitation of the neutravidin/biotin affinity interactions and their subsequent impedimetric analysis. Although this work has gone far in establishing a protocol for the fabrication of these sensors and the site specific immobilisation of antibodies on the electrode surfaces, as with many projects, many more questions have arisen which must be answered to fully demonstrate the potential of these immunosensors. This chapter, therefore, provides a number of suggestions for future research.

Future research relating to immunosensor fabrication will benefit from further enhancement of the screen printing technologies as well ink composition of the electrode substrates. Although, within this research project, we used screen-printed carbon ink electrodes to fabricate the immunosensors, gold or platinum inks could prove to be as or even more successful if irreproducibility issues are overcome.

Most importantly, though, measures towards the enhancement of the fabrication of microelectrode arrays should be taken. Bearing in mind the advantages of the latter, the need to optimise sonication conditions for their mass production becomes apparent. Towards this end, screen-printing technologies can be revisited; however, the considerably more cost-effective approach discussed in Chapter 5 could be optimised instead. From our studies on the sonochemical fabrication of microelectrode arrays, it was recognised that further modifications towards the homogenisation of the applied ultrasound within the ultrasonic tank are necessary. An increase in the number of the transducers for example, could significantly increase the homogeneity of the applied ultrasound. For this reason, a new custom-built sonication tank has been procured that possesses 110 transducers.

Irreproducibility issues concerning later stages of immunosensor fabrication should also be addressed. Although, it has been shown that polyaniline films form a homogeneous and highly reproducible film on the electrode surface with the use of a quartz crystal microbalance, the same level of reproducibility could not be obtained for neutravidin and biotin attachment to the polymer-modified surface.

On top of this, further optimisation of the attachment of biomolecules via affinity approaches should proceed to permit greater antibody loading, control of orientation and increase of the availability of antigen binding sites. The more stable antibody-antigen complexes being formed, the greater will be the potential for enhancing both sensitivity and working concentration response range prior to saturation

As far as the actual recognition of antigens by their complementary antibodies is concerned, work should be directed towards the deeper comprehension of the events that affect the impedance of the sensors. For example, although it has been shown that ciprofloxacin forms chelation complexes with calcium ions in milk and this phenomenon can be recognised by the fabricated anti-ciprofloxacin immunosensors, it is not well understood why this recognition event results in an increase in the system impedance, whereas recognition of non-chelated ciprofloxacin in PBS buffer has the opposite outcome. Most probably, the various stoichemistries of the antibody-antigen complexes dictate whether the impedance of the system will increase or decrease with increasing antigen concentrations, however, this needs to be proven.

Moreover, current experimental interrogation techniques would meet the need for rapid quantification; however, data analysis can be time-consuming. It would be beneficial to have an appropriate written software algorithm to perform the analysis as the impedance spectrum is recorded. Towards this goal, Uniscan, one of the SMEs involved in this research project, has launched a prototype Potentiostat-Galvanostat that is compatible with the screen-printed carbon sensors used throughout this thesis that is capable of performing the user's defined measurement and analysis algorithm as well as storing and displaying the data. Besides this, this prototype device is hand held; hence it could be used for point-of-care applications.

Finally, the spectrum of biomarkers used in immunosensor platforms should also be expanded so as to diagnose many more diseases since their early detection is crucial for their effective treatment. As for the three biomarkers investigated in this thesis, ongoing work with real samples should determine whether the fabricated immunosensors can detect them in complex samples. This is expected to consume considerable time and require a lot of effort as seen in the case of ciprofloxacin immunosensors in milk. For example, significant problems are expected to arise when

the real sample containing an antigen is serum, where albumin is one of the most abundant proteins and has the tendency to bind to all available surfaces thus masking specific responses of less abundant proteins. The fabrication protocol should also be modified in the case of serum samples, since blocking cannot be performed with Bovine Serum Albumin.

References

A.G.N., (1931). The late Baron Shibasaburo Kitashato. *Can. Med. Assoc. J.*, **25(2)**, 206.

a. **Ali S.R., Ma Y., Parajuli R.R., Balogun Y., Lai W.Y., He H., (2007).** A nonoxidative sensor based on a self-doped polyaniline/carbon nanotube composite for sensitive and selective detection of the neurotransmitter dopamine. *Anal. Chem.*, **79(6)**, 2583-2587.

b. **Ali S.R., Ma Y., Parajuli R.R., Balogun Y., He H., (2007).** Interference of ascorbic acid in the sensitive detection of dopamine by a nonoxidative sensing approach. *J. Phys. Chem. B.*, **111(42)**,12275-12281.

Amatore C., Saveant J.M., Tessier D.J. (1983). Charge transfer at partially blocked surfaces: a model for the case of microscopic active and inactive sites. *Electroanal. Chem.*, **147**, 39-51.

Andrieux C.P., Hapiot P., Saveant J.M., (1990). Ultramicroelectrodes for fast electrochemical kinetics. *Electroanalysis*, **2**,183.

Arroyo E.J., Scherer S.S., (2000). On the molecular architecture of myelinated fibers. *Histochem. Cell Biol.,* **113**,1-18.

Bagan P., Berna P., Assouad J., Hupertan V., Le Pimpec Barthes F., Riquet M., (2008). Value of cancer antigen 125 for diagnosis of pleural endometriosis in females with recurrent pneumothorax. *Eur. Respir. J.*, **31**, 140-142.

Bard A.J., Faulkner L.R., (2001). Electrochemical Methods Fundamentals and Applications (2nd ed.). Wiley, New York.

Barker G.C., Jenkin I.L., (1952). Square-wave Polarography, *Analyst*, **77**, 685-696.

Barnett D., Laing D.G., Skopec S., Sadik O.A., Wallace G.G., (1994). Determination of p-cresol (and other phenolics) using a conducting polymer-based electro-immunological sensing system. *Anal. Lett*., **27**, 2417-2429.

Barton A.C., Collyer S.D., Davis F., Gornall D.D., Law K.A., Lawrence E.C.D., Mills D.W., Myler S., Pritchard J.A., Thompson M., Higson S.P.J., (2004). Sonochemically fabricated microelectrode arraysfor biosensors offering widespread applicability. Biosensors and Bioelectronics, **20(2)**, 328-337.

Barton A.C., (2007). PHD thesis, Cranfield University.

Bast R.C., Feeney M., Lazarus H., Nadler L.M., Colvin R.B., Knapp R.C., (1981). Reactivity of a monoclonal antibody with human ovarian carcinoma. *J. Clin. Invest*. **68 (5)**, 1331–1337.

Batt A.L., Bruce I.B., Aga D.S., (2006). Evaluating the vulnerability of surface waters to antibiotic contamination from varying wastewater treatment plant discharges. *Environ. Poll.*, **142**, 295-302.

Baumann N., Pham-Dinh D., (2001). Biology of Oligodendrocyte and Myelin in the Mammalian Central Nervous System. *Physiol Rev*, **81**, 871-927.

Belli S.L., Rechnitz G.A., (1986). Prototype Potentiometric Biosensor Using Intact Chemoreceptor Structures. *Anal. Lett.*, **19**, 403.

Bender S., Sadik O.A., (1998). Direct electrochemical immunosensor for polychlorinated biphenyls. *Environ. Sci. Tech.,* **32**, 788-797.

Berger T., Rubner P., Schautzer F., Egg R., Ulmer H., Mayringer I., Dilitz E., Deisenhammer F., Reindl M., (2003). Antimyelin Antibodies as a Predictor of Clinically Definite Multiple Sclerosis after a First Demyelinating Event. *N. Engl. J. Med., **349**,* 139-145.

Blake J.R., Taib B.B., Doherty G., (1986). Transient cavities near boundaries. I. Rigid boundary. *J. Fluid Mech*, **170**, 479 – 497.

Blitz J. (1963). Fundamentals of Ultrasonics (1st ed.).Butterworths, London, UK.

Bobalek E.G., Moore E.R., Levy S.S., Lee C.C., (1964). Some implications of the gel point concept to the chemistry of alkyd resins. *Journal of Applied Polymer Science*, **3**, 625-657.

Bredas J.L., Street G.B., (1985). Polarons, bipolarons and Solitons in Conducting Polymers. *Accounts of Chemical Research*, **18**, 309-315.

Bridge K.A., (2001). PhD Thesis, UMIST.

Brinton L.A., Moghissi K.S., Scoccia B., Westhoff C.L., Lamb E.J., (2005). Ovulation induction and cancer risk. *Fertil. Steril.*, **83 (2)**, 261-274.

Bucknall S., Silverlight J., Coldham N., Thorne L., Jackman R., (2003). Antibodies to the quinolones and fluoroquinolones for the development of generic and specific immunoassays for detection of these residues in animal products. *Food. Addit. Contam.*, **20***,* 221-228.

Campi P., Pichler W.J., (2003). Quinolone hypersensitivity. *Curr. Opin. Allergy. Clin. Immunol.*, **3**, 275-281.

Cao L.M., Lin H., Mirsky V.M., (2007). Surface plasmon resonance biosensor for enrofloxacin based on deoxyribonucleic acid. *Anal. Chim. Acta,* **589***,* 1-5.

Centonze D., Malitesta C., Palmisano F., Zambonin P.G., (1994). Permeation of solutes through an electropolymerised ultrathin poly *o*-phenylenediamine film used as an anzyme-entrapping membrane, *Electroanalysis*, **6**, 423 – 429.

Chahine G.L., (1982). Experimental and asymptotic study of non-spherical bubble collapse. *Appl. Sci. Res.,* **38**, 187 – 197.

Chandrasekhar P., (1999). Conducting Polymers, Fundamentals and Applications: A Practical Approach, Kluwer Academic Publishers, Boston.

Cheek G., Wales C.P., Nowak R.J., (1983). pH response of platinum and vitreous carbon electrodes modified by electropolymerised films. *Analytical Chemistry*, **55**, 380-381.

Chiba K., Ohsaka T., Ohnuki Y., Oyama N. (1987). Electropolymerisation preparation of a ladder polymer containing phenazine rings. *Journal of Electroanalytical Chemistry,* **219**, 117-124.

Clark L.C. Jr., (1956). Monitor and control of blood and tissue O_2 tensions. *Trans. Am. Soc. Artif. Intern. Organs*, **2**, 41-48.

Clark L.C., Lyons I.R., (1962). Electrode systems for continuous monitoring in cardiovascular surgery. *Ann. New York Academy Sci.*, **102**, 29-45.

Clemens A.H., Chang P.H., Myers R.W., (1976). Development of an automatic system of insulin infusion controlled by blood sugar, its system for the determination of glucose and control algorithms. *Proc. Journes Ann. de Diabtologie de l'Hotel-Dieu*, Paris, 269-278.

Cooney C.L., Weaver J.C., Tannebaum S.R., Faller S.R., Shields D.V., Jahnke M., (1974). *Enzyme Engineering* (Eds. E.K. Pye and L.B. Wingard Jnr.), **2**, 411-417, Plenum, New York.

Cooper J., Cass T., (2004). Biosensors (2nd ed.), Oxford University Press Inc., New York.

Crum L., (1984). Acoustic cavitation series: part five rectified diffusion. *Ultrasonics*, **22**, 215-223.

Cunningham W., Mathieson K., McEwan F.A., Blue A., McGeachy R., McLeod J.A., Morris-Ellis C., O'Shea V., Smith K. M., Litke A., Rahman M., (2001). Fabrication of microelectrode arrays for neural measurements from retinal tissue. *J. Phys. D: Appl. Phys.* **34**, 2804-2809.

Curie J., Curie P., (1880). Développement, par pression, de l'électricité polaire dans les cristaux hémièdres à faces inclinées. *Comptes Rendus de l'Académie des Sciences,* **91**, 294–295.

Dai H.P., Wu Q.H., Sun S.G., Shiu K.K., (1998). Electrochemical quartz crystal microbalance studies on the electropolymerisation processes of *o*-phenylenediamine in sulfuric acid solutions. *Journal of Electroanalytical Chemistry*, **456**, 47-59.

Dai Z., Yan F., Chen J., Ju H., (2003). Reagentless amperometric immunosensors based on direct electrochemistry of horseradish peroxidase for determination of carcinoma antigen-125. *Anal. Chem.*, **75(20),** 5429-5434.

Dannielson B., Winquist F., Lundstrom I., (1985). *Sensors and Actuators B*, **8**, 91-95.

Davidson R.S., Safdar A., Spencer J.D., Robinson B., (1987). Applications of ultrasound to organic chemistry. *Ultrasonics*, **25**, 35-39.

Davis F., Nabok A.V., Higson S.P.J., (2005). Species differentiation by DNA-modified carbon electrodes using an AC impedimetric approach. *Biosens. Bioelec.*, **20***,* 1531-1538.

Davis F., Hughes M. A., Cossins A.R., Higson S.P.J., (2007). Single gene differentiation by DNA-modified carbon electrodes using an AC impedimetric approach. *Anal. Chem.,* **79**, 1153-1157.

Dayton M.A., Brown J.C., Stutts K.J., Wightman R.M., (1980). Faradaic electrochemistry at microvoltammetric electrodes. *Anal. Chem.,* **52(6),** *946 – 950.*

DeLange R.J., Huang T.S., (1971). Egg white avidin. Sequence of the 78-residue middle cyanogen bromide peptide. Complete amino acid sequence of the protein subunit. *J.Biol. Chem*, **246(3)**, 698-709.

D'Elia L.F., Ortíz L.R., Márquez O.P., Márquez J., Martínez Y., (2001). Electrochemical deposition of poly (*o*-phenylenediamine) films on type 304 stainless steel. *Journal of the Electrochemical Society*, 4, C297-C300.

Deng H., Van Berkel G.J., (1999). Electrochemical polymerisation of aniline investigated using on-line electrochemistry/electrospray mass spectrometry. *Anal. Chem.*, **71**, 4284-4293.

Diaz-Gonzalez M., Gonzalez-Garcia M.B. Costa-Garcia A., (2005). Recent advances in electrochemical enzyme immunoassays. *Electroanalysis*, **17**, 1901-1918.

Dimaki M., Bøggild P., (2004). Dielectrophoresis of carbon nanotubes using microelectrodes: a numerical study. *Nanotechnology*, **15**, 1095-1102.

Duan J., Yuan Z.H., (2001). Development of an Indirect Competitive ELISA for Ciprofloxacin Residues in Food Animal Edible Tissues. *J. Agric. Food Chem*., **49***,* 1087-1089.

Edelman G.M., Gally J.A., (1962). The nature of Bence-Jones proteins. Chemical similarities to polypetide chains of myeloma globulins and normal gamma-globulins. *J. Exp. Med.*, **116.** 207-227.

Eggins B., (1997). Biosensors, An introduction, Jonh Wiley & Sons, Chichester, USA,

Ekinci E., Erdogdu G., Karagözler A.E., (2001). Preparation, optimisation, and voltammetric characteristics of poly (*o*-phenylenediamine) film as a dopamine-selective polymeric membrane, *Journal of Applied Polymer Science*, **79**, 327-332.

Ercolini A.M., Miller S.D., (2006). Mechanisms of Immunopathology in Murine Models of Central Nervous System Demyelinating Disease. *J. Immunol.***, 176,** 3293-3298.

Fabre B., Taillebois L., (2003). Poly (aniline boronic acid)-based conductimetric sensor of dopamine. *Chem Commun (Camb),* **24**, 2982-2983.

Fan F., Kwak J., Bard A.J., (1996). Single Molecule Electrochemistry, *J.Am.Chem.Soc*, **118**, 9669.

Farber E., (1970). Baekeland, Leo Hendrik. *Dictionary of Scientific Biography*. p.385, Charles Scribner's Sons, New York.

Feeney R., Kounaves S.P., (2000). Microfabricated ultramicroelectrode arrays: Developments, Advances, and Applications in environmental Analysis. *Electroanalysis*, **12**, 677 – 684.

Fisher A.C. (1996). Electrode Dynamics, Oxford Sci. Publ., Oxford, UK.

Fofonoff T.A. Martel S.M. Hatsopoulos N.G. Donoghue J.P. Hunter, I.W. (2004). Microelectrode array fabrication by electrical discharge machining and chemical etching. *IEEE Trans Biomed Eng*, **51(6)**, 890-895.

Franco E.L. and Duarte-Franco E., (2008). Ovarian cancer and oral contraceptives *The Lancet*, **371,** 277-278.

Free A.H., Adams E.C., Kercher M.L., Free H.M. and Cook, M.H.M, (1957). Simple specific test for uric glucose. *Clinical Chemistry*, **3**, 163-168.

Freitag R., (1996). Biosensors in Analytical Biotechnology, Academic Press, San Diego .

Gaertner W., (1954). Frequency Dependence of Ultrasonice Cavitation. *J. Acoust. Soc. Am*. **26**, 977-980.

Garifallou G-Z., Tsekenis G., Davis F., Millner P. A., Pinacho D. G., Sanchez-Baeza F., Marco M.-P., Gibson T. D., Higson S. P. J., (2007). Labeless immunosensor assay for fluoroquinolone antibiotics based upon an AC impedance protocol. *Anal. Lett.,* **40***,* 1412-1422.

Garjonte R. and Malinaukas A. (1999). Amperometric glucose biosensor based on glucose oxidase immobilised in poly(*o*-phenylenediamine) layer. *Sensors and Actuators B*, **14**, 225-231.

Gendrel D., Chalumeau M., Moulin F. and Raymond J., (2003). Fluoroquinolones in paediatrics: A risk for the patient or for the community. *Lancet Inf. Dis*., **3**, 537-546.

Genies E.M., Tsintavis C. and Syed A.A., (1985). Electrochemical study of polyaniline in aqueous and organic medium. Redox and kinetic properties. *Molecular Crystals and Liquid Crystals Science and Technology,* **121**, 181-186.

Genies E.M., Lapkowski M. and Tsintavis C. (1988). Preparation, properties and applications of polyaniline. New Journal of Chemistry, **12**, 181-196.

Gilmartin M.A.T. and Hart J.P., (1995). Sensing with chemically and biologically modified carbon electrodes. A review. *Analyst*, **120**, 1029–1045.

Glickstein C., (1960). Basic Ultrasonics. J.F.Rider Publisher Inc., New York.

Gornall D.D., (2004). Studies towards the exploitation of Sonochemically formed Microelectrode Arrays of the developments of Electrochemical Sensors, PhD Thesis, Cranfield University

Grant S., Davis F., Pritchard J.A., Law K.A., Higson S.P.J., Gibson T.D., (2003). Labeless and reversible immunosensor assay based upon an electrochemical current-transient protocol. *Analytica Chimica Acta*, **495**, 21-32

Grant, S., Davis, F., Law, K. A., Barton, A. C., Collyer, S. D., Higson, S. P.J. and Gibson, T. D. (2005). A reagentless immunosensor for the detection of bsa at platinum electrodes by an ac impedance protocol. *Anal. Chim. Acta.* **537** , pp. 163-168.p. 537-546.

Green N.M., Konieczny L., Toms E.J. And Valentine R.C., (1971). The use of bifunctional biotinyl compounds to determine the arrangement of subunits in avidin. *Biochem J*., **125**, 781-791.

Grennan K., Killard A.J. and Smyth M.R. (2001). Physical characterisation of screen-printed electrode for use in an amperometric biosensor system. *Electroanalysis,* **13**, 745–750.

Guilbault G.G., Montalvo J., (1969). A Urea specific enzyme electrode. *JACS*, **91**, 2164-2169.

Guilbault G., Hrabankova E., (1970). An electrode for determination of amino acids. *Anal. Lett*., *3*, 53-57.

Guilbault, G.G., (1976). Handbook of Enzymatic Methods of Analysis. Marcel Dekker, New York, pp. 2–188.

Gulce H., Celebi S.S., Ozyoruk H., Yildiz A., (1995). Amperometric enzyme electrode for sucrose determination prepared from glucose oxidase and invertase co-immobilized in polyvinylferrocenium. *Journal of Electroanalytical Chemistry*, **397**, 217-223

Hall E.A., (1990). Biosensors, Open University Press, Cambridge, England.

Hall D.G., (2005) Boronic Acids: Preparation and Applications in Organic Synthesis and Medicine (1st ed.). Wiley VCH, Weinheim, Germany.

Hartmann, A., Golet, E. M., Gartiser, S., Alder, A.C., Koller, T. and Widmer, R.M. (1999). Primary DNA damage but not mutagenicity correlates with ciprofloxacin concentrations in German hospital wastewaters. *Arch. Environ. Contam. Toxicol.,* **36***,* 115-119.

Hassouan, M., Ballesteros, O., Vilchez, J., Zafra, A., Navalon, A., **(2007).** Simple Multiresidue Determination of Fluoroquinolones in Bovine Milk by Liquid Chromatography with Fluorescence Detection. *Anal. Lett.,* **40***,* 779-791.

Heeger A.J., (2001). Nobel Lecture: The Semiconducting and metallic polymers: The fourth generation of polymeric materials. *Rev. Mod. Phys.*, **73**, 681 – 700.

Higson S.P.J., (2004). Analytical Chemistry, Oxford University Press Inc., Cambridge,

Higson S.P.J., (1996). "Sensor", International Patent PCT/GB96/00922 (continuation of UK patent 9507991. Filed on 19 November 1996. Patents granted to date in Europe, US, Canada, Japan and Australia.

Hiller Y., Gershoni J.M., Bayer E.A. and Wilchek. M., (1987). Biotin binding to avidin. Oligosaccharide side chain not required for ligand association. *Biochem J.,* **248**, 167-171.

Hooper D.C., (1999). Mode of action of fluoroquinolones. *Drugs*, **58**, 6-10.

Huh P., Kim S.C., Kim Y., Wang Y., Singh J., Kumar J., Samuelson L.A., Kim B.S.,Jo N.J., Lee J.O., (2007). Optical and electrochemical detection of saccharides with poly (aniline-co-3-aminobenzeneboronic acid) prepared from enzymatic polymerization. *Biomacromolecules*, **8(11)**, 3602-7.

Imisides M.D., John R., Wallace G.G., (1996). Microsensors based on conducting polymers. *Chemtech,* **26(5)**, 19-25.

Ionescu R.E., Jaffrezic-Renault N., Bouffier L., Gondran C., Cosnier S., Pinacho D.G., Marco M.P., Sanchez-Baeza F.J., Healy T., Martelet C., (2007). Impedimetric immunosensor for the specific label free detection of ciprofloxacin antibiotic. *Biosensors &Bioelectronics,* **23***,* 549-555.

Iqbal S.S., Mayo M.W., Bruno J.G., Bronk B.V., Batt C.A., Chambers J.P., (2000). A review of molecular recognition technologies for detection of biological threat agents. *Biosensors &Bioelectronics*, **15**, 549-578.

Janata J., (1975). Immunoelectrode, *Journal of American Chemical Society,* 97, 2914-2916.

Janata J., (2002). Electrochemical sensors and their impedances: A tutorial. *Critical Reviews in Analytical Chemistry*, **32,** 109-120.

Janeway C.A., Murphy K.M., Travers P., Walport M., (2004). Immunobiology. (6^{th} ed.), Garland Science Publishing, London

Jang D.H., Yoo Y.S. and Oh S.M. (1995). Electropolymerisation mechanism for poly (o-phenylenediamine) (PPD) and its electrocatalytic behaviour for O_2 reduction. *Bulletin of the Korean Chemical Society*, **16**, 392-396.

Jenkins D., Kratochvíl P., Stepto R.F.T. and Suter U.W., (1996). Glossary of basic terms in polymer science (IUPAC Recommendations 1996). *Pure Appl. Chem*., **68,** 2287-2312.

Johansson S.G., (2006). The discovery of immunoglobulin E. *Allergy and asthma proceedings*, **27**, 3-6.

John R., Spencer, M., Wallace G.G. and Smyth M.R., (1991). Development of a polypyrrole-based human serum albumin sensor. *Anal. Chim. Acta*., **249**, 381-385.

Kanazawa K.K. and Gordon J.G. (1985). The oscillation frequency of a quartz crystal resonator in contact with a liquid. *Analytica Chimica Acta*, **175**, 99-105.

Kennedy R.., Huang L., Atkinson M., Dush P., (1993). Amperometric monitoring of chemical secretions from individual pancreatic beta-cells. *Anal.Chem*., **65**,1882-1887.

Kilfoyle D.H., Dyck P.J., Wu Y., Litchy W.J., Klein D.M., Dyck P.J.B., Kumar N., Cunningham J.M., Klein C.J., (2006). Myelin protein zero mutation His39Pro: hereditary motor and sensory neuropathy with variable onset, hearing loss, restless legs and multiple sclerosis. *J. Neurol. Neurosur. Pysch.,* **77**, 963-966.

Kiyoyuki W., Okada K., Oda H., Furono K., Gomita Y., Katsu T., (1995). New cocaine-selective membrane electrode. *Anal.Chim. Acta.*, **316**, 371-375.

Kramer E.M., Schardt A., Nave K.A., (2001). Membrane traffic in myelinating oligodendrocytes. *Microsc. Res. Tech.*, **52**, 656-671

Kress-Rogers E., Brimelow J.B.C., (2001). Instrumentation and Sensors for the Food Industry (2^{nd} ed.), Woodhead Printing Ltd., Cambridge, England,

Kuttruff H., (1991). Ultrasonics: Fundamentals and Applications. Elsevier Science Publications, USA.

Labrude P. (2003). Le pharmacien et chimiste Henri Braconnot (Commercy 1780-Nancy 1855). *Rev Hist Pharm*., **51**, 61.

Lakhani S.R., Manek S., Penault-Llorca F., Flanagan A., Arnout L., Merrett S., McGuffog L., Steele D., Devilee P., Klijn J.G.M., Meijers-Heijboer H., Radice P., Pilotti S., Nevanlinna H., Butzow R., Sobol H., Jacquemier J., Lyonet D.S., Neuhausen S.L., Weber B., Wagner T., Winqvist R., Bignon Y., Monti F., Schmitt F., Lenoir G., Seitz S., Hamman U., Pharoah P., Lane G., Ponder B., Bishop D.T. and Easton D.F., (2004). Pathology of Ovarian Cancers in *BRCA1* and *BRCA. Carriers Clinical Cancer Research*, **10**, 2473-2481.

Lamers K.J.B., Vos P., Verbeek M.M., Rosmalen F., van Geel W.J.A., van Engelen B.G.M., (2003). Protein S-100B, neuron-specific enolase (NSE), myelin basic protein (MBP) and glial fibrillary acidic protein (GFAP) in cerebrospinal fluid (CSF) and blood of neurological patients. *Brain Research Bulletin*, **61**, 261-264.

Langevin P., (1918). French Patent No. 505703

Law K.A. and Higson S.P.J. (2005). Sonochemically fabricated acetylcholinesterase micro-electrode arrays within a flow injection analyser for the determination of organophosphate pesticides. *Biosensors and Bioelectronics*, **20**, 1914-1924.

Leighton T.G., (1994). The Acoustic Bubble. , Academic Press, London.

LeRoy A., (1994). Diagnosis and treatment of nephrolithiasis: current perspectives. *AM.J.Roentgenology*, **163(6)**, 1309-1313.

Lewis, D.W. (1990). Peter L. Jensen and the amplification of sound. The MIT Press, Cambridge, Massachusetts, USA, p.190-211.

Li X.G., Huang M.R., Duan W. & Yang Y.L., (2002). Novel multifunctional polymers from aromatic diamines by oxidative polymerizations. *Chem Rev,* **102**, 2925-3030

Licitra C.M., Brooks R.G. and Sieger B.E., (1987). Clinical efficacy and levels of ciprofloxacin in tissue in patients with soft tissue infection. *Antimicrob. Agents Chemother*., **31**, 805-807.

Liedberg B., Nylander C. and Lundstrm I., (1983). Surface plasmon resonance for gas detection and biosensing. *Sensors and Actuators,* **4**, 299-304.

Liuzzi G.M., Mastroianni C.M., Vullo V., Jirillo E., Delia S., Riccio P., (1992). Cerebrospinal fluid myelin basic protein as predictive marker of demyelination in AIDS dementia complex. *J Neuroimmunol*, 36, 251-254.

Lorimer J.P. and Mason T.J., (1987). Sonochemistry Part I-The Physical Aspects *Chem Soc. Rev*., **16**, 239-274.

Losito I., Cioffi N., Vitale M.P., Palmisano F., (2003). Characterization of soluble oligomers produced by electrochemical oxidation of *o*-phenylenediamine by electrospray ionization sequential mass spectrometry. *Rapid Communications in Mass Spectrometry,* **17**, 1169 – 1179.

Losito L., Giglio E.D., Cioffi N. and Malitesta C., (2001). Spectroscopic investigation on polymer films obtained by oxidation of o-phenylenediamine on platinum electrodes at different pHs. *Journal of Materials Chemistry*, **11**, 1812-1817.

Lord Rayleigh (1917). On the maintenance of vibrations by forces of double frequency, and on the propagation of waves through a medium endowed with a periodic structure. *Philosophical magazine*, **24** , 94-98.

Lubbers D.W. and Opitz N.Z., (1975). Naturforsch C. *Biosci.* **30,** 532-533.

Makar A.P.H., Kristensen G.B., Kaern J., Børmer O.P., Abeler V.M. and Trope C.G., (1992). Prognostic Value of Pre-and Postoperative Serum CA 125 Levels in Ovarian Cancer. *Obstetrics & Gynecology*, **79**, 1002-1010.

Malitesta C., Losito L. and Zambonin P.G., (1999). Molecularly imprinted electrosynthesised polymers: new materials for biomimetic sensors. *Analytical Chemistry*, **71**, 1366-1370.

Manzo L., Artigas F., Martinez E., Mutti A., Bergamaschi E., Nicotera. P., Tonini M., Candura S.M., Ray D.E., Costa L.G., (1996). Biochemical markers of neurotoxicity. A review of mechanistic studies and applications. *Human. Expt. Toxicol.,* **15***,* S20-S35.

Martinusz K., Inzelt G. and Horányi G., (1995). Coupled electrochemical and radiometric study of anion migration in poly (*o*-phenylenediamine) films. *Journal of Electroanalytical Chemistry,* **395**, 293-297.

Mason T.J., Berlan, J., (1992). Ultrasonics in industrial Processes: The problems of scale-up. Current trends in Sonochemistry, Edited by G. Price, Royal Society of Chemistry, pp. 148-157

Mason T.J., Lorimer J.P., (2002). Applied Sonochemistry: The Uses of Power Ultrasound in Chemistry and Processing, Wiley-VCH Verlag GmbH, Weinheim, Germany.

Mason D.J., Power E.G., Talsania H., Phillips I. and Gant V.A., (1995). Antibacterial action of ciprofloxacin. *Antimicrob. Agents Chemother*., **39,** 2752-2758.

Mattu T., Pleass R., Willis A., Kilian M., Wormald M., Lellouch A., Rudd P., Woof J., Dwek R., (1998). The glycosylation and structure of human serum IgA1, Fab, and Fc regions and the role of N-glycosylation on Fc alpha receptor interactions. *J Biol Chem*, **273 (4)**, 2260-2272.

Mederos A., Domínguez S., Hernández-Molina R., Sanchiz J. and Brito F., (1999). Coordinating ability of phenylenediamines. *Coordination Chemistry Reviews*, **193-195**, 913-939.

Miller D.L., Bao S., Giles R.A., Thrall B.D., (1999). Ultrasonic Enhancement of Gene Transfection in Murine Melanoma Tumors. *Ultrasound Med. Biol.,* **25 (9),** 1425-1430.

Mills D.W., (2005). The development of a new class of sensor with commercial promise, EngD Thesis, Cranfield University, England.

Mišík V., Riesz P., (2000). Free Radical Intermediates in Sonodynamic Therapy. *Annals of the New York Academy of Sciences*, **899**, 335-348.

Mosbach K. and Danielsson B., (1974). An enzyme thermistor. *Biochim. Biophys. Acta.,* **364**, 140-145.

Mock D.M., Horrowitz P., (1990). A fluorometric assay for avidin-biotin interaction. *Meth. Enzymol.,* **184**, 234-240.

Mu S., Chen C. and Wang J. (1997). The kinetic behavior for the electrochemical polymerization of aniline in aqueous solution. *Synthetic Metals*, **88**, 249-254.

Mukherjee A., Vogt R.F., Linthicum D.S., (1985). Measurement of myelin basic protein by radioimmunoassay in closed head trauma, multiple sclerosis and other neurological diseases.*Clin Biochem,* **18***,* 304-307.

Murray R.W., Ewing A.G., Dust R.A., (1987). Chemically Modified Electrodes - Molecular Design for Electroanalysis. *Anal Chem.,* **59**, 379A-385A.

Mülhaupt, R. (2004). Hermann Staudinger and the Origin of Macromolecular Chemistry. *Angew. Chem. Int. Ed.,* **43**, 1054-1063.

Myler S., (2000). The Exploitation of Thin-Polymer-Films and Microelectrode Arrays for the Development of Electrochemical Biosensors, PhD Thesis, UMIST, UK.

Nagy G., Von Storp H., Guilbault G., (1973). Glucose Enzyme Electrodes Based on the Use of an Iodide Membrane Sensor. *Anal Chim. Acta*, **66**, 443.

Narayan P., Wheatley M.A., (1999). Preparation and characterization of. hollow microcapsules for use as ultrasound contrast agents. *Polymer Engineering & Science.* **39**, 2242 – 2255.

Newman J.D., Warner P.J., Turner A.P.F., Tigwell L.J., (2004). Biosensors: A clearer view. Cranfield Biotechnology Centre, pp 216

Newman J.D., Turner A.P.F., (1994). Biosensors: The analyst's dream? *Chem. Ind.*, **10**, 374-378.

Nicolas M., Fabre B., Marchand G., Simonet J., (2000). New Boronic-Acid and Boronate-Substituted Aromatic Compounds as Precursors of Fluoride-Responsive Conjugated Polymer Films. *Eur. J. Org. Chem.,* **9**, 1703-1710.

Niloff J.M., Klug T.L., Schaetzl E., Zurawski V.R. Jr, Knapp R.C., Bast R.C. Jr., (1984). Elevation of serum CA125 in carcinomas of the fallopian tube, endometrium, and endocervix. *Am J Obstet Gynecol*, **148(8)**, 1057-1058

Nilsson H., Akerlund A., Mosbach K., (1973). Determination of glucose, urea and penicillin using enzyme--pH-electrodes. *Biochim Biophys Acta*, **320**, 529-534.

Niwa O., Tabei H., (1994). Subfemtomole Detection of Catecholamine with Interdigitated Array Carbon Microelectrodes in HPLC. *Anal Chem*, **66,** 285-289.

Nurok D., Koers J.M., and Carmichael A.M., (2003). Role of buffer concentration and applied voltage in obtaining a good separation in planar electrochromatography. *Journal of Chromatography A*, **983**, 247-253.

Nyborg W.L., (1996). Basic physics of low frequency therapeutic ultrasound, in Ultrasound Angioplasty, edited by R. J. Siegel, Kluwer Academic, Boston, USA.

Ogura K., Kokura M., Yano J. and Shiigi H., (1995). Spectroscopic and scanning tunnelling microscope characterisation of virgin and recast films of electrochemically prepared poly (*o*-phenylenediamine). *Electrochimica Acta*, **40**, 2707-2714.

Ogura K., Shiigi H. and Nakayama M., (1996). A new humidity sensor using the composite film derived from poly (*o*-phenylenediamine) and poly (vinyl alcohol). *Journal of the Electrochemical Society*, **143**, 2925-2929.

Ouerghi O., Touhami A., Jaffreiz-Renaul N., Martelet C., Ben Ouada H., Cosnier S., (2002). Impedimetric immunosensor using avidin-biotin for antibody immobilization. *Bioelectrochemistry*, **56**, 131-133.

Owens R.C.Jr, Ambrose P.G., (2000). Antimicrobial Therapy. Clinical Use of the Fluoroquinolones. *Med. Clin. North. Am*., **84**, 1447-1469.

Oyama N., Ohsaka T., Chiba K. and Takahashi K., (1988). Effects of supporting electrolyte and pH on charge transport within electropolymerized poly (*o*-phenylenediamine) films deposited on graphite electrodes, *Bulletin of the Chemical Society of Japan*, **61**, 1095-1101.

Painter P., and Coleman M., (1997). Fundamentals of Polymer Science: an introductory text.

Palmer T., (1991). Understanding Enzymes, Horwood Publishing Ltd., London.

Phillips J.P., Lockman L.A., Shapiro E.G., Blazar B.R., Loes D.J., Moser H.W., Krivit W., (1994). CSF findings in adrenoleukodystrophy: correlation between measures of cytokines, IgG production, and disease severity.*Pediatric Neurology,* **10***,* 289-294.

Prencipe L., Iaccheri E., Manzati C., (1987). Enzymic ethanol assay: a new colorimetric method based on measurement of hydrogen peroxide. *Clin. Chem*., **33**, 486-489.

Preud'homme J.L., Petit I., Barra A., Morel F., Lecron J.C., Lelièvre E., (2000). Structural and functional properties of membrane and secreted IgD. *Mol. Immunol.*, 37, 871-887.

Pritchard J., Law K., Vakurov A., Millner P. and Higson S.P.J., (2004). Sonochemically fabricated enzyme microelectrode arrays for environmental monitoring of pesticides. *Biosensors and Bioelectronics*, **20**, 765-772.

Putnam F.W., Liu Y.S., Low T.L., (1979). Primary structure of a human IgA1 immunoglobulin. IV. Streptococcal IgA1 protease, digestion, Fab and Fc fragments, and the complete amino acid sequence of the alpha 1 heavy chain. *J Biol Chem*, **254**, 2865-74.

Raju T.N., (1999). The Nobel chronicles. 1972: Gerald M Edelman (b 1929) and Rodney R Porter (1917-85). *Lancet,* **354 (9183)**, 1040.

Ray J., Schinich T., Lerner R., (1979). A mutation altering the function of a carbohydrate binding protein blocks cell-cell cohesion in developing Dictyostelium discoideum. *Nature*, **279**, 215-221.

Recksiedler C.L., Deore B.A., Freund M.S., (2006). A novel layer-by-layer approach for the fabrication of conducting polymer/RNA multilayer films for controlled release. *Langmuir,* **22(6)**, 2811-2815.

Rhoades R.A., Pflanzer R.G., (2002). Human Physiology, 4th ed., Thomson Learning.

Ricci F., Amine A., Palleschi G., Moscone D., (2003). Prussian Blue based screen printed biosensors with improved characteristics of long-term lifetime and pH stability. *Biosensors and Bioelectronics*, **18**, 165-174.

Rodriguez-Diaz R.C., Fernandez-Romero J.M., Aguilar-Caballos M.P., Gomez-Hens A., (2006). Determination of Fluoroquinolones in Milk Samples by Postcolumn Derivatization Liquid Chromatography with Luminescence Detection. *J. Agric. Food Chem.,* **54,** 9670-9676.

Rudick R.A., Whitaker J.N., (1987). Cerebrospinal fluid tests for multiple sclerosis. *Neurology and Neurosurgery Update,* **7**, 1-8.

Sadik O.A., John M.J., Wallace G.G., Barnett D., Clarke C. and Laing D.G., (1994). Pulsed amperometric detection of thaumatin using antibody-containing poly(pyrrole) electrodes. *Analyst*. **119**, 1997-2000.

Sadki S., Schottland P., Brodie N., Sabouraud G., (2000). The mechanisms. of pyrrole electropolymerization. *Chem.Soc.Rev*, **29**, 283-293.

Sanderson D.G., Anderson L.B., (1985). Filar electrodes: Steady-state currents and spectroelectrochemistry at twin interdigitated ectrodes. *Anal. Chem*. **57**, 2388-2393.

Santinelli R., Tolone C., D'Avanzo A., del Giudice E. M., Perrone L., D'Avanzo M., (2006). Pontine myelinolysis in a child with carbamate poisoning. *Clin. Toxic.,* **44**, 327-328.

Sarandakou A., Protonotariou E., Rizos D., (2007). Tumor markers in biological fluids associated with pregnancy. *Critical reviews in clinical laboratory sciences,* **44 (2),** 151–78.

Sauerbrey G.Z., (1959). Use of a quartz vibrator for weighing thin films on a microbalance. *Z Physik*, **155**, 206-210.

Seitz W.R., Saari L.A., (1984). Immobilized calcein for metal ion preconcentration. *Anal.Chem*, **56**, 810-813.

Shichiri M., Kawamori R., Yamaski R., Hakai Y. and Abe H., (1982). Wearable artificial endocrine pancreas with needle-type glucose sensor. *The Lancet*, **320**, 1129-1131.

Shlamovitz G.Z., Iakobishvili Z., Matz I., Golovchiner G., Lev E. and Siegel R.J., (2002). In vitro ultrasound augmented clot dissolution—what is the optimal timing of ultrasound application? *Cardiovasc Drugs Ther,* **16**, 521–526

Shuqun C., Xinda Z., Zhaoyou T., Yao Y., Susu B., Dechu Q., (2000). Effects of high-intensity focused ultrasound and anti-angiogenic agents on the ablation of experimental liver cancers. *Chinese Journal of Digestive Diseases*, 1, 35-38.

Silverstein A.M., (2003). Cellular versus humoral immunology: a century-long dispute. *Nat. Immunol*., **4 (5)**, 425-8.

Silverstein A.M., (2004). Labeled antigens and antibodies: the evolution of magic markers and magic bullets. *Nat. Immunol.* **5 (12)**, 1211-7.

Sitampalam G., Wilson G.S., (1983). Surface-Modified Electrochemical Detector for Liquid Chromatography. *Anal. Chem.* **55(9)**, 1608-1610.

Skinner N.G., Hall E.A.H., (1997). Investigation of the origin of the glucose response in a glucose oxidase|polyaniline system. *J. Electroanal. Chem*, **420**, 179-188.

Soto G., Jaffari A.M., Bone S.A., (2001). Characterisation and optimisation of AC conductimetric biosensors. *Biosensors & Bioelectronics*, **16**, 23-29.

Somani P.R., Radhakrishnan S., (2003). Electrochromic materials and devices: present and future. *Materials Chemistry and Physics*, **77**, 117-133.

Stetter J.R., Penrose W.R., Yao S., (2003). Sensors, Chemical Sensors, Electrochemical Sensors, and ECS. *Journal of the Electrochemical Society*, 150, S11-S16.

Stevens F.J., Solomon A., Schiffer M., (1991). Bence Jones proteins: a powerful tool for the fundamental study of protein chemistry and pathophysiology. **Biochemistry, 30**, 6803-6805.

Suslick K.S., Hammerton D.A., Cline R.E. Jr, (1986). *Journal of the American Chemical Society*, **108**, 5641-5642.

Suslick K.S., Price G.J., (1999). Applications of ultrasound to materials chemistry. *Annual Review of Materials Science*, **29**, 295-326.

Suslick K.S., (1994). The Chemistry of Ultrasound, The Yearbook of Science and the Future, Encyclopaedia Britannica, Chicago, 138–155.

Švancara I., Vytřas K., Barek J., Zima J., (2001). Carbon Paste Electrodes in Modern Electroanalysis. *Critical Reviews in Analytical Chemistry*, **31**, 311 – 345.

Teneriello M.G., Park R.C., (1995). Early detection of ovarian cancer. *CA Cancer J Clin.*, **45(2),** 71-87.

Thornycroft J., Barnaby S.W. (1895). Torpedo boat destroyers. *Proc. Inst. Civil. Engineers*, **122**, 51.

Thrust M., Schoning M.S., Vetter J., Kordos P., Lüth H., (1996). A long-term stable penicillin-sensitive potentiometric biosensor with enzyme immobilised by heterobifunctional cross-linking. *Anal. Chim. Acta*, **323**, 115-121.

Tomasi T.B., (1992). The discovery of secretory IgA and the mucosal immune system. *Immunol. Today*, **13 (10)**, 416-418.

Torriero A.A.J., Ruiz-Diaz, J.J.J., Salinas E., Marchevsky E.J., Sanz M.I., Raba J., (2006). Enzymatic rotating biosensor for ciprofloxacin determination. *Talanta,* **69**, 691-699.

Toyoguchi, T., Ebihara, M., Ojima, F., Hosoya, J., Nakagawa, Y., (2005). In vitro study of the adsporption characteristics of drugs. *Biol. Pharm. Bull.,* **2005,** *28,* 841-844.

Tsekenis G., Garifallou G-Z., Davis F., Millner P. A., Gibson T. D., Higson S. P. J., (2008). Label-less immunoprotein assay for myelin basic protein based upon an AC impedance protocol. *Anal.Chem***., 80,** 2058-2062**.**

Turner A.P.F., Karube I. and Wilson G.S., (1987). Biosensors: Fundamentals and Applications, Oxford University Press, Oxford.

Turner A.P.F, Cass A.E.G., Francis D.G., Hill H.A.O., Aston W.J., Higgins I.J., Plotkin E.V., Scott L.D.L., (1984). Ferrocene-mediated enzyme electrode for amperometric determination of glucose. *Anal. Chem.,* **56**, 667-671.

Turner A.P.F., (1989). Biosensors: Fundamentals and Applications., St. Edmundsbury Press, Suffolk, England.

Upadhyay S.K., Kumar P., Arora V., (2006). Complexes of quinolone drugs norfloxacin and ciprofloxacin with alkaline earth metal perchlorates. *J. Struct. Chem.,* **47***,* 1078-1083.

U.S. Food and Drug Administration, Date of access: 22/02/08: http://www.fda.gov/cder/foi/label/2002/19537s41lbl.pdf

Vagdama P., Crump P.W., (1992). Biosensors: Recent trends. *Analyst*., **117**, 1657.

Van Epps H.L., (2006). Michael Heidelberger and the demystification of antibodies. *J. Exp. Med*., **203 (1)**, 5.

Varma S., Shantilatha P., Mitra C.K., (2003**).** Advances in Biosensors 2003: Perspectives in Biosensor, JAI Press.

Vermette P., Gengenbach T., Divisekera U., Kambouris P.A., Griesser H.J. and Meagher L. (2003). Immobilization and surface characterization of NeutrAvidin biotin-binding protein on different hydrogel interlayers, *Journal of Colloid and Interface Science*, **259**, 13-26.

Visintin I., **Feng Z.**, **Longton G.**, **Ward D.C.**, **Alvero A.B.**, **Lai Y.**, **Tenthorey J.**, **Leiser A.**, **Flores-Saaib R.**, **Yu H.**, **Azori M.**, **Rutherford T.**, **Schwartz P.E.**, **Mor G**., (2008). Diagnostic markers for early detection of ovarian cancer. *Clin Cancer Res*. **14(4)**,1065-1072.

Voelkl K.P., Opitz N., Lubbers D.W., Fres Z., (1980). Continuous measurement of concentrations of alcohol using a fluorescence-photometric enzymatic method. *Anal. Chem.* **301**, 162-163.

Volkov A., Tourillon G., Lacaze P.C., and Dubois J.E., (1980). Electrochemical polymerisation of aromatic amines, *Journal of Electroanalytical Chemistry*, **115**, 279-291.

Wang J., (2000). Analytical Electrochemistry (2nd ed.), Wiley-VCH, USA.

Watson L.D., Maynard P., Cullen D.C., Sethi R.S., Brettle J., Lowe C.R., (1987). A microelectronic conductimetric biosensor. *Biosensors*, **3**, 101-115.

Wilchek M. and Bayer E.A., (1988). The avidin-biotin complex in bioanalytical applications. *Analytical Biochemistry*, **171**, 1-32.

Wilder J.L., Pavlik E., Straughn J.M., Kirby T., Higgins R.V., DePriest P.D., Ueland F.R., Kryscio R.J., Whitley R.J., van Nagell J., (2003). Clinical implications of a rising serum CA-125 within the normal range in patients with epithelial ovarian cancer: a preliminary investigation. *Gynecologic Oncology,* 89, 233-235.

Wilson M.S., Nie W., (2006). Multiplex measurement of seven tumor markers using an el ectrochemical protein chip. *Anal Chem*. **78(18)**, 6476-6483.

Winau F., Westphal O., Winau R., (2004). Paul Ehrlich-in search of the magic bullet. *Microbes Infect*., **6(8)**, 786-9.

Wingerchuk D.M., (2006). The clinical course of acute disseminated encephalomyelitis. *Neurol. Res.,* **28**, 341-347.

Winokur M., Moon Y.B., Heeger A.J., Barker J., Bott D.C., Shirakawa H., (1987). X-Ray Scattering from Sodium-Doped Polyacetylene: Incommensurate-Commensurate and Order-Disorder Transformations. *Phys. Rev. Lett.*, **58,** 2329–2332.

Wooley D.W., Longsworth L.G., (1942). Isolation of an antibiotin factor from egg white. *J.Biol. Chem*., **142**, 285-290.

Wu C.C. and Chang H.C., (2004). Estimating the thickness of hydrated ultrathin poly (*o*-phenylenediamine) film by atomic force microscopy. *Analytica Chimica Acta,* 505, 239-246.

Wu L.L., Luo J. and Lin Z.H. (1996). Spectroelectrochemical studies of poly-o-phenylenediamine. Part 1. In situ resonance raman spectroscopy. *Journal of Electroanalytical Chemistry*, **417**, 53-58.

Wu J., Zhang Z., Fu Z., Ju H., (2007). A disposable two-throughput electrochemical immunosensor chip for simultaneous multianalyte determination of tumor markers. *Biosens Bioelectron*, **23(1)**, 114-20.

Yano J., (1995). Electrochemical and structural studies on soluble and conducting polymer from o-phenylenediamine. *Journal of Polymer Science: Part A Polymer Chemistry*, **33**, 2435-2441.

Yin B.W.T., Dnistrian A., Lloyd K.O., (2002). Ovarian cancer antigen CA125 is encoded by the *MUC16* mucin gene. *International Journal of Cancer.* 98(5), 737–740.

Zhai J.., Chi H., Yang R., (1997). DNA based biosensors. *Biotechnol. Adv*., **15**, 43-58.

Zhao X., Xia Y., Whitesides G., (1997). Soft lithographic methods for nano-fabrication. *J.Mater. Chem.,* **7**, 1069-1074.

Zima P., Maršík F. and Sedlář M., (2003). Cavitation rates in water with dissolved gas and other impurities. *Journal of Thermal Science*, **12(2)**, 151-156.

Zoski C.G., (2002). Ultramicroelectrodes: Design, Fabrication, and Characterization. Electroanalysis, **14(15-16)**, 1041 – 1051.

Appendix

List of publications

- **Barton A.C., Collyer S.D., Davis F., Garifallou G.Z., Tsekenis G., Tully E., O'Kennedy R., Gibson T., Millner P.A., Higson S.P., (2008).** Labeless AC impedimetric antibody-based sensors with pgml(-1) sensitivities for point-of-care biomedical applications. *Biosens. Bioelec*., In print.

- **Davis F., Garifallou G-Z., Tsekenis G., Millner P. A., Pinacho D. G., Sanchez-Baeza F., Marco M.-P., Gibson T. D., Higson S. P. J., (2008).** Labeless Immunosensor Assays based upon an AC Impedance Protocol. Conference *Proceedings of the Institution of Engineering and Technology (IET)*. In print.

- **Tsekenis G., Garifallou G-Z., , Davis F., Millner P. A., Pinacho D. G., Sanchez-Baeza F., Marco M.-P., Gibson T. D., Higson S. P. J., (2008).** Detection of Fluoroquinolone Antibiotics in Milk via a Labelless Immunoassay based upon an AC Impedance Protocol, *Anal. Chem.,* Submitted for publication.

- **Tsekenis G., Garifallou G-Z., Davis F., Millner P. A., Gibson T. D., Higson S. P. J., (2008).** Label-less immunoprotein assay for myelin basic protein based upon an AC impedance protocol. *Anal.Chem.,* **80**, 2058-2062.

- **Garifallou G-Z., Tsekenis G., Davis F., Millner P. A., Pinacho D. G., Sanchez-Baeza F., Marco M.-P., Gibson T. D., Higson S. P. J., (2007).** Labeless immunosensor assay for fluoroquinolone antibiotics based upon an AC impedance protocol. *Anal. Lett.,* **40**, 1412-1422.

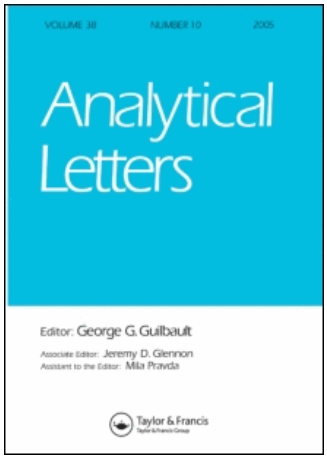

Analytical Letters
Publication details, including instructions for authors and subscription information:
http://www.informaworld.com/smpp/title~content=t713597227

Labeless Immunosensor Assay for Fluoroquinolone Antibiotics Based Upon an AC Impedance Protocol

G.-Z. Garifallou [a]; G. Tsekenis [a]; F. Davis [a]; S. P. J. Higson [a]; P. A. Millner [b]; D. G. Pinacho [c]; F. Sanchez-Baeza [c]; M.-P. Marco [c]; T. D. Gibson [d]
[a] Cranfield Health, Cranfield University, Bedfordshire
[b] University of Leeds, Leeds
[c] Institute of Chemical and Environmental Research (IIQAB-CSIC), Jorge Girona, Barcelona, Spain
[d] T and D Technology, Wakefield, West Yorkshire

Online Publication Date: 01 January 2007
To cite this Article: Garifallou, G.-Z., Tsekenis, G., Davis, F., Higson, S. P. J., Millner, P. A., Pinacho, D. G., Sanchez-Baeza, F., Marco, M.-P. and Gibson, T. D. (2007) 'Labeless Immunosensor Assay for Fluoroquinolone Antibiotics Based Upon an AC Impedance Protocol', Analytical Letters, 40:7, 1412 - 1422
To link to this article: DOI: 10.1080/00032710701327070
URL: http://dx.doi.org/10.1080/00032710701327070

Analytical Letters, 40: 1412–1422, 2007

ISSN 0003-2719 print/1532-236X online
DOI: 10.1080/00032710701327070

Taylor & Francis
Taylor & Francis Group

IMMUNOLOGY

Labeless Immunosensor Assay for Fluoroquinolone Antibiotics Based Upon an AC Impedance Protocol

G.-Z. Garifallou, G. Tsekenis, F. Davis, and S. P. J. Higson
Cranfield Health, Cranfield University, Silsoe, Bedfordshire

P. A. Millner
University of Leeds, Leeds

D. G. Pinacho, F. Sanchez-Baeza, and M.-P. Marco
Institute of Chemical and Environmental Research (IIQAB-CSIC), Jorge Girona, Barcelona, Spain

T. D. Gibson
T and D Technology, Wakefield, West Yorkshire

Abstract: This paper describes the construction of a labeless immunosensor for the antibiotic ciprofloxacin and its interrogation using an AC impedance protocol. Commercial screen-printed carbon electrodes were used as the basis for the sensor. Polyaniline was electrodeposited onto the sensors and then utilized to immobilize a biotinylated antibody for ciprofloxacin using classical avidin-biotin interactions.

Electrodes containing the antibodies were exposed to solutions of antigen and interrogated using an AC impedance protocol. The faradaic component of the impedance of

Received 20 January 2007; accepted 27 February 2007

This work has been supported by the Ministry of Science and Technology (Spain) (Contract numbers AGL2005-07700-C06-01 and NAN2004-09195-C04-04) and by the European Community Framework VI NMP2-CT-2003-505485, "ELISHA" contract. The AMR group is a consolidated Grup de Recerca de la Generalitat de Catalunya and has support from the Departament d'Universitats, Recerca i Societat de la Informació la Generalitat de Catalunya (expedient 2005SGR 00207). DG has a FPI fellowship from the Spanish Ministry of Education.

Address correspondence to S. P. J. Higson, Cranfield Health, Cranfield University, Silsoe, Bedfordshire MK45 4DT. E-mail: s.p.j.higson@scranfield.ac.uk

the electrodes was found to increase with increasing concentration of antigen. Control samples containing a non-specific IgG antibody were also studied and calibration curves obtained by subtraction of the responses for specific and non-specific antibody-based sensors, thereby eliminating the effects of non-specific adsorption of antigen.

Keywords: Fluoroquinolone, ciprofloxacin, AC impedance, immunosensor, polyaniline

INTRODUCTION

The principle of immunoassays was established in 1959 by Yalow and Berson (Yalow and Berson, 1959). Their work developed the widely used radio-immunoassay to examine the properties of insulin-binding antibodies in human serum, using samples obtained from subjects that had been treated with insulin.

Following the newly developed immunoassay technique, the concept of a biosensor was pioneered by Clark and Lyons in 1962 (Clark and Lyons, 1962). The original methodology was to immobilize enzymes on the surface of electrochemical sensors-assuming that this would enhance the ability of a sensor to detect specific analytes. This idea has remained virtually unchanged since this original design, however, technological advances have allowed for the expansion of this field of science.

The incorporation of antibodies into conducting polymer films was first reported in 1991 (John et al. 1991). Anti-human serum albumin (anti-HSA) was incorporated into a polypyrrole film, which was galvanostatically polymerized onto a platinum wire substrate. When grown in the absence of a counterion, a poor polymeric film, both in appearance and electrochemical properties was formed, suggesting that the presence of a counterion was necessary for the polymerization process to be successful. Amino acid analysis of the polymer using a leucine marker showed that approximately 0.1% w/v (0.2 μg) of the antibody was incorporated into the matrix. When the pyrrole anti-HSA electrode was exposed to 50 μg ml^{-1} HSA for 10 min, a new reduction peak was observed at a potential of approximately +600 mV versus Ag/AgCl. This peak increased in magnitude after a further 30 min in the same solution and it was suggested this could be due to an antibody/antigen interaction with the polymer. Further work by the same group gave rise to reports of a reversible real-time immunosensor (John et al. 1991). Other early work utilized a pulsed amperometric detection technique for other analytes, including *p*-cresol (Barnett et al. 1994), thaumatin (Sadik et al. 1994), and polychlorinated biphenyls (Bender and Sadik 1994). Since this work there has been a huge increase in the development of electrochemical immunosensors as detailed in several recent reviews (Cosnier 2005; Diaz-Gonzalez et al. 2005; Rodriguez-Mozaz et al. 2006).

Antibody-antigen interactions are by their very nature complex and the reproducible response characteristics of immunosensors requires that the

affinity reaction occurring is minimally perturbed by the fabrication procedure. We have previously shown that up to 2–3 μg antibodies for BSA and digoxin may be successfully incorporated into conducting polymer films by entrapment in a growing polypyrrole film with no detrimental effect to antibody activity (Grant et al. 2003). Electrochemical interrogation of these films demonstrated selective interactions with the target antigens. Further work utilized an AC impedance protocol (Grant et al. 2005) as the method of interrogation for these films and led to the development of immunosensors for digoxin and bovine serum albumin.

The quinolones are a family of broad-spectrum antibiotics with the majority of quinolones in clinical use being fluoroquinolones, which have a fluoro group attached to the central ring system. They are widely used within adult patients because of excellent tissue penetration which makes them extremely effective against bacteria that grow intracellularly such as salmonella (Gendrei et al. 2003). One of these groups is ciprofloxacin (Fig. 1) which is a broad-spectrum antibiotic active against many bacteria including anthrax (Torriero et al. 2006). Many of these fluoroquinolones are added to farm animal feed since they can lead to greater and more rapid weight gain. Unfortunately the effect of this is thought to have enabled the rise of resistant species of bacteria (Gendrei et al. 2003).

The monitoring of fluoroquinolones within both food and the environment is important since these antibiotics have potential health and environmental damaging effects. Ciprofloxacin concentrations in hospital wastewaters were monitored and correlations with DNA damaging effects made (Hartmann et al. 1999). Levels of ciprofloxacin in hospital outflow water between 0.7–124.5 ng ml^{-1} were measured using high performance liquid chromatography (HPLC) (Hartmann et al. 1999) and shown to display genotoxicity at levels as low as 5.2 ng ml^{-1}. Similar work (Batt et al. 2006) measured wastewater ciprofloxacin using liquid chromatography/mass spectrometry/mass spectrometry (LC/MS/MS) and found levels between 0.031–5.6 ng ml^{-1} (even after treatment) with a limit of detection of 0.030 ng ml^{-1}. Levels *in vivo* have also been widely studied with the therapeutic ranges typically being between 0.57–2.30 μg ml^{-1} in serum and 1.26–4.03 μg g^{-1} in tissue (Licitra et al. 1987).

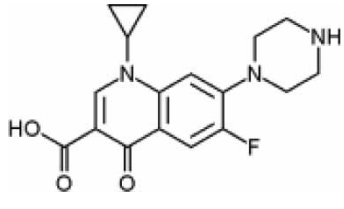

Figure 1. Structure of ciprofloxacin.

A recent publication (Torriero et al. 2006) details the use of a horseradish peroxidase based biosensor for the detection of ciprofloxacin due to its inhibition of the oxidation of catechol, however other piperazine based compounds could potentially interfere with this determination. Linear responses were obtained between 0.02–65 μM with the limit of detection being 0.4 nM. We have within this work developed a labeless immunosensor for ciprofloxacin as a typical fluoroquinolone. The sensor utilizes screen-printed carbon electrodes, modified by deposition of first, a conducting polymer (polyaniline) which is then modified with biotinylating reagent. Complexion of the immobilized biotin with avidin allows the further binding of biotinylated antibodies via standard avidin-biotin interactions (Fig. 2). The resultant electrodes are capable of detecting low levels of the antigen-ciprofloxacin. Control electrodes containing non-specific IgG have also been fabricated and allow the subtraction out of unspecific interactions.

EXPERIMENTAL

Sodium dihydrogen orthophosphate, disodium hydrogen orthophosphate, sodium chloride, and hydrochloric acid, were obtained from BDH (Poole, Dorset). Potassium chloride was obtained from Fisher Scientific UK Ltd, (Loughborough). Aniline, polyclonal IgG from human serum, the biotinylation kit (part no. BK101), biotin 3-sulfo-*N*-hydroxysuccinimide, avidin, bovine serum albumin (BSA), potassium ferrocyanide, and potassium ferricyanide were obtained from Sigma-Aldrich, (Gillingham, Dorset). All water used was obtained from a Purelab UHQ Deioniser (Elga, High Wycombe). Commercial screen-printed carbon electrodes (Fig. 3) containing carbon working and counter electrodes and an Ag/AgCl reference electrode were obtained from Parlex Corp Ltd, Isle of Wight. The surface area of the working electrode was 0.2178 cm^2.

Phosphate Buffered Saline (PBS) at pH 7.4 stock solution was prepared containing 0.14 mol l^{-1} NaH_2PO_4, 0.52 mol l^{-1} Na_2HPO_4, and 0.0051 mol l^{-1} NaCl. Aniline buffer (pH 1–2) was prepared containing 0.5 mol l^{-1} KCl, 0.3 mol l^{-1} HCl, and 0.2 mol l^{-1} aniline.

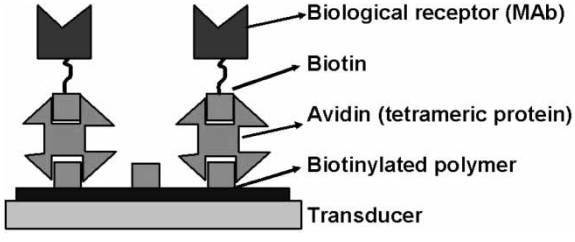

Figure 2. Schematic of antibody modified electrodes.

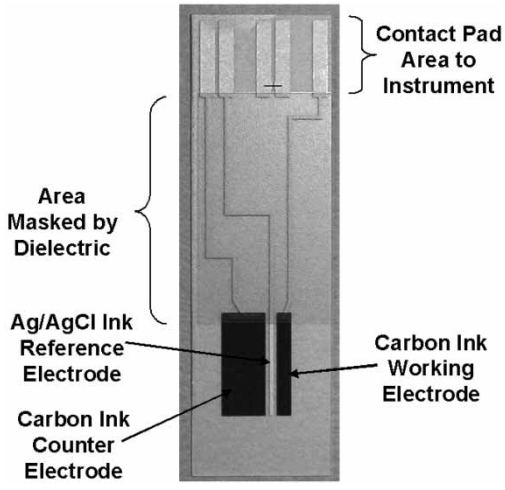

Figure 3. Screen-printed carbon electrodes used within this work.

Polyclonal antiserum (As 171) was raised against 1-(3mercaptopropyl)-6-fluoro-7-(piperanicyl)-1,4-dihydro-4-oxo-quinoline-3-carboxylic acid coupled to HCH. The preparation of the immunogen and of the antibodies will be described elsewhere (Pinacho et al. 2007).

For antibody biotinylation the procedure outlined in the BK101 kit was followed (see manufacturer's instructions for details). Biotinylated antibodies were kept frozen in aliquots of 200-μl at a concentration of 1 mg ml^{-1} until required.

Cyclic voltammetry (Sycopel Potentiometer, Sycopel Scientific, Tyne & Wear) was utilized to deposit polyaniline films on the carbon electrodes. Screen-printed carbon electrodes were placed in aniline buffer and cycled from −200 mV to +800 mV versus Ag/AgCl for approximately 20 cycles (occasionally this was varied slightly to ensure that the same amount of polyaniline was deposited on each electrode. Deposition was terminated at +800 mV to ensure the polyaniline remained in its conducting form. After deposition, electrodes were rinsed in water.

Initially 30 μl of biotin-sulfo-NHS (10 mg ml^{-1} in water) was placed on the polymer coated working electrode surface for 24 h. The sensors were rinsed with copious water and 30 μl of avidin (10 μg ml^{-1} in water) placed on the working electrode for 1 h followed by rinsing in water. Then 30 μl biotinylated antibody (1 mg ml^{-1} in water, 1 hour) was added followed by rinsing. Finally, non-specific interactions were blocked by BSA (10^{-6} M in PBS, 1 hour); the sensors are ready to use at this point, however, if opted, can be stored in PBS at 4°C for no longer than 24 h.

AC impedance measurements were performed using an ACM Auto AC DSP frequency response analyser. Antigen solutions for AC impedance

were prepared by diluting the required concentration of antigen in 30 ml of PBS pH 7.4. A range of concentrations were utilized, since genotoxicity is noted at levels above 5.2 ng ml^{-1}; we set our minimum level at 1 ng ml^{-1} with an upper limit of 10 μg ml^{-1}, which covers the therapeutic/clinical range. However other work within our group suggests detection limits of about 10 pg ml^{-1}. The sensors were first interrogated without antigen addition. Following this, each sensor was exposed to the required antigen concentration for 30 min, rinsed well with deionized water and then subjected to impedance interrogation. Potassium ferrocyanide (10 mM) and potassium ferricyanide (10 mM) in PBS buffer were utilized as a redox couple for impedimetric measurements. Three electrodes were used for each measurement. A frequency range from 10 kHz to 1 Hz was measured, with peak amplitude of 5 mV and a DC offset of +400 mV against Ag/AgCl.

RESULTS AND DISCUSSION

Deposition of Polyaniline

The voltammograms for the deposition of polyaniline/DNA are depicted in Fig. 4 and imply a steady in situ formation of polymer at the electrode surface. As the number of scans increases, peaks appear between +350–400 mV versus Ag/AgCl corresponding to the oxidation and reduction of surface bound polyaniline. The increase in current from scan

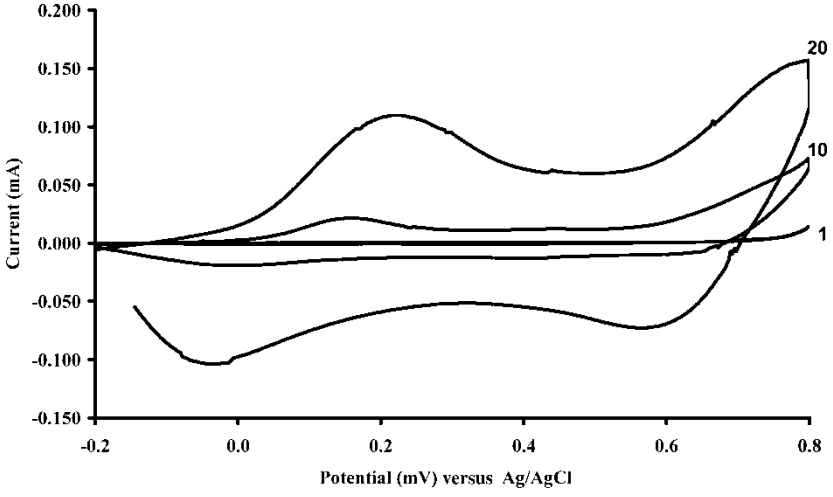

Figure 4. Deposition of conducting polyaniline films by cyclic voltammetry, curves shown after 1, 10, and 20 cycles.

10 to 20 is due to the increase in polyaniline thickness and coverage of the electrode.

Impedance Profiles of the Electrodes

A series of Nyquist curves were obtained for the sensors after exposure to various levels of ciprofloxacin in PBS (Fig. 5a). As can be seen, there is a

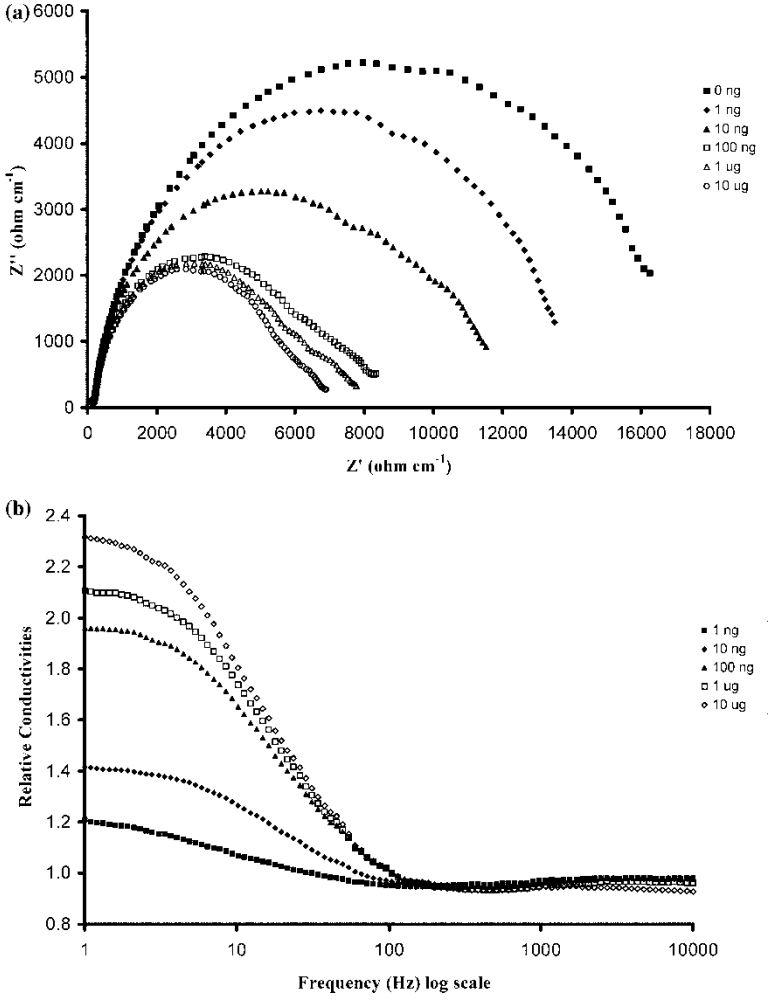

Figure 5. Nyquist plots of a typical antibody modified electrode exposed to various concentrations of antigen.

steady decrease in the impedance of the electrodes with increasing antigen concentration. The relative conductivities of the system, which are obtained by dividing the impedance for each frequency with no antigen present—by the impedance (at the same frequency) for each antigen concentration, are shown in Fig. 5b. As can be seen, we see much larger increases in conductivity at the lower frequencies. Therefore, it was decided that changes in impedance at 1 Hz would be used as a measurement of antigen binding.

The impedance spectra consists of two components, the real (Z') component where the impedance in phase with the AC potential waveform is measured and the imaginary (Z'') where the impedance is 180° out of phase. It is important to differentiate between the individual components of the total impedance of the cell so that the capacitive and Faradaic components of the composite impedimetric response may be identified and quantified. Previous work by our group showed that while both the imaginary and real components increased, the increase in the real component dominated the total increase in the impedance (Grant et al. 2005). Although in this case, changes in both real and imaginary components are visible and again the real component is the major component of total impedance, perhaps more importantly it was also found that the real component offers far greater reproducibility in comparison to the imaginary contribution.

Figures 6a shows the percentage decrease in Z' across a range of antigen concentrations. As can be seen, there is a steady decrease in impedance as antigen concentration increases up to a concentration of about 100 ng ml^{-1}, above which concentration there is a tend towards a plateau, possibly indicating saturation of the specific binding sites. It is possible that any further changes in impedance beyond this level could simply be due to non-specific interactions. Between a concentration range of 1–100 ng ml^{-1}, there is a near linear correlation of the impedance change with the $\log_{10}$ of concentration ($R^2 = 0.96$).

Non-specific interactions could potentially interfere with immunosensor performance. This could be addressed by utilization of a second sensor containing either no antibodies—or alternatively a non-specific antibody. Therefore an identical set of immunosensors were fabricated utilizing a non-specific IgG antibody in place of the specific ciprofloxacin antibody. Results for these electrodes were obtained in exactly the same way and the calibration plot is shown (Fig. 6b). As can be seen, there is a much lower response for the non-specific antibody, showing that although there are non-specific interactions, between the ranges of 1–100 ng ml^{-1}, they comprise a minor component of the detected response. Figure 6c shows the subtracted responses (6a–6b) and again this demonstrates linearity between the response and the $\log_{10}$ of ciprofloxacin concentration between 1–100 ng ml^{-1} ($R^2 = 0.96$).

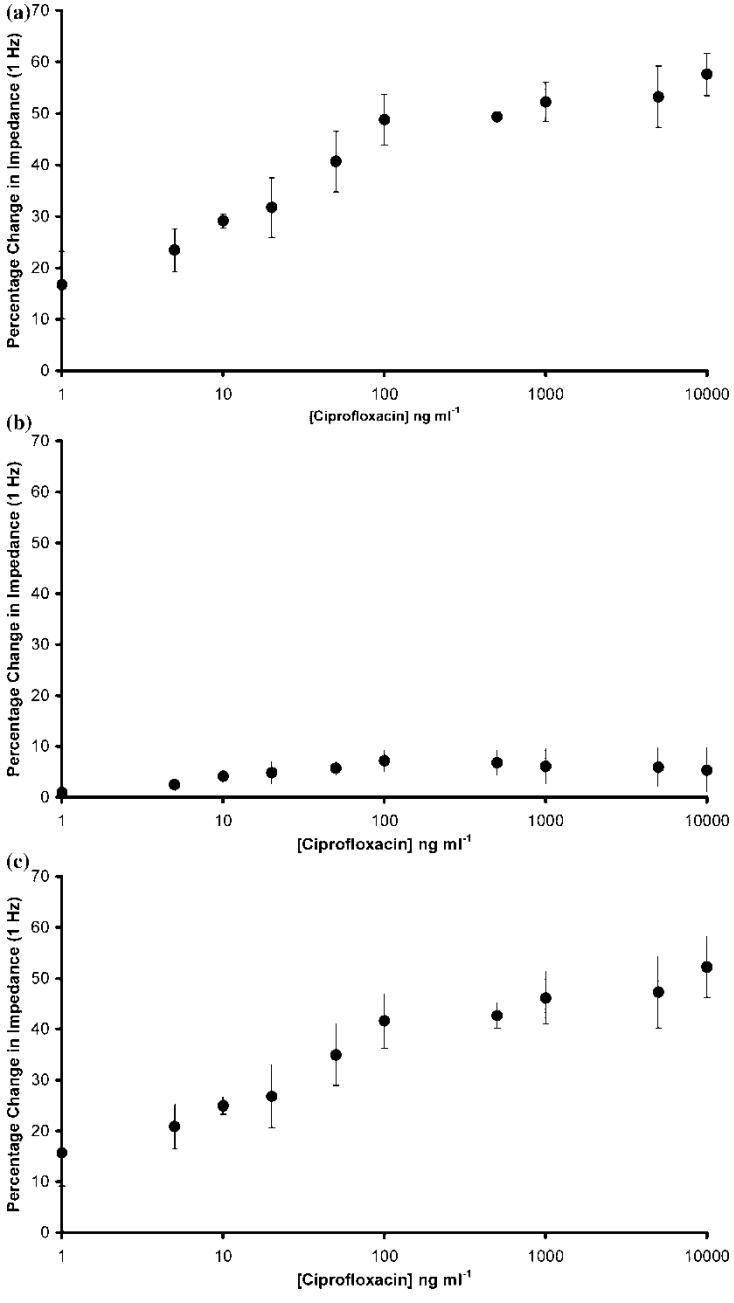

Figure 6. Calibration curves for (a) anti-ciprofloxacin modified electrodes (b) IgG modified electrodes (c) corrected calibration curves (curve a−curve b). All data points are averages of three electrodes; error bars give a measure of the reproducibility of the system.

CONCLUSIONS

We have demonstrated the construction of an immunosensor for the antibiotic ciprofloxacin using a combination of screen-printed electrodes coated with conducting polyaniline and an immobilized polyclonal antibody. Interrogation of the electrodes by AC impedance demonstrated the detection of the antigen. Linear correlation of the impedance change with the $\log_{10}$ of concentration ($R^2 = 0.96$) was observed between concentrations of 1–100 ng ml^{-1}.

REFERENCES

Barnett, D., Laing, D.G., Skopec, S., Sadik, O.A., and Wallace, G.G. 1994. Determination of *p*-cresol (and other phenolics) using a conducting polymer-based electro-immunological sensing system. *Anal. Lett.*, 27: 2417–2429.

Batt, A.L., Bruce, I.B., and Aga, D.S. 2006. Evaluating the vulnerability of surface waters to antibiotic contamination from varying wastewater treatment plant discharges. *Environ. Poll.*, 142: 295–302.

Bender, S. and Sadik, O.A. 1998. Direct electrochemical immunosensor for polychlorinated biphenyls. *Environ. Sci. Tech.*, 32: 788–797.

Clark, L.C. and Lyons, I.R. 1962. Electrode systems for continuous monitoring in cardiovascular surgery. *Ann New York Academy Sci.*, 102: 29.

Cosnier, S. 2005. Affinity biosensors based on electropolymerized films. *Electroanalysis*, 17: 1701–1715.

Diaz-Gonzalez, M., Gonzalez-Garcia, M.B., and Costa-Garcia, A. 2005. Recent advances in electrochemical enzyme immunoassays. *Electroanalysis*, 17: 1901–1918.

Grant, S., Davis, F., Pritchard, J.A., Law, K.A., Higson, S.P.J., and Gibson, T.D. 2003. Labeless and reversible immunosensor assay based upon an electrochemical current-transient protocol. *Anal. Chim. Acta.*, 495: 21–32.

Grant, S., Davis, F., Law, K.A., Barton, A.C., Collyer, S.D., Higson, S.P.J., and Gibson, T.D. 2005. A reagentless immunosensor for the detection of bsa at platinum electrodes by an ac impedance protocol. *Anal. Chim. Acta.*, 537: 163–168.

Gendrei, D., Chalumeau, M., Moulin, F., and Raymond, J. 2003. Fluoroquinolones in paediatrics: A risk for the patient or for the community. *Lancet Inf. Dis.*, 3: 537–546.

Hartmann, A., Golet, E.M., Gartiser, S., Alder, A.C., Koller, T., and Widmer, R.M. 1999. Primary DNA damage but not mutagenicity correlates with ciprofloxacin concentrations in German hospital wastewaters. *Ach. Environ. Contam. Toxicol.*, 115–119.

John, R., Spencer, M., Wallace, G.G., and Smyth, M.R. 1991. Development of a polypyrrole-based human serum albumin sensor. *Anal. Chim. Acta.*, 249: 381–385.

Licitra, C.M., Brooks, R.G., and Sieger, B.E. 1987. Clinical efficacy and levels of ciprofloxacin in tissue in patients with soft tissue infection. *Antimicrob. Agents Chemother.*, 31: 805–807.

Pinacho, D.G., Sanchez-Baeza, F., and Marco, M.P. 2007. Development of a class selective indirect competitive enzyme-linked immunosorbent assay (ELISA) for detection of fluoroquinolone antibiotics, in preparation .

Rodriguez-Mozaz, S., de Alda, M.J.L., and Barcelo, D. 2006. Biosensors as useful tools for environmental analysis and monitoring. *Anal. Bioanal. Chem.*, 386: 1025–1041.

Sadik, O.A., John, M.J., Wallace, G.G., Barnett, D., Clarke, C., and Laing, D.G. 1994. Pulsed amperometric detection of thaumatin using antibody-containing poly(pyrrole) electrodes. *Analyst.*, 119: 1997–2000.

Torriero, A.A.J., Ruiz-Dıaz, J.J.J., Salinas, E., Marchevsky, E.J., Sanz, M.I., and Raba, J. 2006. Enzymatic rotating biosensor for ciprofloxacin determination. *Talanta*, 69: 691–699.

Yalow, R.S. and Berson, S.A. 1959. Assay of plasma insulin in human subjects by immunological methods. *Nature*, 184: 1648–1649.

Anal. Chem. **2008,** *80,* 2058−2062

Label-less Immunosensor Assay for Myelin Basic Protein Based upon an ac Impedance Protocol

Georgios Tsekenis,[†] Goulielmos-Zois Garifallou,[†] Frank Davis,[†] Paul A. Millner,[‡] Tim D. Gibson,[§] and Séamus P. J. Higson*,[†]

Cranfield Health, Cranfield University, Silsoe, Beds, MK45 4DT, U.K., Biosensors and Biocatalysis Group, Research Institute of Membrane and Systems Biology, Garstang Building, University of Leeds, Leeds, LS2 9JT, U.K., and ELISHA Systems Limited, Sigma House, Burlow Road, Buxton, SK17 9JB, U.K.

This paper describes the development and characterization of a label-less immunosensor for myelin basic protein (MBP) and its interrogation using an ac impedance protocol. Commercial screen-printed carbon electrodes were used as the basis for the sensor. Polyaniline was electrodeposited onto the sensors, and this modified surface then utilized to immobilize a biotinylated antibody for MBP using a classical avidin−biotin approach. Electrodes containing the antibodies were exposed to solutions of MBP and interrogated using an ac impedance protocol. The real component of the impedance of the electrodes was found to increase with increasing concentration of antigen. Control samples containing a nonspecific IgG antibody were also studied, and calibration curves were obtained by subtraction of the responses for specific and nonspecific antibody-based sensors, thereby accounting for and eliminating the effects of nonspecific adsorption of MBP. A logarithmic relationship between the concentration of MBP in buffer solutions and the impedimetric response was observed.

The principle of immunoassays was first established by Yalow and Berson[1] in 1959. Their work led to the development of the widely used radioimmunoassay to examine the properties of insulin-binding antibodies in human serum, using samples obtained from subjects that had been treated with insulin.

Independently within unconnected work, the concept of a biosensor was pioneered by Clark and Lyons[2] in 1962. The original methodology involved immobilizing enzymes on the surface of electrochemical sensors so as to exploit the selectivity of enzymes for analytical purposes. This idea has remained virtually unchanged since the original design, although the field has undergone continual technological developments over the last 40 years.

The incorporation of antibodies into conducting polymer films was first reported[3] in 1991. Antihuman serum albumin (anti-HSA) was incorporated into a polypyrrole film, which was galvanostatically polymerized onto a platinum wire substrate. When grown in the absence of a counterion, a poor polymeric film (both in appearance and electrochemical properties) was formed, suggesting that the presence of a counterion was necessary for the polymerization process to be successful. Amino acid analysis of the polymer using a leucine marker showed that approximately 0.1% w/v (0.2 μg) of the antibody was incorporated into the matrix. When the pyrrole anti-HSA electrode was exposed to 50 μg mL^{-1} HSA for 10 min, a new reduction peak was observed at a potential of approximately +600 mV versus Ag/AgCl. This peak increased in magnitude after a further 30 min in the same solution—and it was suggested this could be due to an antibody/antigen interaction with the polymer. Further work by the same group gave rise to reports of a reversible real-time immunosensor.[3] Other early work utilized a pulsed amperometric detection technique for other analytes, including *p*-cresol,[4] thaumatin,[5] and polychlorinated biphenyls.[6] Since this early work there has been burgeoning interest in the development of electrochemical immunosensors—as detailed in several recent reviews.[7−9]

Antibody−antigen interactions are by their very nature complex, and the reproducible response characteristics of immunosensors requires that the affinity reaction is minimally perturbed by the fabrication procedure. We have previously shown that up to 2−3 μg of antibodies for bovine serum albumin and digoxin may be successfully incorporated into conducting polymer films by entrapment in a growing polypyrrole film with no detrimental effect to antibody activity.[10] Electrochemical interrogation of these films demonstrated selective interactions with the target antigens. Further work utilized an ac impedance protocol[11] as the method of interrogation for these films—and led to the development of immunosensors for digoxin and bovine serum albumin. Later work

* Corresponding author. Fax: (+44) 01525 863433. E-mail: s.p.j.higson@cranfield.ac.uk.

† Cranfield University.

‡ University of Leeds.

§ ELISHA Systems Ltd.

(1) Yalow, R. S.; Berson, S. A. *Nature* **1959**, *184*, 1648−1649.

(2) Clark, L.C.; Lyons, I. R. *Ann. N.Y. Acad. Sci.* **1962**, *102*, 29.

(3) John, R.; Spencer, M.; Wallace, G. G.; Smyth, M. R. *Anal. Chim. Acta* **1999**, *249*, 381−385.

(4) Barnett, D.; Laing, D. G.; Skopec, S.; Sadik, O. A.; Wallace, G. G. *Anal. Lett.* **1994**, *27*, 2417.

(5) Sadik, O. A.; John, M. J.; Wallace, G. G.; Barnett, D.; Clarke, C.; Laing, D. G. *Analyst* **1994**, *119*, 1997−2000.

(6) Bender, S.; Sadik, O. A. *Environ. Sci. Technol.* **1998**, *32*, 788−797.

(7) Rodriguez-Mozaz, S.; de Alda, M. J. L.; Barcelo, D. *Anal. Bioanal. Chem.* **2006**, *386*, 1025−1041.

(8) Diaz-Gonzalez, M.; Gonzalez-Garcia, M. B.; Costa-Garcia, A. *Electroanalysis* **2005**, *17*, 1901−1918.

(9) Cosnier, S. *Electroanalysis* **2005**, *17*, 1701−1715.

(10) Grant, S.; Davis, F.; Pritchard, J. A.; Law, K. A.; Higson, S. P. J.; Gibson, T. D. *Anal. Chim. Acta* **2003**, *495*, 21−32.

(11) Grant, S.; Davis, F.; Law, K. A.; Barton, A. C.; Collyer, S. D.; Higson, S. P. J.; Gibson, T. D. *Anal. Chim. Acta* **2003**, *537*, 163−168.

10.1021/ac702070e CCC: $40.75
Published on Web 02/09/2008

by our group studied approaches for immobilization of antibodies onto polyaniline-coated screen-printed carbon electrodes utilizing a classical avidin−biotin chemistry. This enabled the construction of immunosensors for the fluoroquinolone antibody ciprofloxacin.[12]

Myelin is a complex membrane which forms a sheath around axons in vertebrate species.[13] It is the most abundant membrane structure within the vertebrate nervous system, allowing the fast conduction of nerve impulses through the nerve fibers[14] due to its high resistance and low capacitance. Myelin basic protein (MBP) is a cytoplasmic protein important in the process of myelination of nerves in the central nervous system since it comprises the bulk of the main line of compact myelin[13] and up to 30% of the protein content of myelin overall.[14]

A demyelinating disease is any disease of the nervous system in which the myelin sheath of neurons becomes damaged. This impairs the conduction of signals in the affected nerves, causing impairment in sensation, movement, cognition, or other functions, depending on which nerves are involved. Multiple sclerosis (MS), which is a chronic and inflammatory disease of the central nervous system, is an example of a demyelinating disease. Multiple sclerosis affects neurons within the brain and spinal cord that are involved with sensory and motor control functions. The name multiple sclerosis is derived from the multiple scars (or scleroses) that can be observed on the myelin sheaths. At the time of writing MS does not have a cure, although several treatments are available that may slow the appearance of new symptoms.

Multiple sclerosis is currently often diagnosed following occurrence of a number of indicative symptoms. Magnetic resonance imaging (MRI) may be used to evaluate patients who display these symptoms. MRI is capable of imaging areas where demyelination is occurring, with lesions caused by demyelination showing up as bright areas on the scan. Cerebrospinal fluid can also be utilized in the diagnosis of MS, and the presence of immunoglobins can be detected in the majority of MS sufferers. It should be noted, however, that other conditions can also lead to the presence of these species.[15]

Other demyelinating diseases include transverse myelitis, Guillain−Barré syndrome, and progressive multifocal leukoencephalopathy. There are various identified potential causes of demyelination, including autoimmune reactions,[16] infectious agents,[17] genetic conditions,[18] and also exposure to compounds such as carbamate pesticides.[19]

The presence of antibodies against myelin proteins such as MBP can be a predictor of MS.[20] Clinical studies of 103 patients suffering from MS demonstrated that the presence of antibodies

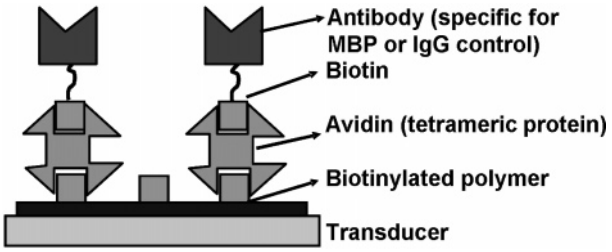

Figure 1. Schematic of antibody-modified electrodes showing the assembly of avidin and biotinylated electrodes and binding of biotinylated antibody.

for MBP and myelin oligodendrocyte glycoprotein within serum could be correlated with a greatly increased level of relapse compared to patients without these antibodies. Other demyelinating conditions also lead to elevated levels of MBP in cerebrospinal fluid,[21,22] for example, in cases of closed head trauma[23] or acquired immunodeficiency syndrome (AIDS) dementia complex (ADC).[24] A significant correlation has also been determined between the clinical stage of the childhood-onset cerebral form of adrenoleukodystrophy and cerebrospinal fluid MBP levels.[25] MBP levels between 4 and 8 ng L^{-1} in cerebrospinal fluid may indicate a chronic breakdown of myelin or recovery from an acute episode. MBP levels greater than 9 ng mL^{-1} indicate that active demyelination may be occurring. Normally there should be less than 4 ng mL^{-1} of MBP in the cerebral spinal fluid.

Increased MBP levels can also occur as a result of a stroke. A stroke, also known as cerebrovascular accident (CVA), is an acute neurological injury in which blood supply to a part of the brain is interrupted. Strokes involve a sudden loss of neuronal function due to arterial or even venous disturbance in cerebral perfusion. The part of the brain with disturbed perfusion no longer receives an adequate supply of oxygen. This initiates the ischemic cascade which causes brain cells to die or be seriously damaged, impairing local brain function. An indirect result of stroke is an active breakdown of myelin or demyelination, and therefore, the levels of MBP in cerebral spinal fluid (CSF) can act as markers for stroke.

Commercial ELISA tests exist for MBP; Diagnostic Systems Laboratories (Texas), for example, manufactures an ELISA which can measure levels of MBP in cerebrospinal fluid in 4 h.

We have within this work developed a label-less immunosensor for MBP. The sensor utilizes screen-printed carbon electrodes and is modified first by deposition of a conducting polymer (polyaniline) and thence biotinylating reagent. Complexion of the immobilized biotin with avidin allows the further binding of biotinylated antibodies via standard avidin−biotin interactions as described earlier[12] and as shown schematically in Figure 1. The resultant electrodes are capable of detecting the antigen within

(12) Garifallou, G.-Z.; Tsekenis, G.; Davis, F.; Millner, P. A.; Pinacho, D. G.; Sanchez-Baeza, F.; Marco, M.-P.; Gibson, T. D.; Higson, S. P. J. *Anal. Lett.* **2007**, *40*, 1412−1442.
(13) Arroyo, E. G.; Scherer, S. S. *Cell Biol.* **2000**, *113*, 1−18.
(14) Baumann, N.; Pham-Dinh, D. *Physiol. Rev.* **2001**, *81*, 871−927.
(15) Rudick, R. A.; Whitaker, J. N. In *Neurology/Neurosurgery Update*; Scheinberg, P., Ed.; CPEC: Princeton, NJ, 1987; Vol. 7.
(16) Ercolini, A. M.; Miller, S. D. *J. Immunol.* **2006**, *176*, 3293−3298.
(17) Wingerchuk, D. M. *Neurol. Res.* **2006**, *28*, 341−347.
(18) Kilfoyle, D. H.; Dyck, P. J.; Wu, Y.; Litchy, W. J.; Klein, D. M.; Dyck, P. J. B.; Kumar, N.; Cunningham, J. M.; Klein, C. J. *J. Neurol., Neurosurg. Psychiatry* **2006**, *77*, 963−966.
(19) Santinelli, R.; Tolone, C.; D'Avanzo, A.; del Giudice, E. M.; Perrone, L.; D'Avanzo, M. *Clin. Toxic.* **2006**, *44*, 327−328.
(20) Berger, T.; Rubner, P.; Schautzer, F.; Egg, R.; Ulmer, H.; Mayringer, I.; Dilitz, E.; Deisenhammer, F.; Reindl, M. *N. Engl. J. Med.* **2003**, *349*, 139−45.
(21) Manzo, L.; Artigas, F.; Martinez, E.; Mutti, A.; Bergamaschi, E.; Nicotera, P.; Tonini, M.; Candura, S. M.; Ray, D. E.; Costa, L. G. *Hum. Exp. Toxicol.* **1996**, *15*, S20−S35.
(22) Lamers, K. J. B.; Vos, P.; Verbeek, M. M.; Rosmalen, F.; Van Geel, W. J. A.; Van Engelen, B. G. M. *Brain Res. Bull.* **2003**, *61*, 261−264.
(23) Mukherjee, A.; Vogt, R. F.; Linthicum, D. S. *Clin. Biochem.* **1985**, *18*, 304−307.
(24) Liuzzi, G. M.; Mastroianni, C. M.; Vullo, V.; Jirillo, E.; Delia, S.; Riccio, P. *J. Neuroimmunol.* **1992**, *36*, 251−254.
(25) Phillips, J. P.; Lockman, L. A.; Shapiro, E. G.; Blazar, B. R.; Loes, D. J.; Moser, H. W.; Krivit, W. *Pediatr. Neurol.* **1994**, *10*, 289−294.

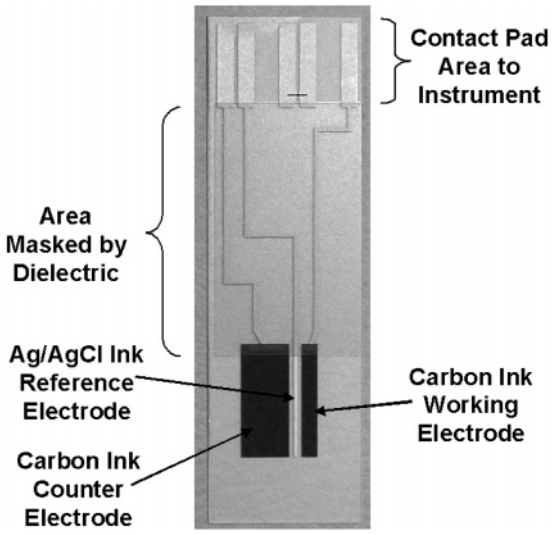

Figure 2. Screen-printed carbon electrodes used within this work.

the required physiological range. Control electrodes containing nonspecific IgG have also been fabricated to measure the effects of nonspecific binding and permit the subtraction of these unspecific interactions from the response toward specific binding of MBP. This approach helps to increase the stability and reliability of these sensors when applied to clinical samples.

EXPERIMENTAL SECTION

Sodium dihydrogen orthophosphate, disodium hydrogen orthophosphate, sodium chloride, and hydrochloric acid were obtained from BDH (Poole, Dorset, U.K.). Potassium chloride was obtained from Fisher Scientific U.K. Ltd., Loughborough, U.K. Aniline, MBP (from mouse, M2941), myelin basic protein antibody (monoclonal anti-MBP from rat, M9434), polyclonal IgG (from mouse, I5381), the biotinylation kit (part no. BK101), biotin 3-sulfo-*N*-hydroxysuccinimide, neutravidin, bovine serum albumin (BSA), potassium ferrocyanide, and potassium ferricyanide were obtained from Sigma-Aldrich, Gillingham, Dorset, U.K. All water used was obtained from a Purelab UHQ Deionizer (Elga, High Wycombe, U.K.). Commercial screen-printed carbon electrodes (Figure 2) containing carbon working and counter electrodes and a Ag/AgCl reference electrode were obtained from Microarray Ltd., Manchester, U.K. The surface area of the working electrode was 0.2178 cm^2.

Phosphate-buffered saline (PBS), pH 7.4 stock solution was prepared containing 0.14 mol L^{-1} NaH_2PO_4, 0.52 mol L^{-1} Na_2HPO_4, and 0.0051 mol L^{-1} NaCl. Aniline buffer, pH 1−2, was prepared containing 0.5 mol L^{-1} KCl, 0.3 mol L^{-1} HCl, and 0.2 mol L^{-1} aniline.

For antibody biotinylation, the procedure outlined in the BK101 kit was followed (see manufacturers instructions for details). Biotinylated antibodies were kept frozen in aliquots of 200 μL at a concentration of 1 mg mL^{-1} until required.

Cyclic voltammetry (Sycopel potentiometer, Sycopel Scientific, Tyne & Wear, U.K.) was utilized to deposit polyaniline films on the carbon electrodes. Screen-printed carbon electrodes were placed in aniline buffer and cycled from −200 to +800 mV versus Ag/AgCl for approximately 20 cycles, (the number of cycles could be varied to ensure the same quantity of polyaniline was deposited on each electrode). Deposition was terminated at +800 mV to ensure the polyaniline remained in its conducting form. Following deposition the polymer-coated electrodes were rinsed in water.

A volume of 30 μL of biotin−sulfo−NHS (10 mg mL^{-1} in water) was placed on the polymer-coated working electrode surface for 24 h. The sensors were rinsed with copious water and 30 μL of avidin (10 μg mL^{-1} in water) placed on the working electrode for 1 h—followed by further rinsing in water. Then 30 μL of biotinylated antibody (1 mg mL^{-1} in water) was added followed by rinsing. Finally, nonspecific interactions were blocked by BSA (10^{-6} M in PBS); the sensors are ready to use at this point; however, if opted, they can be stored in PBS at 4 °C up to 24 h.

The ac impedance measurements were performed using an ACM auto ac DSP frequency response analyzer (ACM Instruments, Grange over Sands, UK). Antigen solutions for ac impedance were prepared by diluting the required concentration of antigen in 30 mL of PBS, pH 7.4. A range of concentrations were utilized; since levels should be less than 4 ng mL^{-1} for a healthy individual, we set our minimum level at 1 ng mL^{-1} with an upper limit of 1 μg mL^{-1}, so as to cover the clinical range.

The sensors were first interrogated without antigen addition. Following this, each sensor was exposed to the required antigen concentration for 30 min, rinsed well with deionized water, and then subjected to impedance interrogation. Potassium ferrocyanide (10 mM) and potassium ferricyanide (10 mM) in PBS buffer were utilized as a redox couple for impedimetric measurements. Three electrodes were used for each measurement. A frequency range from 10 kHz to 1 Hz was measured, with a peak amplitude of 5 mV and a dc offset of +400 mV against Ag/AgCl.

RESULTS AND DISCUSSION

Deposition of Polyaniline. The voltammograms for the deposition of polyaniline onto the screen-printed carbon electrodes[12] are depicted in Figure 3 and imply a steady in situ formation of polymer at the electrode surface. As the number of scans increases, voltammetric peaks are seen between +350 and 400 mV versus Ag/AgCl, corresponding to the oxidation and reduction of surface bound polyaniline. The increase in current from scan 10 to 20 is due to the increase in polyaniline thickness and coverage of the electrode.[11]

Impedance Profiles of the Electrodes. A series of Nyquist curves were obtained for the sensors after exposure to various levels of MBP in PBS (Figure 4a). As can be seen, there is a steady decrease in the impedance of the electrodes with increasing antigen concentration. The relative impedances of the system for various antigen concentrations can be obtained by dividing the impedance for each frequency when a given concentration of antigen has been applied by the impedance (at the same frequency) for the sensor exposed to zero antigen concentration; these are shown in Figure 4b. This figure clearly shows that the impedance of the electrodes steadily increases with the concentration of MBP. Myelin basic protein is a mixture of epitopes with molecular weights of 14−21 kDa.[14] However the commercial antibody recognizes the peptide strand between amino acids 36 and 50 which is common to all the epitopes. The increases in impedance are most probably due to binding of the protein to the surface, since the protein molecules are likely to be insulating in nature. As can be seen, much larger increases in impedance are observed at the lower frequencies, which again indicates

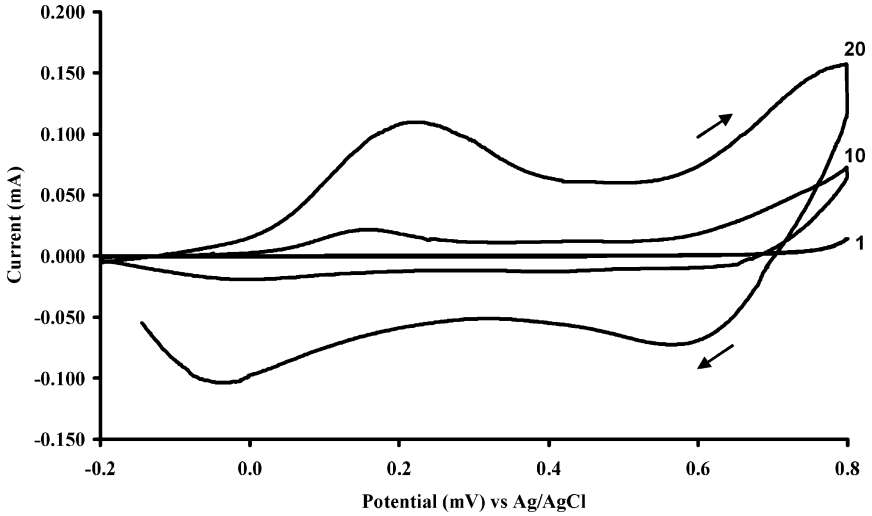

Figure 3. Deposition of conducting polyaniline films by cyclic voltammetry between −0.2 and +0.8 V at 50 mV s^{-1}; current transients are shown for the 1st, 10th, and 20th cycles.

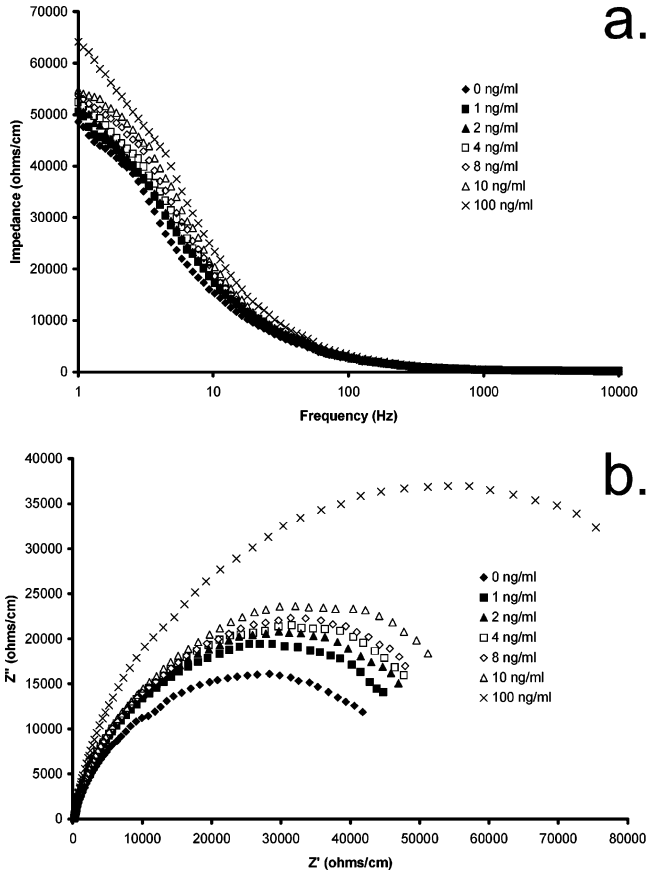

Figure 4. (a) Bode and (b) Nyquist plots of a typical specific anti-MBP-modified electrode exposed to various concentrations of antigen (MBP); for brevity not all concentrations are shown, but just for 0, 1, 2, 4, 8, 10, and 100 ng mL^{-1}.

deposition of insulating material. Therefore, it was decided that changes in impedance at 1 Hz would be used as a measurement of antigen binding.

The impedance spectra consists of two components: the real (Z') component, where the impedance in phase with the ac potential waveform is measured, and the imaginary (Z''), where the impedance is 180° out of phase. It is important to differentiate between the individual components of the total impedance of the cell. Previous work by our group showed that while both the imaginary and real components increase, the increase in the real component dominated the total increase in the impedance.[11,12] Although in this case changes in both real and imaginary components are visible and again the real component is the major component of the total impedance, it was also found (perhaps more importantly) that the real component offers far greater reproducibility in comparison to the imaginary contribution.[11,12]

Figure 5a shows the percentage increase in Z' across a range of antigen concentrations. As can be seen, there is a steady increase in impedance as antigen concentration increases toward a concentration of about 100 ng mL^{-1}. Levels higher than 100 ng mL^{-1} do not appear to lead to even higher impedances, but rather tend toward a plateau, Figure 5a. This possibly indicates saturation of the specific binding sites. Any further changes in impedance beyond this level are likely to be due to nonspecific interactions.

Nonspecific interactions have the potential to interfere with immunosensor performance, leading to erroneously elevated results. This could be addressed by utilization of a second sensor containing either no antibodies or, alternatively, by exploitation of a nonspecific antibody. For this reason an identical set of immunosensors were fabricated utilizing a nonspecific IgG antibody in place of the specific MBP antibody. The nonspecific antibody was a commercial polyclonal IgG antibody, from the same species (mouse) as the specific MBP antibody. This was biotinylated using an identical protocol and then incorporated into the sensor using identical conditions, buffers, concentrations, etc. as utilized for the specific antibody electrodes. Whereas specific binding of MBP will only occur when the anti-MBP antibody is present, electrodes fabricated using a nonspecific antibody should undergo the same nonspecific binding events as those fabricated using specific antibodies. It therefore follows that utilization of both types of electrodes followed by simple subtraction of nonspecific electrode response from those of the specific electrodes should allow the nonspecific responses to be cancelled out.

Results for the nonspecific IgG electrodes were obtained in exactly the same manner as for the specific electrodes, and the calibration plot for these measurements is shown within Figure 5b. As can clearly be seen, there is a much lower response for

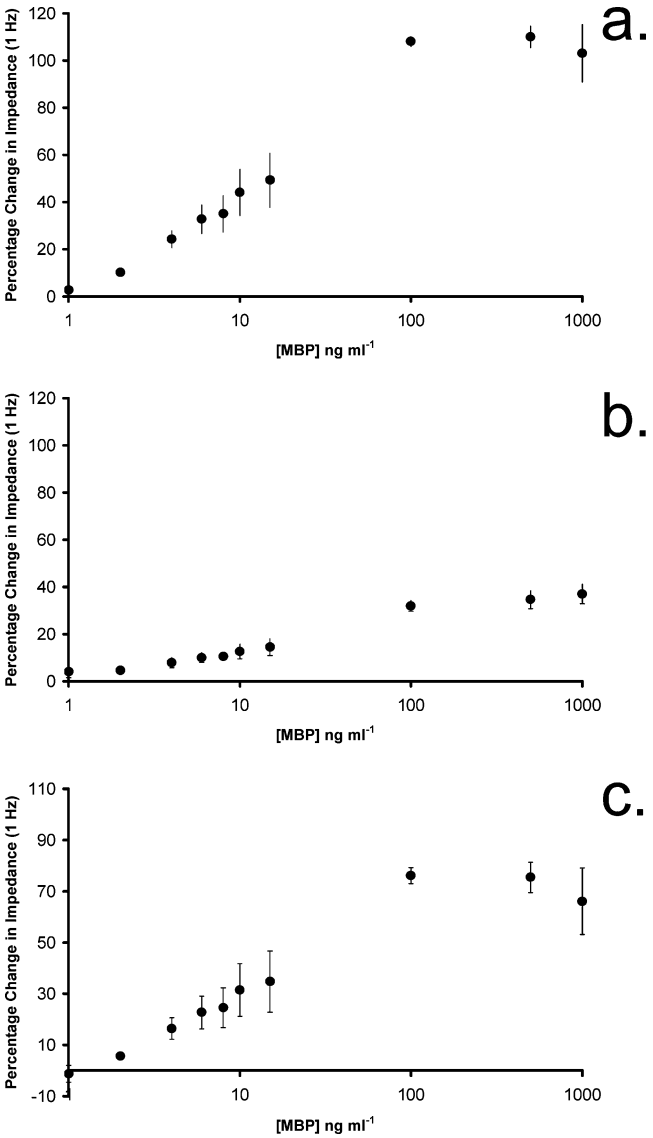

Figure 5. Calibration curves showing the increase in the real component of impedance at 1 Hz for (a) specific anti-MBP-modified electrodes exposed to varying concentrations of antigen (MBP), (b) IgG-modified electrodes exposed to antigen under identical conditions, and (c) corrected calibration curves where the nonspecific response has been subtracted from the specific response (curve a − curve b). All data points are means for the responses of three electrodes; error bars give a measure of the reproducibility of the system.

the nonspecific antibody, showing that although there are nonspecific interactions, between the concentration ranges of 1−100 ng mL^{-1}, they comprise a minor component of the detected response.

Once the nonspecific responses have been subtracted (Figure 5a − Figure 5b), a corrected plot (Figure 5c) shows the calibration curve for the corrected sensor response. Between a concentration range of 1−100 ng mL^{-1}, there is a near linear correlation of the corrected impedance change with the log of concentration (R^2 = 0.976). Between the lower range of 1−15 ng mL^{-1}, the correlation of the impedance change with the log of concentration is further improved (R^2 = 0.990). The limit of detection of this system was found to be approximately 1 ng mL^{-1}, based on a multiple of 3× the standard deviation of the baseline samples—and combined with the good linear response, indicates that we have developed a sensor with good performance within the required range of detection for MBP.

As yet we have not attempted to either reverse the antibody−antigen binding process or remove the antibody and replace it with fresh protein. In view of the low potential unit cost of the electrodes it would be simpler just to use sensors as single-use devices. However, for this to be feasible there must be both good sensor-to-sensor and batch-to-batch reproducibility. We have found that repeated runs on the same electrode give reproducible results with RSDs < 2%. We have also determined the electrode-to-electrode reproducibility of responses to have RSDs < 5% variability in a series of trials.

CONCLUSIONS

We have demonstrated the construction of an immunosensor for the MBP using a combination of screen-printed electrodes coated with conducting polyaniline and an immobilized polyclonal antibody. Interrogation of the electrodes by ac impedance demonstrated the detection of the antigen. Linear correlation of the impedance change with the log of concentration (R^2 = 0.977) was observed between concentrations of 1−100 ng mL^{-1}. A similar logarithmic relationship was observed in our earlier work with ciprofloxacin immunosensors.[12]

Further work utilizing samples of cerebrospinal fluid with various levels of MBP will be undertaken, and it is expected that the use of a dual-antibody (specific and nonspecific) electrode system should allow subtraction of any nonspecific binding events to allow the detection of MBP levels in "real" samples. These studies will be reported in a future publication.

One major drawback associated with immunosensors is the strength of the antibody/antigen binding which can render the interaction essentially irreversible. This would lead to the sensor rapidly becoming saturated upon multiple usage, a process which would be very difficult to reverse by simple washing. The use of inexpensive screen-printed electrodes as a template for these sensors will allow for the production of simple and, more importantly, inexpensive single-use immunosensors, thereby eliminating the need for washing and reuse of sensors.

Commercialization of this research is proceeding through a new spin-out company ELISHA Systems Ltd., which is in the process of developing a range of label-less immunosensors for a number of different antigens.

ACKNOWLEDGMENT

This work, including funding for G.T., G.-Z.G., and F.D., has been supported by the European Community Framework VI NMP2-CT-2003-505485, "ELISHA" contract.

Received for review October 8, 2007. Accepted December 21, 2007.

AC702070E

Detection of Fluoroquinolone Antibiotics in Milk via a Labelless Immunoassay based upon an AC Impedance Protocol

Georgios Tsekenis[1], Goulielmos-Zois Garifallou[1], Frank Davis[1], Paul A. Millner[2] Daniel G. Pinacho[3], Francisco Sanchez-Baeza[3], M.-Pilar Marco[3], Tim D. Gibson[4] and Séamus P. J. Higson[*1].

[1]Cranfield Health, Cranfield University, Silsoe, Beds, MK45 4DT, UK.

[2]School of Biochemistry and Molecular Biology, University of Leeds, Leeds, LS2 9JT, UK.

[3]Applied Molecular Receptors Group (AMRg). Department of Biological Organic Chemistry. IIQAB-CSIC. Jorge Girona, 18-26, 08034-Barcelona, Spain

[4]T and D Technology, Wakefield, W. Yorks, WF3 4AA, UK.

[*].Corresponding author. Fax (+44) 01525 863433, email s.p.j.higson@cranfield.ac.uk

Abstract.

This paper describes the construction of a labeless immunosensor for the antibiotic ciprofloxacin in milk and its interrogation using an AC impedance protocol. Commercial screen-printed carbon electrodes were used as the basis for the sensor. Polyaniline was electrodeposited onto the sensors and then utilised to immobilise a biotinylated antibody for ciprofloxacin using classical avidin-biotin interactions.

Electrodes containing the antibodies were exposed to solutions of antigen in milk and interrogated using an AC impedance protocol. The faradaic component of the impedance of the electrodes was found to increase with increasing concentration of antigen. Control samples containing a non-specific IgG antibody were also studied but found to display large non-specific responses, probably due to the antibody binding some of the large number of components found in milk. Control sensors however could be fabricated using antibodies specific for species not found in milk. Calibration curves could be obtained by subtraction of the responses for specific and control antibody based sensors, thereby eliminating the effects of non-specific adsorption of antigen. Sensors exposed to ciprofloxacin in milk gave increases in impedance whereas ciprofloxacin in phosphate buffer lead to decreases, indicating the sensors can both detect and differentiate between free and chelated antigen.

Keywords: fluoroquinolone, ciprofloxacin, AC impedance, immunosensor, polyaniline.

INTRODUCTION

The principle of immunoassays was first established by Yalow and Berson[1] in 1959 and led to the development of the widely used radioimmunoassay technique, initially to determine insulin-binding antibodies in human serum, using samples obtained from subjects that had been treated with insulin. Independently within unconnected work, Clark and Lyons[2] in 1962 developed the concept of a biosensor. The original methodology involved immobilising enzymes on the surface of electrochemical sensors so as to exploit the selectivity of enzymes for analytical purposes. Although the field has undergone continual technological developments over the last forty years, the basic idea has remained virtually unchanged since the original design.

The incorporation of antibodies into conducting polymer films was first reported[3] in 1991. Polypyrrole films were galvanostatically polymerised onto a platinum wire substrate. When grown in the absence of a counterion, a poor polymeric film (both in appearance and electrochemical properties) was formed, suggesting that the presence of a counterion was necessary for the polymerisation process to be successful. Anti-human serum albumin (anti-HSA) could be incorporated into the film with amino acid analysis of the resulting polymer using a leucine marker determining that approximately 0.1% w/v (0.2 μg) of the antibody was incorporated into the matrix. Exposure of the pyrrole anti-HSA electrode a to 50 μg ml^{-1} HSA solution for ten minutes led to the formation of a new reduction peak at a potential of approximately +600mV vs. Ag/AgCl. This peak increased in magnitude after a further thirty minutes in the same solution – suggesting that this could be due to an antibody/antigen interaction with the polymer. Further work by the same group gave rise to reports of a reversible real-time immunosensor[3]. Other early work utilised a pulsed amperometric detection technique for other analytes, including p-cresol[4], thaumatin[5] and polychlorinated biphenyls[6]. Since this early work there has been burgeoning interest in the development of electrochemical immunosensors - as detailed in several recent reviews[7-9].

Antibody-antigen interactions are by their very nature complex and it follows that the affinity reaction must be only minimally perturbed by the fabrication procedure to allow the immunosensors to display reproducible response characteristics. Previously within our group we have shown that up to 2-3 μg antibodies for BSA and digoxin may be successfully incorporated into conducting polymer films by entrapment in a growing polypyrrole film with no detrimental effect to antibody activity[10]. Electrochemical interrogation of these films demonstrated selective interactions with the target antigens. Further work utilised an AC impedance protocol[11] as the method of interrogation for these films - and led to the development of immunosensors for digoxin and bovine serum albumin. Later work by our group studied approaches for immobilisation of antibodies onto polyaniline coated screen-printed carbon electrodes utilising a classical avidin-biotin chemistry. This enabled the construction of immunosensors for the fluoroquinolone antibody ciprofloxacin[12] in buffer solutions. We have also demonstrated selective immunosensors for myelin basic protein[13], prostate specific antigen[14] and the stroke marker proteins neuron specific enolase[15] and S-100 [β][16].

Fluoroquinolones are members of the quinolone family of broad-spectrum antibiotics and comprise the majority of quinolones in clinical use, the name fluoroquinolone deriving from the fact they have a fluoro group attached to the central ring system. They have excellent tissue penetration which makes them extremely

effective against bacteria that grow intracellularly such as salmonella, leading to widespread use within adult patients[17]. One of this group is ciprofloxacin (Figure 1) which is a broad-spectrum antibiotic active against many bacteria including anthrax [18]. Many of these fluoroquinolones are added to farm animal feed since they can lead to greater and more rapid weight gain. Unfortunately the effect of this is thought to have enabled the rise of resistant species of bacteria[17].

The monitoring of fluoroquinolones within both food and the environment is important since these antibiotics have potential health and environmental damaging effects. Ciprofloxacin concentrations in hospital wastewaters were monitored and correlations with DNA damaging effects made[19]. HPLC techniques have been utilised to measure levels of ciprofloxacin in hospital outflow water[19] and found levels between 0.7-124.5 ng ml^{-1} and shown to display genotoxicity at levels as low as 5.2 ng ml^{-1}. Similar work utilised LC/MS/MS methods[20] and found wastewater ciprofloxacin levels between 0.031-5.6 ng ml^{-1} (even after treatment) with a limit of detection of 0.030 ng ml^{-1}. Levels *in vivo* have also been widely studied with the therapeutic ranges typically being between 0.57-2.30 μg ml^{-1} in serum and 1.26-4.03 μg g^{-1} in tissue[21].

A horseradish peroxidase based biosensor[18] has been developed for the detection of ciprofloxacin due to its inhibition of the oxidation of catechol. Linear responses were obtained between 0.02-65 μM with the limit of detection being 0.4 nM, however other piperazine based compounds could potentially interfere with this determination. We have within earlier work developed a labeless immunosensor for ciprofloxacin as a typical fluoroquinolone which utilises screen-printed carbon electrodes, modified by deposition of first, a conducting polymer (polyaniline) which is then modified with biotinylating reagent[12]. Complexion of the immobilised biotin with avidin allows the further binding of biotinylated antibodies via standard avidin-biotin interactions (Figure 2). The resultant electrodes are capable of detecting low levels of the antigen – ciprofloxacinin dissolved in phosphate buffer[12]. However for an immunosensor to be of practical use it must be capable of the analysis of the substrate within a wide range of matrices. Since there is a wide use of fluoroquinonolones within the animal industry, it was decided to investigate whether ciprofloxacin can be detected in milk. The European Union has set a maximum residue limit of 100 ng ml^{-1} for enrofloxacin plus ciprofloxacin in milk[22]. Previous studies have utilised techniques such as HPLC to detect various fluoroquinolone antibodies in bovine milk[22] with a detection limit of 3 ng ml^{-1} for ciprofloxacin and LC with luminescence detection[23] to measure ciprofloxacin in milk with a linear range of 8-3500 ng ml^{-1} and a detection limit of 3 ng ml^{-1}. A number of ELISA based tests[24,25] have also been developed to detect fluoroquinolones in milk with detection limits of several ng ml^{-1}. Recent work has also described the construction of a DNA based sensor which combined with a surface plasmon resonance method allows quantification of enrofloxacin between 3-20 μg ml^{-1} in milk[26]. An immunosensor for ciprofloxacin based on polypyrrole films combined with an AC impedance technique[27] has also been described with sensitivities as low as 10 pg ml^{-1}.

RESULTS AND DISCUSSION

Deposition of polyaniline

The voltammograms for the deposition of polyaniline/DNA were as found in earlier work[12,13] and imply a steady in situ formation of polymer at the electrode surface. As the number of scans increases, peaks appear between +350-400 mV vs Ag/AgCl corresponding to the oxidation and reduction of surface bound polyaniline,

with the current passed increasing with number of scans due to the increase in polyaniline thickness and coverage of the electrode.

Impedance profiles of the electrodes

A series of Bode (Figure 4a) and Nyquist curves (Figure 4b) were obtained for the sensors after exposure to various levels of ciprofloxacin in PBS. As can be seen, there is a steady increase in the impedance of the electrodes with increasing antigen concentration. This was unexpected since our work on ciprofloxacin in phosphate buffer clearly demonstrates that binding of the antigen leads to a drop in impedance. As can be seen, we see much larger increases in impedance at the lower frequencies. Therefore it was decided that changes in impedance at 1 Hz would be used as a measurement of antigen binding.

The Nyquist plots display the two components of the impedance spectra, the real (Z') component where the impedance in phase with the AC potential waveform is measured and the imaginary (Z'') where the impedance is 180^{o} out of phase. Both of the individual components contribute to the total impedance of the cell. However it is important to differentiate between them so that the capacitive and Faradaic components of the composite impedimetric response may be identified and quantified.

In this system, the Z' (real) component of the impedance can be seen to steadily increase with decreasing frequency. In the baseline plot the Z'' (imaginary) component increases to a maximum value before falling as the frequency approaches 1 Hz. Similar behaviour appears to occur as antigen bending increases except that for the higher concentrations of ciprofloxacin the maximu value is beyond the range of our frequency range This type of impedance spectrum is indicative of a surface-modified electrode system where the electron transfer is slow and the impedance is controlled by the interfacial electron transfer[28].

In previous pieces of work within our group we have demonstrated that although both the imaginary and real components increase, the increase in the real component dominates the total increase in the impedance[11-13]. Although in this case and in previous work[11-13] changes in both real and imaginary components are visible, once again the real component is the major component of total impedance and perhaps more importantly we have repeatedly found that the real component offers far greater reproducibility in comparison to the imaginary contribution.

Figure 5a shows the percentage increase in Z' (measured at 1 Hz) across a range of antigen concentrations. As can be seen, there is a steady increase in the real component of impedance as antigen concentration increases up to a concentration of about 100 ng ml^{-1}, above which concentration there is a tend towards a plateau, possibly indicating saturation of the specific binding sites. It is possible that any further changes in impedance beyond this level could simply be due to non-specific interactions. Between a concentration range of 1-100 ng ml^{-1}, there is a near linear correlation of the impedance change with the $\log_{10}$ of concentration (R^2=0.96).

Non-specific interactions could potentially interfere with immunosensor performance. We have previously described the utilisation of control electrodes containing a non-specific IgG antibody[11-13] These permit the subtraction of unspecific interactions from the specific binding response and also may help to increase the stability and reliability of these sensors when applied to complex mixtures such as milk, other foodstuffs or clinical samples. Therefore an identical set of immunosensors were fabricated utilising a non-specific IgG antibody in place of the specific ciprofloxacin antibody. Results for these electrodes were obtained in exactly the same way and the calibration plot is shown (Figure 5b). As can be seen, there is a

very high decrease in impedance for the non-specific antibody. However further experiments showed that these results are a function of the time of exposure rather than ciprofloxacin concentration. The explanation for this is that since milk is such a complex mixture of components, some of these specifically bind to certain fractions of the IgG. In order to test this theory, another set of control electrodes were utilised, where instead of non-specific IgG antibody, a specific antibody for an antigen not found in milk was utilised. Figure 5c shows the results upon exposure to ciprofloxacin in milk for electrodes fabricated using a specific antibody for prostate specific antigen, used in earlier work[14]. Results for these electrodes showed that although there are non-specific interactions, between the ranges of 0.1-100 ng ml^{-1}, they comprise a minor component of the detected response and in fact lead to a drop rather than a gain in impedance, as was found within our earlier work on ciprofloxacin in PBS[12]. Figure 5d shows the subtracted responses (5a-5c). As can be seen this demonstrates linearity between the response and the $\log_{10}$ of ciprofloxacin concentration between 0.1-100 ng ml^{-1} (R^2=0.98). Above 100 ng ml^{-1} the receptors appear to be saturated.

Figure 5d also displays our earlier results for ciprofloxacin in PBS[12] overlaid over those for milk. As can be seen, the results are very similar in that they give linear ranges with very similar gradients in the region 0-100 ng ml^{-1} and above 100 ng ml^{-1} appear to be saturated. However they are of opposite nature; adsorption of ciprofloxacin from milk gives an increase in Z' whereas from PBS a decrease is observed. It is reported however that in the presence of calcium ions, many fluoroquinolone antibiotics, including ciprofloxacin readily form calcium chelate complexes[29,30]. These complexes are usually dimeric in nature with two ciprofloxacin units complexed to a single calcium ion[29]. It appears from our results that the antibody is capable of binding ciprofloxacin in either its free or chelated form over similar concentration ranges, as shown by responses compared to control samples. However the great structural differences between the free and complexed forms of the antigen leads to different effects on the AC impedance results. The effects of adsorption of various moieties on the AC impedance behaviour is highly complex and not well understood. For example in previous work by our group on DNA based sensors, adsorption of complementary DNA stands has been shown to lead to drops in the AC impedance of our electrodes whereas adsorption of non-complementary DNA leads to an increase[31,32]. This means that it is possible to differentiate between complexed and free ciprofloxacin. This is of interest since the FDA recommend that ciprofloxacin is not taken with dairy products, calcium fortified juices or calcium containing antacids[33] as they may reduce adsorption of the drug.

CONCLUSIONS

We have demonstrated the construction of an immunosensor for the antibiotic ciprofloxacin using a combination of screen-printed electrodes coated with conducting polyaniline and immobilised antibodies. The electrodes were then exposed to solutions of the antigen in milk. Interrogation of the electrodes by AC impedance demonstrated the detection of the antigen. Linear increases of the impedance change with the $\log_{10}$ of concentration (R^2=0.98) was observed between concentrations of 0.1-100 ng ml^{-1}. The sensor not only bound the antigen from PBS or milk but also proved capable of distinguishing from which matrix the ciprofloxacin was adsorbed, possibly due to formation of a dimeric calcium chelated form of the antibiotic in milk. This is especially of interest, since free and chelated ciprofloxacin have very different adsorption characteristics when ingested.

ACKNOWLEDGEMENTS

This work has been supported by the Ministry of Science and Technology (Spain) (Contract numbers AGL2005-07700-C06-01 and NAN2004-09195-C04-04) and by the European Community Framework VI NMP2-CT-2003-505485, "ELISHA" contract. The AMR group is a consolidated Grup de Recerca de la Generalitat de Catalunya and has support from the Departament d'Universitats, Recerca i Societat de la Informació la Generalitat de Catalunya (expedient 2005SGR 00207). DG has a FPI fellowship from the Spanish Ministry of Education.

EXPERIMENTAL

Sodium dihydrogen orthophosphate, disodium hydrogen orthophosphate, sodium chloride, hydrochloric acid, were obtained from BDH (Poole, Dorset, UK). Potassium chloride was obtained from Fisher Scientific UK Ltd, Loughborough, UK. Aniline, polyclonal IgG from human serum, the biotinylation kit (part no. BK101), biotin 3-sulfo-N-hydroxysuccinimide, avidin and bovine serum albumin (BSA) were obtained from Sigma-Aldrich, Gillingham, Dorset, UK. Ciprofloxacin hydrochloride was purchased from UQUIFA (Barcelona, Spain). All water used was obtained from a Purelab UHQ Deioniser (Elga, High Wycombe, UK). Commercial screen-printed carbon electrodes (Figure 3) containing carbon working and counter electrodes and an Ag/AgCl reference electrode were obtained from Parlex Corp Ltd, Isle of Wight, UK. The surface area of the working electrode was 0.2178 cm^2. Semi-skimmed bovine milk was purchased from a local supermarket.

Phosphate Buffered Saline (PBS) at pH 7.4 stock solution was prepared containing 0.14 mol l^{-1} NaH_2PO_4, 0.52 mol l^{-1} Na_2HPO_4 and 0.0051 mol l^{-1} NaCl. Aniline buffer (pH 1-2) was prepared containing 0.5 mol l^{-1} KCl, 0.3 mol l^{-1} HCl and 0.2 mol l^{-1} aniline.

Polyclonal antiserum (As 171) was a gift from AMRg and was raised against 1-(3-mercaptopropyl)-6-fluoro-7-(piperanicyl)-1,4-dihydro-4-oxo-quinoline-3-carboxylic acid coupled to HCH. The preparation of the immunogen and of the antibodies will be described elsewhere[34]. Monoclonal antibody to prostate specific antigen with sodium azide preservative was supplied by Canag Diagnostics, Ltd. (Gothenburg, Sweden).

For antibody biotinylation the procedure outlined in the BK101 kit was followed (see manufacturers instructions for details). Biotinylated antibodies were kept frozen in aliquots of 200 µl at a concentration of 1 mg ml^{-1} until required.

Cyclic voltammetry (Sycopel Potentiometer, Sycopel Scientific, Tyne & Wear, UK) was utilised to deposit polyaniline films on the carbon electrodes. Screen-printed carbon electrodes were placed in aniline buffer and cycled from -200 mV to +800 mV vs. Ag/AgCl for approximately 20 cycles (occasionally this was varied slightly to ensure the same amount of polyaniline was deposited on each electrode. Deposition was terminated at +800 mV to ensure the polyaniline remained in its conducting form. After deposition electrodes were rinsed in water.

30 µl of biotin-sulfo-NHS (10 mg ml^{-1} in water) was placed on the polymer coated working electrode surface for 24 hours. The sensors were rinsed with copious water and 30 µl of avidin (10 µg ml^{-1} in water) placed on the working electrode for 1 hour followed by rinsing in water. Then 30 µl biotinylated antibody (1 mg ml^{-1} in water) was added followed by rinsing. Finally, non-specific interactions were blocked by BSA (10^{-6} M in PBS); the sensors are ready to use at this point, however, if opted, can be stored in PBS at 4^oC for no longer than 24 hours.

AC impedance measurements were performed using an ACM Auto AC DSP frequency response analyser. Antigen solutions were prepared by initially dissolving ciprofloxacin in PBS, then diluting to the required concentration of antigen in 30ml of milk. A range of concentrations were utilised; we set our minimum level at 0.1 ng ml^{-1} with an upper limit of 10 μg ml^{-1}. The sensors were first interrogated without antigen addition. Following this, each sensor was exposed to the required antigen concentration for 30 minutes, rinsed well with deionised water and then subjected to impedance interrogation in fresh milk. Three electrodes were used for each measurement. A frequency range from 10 kHz to 1 Hz was measured, with a peak amplitude of 5 mV and a DC offset of +400 mV against Ag/AgCl.

REFERENCES

1. Yalow R. S., Berson S. A,, *Nature.* **1959,** *184* 1648-1649.
2. Clark L..C., Lyons I..R., *Ann New York Academy Sci.* **1962,** *102,* 29.
3. John R., Spencer M., Wallace G. G., Smyth M. R., *Anal. Chim. Acta*. **1999,** *249,* 381-385.
4. Barnett D., Laing D. G., Skopec S., Sadik O. A., Wallace G. G., *Anal. Lett*. **1994,** *27,* 2417.
5. Sadik O. A., John M. J., Wallace G. G., Barnett D., Clarke C., Laing D. G., *Analyst*. **1994,** *119,* 1997-2000.
6. Bender S. Sadik O. A., *Environ. Sci. Tech*., **1998,** *32,* 788-797.
7. Rodriguez-Mozaz S., de Alda M. J. L., Barcelo D., *Anal. Bioanal. Chem.,* **2006,** *386,* 1025-1041.
8. Diaz-Gonzalez M., Gonzalez-Garcia M. B., Costa-Garcia A., *Electroanalysis*, **2005,** *17,* 1901-1918.
9. Cosnier S., *Electroanalysis,* **2005,** *17,* 1701-1715.
10. Grant S., Davis F., Pritchard J. A., Law K. A., Higson S. P. J., Gibson T. D., *Anal. Chim. Acta.,* **2003,** *495,* 21-32.
11. Grant S., Davis F.,. Law K. A.,. Barton A. C., Collyer S. D., Higson S. P. J., Gibson, T. D., *Anal. Chim. Acta.,* **2005,** *537,* 163-168.
12. Garifallou G-Z., Tsekenis G., Davis F., Millner P. A., Pinacho D. G., Sanchez-Baeza F., Marco M.-P., Gibson T. D., Higson S. P. J., *Anal. Lett.,* **2007**, *40,* 1412-1442.
13. Tsekenis G., Garifallou G-Z., Davis F., Millner P. A., Gibson T. D., Higson S. P. J., *Anal. Chem.,* **2008,** *in press.*
14. PSA ref
15. NSE ref.
16. S-100 ref.
17. Gendrei, D., Chalumeau, M., Moulin, F., Raymond, J., *Lancet Inf. Dis.,* **2003,** *3*: 537-546.
18. Torriero, A. A. J., Ruiz-Dıaz J. J. J., Salinas, E., Marchevsky, E. J., Sanz, M. I., Raba, J., *Talanta,* **2006,** *69,*: 691-699.
19. Hartmann, A., Golet, E. M., Gartiser, S., Alder, A. C., Koller, T., Widmer, R. M.,. *Ach. Environ. Contam. Toxicol.,* **1999,** 115-119.
20. Batt, A. L., Bruce, I. B., Aga, D. S., *Environ. Poll.,* **2006,** *142,*: 295-302.
21. Licitra, C. M., Brooks, R. G., Sieger, B. E., *Antimicrobial Agents and Chemotherapy,* **1987,** *31,*: 805-807.

22. Hassouan, M., Ballesteros, O., Vilchez, J., Zafra, A., Navalon, A., *Anal. Lett.*, **2007,** 779-791.
23. Rodriguez-Diaz, R. C., Fernandez-Romero, J. M., Aguilar-Caballos, M. P., Gomez-Hens, A., *J. Agric. Food Chem.*, **2006,** 9670-9676.
24. Bucknall, S., Silverlight, J., Coldham, N., Thorne, L., Jackman, R., *Food. Addit. Contam.* **2006,** *20,* 221-228.
25. Duan, J., Yuan, Z. H., *J. Agric. Food Chem.*, **2001,** *49,* 1087-1089.
26. Cao, L. M., Lin, H., Mirsky, V. M., *Anal. Chim. Acta,* **2007**, *589,* 1-5.
27. Ionescu, R. E., Jaffrezic-Renault, N., Bouffier, L., Gondran, C., Cosnier, S., Pinacho, D. G., Marco M. P., Sanchez-Baeza, F. J., Healy, T., Martelet, C., *Biosens. Bioelec,* **2007,** *23,* 549-555.
28. Katz, E., Willner, I., *Electroanalysis*, **2003**, *15,* 913-947.
29. Upadhyay, S. K., Kumar, P., Arora, V., *J. Struct. Chem.*, **2006,** *47,* 1078-1083.
30. Toyoguchi, T., Ebihara, M., Ojima, F., Hosoya, J., Nakagawa, Y., *Biol. Pharm. Bull.*, **2005,** *28,* 841-844.
31. Davis F., Nabok A. V., Higson S. P. J., *Biosens. Bioelec.*, **2004**, *20,* 1531-1538.
32. Davis F., Hughes, M. A., Cossins, A. R., Higson S. P. J., *Anal. Chem.,* **2007,** *79,* 1153-1157.
33. http://www.fda.gov/cder/foi/label/2002/19537s41lbl.pdf
34. Pinacho, D. G., Sanchez-Baeza, F., Marco, M. P., paper in preparation.

LIST OF FIGURES.

Figure 1. Structure of ciprofloxacin.
Figure 2. Schematic of antibody modified electrodes.
Figure 3. Screen-printed carbon electrodes used within this work.
Figure 4 (a) Bode and (b) Nyquist plots of a typical ciprofloxacin-specific antibody modified electrode exposed to ciprofloxacin.
Figure 5. Calibration curves for (a) anti-ciprofloxacin modified electrodes (b) IgG modified electrodes (c) PSA modified electrodes (d) ● corrected calibration curves (curve a – curve c). All data points are averages of three electrodes; error bars give a measure of the reproducibility of the system. Plot (d) also contains for comparison purposes the calibration curve for ciprofloxacin in phosphate buffer previously reported ■ [12].

Fig 1

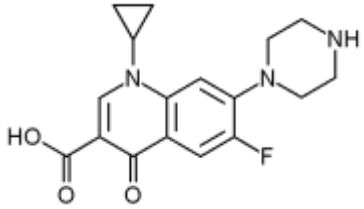
NH
N
N
HO
F
O
O

Fig 2

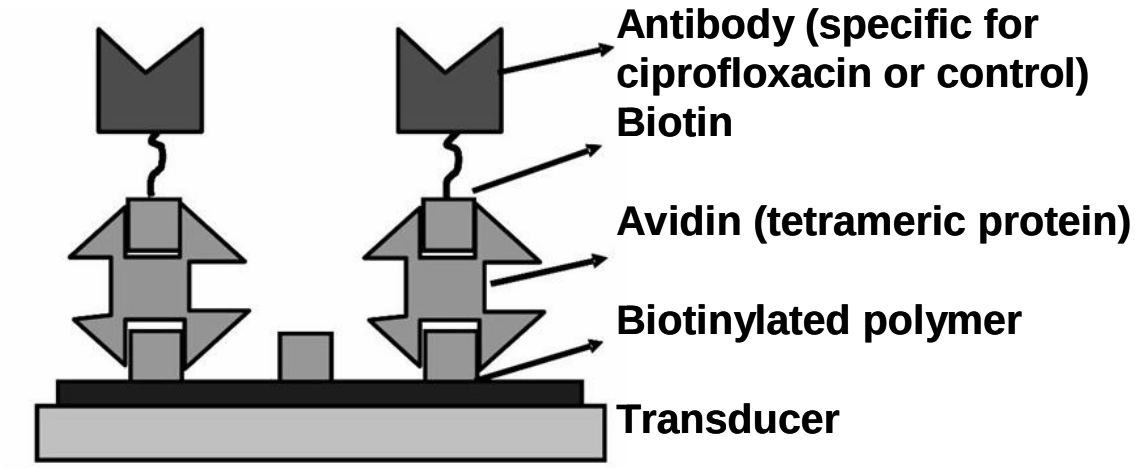
Antibody (specific for ciprofloxacin or control)
Biotin
Avidin (tetrameric protein)
Biotinylated polymer
Transducer

Fig 3

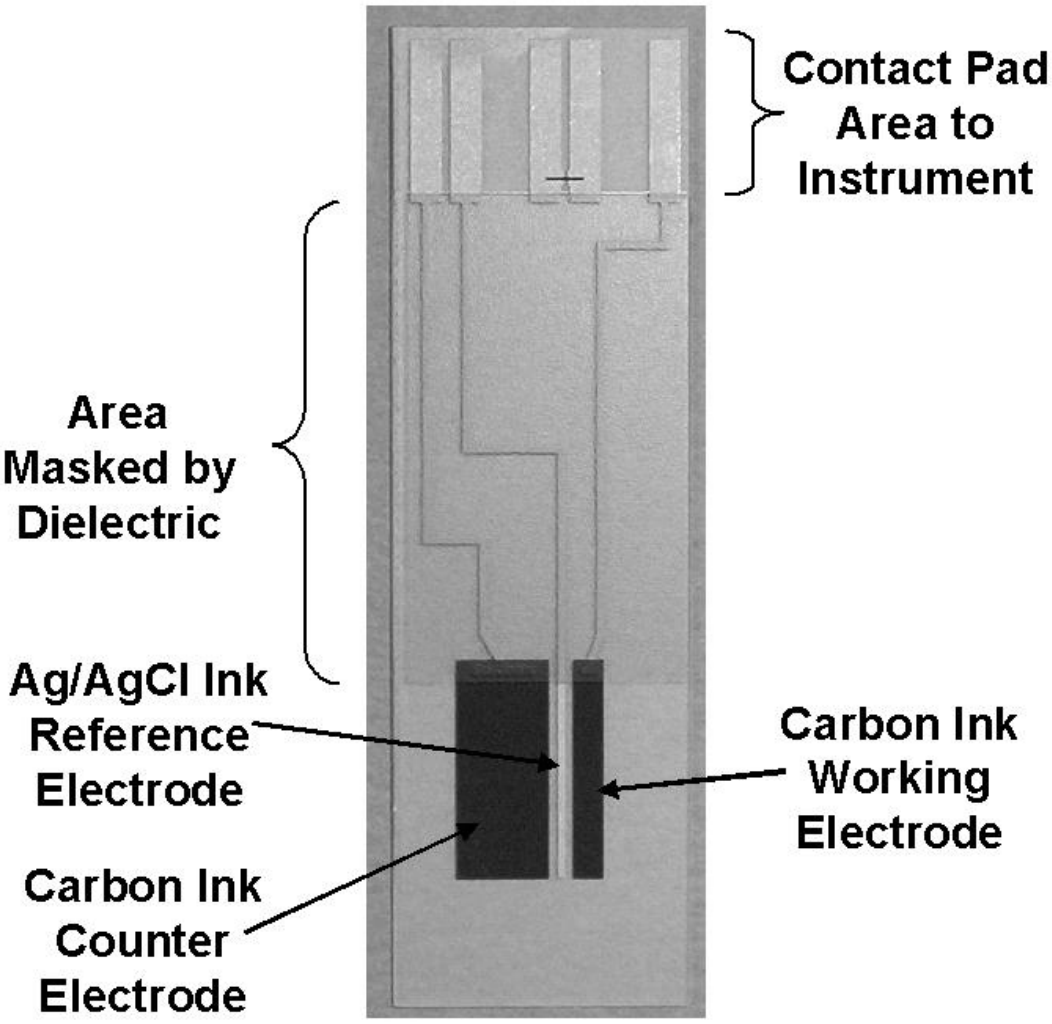
Contact Pad
Area to
Instrument
Area
Masked by
Dielectric
Ag/AgCl Ink
Reference
Electrode
Carbon Ink
Working
Electrode
Carbon Ink
Counter
Electrode

Fig 4

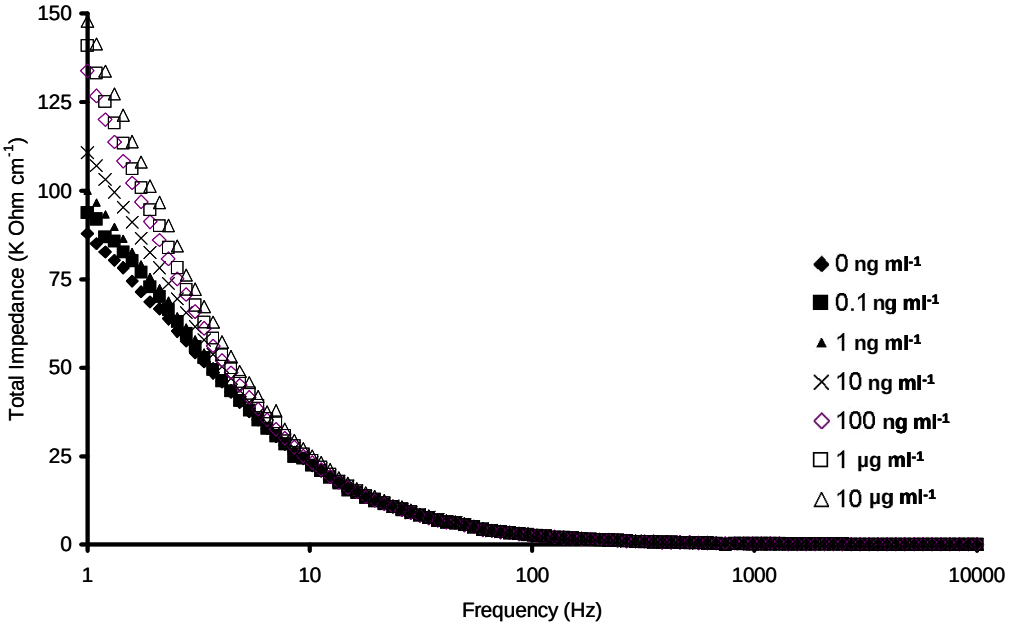
Total Impedance (K Ohm cm-1)
Frequency (Hz)
0 ng ml-1
0.1 ng ml-1
1 ng ml-1
10 ng ml-1
100 ng ml-1
1 µg ml-1
10 µg ml-1

a.

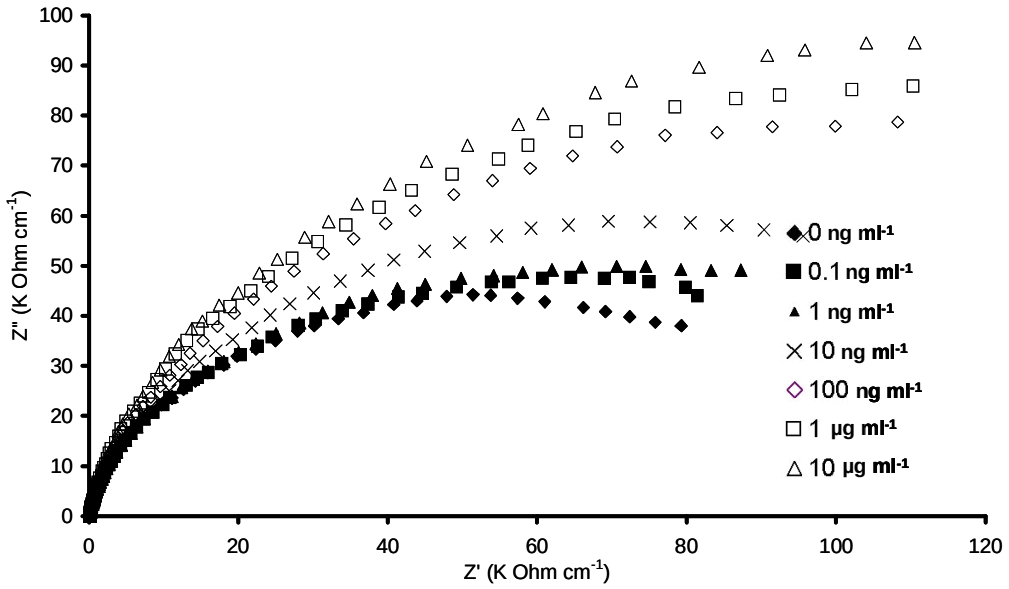
Z'' (K Ohm cm-1)
Z' (K Ohm cm-1)
0 ng ml-1
0.1 ng ml-1
1 ng ml-1
10 ng ml-1
100 ng ml-1
1 µg ml-1
10 µg ml-1

b.

Fig 5.

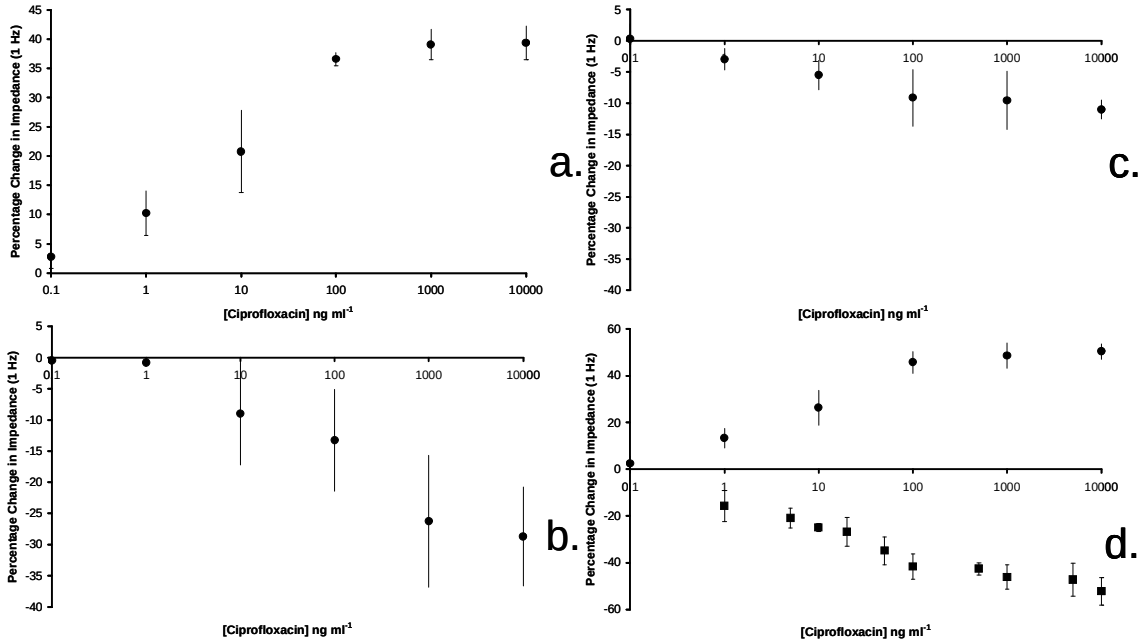
a.
b.
c.
d.
Percentage Change in Impedance (1 Hz)
[Ciprofloxacin] ng ml-1
0.1
1
10
100
1000
10000

Labeless Immunosensor Assays based upon an AC Impedance Protocol

Frank Davis[1], Goulielmos-Zois Garifallou[1], Georgios Tsekenis[1], Paul A. Millner[2] Daniel G. Pinacho[3], Francisco Sanchez-Baeza[3], M.-Pilar Marco[3], Tim D. Gibson[4] and Séamus P. J. Higson[*1].

[1]Cranfield Health, Cranfield University, Silsoe, Beds, MK45 4DT, UK.

[2]School of Biochemistry and Molecular Biology, University of Leeds, Leeds, LS2 9JT, UK.

[3]Applied Molecular Receptors Group (AMRg). Department of Biological Organic Chemistry. IIQAB-CSIC. Jorge Girona, 18-26, 08034-Barcelona, Spain

[4]T and D Technology, Wakefield, W. Yorks, WF3 4AA, UK.

[*].Corresponding author. Fax (+44) 01525 863433, email s.p.j.higson@cranfield.ac.uk

Abstract.

This paper describes the construction of labeless immunosensors for the selective determination of an antigen, of which two immunosensors for ciprofloxacin and myelin basic protein are described in more detail. Commercial screen-printed carbon electrodes were used as the basis for the sensor. Polyaniline was electrodeposited onto the sensors and then utilised to immobilise biotinylated antibodies for ciprofloxacin and myelin basic protein using avidin-biotin interactions.

Electrodes containing the antibodies were exposed to solutions of antigen and the AC impedance of the electrodes measured over a range of frequencies. The faradaic component of the impedance of the electrodes was found to increase with increasing concentration of antigen. Control samples containing a non-specific IgG antibody were also studied and calibration curves obtained by subtraction of the responses for specific and non-specific antibody based sensors, thereby eliminating the effects of non-specific adsorption of antigen.

Introduction

The principle of immunoassays was established in 1959 (Yalow & Berson, 1959) and led to the development of the widely used technique. Later in 1962 the concept of a biosensor was pioneered (Clark & Lyons, 1962). The original methodology was to immobilise enzymes on the surface of electrochemical sensors-assuming that this

would enhance the ability of a sensor to detect specific analytes. This idea has remained virtually unchanged since this original design, however, technological advances have allowed for the expansion of this field of science.

The incorporation of antibodies into conducting polymer films was first reported in 1991 (John *et al* 1991). Anti-human serum albumin (anti-HSA) was incorporated into a polypyrrole film, polymerised onto a platinum wire substrate. When the pyrrole anti-HSA electrode was exposed to 50 μg ml^{-1} HSA for ten minutes, a new reduction peak was observed at a potential of approximately +600mV vs. Ag/AgCl, increasing in magnitude after a further thirty minutes in the same solution This was thought to be due to an antibody/antigen interaction with the polymer. Other work utilised a pulsed amperometric detection technique for other analytes, including p-cresol (Barnett *et al* 1994), Thaumatin (Sadik *et al* 1994) and polychlorinated biphenyls (Bender and Sadik 1994). Since this work there has been a huge increase in the development of electrochemical immunosensors as detailed in several recent reviews (Rodriguez-Mozaz *et al* 2006, Diaz-Gonzalez *et al* 2005, Cosnier 2005).

We have previously shown that up to 2-3 μg antibodies for BSA and digoxin may be successfully incorporated into conducting polymer films by entrapment in a electrochemically deposited polypyrrole film with no detrimental effect to antibody activity (Grant *et al* 2003). Measuring the electrochemical properties of these films demonstrated selective interactions with the target antigens. Further work utilised an AC impedance protocol (Grant *et al* 2005) as the method of interrogation for these films and led to the development of immunosensors for digoxin and bovine serum albumin. The AC protocol consisted of measuring the AC impedance of the system across a frequency range of 1-10000 Hz, peak amplitude 5 mV.

We review within this work our studies on immunosensors for ciprofloxacin (Garifallou *et al* 2007) and myelin basic protein (Tsekenis *et al* 2008). Ciprofloxacin is a member of the fluoroquinolone family of broad-spectrum antibiotics, widely used within adult patients because of excellent tissue penetration which makes them extremely effective against bacteria that grow intracellularly such as salmonella (Gendrei *et al* 2003) and anthrax (Torriero *et al* 2006). The monitoring of fluoroquinolones within both food and the environment is important since these antibiotics have potential health and environmental damaging effects. Ciprofloxacin concentrations in hospital wastewaters were monitored and correlations with DNA

damaging effects made (Hartmann *et al* 1999). Levels of ciprofloxacin in hospital outflow water between 0.7-124.5 ng ml^{-1} were measured using HPLC (Hartmann *et al* 1999) and shown to display genotoxicity at levels as low as 5.2 ng ml^{-1}. Levels *in vivo* have also been widely studied with the therapeutic ranges typically being between 0.57-2.30 μg ml^{-1} in serum and 1.26-4.03 μg g^{-1} in tissue (Licitra *et al* 1987).

Myelin basic protein (MBP) is a cytoplasmic protein important in the process of myelination of nerves in the central nervous system since it comprises the bulk of the main line of compact myelin (Arroyo and Scherer 2000) and up to 30% of the protein content of myelin overall (Baumann and Pham-Dinh 2001). A demyelinating disease is any disease of the nervous system in which the myelin sheath of neurons becomes damaged. This impairs the conduction of signals in the affected nerves, causing impairment in sensation, movement, cognition, or other functions, depending on which nerves are involved. Examples are multiple sclerosis, transverse myelitis, Guillain-Barré syndrome, and progressive multifocal leukoencephalopathy. The normal level of MBP in cerebrospinal fluid is less than 4 ng ml^{-1}, levels between 4 and 8 ng ml^{-1} in cerebrospinal fluid may indicate a chronic breakdown of myelin, or recovery from an acute episode. MBP levels greater than 9 ng ml^{-1} indicate that active demyelination may be occurring.

Ciprofloxacin is usually measured by HPLC and commercial ELISA tests exist for myelin basic protein; Diagnostic Systems Laboratories (Texas) for example manufacture an ELISA which can measure levels of MBP in cerebrospinal fluid in four hours. These methods both require expensive equipment and trained personnel in a laboratory setting. The development of inexpensive single use immunosensors will reduce costs and increase the speed and simplicity of testing.

Results of the study

The sensors described within this work utilise screen-printed carbon electrodes, modified by deposition of first, a conducting polymer (polyaniline) which is then modified with biotinylating reagent. Complexion of the immobilised biotin with avidin allows the further binding of biotinylated antibodies via standard avidin-biotin interactions (Figure 1). Control electrodes containing non-specific IgG have also been fabricated and allow the subtraction out of unspecific interactions.

Polycolonal antibodies for ciprofloxacin, raised in rabbit by the Applied Molecular Receptors Group (AMRg). Department of Biological Organic Chemistry.

University of Barcelona (Garifallou *et al* 2007), and MBP (monoclonal anti-MBP from rat, Sigma catalogue number M9434) incorporated within the immunosensors as described previously (Garifallou *et al* 2007, Tsekenis *et al* 2008). Commercial (Sigma) IgG antibodies from the same species were used as controls. As described within these papers, the sensors were then exposed to various concentrations of antigen in solutions containing a ferri/ferrocyanide redox couple. It was found for both antigens that there were large changes in the faradaic component of the ac impedance spectrum, especially at low frequencies. In both cases, control electrodes were fashioned using a non-specific IgG antibody. The control electrodes provide a measure of the non-specific binding within the system and allow for its subtraction.

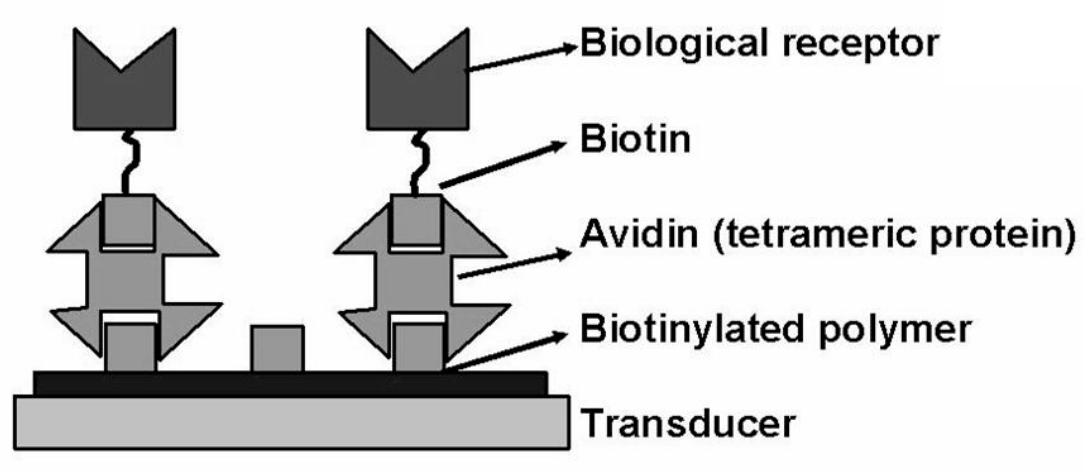

Figure 1. Schematic of antibody modified electrodes.

Figure 2a shows the Nyquist plots for the anti-ciprofloxacin electrodes upon exposure to the antigen. These plots show the increases in faradaic (x-axis) and capacitive (y-axis) impedance with decreasing frequency. As can be seen, there is a steady decrease in the impedance of the electrodes with increasing antigen concentration and it is most pronounced at the lower frequencies. Previous work by our group found that the real component offers far greater reproducibility in comparison to the imaginary contribution. Therefore it was decided that changes in impedance at 1 Hz would be used as a measurement of antigen binding.

Figure 2b shows the percentage decrease in Z' across a range of antigen concentrations. As can be seen, there is a steady decrease in impedance as antigen concentration increases up to a concentration of about 100 ng ml^{-1}, above which concentration there is a tend towards a plateau, possibly indicating saturation of the specific binding sites. Results for the IgG electrodes were obtained in exactly the

same way and the calibration plot is shown (Figure 2c). As can be seen, there is a much lower response for the non-specific antibody, showing that although there are non-specific interactions, between the ranges of 1-100 ng ml^{-1}, they comprise a minor component of the detected response. Figure 2d shows the subtracted responses and this demonstrates linearity between the response and the log_{10} of ciprofloxacin concentration between 1-100 ng ml^{-1} (R^2=0.96). The limit of detection (three times the standard deviation of the baseline) was 1 ng ml^{-1}, suitable for testing environmental levels of ciprofloxacin and with sample dilution, physiological levels.

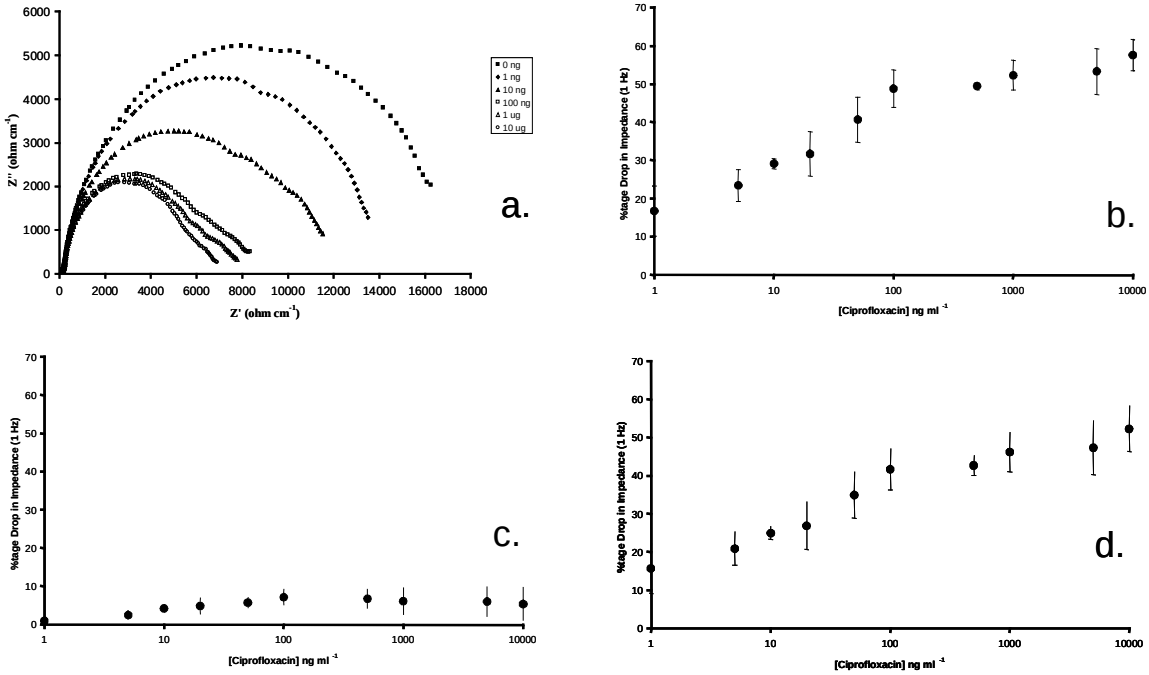

Figure 2. (a) Nyquist plots of a typical antibody modified electrode exposed to various concentrations of antigen, calibration curves for (b) anti-ciprofloxacin modified electrodes (c) IgG modified electrodes (d) corrected calibration curves. Points are means of responses of three electrodes; error bars show standard deviation.

Using an identical method, electrodes containing antibodies to MBP were constructed and interrogated as above. Figure 3a shows the Nyquist plots for this system. In this case exposure to the antigen led to increases in the ac impedance, probably because MBP is a large molecule and binding of this protein leads to formation of a resistive layer at the surface of the electrode. Figure 3b shows there is a steady increase in impedance as antigen concentration increases up to a concentration of about 100 ng ml^{-1}, above which concentration there is a tend towards a plateau, possibly indicating saturation of the specific binding sites. The calibration plot for the control electrodes is shown (Figure 3c) again displaying a much lower response for

the non-specific antibody. Figure 3d shows the subtracted responses and this demonstrates linearity between the response and the $\log_{10}$ of MBP concentration between 1-100 ng ml^{-1} (R^2=0.98). Within the lower range of 1-15 ng ml^{-1} (which covers the physiological range) the correlation of the impedance change with the $\log_{10}$ of concentration is further improved (R^2=0.99). Limit of detection (3 x standard deviation of baseline) was 1 ng ml^{-1}.

Conclusions

We have demonstrated the construction of an immunosensor for the antibiotic ciprofloxacin and for MBP using a combination of screen-printed electrodes coated with conducting polyaniline and an immobilised antibody. Interrogation of the electrodes by AC impedance demonstrated the detection of the antigen. Linear correlation of the impedance change with the $\log_{10}$ of antigen concentration was observed between concentrations of 1-100 ng ml^{-1}. Commercialisation of this research is proceeding through a new spin-out company ELISHA Systems Ltd., who are developing a range of labeless immunosensors for a number of different antigens.

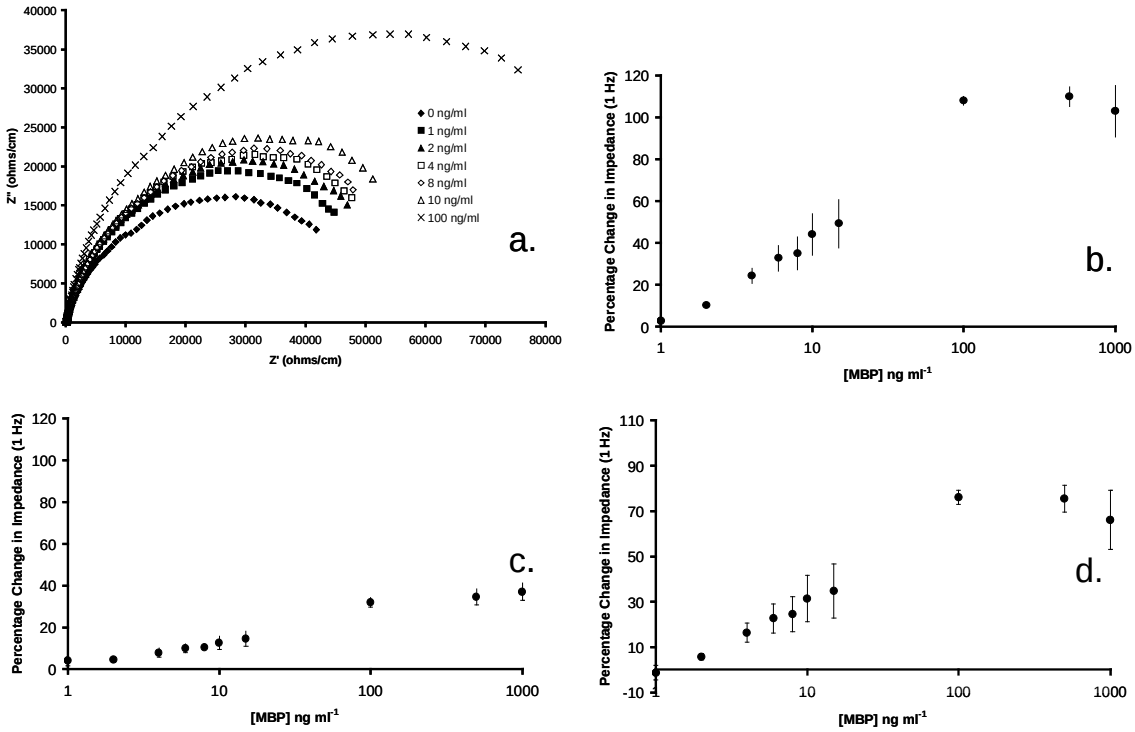

Figure 3. (a) Nyquist plots of a anti-MBP modified electrode exposed to various concentrations of MBP, calibration curves for (b) anti-MBP modified electrodes (c) IgG modified electrodes (d) corrected calibration curves. Points are means of responses of three electrodes; error bars show standard deviation.

REFERENCES

Arroyo E. G., Scherer S. S., 2000, *Cell Biol.* 113, 1-18.

Barnett, D. Laing, D. G. Skopec, S. Sadik, O. A. Wallace, G. G. 1994, *Anal. Lett*. 27: 2417-2429.

Baumann N., Pham-Dinh D., 2001, *Physiol. Rev.*, 81, 871-927.

Bender, S. Sadik, O. A. 1998, *Environ. Sci. Tech*., 32: 788-797.

Clark, L.C and Lyons, I.R. 1962, *Ann New York Academy Sci*. 102: 29.

Cosnier, S., 2005, *Electroanalysis*, 17: 1701-1715.

Diaz-Gonzalez, M., Gonzalez-Garcia, M. B., Costa-Garcia, A. 2005*Electroanalysis*, 17: 1901-1918.

G-Z. Garifallou G. Z., Tsekenis G., Davis F., Millner P. A., Pinacho D. G., Sanchez-Baeza F., Marco M.P., Gibson T. D., Higson S. P. J., 2007 *Anal. Lett.*, 40, 1412-1442.

Gendrei, D., Chalumeau, M., Moulin, F., Raymond, J., 2003, *Lancet Inf. Dis.*, 3: 537-546.

Grant, S., Davis, F.,. Pritchard, J. A., Law, K. A.,. Higson S. P. J.,. Gibson, T. D. 2003, , *Anal. Chim. Acta.*, 495: 21-32.

Grant, S., Davis, F.,. Law, K. A.,. Barton, A. C., Collyer, S. D., Higson S. P. J.,. Gibson, T. D. 2005, *Anal. Chim. Acta.*, 537: 163-168.

Hartmann, A. Golet, E. M. Gartiser, S. Alder, A. C. Koller, T. Widmer, R. M. 1999, *Ach. Environ. Contam. Toxicol.*, 115-119.

John, R. Spencer, M. Wallace, G. G. Smyth, M. R. (1991) *Anal. Chim. Acta*. 249: 381-385.

Licitra, C. M., Brooks, R. G., Sieger, B. E. (1987), *Antimicrobial Agents And Chemotherapy*, 31: 805-807.

Rodriguez-Mozaz, S., de Alda, M. J. L., Barcelo, D. 2006, *Anal. Bioanal. Chem.*, 386: 1025-1041.

Sadik, O. A. John, M. J. Wallace, G. G. Barnett, D. Clarke, C. Laing, D. G. (1994), *Analyst*. 119: 1997-2000.

Tsekenis G., Garifallou G-Z., Davis F., Millner P. A., Gibson T. D., Higson S. P. J., 2008, *Anal. Chem.*, 20: 2058-2062.

Torriero, A. A. J., Ruiz-Dıaz J. J. J., Salinas, E., Marchevsky, E. J., Sanz, M. I., Raba, J., 2006, *Talanta*, 69: 691-699.

Yalow, R. S. Berson, S. A 1959, *Nature*. 184: 1648-1649.

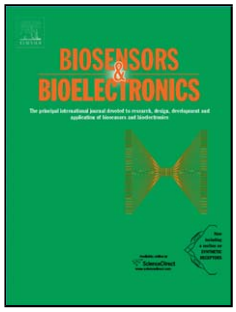

Title: Labeless AC Impedimetric Antibody Based Sensors with pg ml-1 Sensitivities for Point-Of-Care Biomedical Applications

Authors: Andrew C. Barton, Goulielmos-Zois Garifallou, Frank Davis, Stuart D. Collyer, Georgios Tsekenis, Paul A. Millner, Tim D. Gibson, Séamus P.J. Higson

PII: S0956-5663(08)00255-8
DOI: doi:10.1016/j.bios.2008.06.001
Reference: BIOS 2774

To appear in: *Biosensors and Bioelectronics*

Received date: 4-3-2008
Revised date: 16-4-2008
Accepted date: 4-6-2008

Please cite this article as: Barton, A.C., Garifallou, G.-Z., Davis, F., Collyer, S.D., Tsekenis, G., Millner, P.A., Gibson, T.D., Higson, S.P.J., Labeless AC Impedimetric Antibody Based Sensors with pg ml-1 Sensitivities for Point-Of-Care Biomedical Applications, *Biosensors and Bioelectronics* (2007), doi:10.1016/j.bios.2008.06.001

Labeless AC Impedimetric Antibody Based Sensors with pg ml^{-1} Sensitivities for Point-Of-Care Biomedical Applications.

Andrew C. Barton[1], Goulielmos-Zois Garifallou[1], Frank Davis[1], Stuart D. Collyer[2], Georgios Tsekenis[1], Paul A. Millner[3], Tim D. Gibson[4] and Séamus P. J. Higson[*1].

[1]Cranfield Health, Cranfield University, Silsoe, Beds, MK45 4DT, UK.

[2]Microarray Ltd, PO Box 88, Manchester, M60 1QD, UK.

[3]School of Biochemistry and Molecular Biology, University of Leeds, Leeds, LS2 9JT, UK.

[4]T and D Technology Ltd, Wakefield, W. Yorks, WF3 4AA, UK.

[*]Corresponding author. Fax (+44) 01525 863433, email s.p.j.higson@cranfield.ac.uk

Abstract.

This paper describes the development and characterisation of labeless immunosensors for (a) the cardiac drug digoxin and (b) bovine serum albumin (BSA). Commercial screen-printed carbon electrodes were used as the basis for the sensors. Two methods were used to immobilise antibodies at the electrode surface. Aniline was electropolymerised onto these electrodes to form a thin planar film of conductive polyaniline; the polyaniline film was then utilised as a substrate to immobilise biotinylated anti-digoxin using a classical avidin-biotin affinity approach. As an alternative approach, poly(1,2-diaminobenzene) was electrodeposited onto the carbon electrodes - and this modified surface was then sonochemically ablated to form an array of micropores. A second electropolymerisation step was then used to co-deposit

conductive polyaniline along with antibodies for BSA within these pores to produce a microarray of polyaniline protrusions with diameters of several μm containing entrapped anti-BSA.

The resulting antibody grafted electrodes were interrogated using an AC impedance protocol before and following exposure to digoxin or BSA solutions, along with control samples containing a non-specific IgG antibody. The impedance characteristics of both types of electrode were changed by increasing concentrations of antigen up to a saturation level. Calibration curves were obtained by subtraction of the non-specific response from the specific response, thereby eliminating the effects of non-specific adsorption of antigen. Both the use of microelectrode arrays and affinity binding protocols showed large enhancements in sensitivity over planar electrodes containing entrapped antibodies and gave similar sensitivities to our other published work using affinity based planar electrodes. Detection limits were of the order of 0.1 ng ml^{-1} for digoxin and 1.5 ng ml^{-1} for BSA.

Keywords. ac impedance, immunosensor, polyaniline, microelectrode, BSA, digoxin.

1. Introduction

The principle of immunoassays was first established in 1959 (Yalow and Berson 1959) and their work led to the development of the widely used radioimmunoassay to determine insulin-binding antibodies in human serum, using samples obtained from subjects that had been treated with insulin. Later, within unconnected work (Clark and Lyons 1962), the concept of a biosensor was pioneered. These workers exploited the selectivity of enzymes for analytical purposes via a methodology which involved immobilising enzymes on the surface of electrochemical sensors and measuring the oxygen consumption by the glucose oxidase enzymatically catalysed oxidation of glucose. This basic idea has remained virtually unchanged since the original design, although the field has undergone continual technological developments over the last forty years.

The incorporation of antibodies into conducting polymer films was first reported (John *et* al 1991) in 1991. Pyrrole was galvanostatically polymerised onto a platinum wire substrate from a solution which contained anti-human serum albumin (anti-HSA). The antibody was incorporated into the polypyrrole film and the pyrrole anti-HSA electrode found to give a specific electrochemical response to HSA. Since this early work there has been burgeoning interest in the development of electrochemical immunosensors - as detailed in several recent reviews (Rodriguez-Moraz *et al* 2006, Diaz-Gonzales *et al* 2005, Cosmier 2005).

Antibody-antigen interactions are by their very nature complex and it is thought necessary that the affinity reaction be minimally perturbed by the fabrication procedure to give reproducible response characteristics. We have previously shown that up to 2-3 μg antibodies for BSA and digoxin may be successfully incorporated

into conducting polymer films by entrapment in a growing polypyrrole film with no detrimental effect to antibody activity (Grant *et al* 2003). Electrochemical interrogation of these films demonstrated selective interactions with the target antigens. Further work utilised an AC impedance protocol (Grant *et al* 2005) as the method of interrogation for these films - and led to the development of immunosensors for digoxin and bovine serum albumin. Later work by our group utilised polyaniline coated screen-printed planar carbon electrodes as substrates for immobilisation of antibodies utilising the classical avidin-biotin interaction. This enabled the construction of immunosensors for the fluoroquinolone antibody ciprofloxacin (Garifallou *et al* 2007) and myelin basic protein - a marker for conditions such as stroke and multiple sclerosis (Tsekenis *et al* 2008).

Our group has also pioneered the development of sonochemically fabricated microarrays of conductive polymers (Higson 1996), the schematic for the formation of which is shown within figure 1. Poly(1,2-diaminobenzene) can be electrodeposited on a variety of conductive surfaces to form an insulating layer[15]. We have utilised commercial screen printed 3 electrode strips as the basis for these sensors. The working electrodes are initially coated with a thin film (50-70 nm thickness) of an insulating polymer formed by the electrochemical deposition of 1,2-diaminobenzene (Myler *et al* 1997). An advantage of this process is that it is self-limiting, making it highly reproducible. Sonochemical ablation is then used to ablate or "drill" holes in this insulating material with diameters of 0.1 to several microns and a density of up to 120000 pores cm^{-2}. We have used these micropore arrays for the detection of aqueous chlorine (Davis *et al* 1997). The arrays may be used as substrates for further electropolymerisation reactions, generating arrays of conducting polyaniline protrusions, consisting of just the polymer or alternatively containing entrapped

biological species (Barton *et al* 2004). Previous work within our group has utilised these microarrays containing entrapped enzymes for the amperometric detection of glucose (Barton *et al* 2004, Myler *et al* 2004), alcohol (Myler *et al* 2005). and a range of organophosphate pesticides (Pritchard *et al* 2004, Law *et al* 2005) with extreme sensitivity (10^{-17} M).

One difficulty often encountered when using sensors for practical analytical applications is that the species being detected can in some situations be present only at very low concentration while being contained within a complex biological system such as blood. This means that any sensor must display high sensitivities and also low non-specific adsorption of possible foulants or interferents. As can be seen from previous work using enzymes, use of microelectrodes rather than planar electrodes can lead to extremely high sensitivities (Pritchard *et al* 2004, Law *et al* 2005). Attempts therefore were made within this study to determine whether the use of microelectrodes rather than planar electrodes within immunosensors similar to those previously reported (Grant *et al* 2003, 2005) would lead to sensitivity enhancements. Microelectrode arrays containing entrapped anti-BSA were constructed and their performance compared with our previous work on planar, entrapped sensors.

A disadvantage associated with the entrapment method used within much of our previous work for antibody immobilisation is that the antigen will often be too bulky to diffuse through the polymer matrix and so only antibodies located at the surface of the polymer film or microelectrode - and suitably orientated, will be available for antigen binding. Other work comparing monolayers of randomly and specifically orientated antibody fragments (Bonroy *et al* 2006) showed that immunosensor responses typically double when the fragment is specifically orientated.

Digoxin (supplementary information, figure S2) is a cardiac drug, widely used in the treatment of various heart conditions such as atrial fibrillation and atrial flutter, with a narrow therapeutic range of 0.8-2.0 ng ml^{-1} (Terra *et al* 1999). Previous work by our group demonstrated the construction of an immunosensor for digoxin, however, these sensors were only capable of detecting the antigen in the mg-μg ml^{-1} ranges (Grant *et al* 2003). The anti-digoxin antibodies used in this early study were entrapped within a planar, electropolymerised film. We therefore within this work also compare results obtained using an affinity method to graft antibodies to the surface of the film with those obtained previously by entrapment (Grant *et al* 2003) in an attempt to improve sensitivity.

The focus of this paper is not just to describe the development of particular sensors - but rather to compare the behaviour of sensors fabricated using a variety of methods, namely our earlier work on entrapment in planar polymer films with affinity grafted planar films and also entrapment of the antibodies within conductive polymer protrusions. As will be demonstrated, both methods lead to an enhancement in sensitivity.

2. Experimental

2.1. Materials and equipment

Sodium dihydrogen orthophosphate, disodium hydrogen orthophosphate, sodium chloride and hydrochloric acid were obtained from BDH (Poole, Dorset, UK). Aniline, polyclonal human anti-IgG (AIgG), biotin 3-sulfo-N-hydroxysuccinimide, the biotinylation kit (part no. BK101), neutravidin, human serum albumin (HSA), bovine serum albumin (BSA), anti-bovine serum albumin (ABSA, developed in rabbit), digoxin, anti-digoxin (developed in rabbit-whole antiserum), sodium acetate,

acetic acid, sodium perchlorate, potassium ferrocyanide and potassium ferricyanide were obtained from Sigma-Aldrich, Gillingham, Dorset, UK. All water used was obtained from a Purelab UHQ Deioniser (Elga, High Wycombe, UK). Commercial screen-printed carbon electrodes (Figure S1, supplementary information) containing carbon working and counter electrodes and an Ag/AgCl reference electrode were obtained from Microarray Ltd, Manchester, UK. The surface area of the working electrode was 0.2178 cm^2. AC impedance measurements were performed using an ACM Auto AC DSP frequency response analyser (ACM Instruments, Grange-over-Sands, UK). Cyclic voltammetry was performed using a Sycopel potentiometer (Sycopel Scientific, Tyne & Wear, UK) to electrodeposit polyaniline.

Aniline buffer (pH 1-2) was prepared containing 0.5 mol l^{-1} KCl, 0.3 mol l^{-1} HCl and 0.2 mol l^{-1} aniline. Phosphate buffer (PBS, pH 7.4) was prepared comprising 52.8 mmol l^{-1} disodium hydrogen orthophosphate 12-hydrate, 13 mmol l^{-1} sodium dihydrogen orthophosphate 1-hydrate and 5.1 mmol l^{-1} sodium chloride. Acetate buffer (pH 4.0) was prepared comprising 0.4 mol l^{-1} sodium acetate, 0.4 mol l^{-1} acetic acid and 0.4 mol l^{-1} sodium perchlorate.

The anti-digoxin was supplied as a solution in whole antiserum and was purified using a 5 ml protein G-column (Pharmacia). IgG fraction was eluted using glycine buffer (pH 2.7) and dialyzed overnight. For antibody biotinylation, the procedure outlined in the BK101 kit was followed (see manufacturers instructions for details). The biotinylated anti-digoxin was very dilute (0.01 mg ml^{-1}) and was concentrated using a Centriprep centrifugal filter unit (Millipore, Hertfordshire, UK) fitted with an Ultracel YM-30 membrane containing glycerol, to prevent drying. This procedure also ensured the removal of sodium azide from the antibody solution. The procedure involved three subsequent centrifugations in a cold room (4ºC), each for 20

minutes at 30,000 rpm; the final concentration was 0.5 mg ml^{-1}. Biotinylated antibodies were kept frozen in aliquots of 200 μl until required.

2.2. Formation of microarrays.

Sonochemically fabricated microarrays were constructed as previously described (Barton *et al* 2004). To deposit the insulating layer, a 5 mmol l^{-1} solution of 1,2-diaminobenzene in pH 7.4 phosphate buffer was utilised. Prior to the immersion of the carbon electrode, the monomer solution used was thoroughly purged with N_2 for 20 minutes in a sealed cell to provide an oxygen free atmosphere. An initial 1-second blast of ultrasound was also applied to a submerged electrode to displace air bubbles trapped at the surface of the electrodes. Homogenous insulation of a planar carbon electrode was achieved by sequentially scanning the working electrode potential from 0 mV through to +1000 mV (vs. Ag/AgCl) and back to the starting potential at a scan rate of 50 mVs^{-1} for 20 sweeps.

Sonication experiments were performed using a custom built 2 kW, 25 kHz ultrasound tank with internal dimensions of 750 x 750 x 600 mm (working volume 750 x 750 x 500 mm) (Ultrawave Ltd., Cardiff, UK). Ultrasound was applied at a frequency of 25 KHz for 10 seconds duration.

2.3. Incorporation of antibody within microarrays via electrochemical deposition.

A 0.2 M aniline hydrochloride solution was prepared in a pH 4.0 acetate buffer. The solution pH fell to approximately 2.6 upon addition of monomer. Monoclonal antibody receptor was incorporated into the buffered monomer solution prior to polymerisation at a resultant concentration of 0.5 mg ml^{-1}. The pH of the monomer solution increases upon addition of antibody, this was monitored to ensure

the pH remained below 4.0 so that the conductive protonated 'emeraldine' form of polyaniline was deposited at the working electrode. Electrochemical deposition of the polyaniline was performed by sequentially cycling the working electrode potential from –200 mV through to +800 mV (vs. Ag/AgCl) and back to the starting potential at a scan rate of 50 mVs^{-1}. A linear sweep from -200 to +800 mV (50 mVs^{-1}) was performed at the end of cyclic voltammetry to leave the polyaniline in its protonated emeraldine salt form. This lead to formation of polyaniline protrusions containing entrapped antibodies as previously described (Barton *et al* 2004, Law *et al* 2005).

2.4. Construction of planar antibody electrodes via an affinity protocol

Anti-digoxin was immobilised at the surface of planar electrodes by the methods previously described (Garifallou *et* al 2007, Tsekenis *et* al 2008) and the immunosensor structure is shown schematically in figure 2. The potentiodynamic electrodeposition of polyaniline from aniline buffer, pH 1-2 into the microelectrode array was achieved electrochemically as described for the microarrays.

30 µl of biotin-sulfo-NHS (10 mg ml^{-1} in water) was placed on the working electrode surface for 24 hours. The sensors were rinsed with copious water and 30 µl of neutravidin (10 µg ml^{-1} in water) placed on the working electrode for 1 hour - followed by further rinsing in water. 30 µl biotinylated anti-digoxin (0.5 mg ml^{-1} in water, 1 hour) was then added followed by rinsing. Finally, non-specific interactions were blocked by HSA (10^{-6} mol l^{-1} in PBS, 1 hour).

2.5. Determination of antigen concentration

AC impedance measurements were performed using an ACM Auto AC DSP frequency response analyser. Following immobilisation of antibody, impedance

analyses were performed from 1 Hz to 10,000 Hz (+/- 5 mV amplitude perturbation) in pH 7.4 phosphate buffer, i.e. containing no antigen, as a baseline trace. This buffer solution did, however, contain a 50:50 mixture of $[Fe(CN)_6]^{3-/4-}$, at a concentration of 10 mmol l^{-1} as redox mediator so as to perform faradaic impedance spectroscopy. The potential of the electrochemical cell is offset to the formal potential of the redox probe (+0.12 V vs. Ag/AgCl identified via amperometric cyclic voltammetry). Following the recording of a baseline spectral trace (0 ng ml^{-1} antigen), the same sensor is used for all concentrations and exposed for 30 minute time periods to the increasing concentrations of antigen in phosphate buffered test solution.

After each 30 minutes exposure to a known concentration, the sensor was thoroughly flushed with 50ml of pH 7.4 phosphate buffer (containing $[KFe(CN)_6]^{3-/4-}$ & no antigen) to remove any non-specifically adsorbed matter before ac impedance spectra were recorded in the phosphate buffered test solution (containing $[KFe(CN)_6]^{3-/4-}$ & no antigen). This sensor was then exposed to an increasing antigen concentration and the process repeated for the full range of applied antigen concentrations under investigation. Traces recorded may then be compared to the baseline trace. Immunosensors were also tested where the electrode was exposed to a diminishing series of antigen concentrations i.e. starting with the highest and gave similar results (Garifallou 2008).

The electrode assemblies were found to be very stable, for example a sensor placed in pH 7.4 phosphate buffer (containing $[KFe(CN)_6]^{3-/4-}$ showed no change in the ac impedance curves even after 90 minutes equillibration (Tsekenis 2008).

3. Results and discussion

3.1. Impedance results for planar, affinity immobilised anti-digoxin electrodes:

Figure 3 shows the (a) Bode and (b) Nyquist curves obtained for a planar polyaniline/anti-digoxin modified, carbon electrode exposed to various concentrations in the range of 0-10 ng $ml^{-1}$of antigen. The Nyquist curve (figure 3b) demonstrates that the Z' (real) component of the impedance increases steadily with decreasing frequency whereas the Z'' (imaginary) component increases to a maximum value (at frequencies in the range 5-10 Hz) before falling as the frequency approaches 1 Hz. This type of impedance spectrum is indicative of a surface-modified electrode system where the electron transfer is slow and the impedance is controlled by the interfacial electron transfer (Katz and Willner 2003).

As can be seen, there is a steady decrease in impedance as antigen concentration increases towards a concentration of about 1.5 ng ml^{-1}. Levels of 2 ng ml^{-1} and 10 ng ml^{-1} did not lead to even lower impedances, but rather tend towards a plateau, indicating saturation of the specific binding sites. Any further changes in impedance beyond 1.5 ng ml^{-1} are likely to be due to non-specific interactions. The corresponding Bode plots (figure 3a) also show a decrease in the total impedance as the digoxin levels increase. This indicates that the binding of digoxin is facilitating electron transfer between the electrode and the redox probe. Since the therapeutic range is 0.8-2.0 ng ml^{-1} (Terra *et al* 1999) this indicates that these sensors will be sufficiently sensitive and in fact there may be a need to undertake some dilution of the sample. However the range of these sensors is unfortunately rather small, which may preclude their use in real situations. What is of interest though is the much higher sensitivity compared to digoxin sensors fabricated by entrapment, indicating that controlled immobilisation does lead to enhanced sensitivity.

The impedance spectra consists of two components, the real (Z') component where the impedance in phase with the AC potential waveform is measured and the

imaginary (Z") where the impedance is 180^{o} out of phase. Previous work by our group has demonstrated that in these type of systems, the increase in the real component dominated the total increase in the impedance and perhaps more importantly the real component offers far greater reproducibility in comparison to the imaginary contribution (Garifallou *et* al 2007, Tsekenis *et* al 2008).

Our previous work demonstrated that the sensors of this type gave the largest relative changes at the lower frequencies (Garifallou *et* al 2007, Tsekenis *et* al 2008). Calibration curves could be drawn (figure 4a) showing the percentage decrease in Z' at 1 Hz across a range of antigen concentrations. Again these show a relationship between antigen concentration and the decrease in Z'.

Non-specific interactions have the potential to either exaggerate or mask specific interactions. Whereas specific binding of antigens will only occur when their antibodies is present, electrodes fabricated using a non-specific antibody should undergo the same non-specific binding events as those fabricated using specific antibodies. The calibration curve showing the percentage decrease in Z' at 1 Hz is shown for sensors fabricated using an identical protocol except that the specific antibody is replaced by a non-specific IgG antibody (figure 4b). As can clearly be seen, there is a much lower response for the non-specific antibody, showing that although there are non-specific interactions, between the concentration ranges of 0-2 ng ml^{-1}, they comprise a minor component of the detected response.

Once the non-specific responses have been subtracted (figure 4a - figure 4b), a corrected plot (figure 4c) shows the calibration curve for the corrected sensor response. Between a concentration range of 0-1.5 ng ml^{-1}, there is a clear correlation of the corrected impedance change with the concentration. The limit of detection, calculated as 3x the standard deviation of the baseline sample of this system

(Analytical methods committee, 1987) is approximately 0.1 ng ml^{-1}. Our previous system using entrapment of digoxin within a polymer film combined with pulsed waveform detection (Grant *et al* 2003) was only capable of resolving digoxin at levels higher than 50 μg ml^{-1}, so as can be seen the combination of an ac interrogation protocol and an affinity based immobilisation procedure leads to at least a two orders of magnitude increase in sensitivity. The responses for 10 ng ml^{-1} digoxin (not shown in plots) were indistinguishable from those at 2 ng ml^{-1}.

3.2. Impedance results for entrapment immobilised anti-BSA microelectrodes:

Impedance traces for polyaniline microelectrode sensors containing entrapped ABSA were obtained as for the anti-digoxin based electrodes. These were very similar in appearance to those obtained for previous electrodes, again indicating a electrochemical system where the electron transfer is slow and the impedance is controlled by the interfacial electron transfer (Katz and Willner 2003). Rather than just studying the change in Z' at 1 Hz, it was decided to undergo a more detailed investigation of the electrochemical system. A computer fitting of the experimental data to a theoretical model, represented by a simple equivalent circuit, may be performed by the software accompanying the frequency response analyser. In this case, the interface is modelled by an equivalent circuit (supplementary information, figure S3), also called a Randles circuit (Randles, 1947), consisting of a double-layer capacitor in parallel with a polarization resistor (also known as a charge transfer resistor with certain constraints) and a Warburg impedance, connected in series with a resistor that measures the resistance of the electrolyte solution. For a more thorough evaluation of the data obtained, the changes in the Nyquist curves may be translated into electron transfer resistance changes to provide a clear and consistent format.

The relative electron transfer resistance changes from the baseline response at each concentration of BSA for a typical electrode modified with ABSA are plotted in figure 5a. The electron transfer resistance increases with increasing BSA concentration and demonstrates that an entrapped ABSA immunosensor gave a linear response to the analyte from 0 ng ml^{-1} to 100 ng ml^{-1} ABSA.

The insulation of the modified electrode upon formation of stable antibody-antigen immunocomplexes hinders the electron transfer kinetics of the redox probe resulting in the increase of electron transfer resistance. The electron transfer resistance increases with increasing antigen concentration for both types of electrode. The limit of detection (three times the standard deviation of the baseline value) of the entrapped ABSA immunosensor is 1 ng ml^{-1}. There is negligible change from 100 ng ml^{-1} to 300 ng ml^{-1} suggesting that the immunosensor approaches saturation.

Non-specific interactions have the potential to interfere with immunosensor performance, leading to erroneously elevated results. For this reason, identical sets of immunosensors were fabricated by both methods utilising a non-specific IgG antibody in place of the specific ABSA antibody. Results for these electrodes were obtained in exactly the same manner as for the specific electrodes. From the Nyquist plots for these systems (not shown), it could be seen that while binding of BSA to the non-specific immunosensors occurs, the responses are smaller than for ABSA modified sensors. A calibration plot for this system can also be drawn (figure 5b) and shows a linear-type non-specific response is observed for the affinity based anti-IgG immunosensor from 1 to 100 ng ml^{-1} BSA with a plateau above this concentration. Upon comparison of figure 5a with figure 5b, it is apparent that approximately 50% of the ABSA-affinity immobilised sensor response encountered is, in fact, non-specific.

This is most likely due to the fact that BSA is a protein with a high affinity for surfaces and no blocking reagents have been utilised for these electrodes.

To obtain a calibration profile, in terms of 'corrected' electron transfer resistance change for an ABSA immunosensor, accounting for any non-specific responses, the non-specific response was subtracted from the specific response over the entire analytical concentration range. In total 10 ABSA immobilised sensors of each type and 10 corresponding anti-IgG immobilised sensors were interrogated over their active concentration range, to allow an assessment of the reproducibility of the responses for this system. Results are presented in figure 6. The error bars are the standard deviations obtained for the 10 matched sensor pairs from the mean 'corrected' values.

From figure 6 a linear response was observed for the immunosensors from 0-100 ng ml^{-1} BSA. Figure 6 (inset) shows an expanded view from 0 to 10 ng ml^{-1} BSA and shows linear behaviour with R^2>0.99. At concentrations above 100 ng ml^{-1}, the sensor becomes saturated. From the standard deviations obtained, we can say that discrimination of BSA antigen analyte is possible at 5 ng ml^{-1}. The limit of detection of the ABSA immunosensor is 1.5 ng ml^{-1} BSA and is calculated from 3x the standard deviation of the baseline response and extrapolated from the line of best-fit according to IUPAC guidelines (Analytical methods committee, 1987). Previous work (Grant *et al* 2003, 2005) allowed detection of BSA at levels as low as 10 μg ml^{-1}. As can be seen the use of polyaniline microelectrodes has greatly increased sensitivity, although in this instance there is a problem with high non-specific responses.

3.3 Stability of the BSA immunosensors and regeneration studies.

Although a long-term sensor stability test was not performed, a batch of 18 sensor pairs was assessed from storage in dry state, at 4ºC, for a period of 12 weeks. Again an identical experimental protocol was employed for electrochemical impedance interrogation and the 'corrected' electron transfer change was the analysis method for response recovery.

Every 2 weeks a set of 3 matched sensor pairings was removed from storage and interrogated over the full BSA antigen analyte concentration range from 1 to 300 ng ml^{-1}. After 2 weeks no loss of sensor response occurred but after 4 weeks there was a 10% loss in response and further steady decreases until after 10 weeks storage only 10% of the original response was detected.

Some of our previous work demonstrated that acid washing of some immunosensors led to their regeneration (Barton 2007). Attempts were made so see whether it was possible to regenerate the sensors by acid washing. 5 ABSA-immobilised sensors and 5 matched non-specific AIgG-immobilised sensors are exposed to the full interrogation procedure prior to reversibility investigations. In order to split the antibody-antigen complex and to regenerate the sensors, 0.1M HCl acidic buffer (pH 2.3) was applied for 3 separate 1 minute time periods. In between each acidic buffer exposure, pH 7.4 PBS was used to rinse the sensor surface. Finally the sensors were rinsed with 50ml PBS to produce PSA-free sensors which could then be used for fresh analysis. Unfortunately in all cases the washing removed all activity. An identical baseline response could be achieved which suggests that the sensor surface integrity remains, yet the antigen recognition and binding capabilities of the receptor antibodies are severely damaged by the treatments.

4. Conclusions

Our work verifies several fabrication techniques and an ac experimental interrogation protocol as a viable approach towards the labeless sensing of BSA and digoxin. Affinity based sensors where anti-digoxin is immobilised on planar electrodes using avdin-biotin interactions have been shown to display much higher sensitivities (by two orders of magnitude, capable of detection of ng ml^{-1} levels of antigen) than sensors developed in earlier work utilising entrapment within planar conductive polymer electrodes as the method of immobilisation. Low non-specific binding of these electrodes was also observed. However the range of these electrodes was very limited which could preclude their use in real analyses.

Similarly sensors developed where ABSA is entrapped in conductive polymer microelectrodes rather than planar polymer films have been studied. The microelectrode array sensors were three orders of magnitude more sensitive, again allowing detection of ng ml^{-1} levels of antigen. These types of sensors however displayed higher non-specific binding. However BSA is a protein noted for its high binding ability to surfaces and future sensors for other analytes will include a BSA blocking step to reduce non-specific interactions.

The next step involved combining these two methods in an attempt to enhance the sensitivity levels even further. Sensors have been developed involving a multi-step procedure. Initially conductive polyaniline microarrays were constructed. The polyaniline was then modified with biotinylating reagents and biotinylated antibodies immoblised by the affinity procedures described above. Finally the sensors are blocked with HSA. Ongoing work has demonstrated the construction of sensors for prostate specific antigen, neuron specific enolase and the stroke marker protein S-100[β]. ***These immunosensors have been shown capable of quantifying antigens at levels as low as 1 pg ml^{-1}, these will be the subject of a further series of***

publications to be submitted for publication shortly and will be described in detail at the 10th World Congress in Biosensors, Shanghai, May 14th-18th 2008.

Acknowledgements

This work, including funding for ACB, G-Z G, GT and FD, has been supported by the European Community QLRT-2001-02583 (SMILE) and NMP2-CT-2003-505485, (ELISHA) Framework VI contracts.

References

Analytical Methods Committee, 1987. Analyst 112, 199-204.

Barnett, D., Laing, D. G., Skopec, S., Sadik, O. A., Wallace, G. G., 1994. Anal. Lett. 27, 2417-2429.

Barton, A.C., Collyer, S. D., Davis, F., Gornall, D. D., Law, K. A., Lawrence, E. C. D., Mills, D. W., Myler, S., Pritchard, J. A., Thompson, M., Higson, S. P. J., 2004. Biosens. Bioelec. 20, 328-337.

Barton, A.C., 2007, PhD Thesis, Cranfield University.

Bender, S. Sadik, O. A., 1998. Environ. Sci. Tech. 32, 788-797.

Bonroy, K., Frederix, F., Reekmans, G., Dewolf, E., De Palma, R., Borghs, G., Declerck, P., Goddeeris, B., 2006. J. Immunolog. Met. 312, 167-181.

Clark, L. C., Lyons, I. R.,1962. Ann New York Academy Sci. 102, 29-45.

Cosnier S., 2005. Electroanalysis 17, 1701-1715.

Davis, F., Collyer, S. D., Gornall, D. D., Law, K. A., Mills, D. W., Higson, S. P. J., 2007. Chimica Oggi/Chemistry Today 25, 28-31.

Diaz-Gonzalez, M., Gonzalez-Garcia, M. B., Costa-Garci, A., 2005. Electroanalysis 17, 1901-1918.

Garifallou, G.-Z., Tsekenis, G., Davis, F., Higson, S. P. J., Millner, P. A., Pinacho, D. G., Sanchez-Baeza, F., Marco, M.-P., Gibson, T. D. 2007. Anal. Lett. 40, 1412-1442.

Garifallou, G.-Z., 2008, PhD Thesis, Cranfield University.

Grant, S., Davis, F., Pritchard, J. A., Law, K. A., Higson, S. P. J., Gibson, T. D., 2003. Anal. Chim. Acta. 495, 21-32.

Grant, S., Davis, F., Law, K. A., Barton, A. C., Collyer, S. D., Higson, S. P. J., Gibson, T. D., 2005. Anal. Chim. Acta. 537, 163-168.

Higson, S. P. J., 'Sensor', International Patent: PCT/GB96/0092, 1996.

John, R., Spencer, M., Wallace, G. G., Smyth, M. R., 1999. Anal. Chim. Acta. 249, 381-385.

Katz, E, Willner, I., 2003. Electroanalysis 15, 913-947.

Law, K. A., Higson, S. P. J., 2005. Biosens. Bioelec. 21, 1914-1924.

Myler, S., Eaton, S., Higson, S. P. J., 1997. Anal. Chim. Acta. 357, 55-61.

Myler, S., Davis. F., Collyer. S. D., Higson. S. P. J., 2004. Biosens. Bioelec., 20, 408-412.

Myler, S., Davis, F., Collyer, S. D., Gornall, D. D., Higson, S. P. J., 2005. Biosens. Bioelec. 21, 666-671.

Pritchard, J. A., Law, K. A., Vakurov, A., Millner, P. A., Higson, S. P. J., 2004. Biosens. Bioelec. 20, 765-772.

Randles, J.E.B. 1947, Discussions of the Faraday Society, 1, .11-19.

Rodriguez-Mozaz, S., de Alda, M. J. L., Barcelo, D., 2006. Anal. Bioanal. Chem. 386, 1025-1041.

Sadik, O. A., John, M. J., Wallace, G. G., Barnett, D., Clarke, C., Laing, D. G., 1994. Analyst 119, 1997-2000.

Terra, S. G., Washam, J. B., Dunham, G. D., Gattis, W. A., 1999. Pharmacotherapy 19(10) 1123-1126.

Tsekenis, G., Garifallou, G. Z., Davis, F., Millner, P. A., Gibson, T. D., Higson, S. P. J.2008. Anal. Chem., 20, 2058-2062.

Tsekenis, G., 2008, PhD Thesis, Cranfield University.

Yalow, R. S., Berson, S. A., 1959. Nature. 184, 1648-1649.

LIST OF FIGURES.

Figure 1. Formation of polyaniline microarrays (a) deposition of insulating layer (b) sonochemical formation of pores (c) polymerisation of aniline.

Figure 2. Schematic of the affinity binding procedure used to immoblise anti-digoxin

Figure 3. (a) Bode and (b) Nyquist plots of a typical specific anti-digoxin modified electrode exposed to various concentrations in the range 0-10.0 ng ml^{-1} of digoxin in PBS.

Figure 4. Calibration curves showing the increase in the real component of impedance (in the range 0-2.0 ng ml^{-1} digoxin) at 1Hz for: (a) specific anti-digoxin modified electrodes exposed to varying concentrations of antigen (b) IgG modified electrodes exposed to antigen under identical conditions (c) corrected calibration curves where the non-specific response has been subtracted form the specific response (curve a – curve b). All data points are means for the responses of three electrodes; error bars give a measure of the reproducibility of the system.

Figure 5. Calibration plot showing changes in electron transfer resistance vs. BSA concentration. (a) entrapped ABSA (0-300 ng ml^{-1}) (b) entrapped anti-IgG (0-300 ng ml^{-1})

Figure 6. Corrected calibration curves where the non specific response has been subtracted from the specific response (0-300 ng ml^{-1}) (inset) corrected calibration plot (0-10 ng ml^{-1}).

Figure(s)

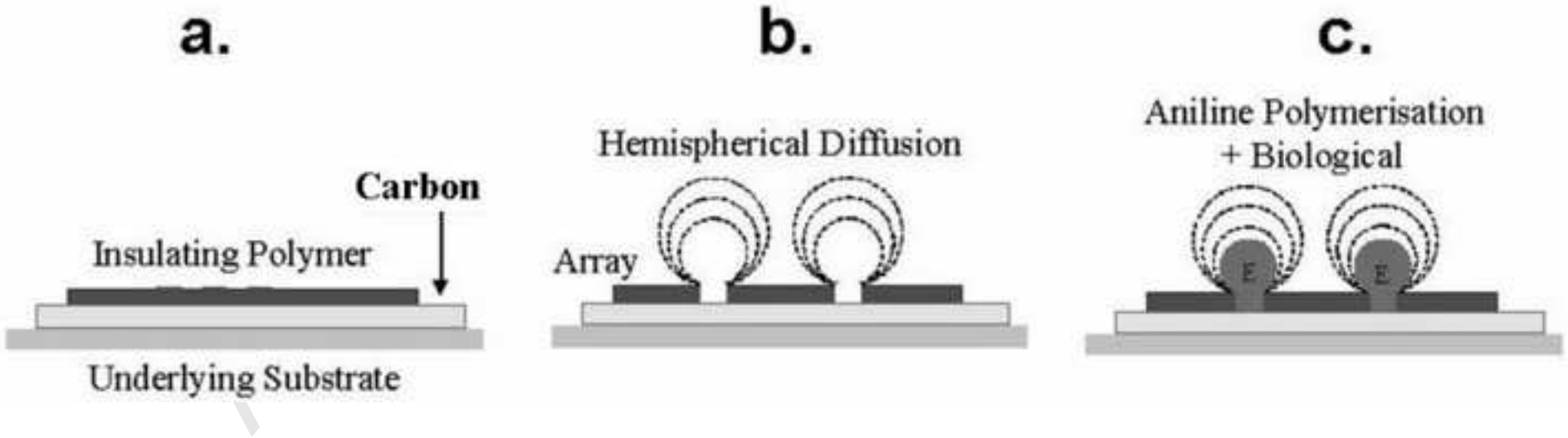
a.
Carbon
Insulating Polymer
Underlying Substrate
b.
Hemispherical Diffusion
Array
c.
Aniline Polymerisation
+ Biological
E
E

Figure(s)

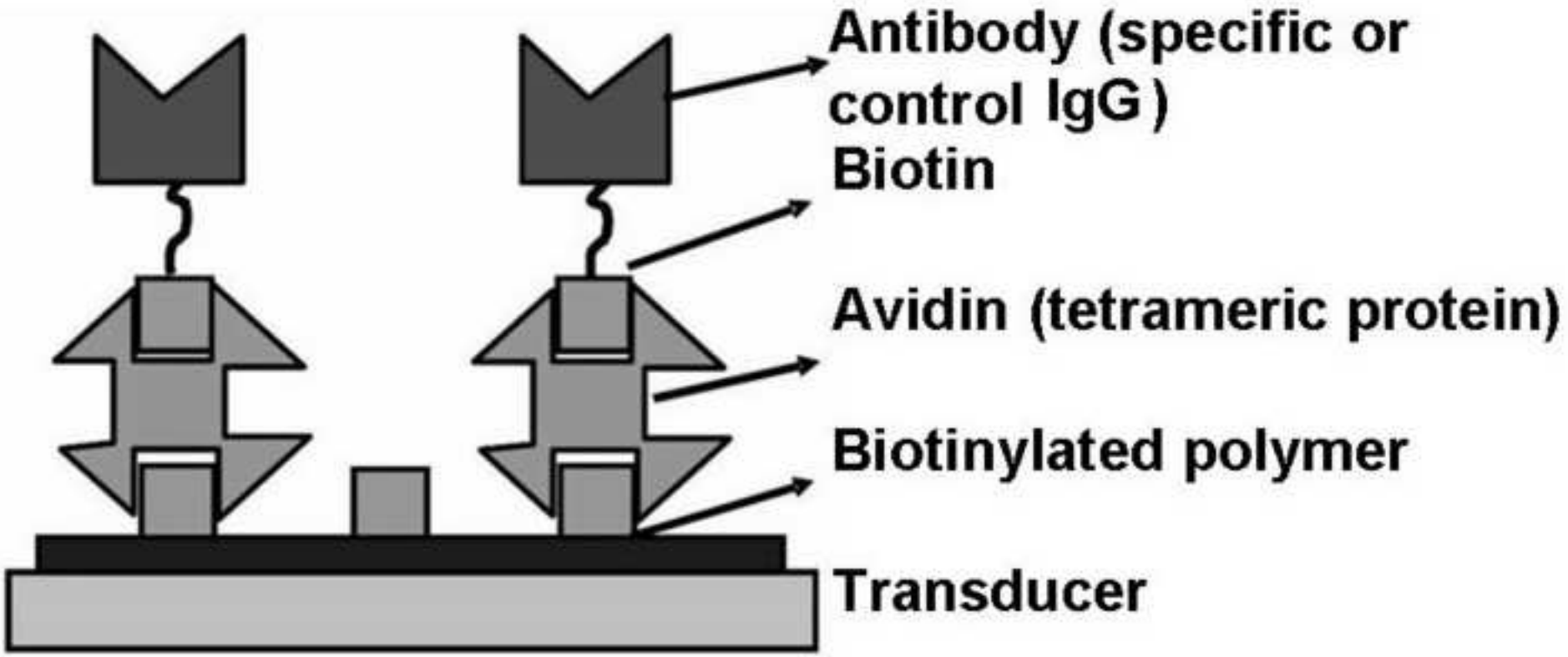
Antibody (specific or control IgG)
Biotin
Avidin (tetrameric protein)
Biotinylated polymer
Transducer

Figure(s)

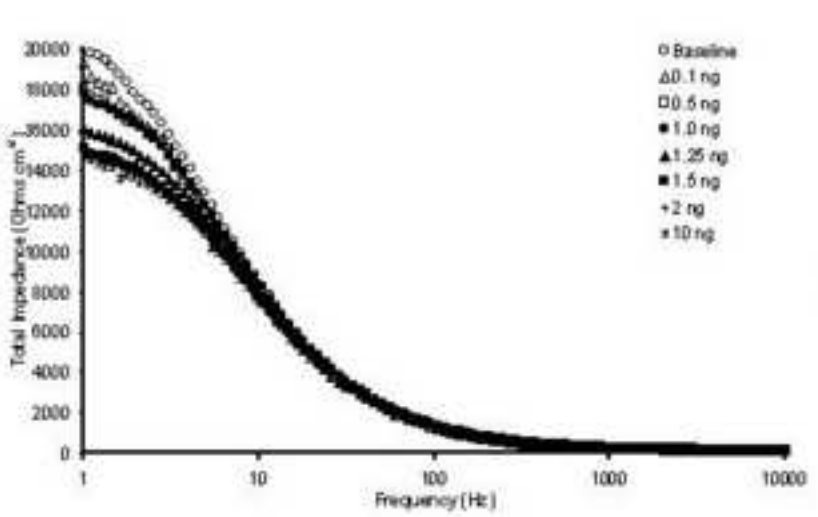

a.

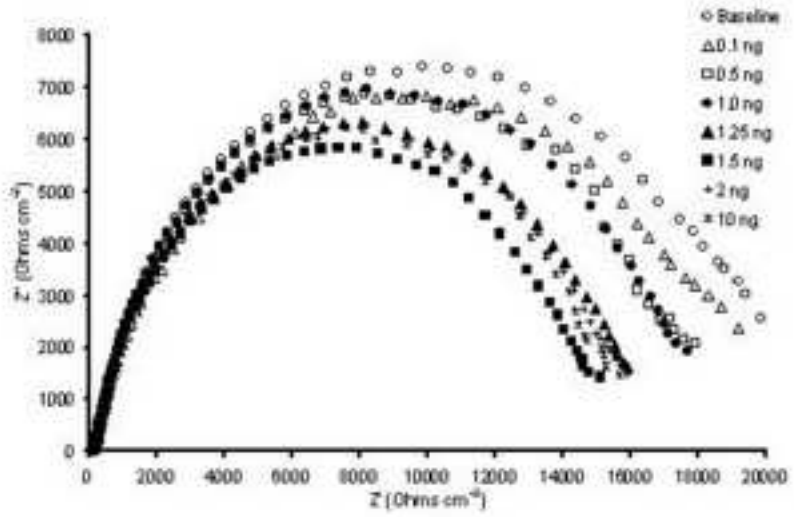

b.

Figure(s)

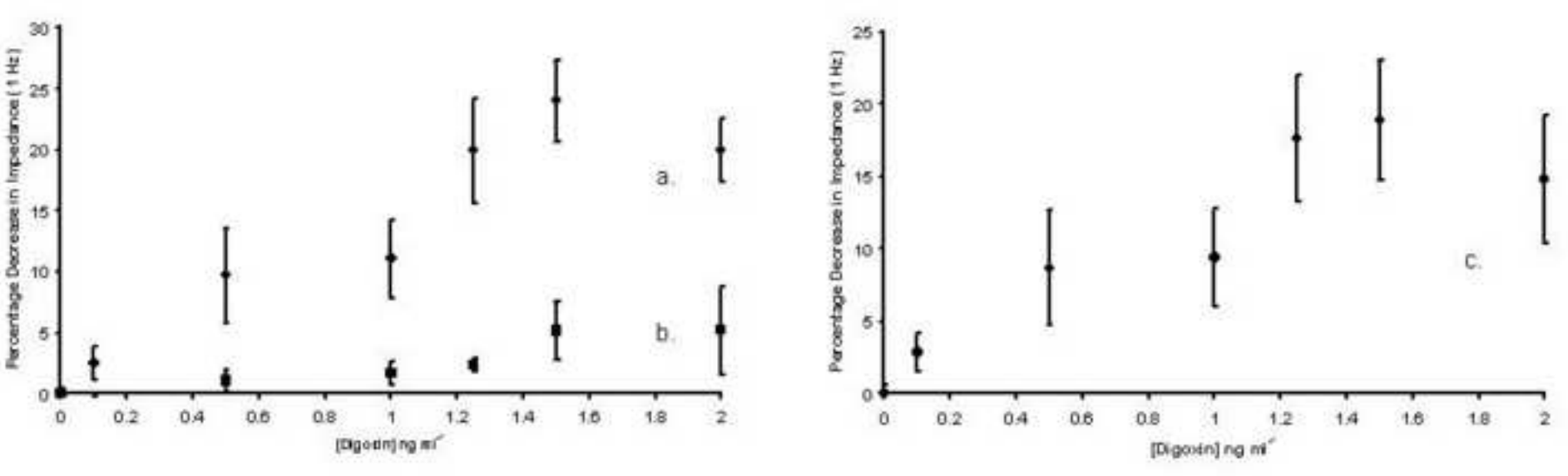

Figure(s)

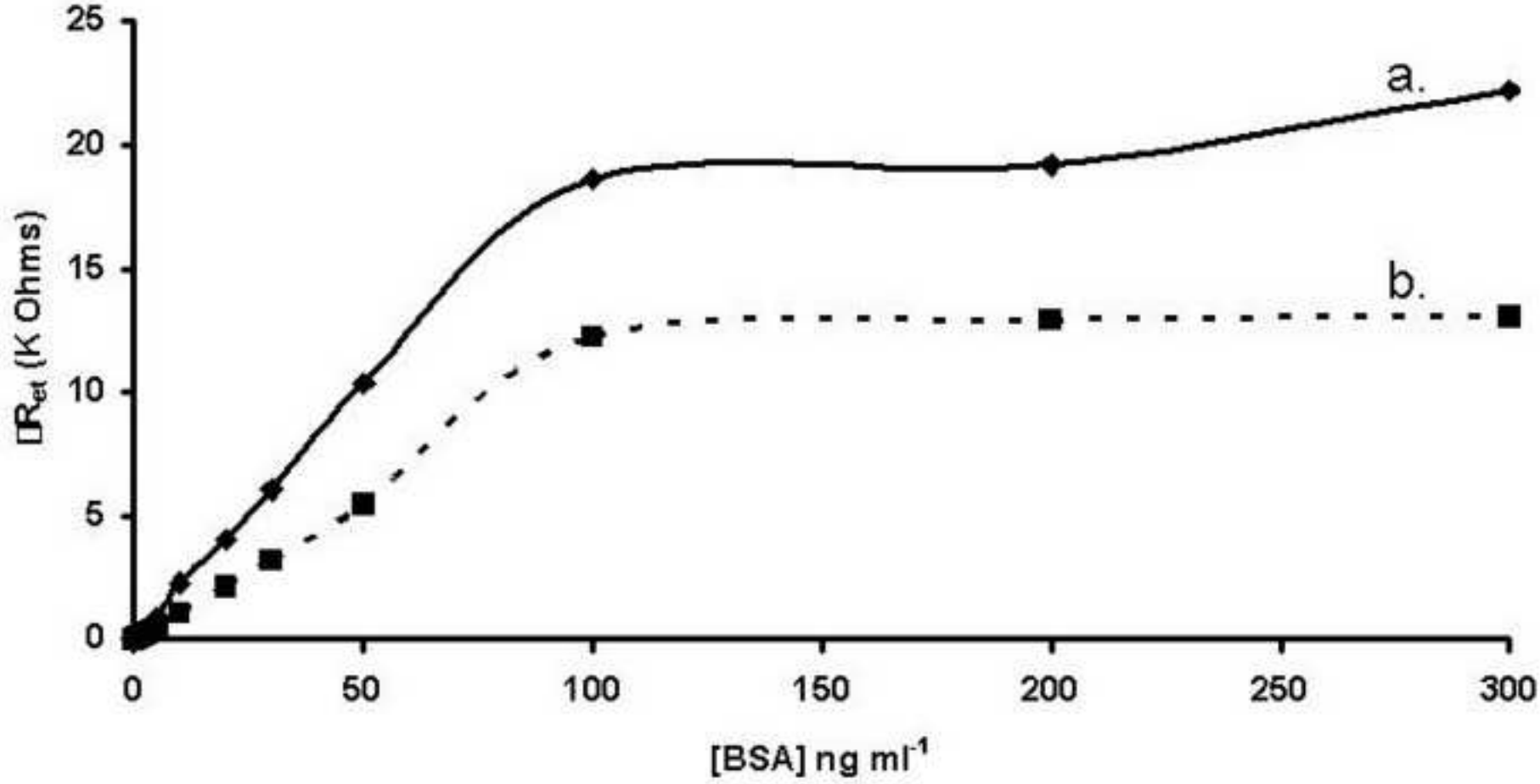

Figure(s)